

**Luminescent conjugated oligothiophenes
as diagnostic tools and potential pharmacophores
in Alzheimer's disease**

Inaugural-Dissertation

to obtain the academic degree

Doctor rerum naturalium (Dr. rer. nat.)

submitted to the Department of Biology, Chemistry and Pharmacy
of Freie Universität Berlin

by

Susann Handrick

from Räckelwitz

2014

The present dissertation was prepared from June 2010 to April 2014 under the
direction of Prof. Dr. med. Frank L. Heppner and
supervision of Stefan Prokop, MD
at the Department of Neuropathology, Charité – Universitätsmedizin Berlin.

1st Reviewer: Prof. Dr. med. Frank L. Heppner

2nd Reviewer: Prof. Dr. Fritz G. Rathjen

date of defence: 29.09.2014

**Life is not about waiting in the storm to pass,
it is about learning to dance in the rain.**

Acknowledgment

First and foremost I want to thank Prof. Dr. med. Frank L. Heppner for his support and for giving me the opportunity to do my thesis in his department.

I want to thank Prof. Dr. Fritz G. Rathjen to review my thesis. I also thank the members of the promotion committee to evaluate my thesis.

My special thanks go to Stefan Prokop, MD for his guidance, supervision and scientific support during my thesis. I am also grateful to have given this very interesting project. His perpetual enthusiasm in scientific research motivated me during the last years a lot. In addition, I would like to thank him for the constructive comments and discussions to sum up my thesis.

Further, I want to thank all collaborators on the EU project LUPAS for motivating scientific discussions during our biannual meetings. Special thanks go to all direct collaborations including the Linköping University in Sweden, the Université Claude Bernard Lyon 1 in France, the Norwegian University of Science and Technology in Norway and to the company Genovis AB in Sweden. I want to express my sincere gratitude to Prof. Per Hammarström, PhD, K. Peter R. Nilsson, PhD and Sofie Nyström, PhD who enabled my research visit at the Linköping University to perform the spectral analyses within my project. I enjoyed working at the Linköping University in December 2012 a lot.

The financial support provided from the “Sonnenfeld Stiftung” for the finalization of this project is greatly appreciated.

I would like to thank all the current and previous members of the Department of Neuropathology at the Charité – Universitätsmedizin Berlin for the great working environment. Especially, I would like to thank Carola and Gordon for reading this thesis and giving me constructive criticism. I loved to spend my days and work at the Department of Neuropathology together with my colleagues and friends Josi, Gordon, Carola, Alex D., Alex H., Steffi, Kelly and Adnan. Remembering the fruitful and stimulating discussions and also fun times will always put a smile on my face.

In this line, I would like to thank some very special persons of my private life who supported me throughout my thesis and have made my life so colorful. Sophie, Sarah, Josi and my sister Rony carried me through all phases of this thesis, listened patiently, always encouraged and supported me. Furthermore I am grateful to have friends like Luisa, Mathilde, Clemens, Diana, Jule and Tim, who carried me with love and trust through the last years.

Najwutrobniji dzak chcu tež mojimaj staršimaj wuprajić. Dołhož móžu myslić, staj wój mje bjez wuměnjenjow při přesadženju mojich sonow podpěrałoj. Sym wamaj tež z cyłeje wutroby dzakowna, zo sym stajnje lubje doma witana a zo mje lubujetaj. Přerady přijědu domoj, tež dokelž wěm, zo zamóžeće mje w kóždyj situaciji popadnyć a znowa motiwěrować. Za wšitko to sym wamaj njesměrnje dzakowna!

Table of contents

List of abbreviations	1
1. Introduction	3
1.1 Dementia and neurodegenerative diseases.....	3
1.2 Alzheimer's disease.....	5
1.2.1 Epidemiology and genetics of Alzheimer's disease	5
1.2.2 Clinical symptoms and pathological alterations of Alzheimer's disease.....	5
1.2.3 Treatment of Alzheimer's disease	9
1.2.4 Diagnostics of Alzheimer's disease.....	10
1.2.5 Alzheimer's disease mouse models.....	13
1.3 Luminescent conjugated oligothiophenes as novel amyloid binding agents.....	14
1.4 Aims and hypotheses of the thesis	17
1.4.1 LCOs as <i>in vivo</i> imaging tracer for detecting cerebral A β deposits in Alzheimer's disease.....	17
1.4.2 Effect of LCOs on Alzheimer's disease pathology <i>in vivo</i>	18
2. Material and Methods.....	20
2.1 LCOs, LCO derivatives and LCO-MNPs.....	20
2.2 <i>In vivo</i> manipulations in mouse models.....	22
2.2.1 Alzheimer's disease mouse model <i>APP/PS1</i>	22
2.2.2 Genotyping of <i>APP/PS1</i> mice	23
2.2.3 Intravenous and intraperitoneal applications in <i>APP/PS1</i> mice	25
2.2.4 Blood sampling from <i>APP/PS1</i> mice	25
2.2.5 Euthanasia and organ sampling.....	26
2.3 Histology	27
2.3.1 Cutting of tissue	27
2.3.2 Staining of tissue.....	28
2.3.2.1 Hematoxylin and eosin staining.....	28
2.3.2.2 Amyloid stainings.....	28
2.3.2.3 Immunohistology.....	29
2.4 Quantitative analyses of cerebral free floating sections	31
2.4.1 Quantification of area covered by a specific staining.....	31
2.4.2 Counting A β plaques.....	32
2.4.3 A β plaque size distribution analysis.....	32
2.5 Biochemical analyses of cerebral Aβ burden.....	33
2.5.1 Extraction of cerebral A β by homogenization of frozen hemispheres.....	33

2.5.2	Biochemical quantification of cerebral A β by an electroluminescence linked immunosorbent assay system.....	33
2.5.3	Biochemical quantification of cerebral A β by SDS-polyacrylamid gel electrophoresis and Western Blotting.....	34
2.6	Spectral imaging of Aβ plaques after pFTAA and hFTAA co-staining	35
2.6.1	Fluorescence microscopy	35
2.6.2	Confocal microscopy.....	36
2.7	Electrophysiological measurements in the CA1 region of hippocampal slices	36
2.7.1	Generation of hippocampal slices	36
2.7.2	Long term potentiation in the hippocampal CA1 region.....	36
2.7.3	Paired pulse facilitation in the hippocampal CA1 region.....	37
2.8	Microscopy.....	37
2.9	Magnetic resonance imaging and intracranial pressure measurement.....	39
2.10	Statistical analyses	39
3.	Results	40
3.1	Efficient labeling of Aβ deposits with pFTAA on tissue sections and <i>in vivo</i>	40
3.1.1	Labeling of A β deposits in murine and human tissue samples.....	40
3.1.2	<i>In vivo</i> labeling of cerebral A β deposits in the transgenic Alzheimer’s disease mouse model <i>APP/PS1</i>	45
3.1.2.1	Intravenous <i>versus</i> intraperitoneal pFTAA application.....	45
3.1.2.2	Titration of pFTAA dosage for <i>in vivo</i> application in <i>APP/PS1</i> mice.....	49
3.1.2.3	Time course of pFTAA <i>in vivo</i> binding to cerebral A β plaques.....	51
3.1.2.4	Histological analyses of peripheral organs after short term pFTAA application	53
3.2	LCOs coupled to magnetic nanoparticles as novel MRI contrast agents for diagnostics of Alzheimer’s disease.....	59
3.2.1	Staining of murine brain tissue with LCO derivatives and LCO-MNPs	59
3.2.2	Investigation of LCO derivatives and LCO-MNPs for blood brain barrier crossing after peripheral application.....	67
3.2.3	Summary of MRI results after short term application of LCO-MNPs to <i>APP/PS1</i> mice.....	80
3.2.4	Summary of LCOs as novel MRI contrast agents for diagnostics of Alzheimer’s disease	82
3.3	Long term pFTAA treatment of young experimental animals.....	83
3.3.1	Experimental setup of long term pFTAA treatment of young experimental animals	83
3.3.2	Monitoring toxic side effects during and after long term pFTAA treatment of young experimental animals	84
3.3.2.1	Weight gain of young experimental animals during long term pFTAA treatment	84
3.3.2.2	Blood analyses during and after long term pFTAA treatment of young experimental animals	86

3.3.2.3	<i>Postmortem</i> screening of peripheral organs after long term pFTAA treatment of young experimental animals	91
3.3.3	Histological analyses of cerebral sections after long term pFTAA treatment of young experimental animals	98
3.3.3.1	Quantification of cerebral A β plaque burden by conventional amyloid stainings	99
3.3.3.2	Quantification of cerebral A β plaque burden by immunohistological stainings	101
3.3.3.3	Spectral analyses of A β plaques after long term pFTAA treatment	105
3.3.3.4	Quantification of dystrophic neurites around cerebral A β plaques	109
3.3.3.5	Histological analyses of neuronal loss in distinct cerebral regions.....	110
3.3.3.6	Histological analyses of cortical gliosis.....	111
3.3.4	Biochemical analysis of cerebral A β burden after long term treatment of young <i>APP/PS1</i> mice	114
3.3.4.1	Detection of cerebral A β amounts by MSD 6E10 assay and by SDS-polyacrylamid gel electrophoresis and Western Blotting	114
3.3.4.2	Impact of pFTAA on A β extraction from brain tissue.....	124
3.3.5	Summary of long term pFTAA treatment in young experimental animals.....	129
3.4	Functional impact of short term pFTAA treatment in aged experimental animals... 129	
3.4.1	Hippocampal long term potentiation measurements in young and aged <i>APP/PS1</i> versus WT mice..	130
3.4.2	Short term pFTAA treatment of aged experimental animals	131
4.	Discussion.....	137
4.1	LCOs as <i>in vivo</i> tracer for detecting Aβ in Alzheimer's disease.....	137
4.2	Effect of LCOs on Alzheimer's disease pathology <i>in vivo</i>	143
4.2.1	Effect of pFTAA on A β plaque pathology <i>in vivo</i>	143
4.2.2	Effect of pFTAA on A β oligomer toxicity <i>in vivo</i>	146
4.2.3	Conclusions of peripheral pFTAA treatment in <i>APP/PS1</i> mice	147
5.	Zusammenfassung.....	149
6.	Abstract.....	151
7.	References	153
8.	List of publications.....	160

List of abbreviations

A β	Amyloid- β
aCSF	Artificial cerebrospinal fluid
AD	Alzheimer's disease
ALT	Alanine aminotransferase
APP	Amyloid precursor protein
APPPS1	AD transgenic mice carrying the Swedish APP and the presenilin 1 mutation L166P
AST	Aspartat aminotransferase
BBB	Blood brain barrier
CAA	Cerebral amyloid angiopathy
CERAD	Consortium to Establish a Registry for AD
CP	Conjugated polymer
CSF	Cerebrospinal fluid
ddH ₂ O	Double-distilled water
DLB	Dementia with Lewy bodies
DNA	Desoxyribonucleic acid
dpi	Days post initial injection
FA	Formic acid
FAD	Familial Alzheimer's disease
FDG-PET	Fluorodeoxyglucose positron emission tomography
FeO	Iron oxide
fEPSP	Field excitatory postsynaptic potential
FTD	Frontotemporal dementia
GdF3	Gadolinium fluoride
GLDH	Glutamate dehydrogenase
H&E	Hematoxylin and eosin
HFS	High frequent stimulation
hFTAA	Heptameric formyl thiophene acetic acid
i.c.	Intracranial
ICP	Intracranial pressure
i.p.	Intraperitoneal
i.v.	Intravenous
LCOs	Luminescent conjugated oligothiophenes
LCPs	Luminescent conjugated polymers
LOAD	Late-onset Alzheimer's disease
LTP	Long term potentiation
MCH	Mean corpuscular hemoglobin
MCHC	Mean corpuscular hemoglobin concentration
MCV	Mean corpuscular volume
MCI	Mild cognitive impairment
MNPs	Magnetic nanoparticles
MRI	Magnetic resonance imaging
n	Number of subjects per group

NFTs	Neurofibrillary tangles
NPs	Nanoparticles
NTNU	Norwegian University of Science and Technology
PBS	Phosphate buffered saline
PCR	Polymerase chain reaction
PEG	Polyethylene glycol
PET	Positron emission tomography
PFA	Paraformaldehyd
pFTAA	Pentameric formyl thiophene acetic acid
PiB	Pittsburgh compound B
PPF	Paired pulse facilitation
PrP	Prion protein
PSEN	Presenilin
p-tau	Phosphorylated tau
RFU	Relative fluorescence unit
rpm	Revolutions per minute
RT	Room temperature
SAD	Sporadic Alzheimer's disease
SDS	Sodium dodecyl sulfate
SDS-PAGE	SDS-polyacrylamid gel electrophoresis
SMA β BA's	Small molecule A β -binding agents
TAE	Tris-acetate-EDTA
TBS	Tris buffered saline
TBS-T	Tris buffered saline containing 1 % triton X-100
TEG	Triethylene glycol
TEM	Transmission electron microscopy
ThS	Thioflavin S
ThT	Thioflavin T
Tris	Tris(hydroxymethyl)-aminomethan
t-tau	Total tau
WB	Western Blotting
WT	Wildtype mice
wpi	Weeks post initial injection

1. Introduction

1.1 Dementia and neurodegenerative diseases

Dementia represents a syndrome of impaired cognition and behavior caused by brain dysfunction, severe enough to interfere with daily life¹. Symptoms of dementia vary greatly and include impairment of the ability to acquire and remember new information as well as restricted visuospatial abilities and language functions. Demented patients show limitations in reasoning and handling of complex tasks, reveal changes in personality and behavior including apathy, loss of drive and empathy or social withdrawal². Advanced age is the greatest risk factor for dementia (Tab. 1) whereas female elderlies reveal a higher prevalence of dementia than males³.

Table 1: The international prevalence rate of dementia is plotted against increasing age groups

Source: Alzheimer's Disease International (2009). *World Alzheimer Report*.

Prevalence of dementia	
Age group	International prevalence rate
60 - 64	1.3 %
65 - 69	2.2 %
70 - 74	3.8 %
75 - 79	6.5 %
80 - 84	11.6 %
85 - 89	20.1 %
90 +	41.5 %

The term neurodegeneration defines a progressive loss of structure and function of neurons, causing ultimately neuronal death⁴. Abnormal aggregation of misfolded proteins characterizes the majority of neurodegenerative disorders. Dementias associated with protein misfolding (so called proteopathies) include Alzheimer's disease (AD), dementia with Lewy bodies (DLB), frontotemporal dementia (FTD) or Creutzfeldt-Jakob disease. In contrast, examples for non-proteopathic dementias, which do not exhibit major deposits of misfolded proteins, are vascular dementia, normal pressure hydrocephalus, subdural hematomas, brain tumors or infections for example with the human immunodeficiency virus or herpes simplex viruses.

The most common type of dementia is AD, which accounts for an estimated 54 % of all cases worldwide. DLB, FTD and mixed-dementias (most commonly AD associated changes and

vascular lesions) combined make up 30 % and vascular dementia accounts for 16 % of dementia cases (Fig. 1)⁵.

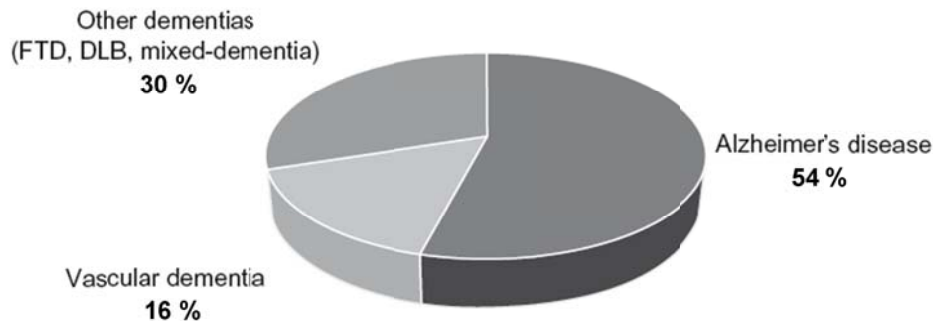


Figure 1: Worldwide subtypes of late onset dementia (≥ 65 years). Late onset dementias are differentiated in three subtypes: i) AD, ii) FTD, DLB, mixed-dementia and iii) vascular dementia, which occur with a distinct prevalence rate. Adapted with permission from Grand et al., *J Multidiscip Healthc*, 2011, 4, 125-47. Copyright © 2011, Dove Medical Press.

The underlying cause of different types of dementia is brain cell damage in regions responsible for memory, judgement and movement. The permanent and progressive changes in the brain accompanying atypical protein deposition in many neurodegenerative disorders are generally irreversible. Characteristic atypical cerebral protein deposits, termed amyloids, contain insoluble protein fibrils that share similar morphological features but comprise many different proteins⁶. Extracellular plaques and intracellular neurofibrillary tangles (NFTs) as histopathological hallmarks of AD brains consist for example of aggregated amyloid- β ($A\beta$) fibrils and hyperphosphorylated tau proteins⁷, whereas α -synuclein accumulates in intraneuronal inclusions known as Lewy bodies and Lewy neurites that characterize Parkinson's disease and DLB⁸. Prion diseases as infectious neurodegenerative disorders are distinguished by the extracellular deposition of β -sheet rich prion protein (PrP) aggregates⁹. Despite significant advances in the understanding of the nature of deposited proteins, detailed knowledge on the initiation of protein misfolding and spread of amyloidogenic proteins causing these proteopathic neurodegenerative diseases is lacking, making the development of novel therapeutic approaches difficult.

1.2 Alzheimer's disease

1.2.1 *Epidemiology and genetics of Alzheimer's disease*

Most cases of AD, the leading cause of dementia, are sporadic (SAD or late-onset AD (LOAD)) with unknown causes and appear at ages above 65 years, while only 1-10 % account for the familial or inherited form of AD (FAD or early-onset AD). The prevalence rates for AD rise exponentially with age and double every five years after the age of 65 years¹⁰. 32 % of people age 85 and older are affected¹¹, showing that advancing age is the greatest risk factor for SAD. The prevalence of AD in Germany is estimated to be as high as 1.2 million cases¹²; worldwide 24 million people are affected and 4.6 million new cases arise every year¹³. Due to the considerable aging of society in first world countries, the frequency of AD is expected to double every 20 years until 2040¹⁴, which implicates a tremendous cost burden on the public health care system in the future.

SAD is influenced by genetic variants combined with life exposure factors. The high-risk allele $\epsilon 4$ of apolipoprotein E represents the strongest common genetic variant for typical LOAD¹⁵. Recently also a single-nucleotide polymorphism in the gene encoding the triggering receptor expressed on myeloid cells 2 (*TREM2*) was associated with AD^{16,17}. Further factors that increase the risk of SAD are cardiovascular diseases, smoking, hypertension, type II diabetes, obesity or traumatic brain injury. In contrast, leisure activity, mediterranean diet and physical activity are known protective factors reducing the risk of AD¹⁸. Inherited cases of AD are caused by rare mutations in one of three genes, which are most often inherited in an autosomal dominant pattern. These genes are i) the amyloid precursor protein (*APP*) on chromosome 21, ii) presenilin 1 (*PSEN1*) on chromosome 14 and iii) presenilin 2 (*PSEN2*) on chromosome 1. Mutations in these three genes lead to an increased production of the A β peptide, triggering its cerebral extracellular aggregation and deposition into A β plaques, an event believed to start the pathogenic cascade in AD¹⁹.

1.2.2 *Clinical symptoms and pathological alterations of Alzheimer's disease*

Humans affected by AD experience initially a mild memory loss and show difficulties in remembering names or recent events. Early symptoms, including problems with memory, apathy and depression, usually develop slowly and get worse over time. Later symptoms include impaired judgment, disorientation, confusion, behavioral changes, and problems with speaking, swallowing, and walking¹¹.

Brains of AD affected individuals show characteristic pathological alterations. A macroscopic feature of the AD brain is the typical symmetric pattern of cortical atrophy resulting in a progressive cerebral shrinkage (Fig. 2). The earliest site of atrophy is typically the entorhinal cortex, followed by the hippocampus and the amygdala – cerebral regions important for memory and emotions. Narrowed cerebral gyri, widened sulci and enlarged ventricles are visible macroscopically as well²⁰ (Fig. 2).

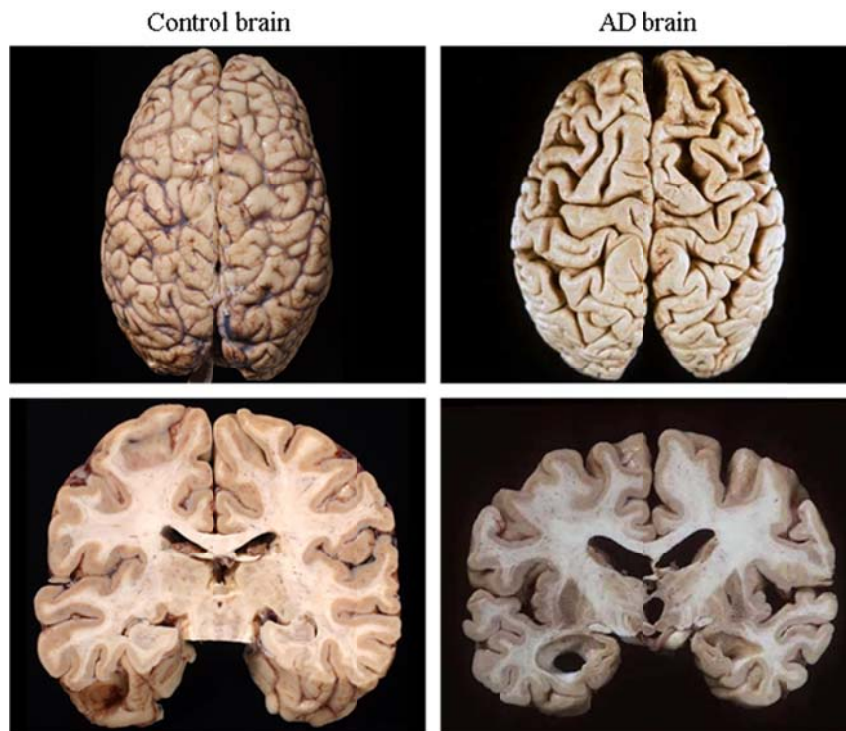


Figure 2: Macroscopic features of a typical AD brain. The topview (upper row) and a cross section (lower row) of a control and an AD brain are depicted. Image courtesy of Stefan Prokop, MD, Department of Neuropathology, Charité – Universitätsmedizin Berlin.

Neuronal and synapse loss are the histopathological correlates of cerebral atrophy in the AD brain resulting from dystrophic neurites in neocortical terminal fields containing hyperphosphorylated tau proteins^{21–23} (Fig. 3d). Other histopathological features of AD brains are parenchymal, extracellular A β plaques (Fig. 3a) and NFTs (Fig. 3c) in medial temporal-lobe structures. Furthermore, astrogliosis and microglial cell activation around A β plaques and NFTs, cerebral amyloid angiopathy (CAA, Fig. 3b) and granulovacuolar degeneration in neurons of the hippocampal formation are commonly encountered pathological changes^{24–27}.

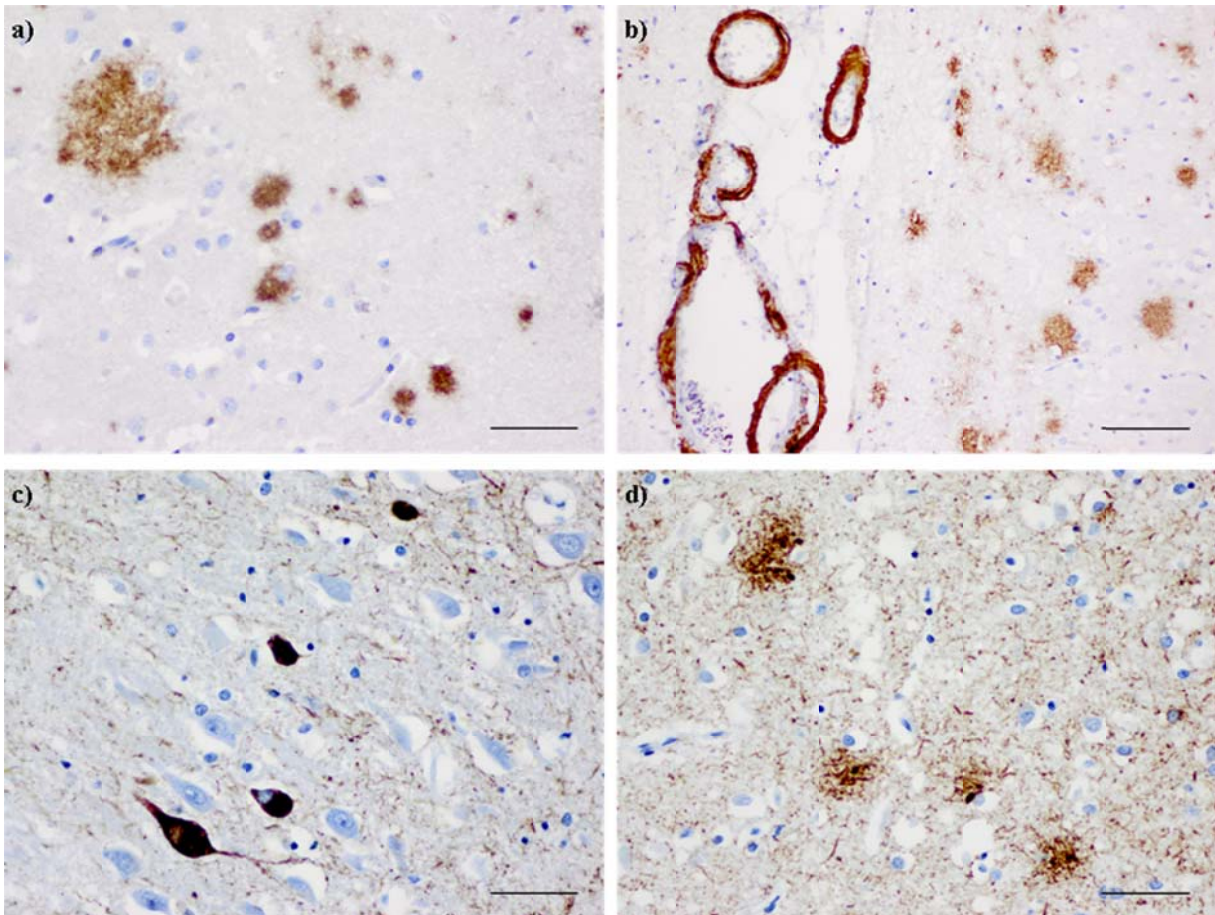


Figure 3: Pathological alterations in a human AD brain. Depicted are characteristic pathological features of a human AD brain: A β plaques (a) and A β deposition in cerebral vessel walls (CAA, b) labeled by antibody 4G8, as well as deposits of hyperphosphorylated tau (labeled by antibody AT8) in NFTs (c) and dystrophic neurites (d), clustering around A β plaques. a), c), d) Scale bar = 50 μ m. b) Scale bar = 100 μ m.

Cerebral A β plaques formed mainly by aggregated A β proteins and NFTs consisting primarily of hyperphosphorylated tau proteins are the two prominent histopathological hallmarks of AD. Based on their morphology and their stainability with common amyloid binding dyes such as Congo red or thioflavin S (ThS), extracellular A β plaques are classified in diffuse deposits and dense-core plaques, with only the latter containing classical amyloid in their core. Diffuse plaques represent amorphous A β deposits with ill-defined contours, which are typically not labeled by Congo red or ThS. Diffuse A β plaques can be found in brains of cognitively intact elderly people as well. In contrast, since their presence is generally associated with cognitive impairment, the identification of amyloid containing dense-core plaques is used for the pathological diagnosis of AD⁷. These plaques consist of a compact amyloid core, which is labeled by Congo red and ThS. Dense-core plaques are typically surrounded by dystrophic neurites and activated microglia and astrocytes. NFTs represent intraneuronal deposits of misfolded and hyperphosphorylated tau proteins. Under normal conditions tau is a microtubule-associated protein facilitating axonal transport by binding and

Introduction

stabilizing microtubules²⁸. Pathological hyperphosphorylation of tau leads to a detachment of tau proteins from microtubules and to a subsequent intracellular mislocation. These events cause the typical intraneuronal aggregate formation and deposition.

According to the amyloid cascade hypothesis¹⁹, accumulation of A β in the brain, caused by an imbalance between A β production and clearance, is the primary force driving AD pathogenesis. Mutations identified in FAD patients promote cerebral A β production by favoring proteolytic processing of APP by β - or γ -secretase and/or increase the likelihood of self-aggregation of A β peptides into amyloid fibrils²⁹. These processes strongly support the amyloid hypothesis as a pathogenetic concept for AD¹⁹.

A β peptides, the main component of cerebral A β plaques mainly consist of 36-43 amino acids and originate from the amyloidogenic processing of APP. Soluble A β is constitutively produced by a variety of cell types and is known to be a normal component of human biological fluids³⁰. APP as the precursor of the A β peptide is naturally processed by three proteases. The generation of A β peptides within the amyloidogenic pathway requires sequential enzymatic cleavage of the membrane-anchored β -secretase BACE1 (beta-site amyloid precursor protein cleaving enzyme 1) and the γ -secretase, a protein complex with PSEN1 or PSEN2 at its catalytic core (Fig. 4a). In contrast, processing by α - and γ -secretase mediates the non-amyloidogenic pathway³¹ (Fig. 4a), which is predominant under normal circumstances. A β peptides spontaneously self-aggregate into several physical forms including soluble oligomers (2-6 peptides), intermediate assemblies or grow into larger fibrils, which form the characteristic A β plaques (Fig. 4b). A β ₄₂ is known to be the most aggregation prone and damaging A β species³² and soluble A β oligomers are believed to be the main toxic species causing synaptic dysfunction, neuronal cell death and cognitive impairment in AD³³⁻³⁵. In human AD brains the concentration of soluble A β species correlates better with synaptic loss and cognitive decline than the number of senile plaques^{36,37}.

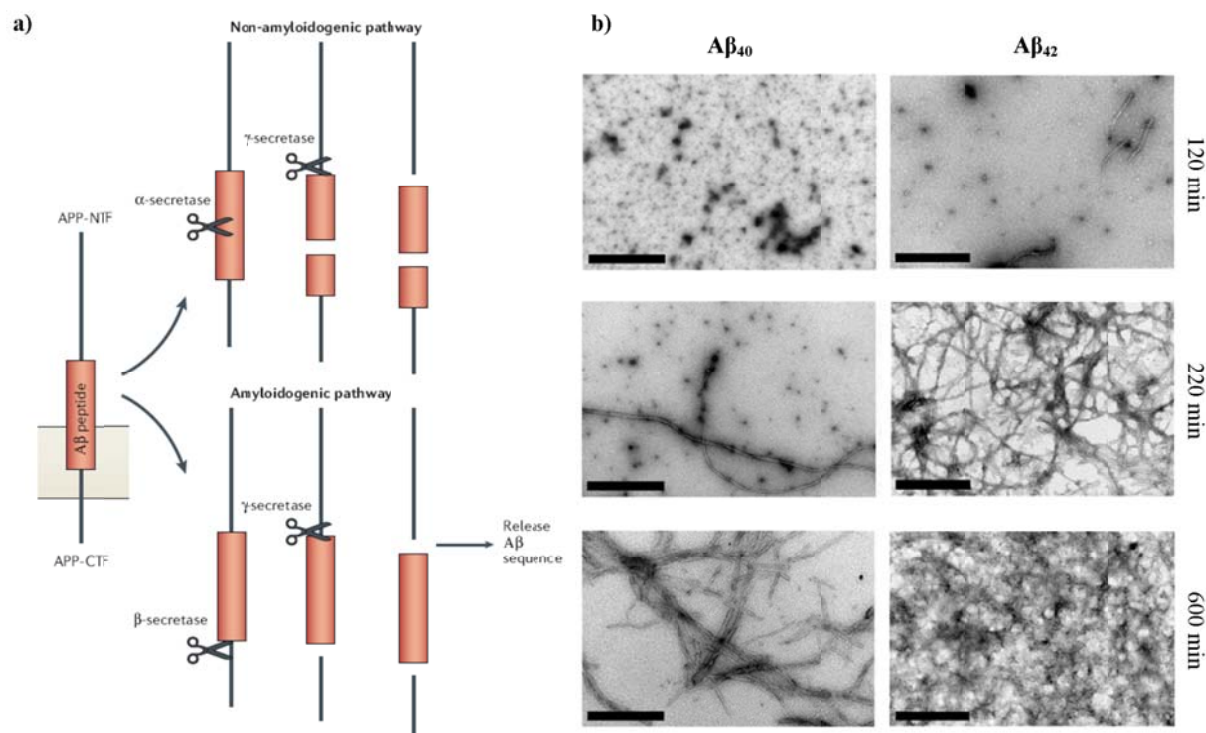


Figure 4: Schematic depiction of APP processing and transmission electron microscopic images of time related A β aggregation *in vitro*. APP can be processed in two different ways: i) by the amyloidogenic and ii) by the non-amyloidogenic pathway, driven by α - and γ -secretase. The two enzymes β - and γ - secretase mediate the amyloidogenic pathway, which results in the release of A β (a). Transmission electron microscopic (TEM) images show the time dependent (120 min, 220 min, 600 min) self-aggregation of A β_{40} and A β_{42} *in vitro* (b). Adapted with permission from Van Dam & De Deyn, *Nat Rev Drug Discov*, 2006, 5, 956-970; Copyright © 2006, Nature Publishing Group (a) and Aslund et al., *ACS Chem Biol*, 2009, 4(8), 673-684; Copyright © 2009, American Chemical Society (b).

1.2.3 Treatment of Alzheimer's disease

Current treatment strategies approved by the food and drug administration aim at slowing the progression of symptoms and improving the quality of life for patients. The drugs are classified into acetylcholinesterase inhibitors and N-methyl-D-aspartate receptor modulators. They temporarily help to improve memory and thinking problems in about half of the patients for a limited amount of time, but these drugs are generally not modifying or stopping the pathogenic cascade of the disease⁴⁰.

Novel treatment strategies for AD, currently in the stage of clinical trials are targeting A β and its aggregation as well as tau, selected kinases or related neuronal proteins. They intend to stop or even reverse the underlying pathological process of protein aggregation and neuronal dysfunction. Therapeutic approaches targeting A β can be differentiated into: i) blocking A β production by β - and γ -secretase inhibition, ii) preventing A β aggregation and iii) promoting A β clearance by active and passive A β immunotherapy⁴¹. Currently numerous clinical trials assessing the efficacy of active and passive A β immunotherapy are ongoing. Besides A β

immunotherapy, approaches targeting the inhibition, reversion and elimination of A β aggregation have been shown to be successful therapeutic strategies reaching clinical trials. Four different strategies can be distinguished⁴²: i) inhibition of amyloid formation by small-molecules, ii) inhibition of A β aggregation by small rationally-designed peptides, iii) use of amyloid-binding proteins and agents, which block the A β protein interaction and iv) clearance of misfolded A β proteins by immunotherapy. Small molecules like the amyloid binding dyes Congo red, methoxy-XO4 and other sulfonated dyes were shown to inhibit A β toxicity and to prevent A β fibrillogenesis *in vitro*^{43–45}. The cationic surfactant hexadecyl-N-methylpiperidinium bromide, a small molecule as well, inhibits the aggregation of A β peptides probably by binding to regions of the peptide necessary for the self-assembly⁴⁶. Interestingly compounds like curcumin and rosmarinic acid have also been reported to exhibit anti-amyloidogenic properties⁴⁷. Most of the small A β binding molecules however, lack specificity, reveal unwanted side effects and their mechanism of action is unknown. Nevertheless, they have good drug-like properties, which enable an oral treatment and blood brain barrier (BBB) crossing⁴⁸ that are most useful for further clinical applications.

1.2.4 Diagnostics of Alzheimer's disease

In the majority of cases the diagnosis of AD can be made with high accuracy in the living patient¹. The clinical workup for the diagnosis of AD in symptomatic individuals includes mental status testing, physical and neurological exams as well as the sampling of cerebrospinal fluid (CSF) for the analysis of specific AD biomarkers⁴⁶. Additionally, distinct imaging techniques play a key role for the clinical diagnosis of AD. Neuropathological analyses by immunohistological A β and tau stainings may be performed *postmortem* to confirm the clinical diagnosis and detect accompanying pathological processes. Ideally a pre-symptomatic diagnostic detection of amyloid pathophysiology in subjects at risk could be established. This would allow to treat patients before the progressive cerebral A β plaque pathology initiates subsequent neuronal loss and irreversible cognitive impairments.

Three preclinical stages of AD (I. asymptomatic amyloidosis, II. amyloidosis and neurodegeneration, III. amyloidosis, neurodegeneration and subtle cognitive decline) and the stage of mild cognitive impairment (MCI) due to AD precede full blown AD dementia. The most prominent cognitive deficits in AD dementia are impaired learning and recall of recent information (amnestic presentation), deficits in word finding and spatial cognition (language and visuospatial presentation) as well as impairments in reasoning, judgment and problem

solving (executive dysfunction). Cognitive deficits are assessed by a number of neuropsychological tests. The Consortium to Establish a Registry for AD (CERAD) for example was established to standardize procedures for the evaluation and diagnosis of AD patients. Standardized instruments of CERAD to assess the various manifestations of AD include clinical- and neuro-psychology, neuropathology, a behaviour rating scale for dementia, family history interviews and the assessment of service needs. The clinical diagnosis of AD requires the exclusion of other neurological diseases including absence of core features of DLB, FTD or progressive aphasia⁴⁹.

A β_{42} , total tau (t-tau) and phosphorylated tau (p-tau) levels in the CSF have been assessed as potential biomarkers for AD. Besides guiding clinical diagnosis, they can provide a useful tool to evaluate disease risk or prognosis, or to monitor therapeutic interventions⁵⁰. A β_{42} levels function as a measure of cerebral A β plaque load. Increased t-tau levels generally reflect neuronal and axonal damage in neurodegenerative diseases. Higher p-tau levels are specifically associated with faster progression from MCI to AD and more rapid cognitive decline. With above 80 % sensitivity and specificity, AD patients can be discriminated from non-demented age matched control subjects by increased t- and p-tau and decreased A β_{42} levels in the CSF. But these CSF biomarkers are not optimal to discriminate AD from other dementias and since they are measured in the CSF and require a lumbar puncture, their applicability is limited.

Biomarker quantification in the peripheral blood has not been proven to be reliable so far. Combined multivariate analysis of several inflammatory and signaling proteins detected in the plasma was shown to be promising, however it needs further investigation to determine its diagnostic value⁵¹. Additionally, there is a number of micro ribonucleic acids under investigation, which were shown to correlate with AD and could be detected in biological fluids like CSF, blood or urine^{52,53}. Recently also a set of ten lipids from peripheral blood reflecting cell membrane integrity were discovered and validated as biomarker for the detection of preclinical Alzheimer's disease⁵⁴.

Besides the use of distinct biomarkers for the clinical diagnosis of AD, there are several functional and structural imaging techniques available. Fluorodeoxyglucose positron emission tomography (FDG-PET) represents a functional imaging technique using the glucose analog FDG, labeled with radioactive fluorine-18, to measure by glucose consumption the general metabolic activity of neurons in the brain tissue^{55,56}. Magnetic resonance imaging (MRI) is used for structural imaging of the symptomatic AD brain and characteristic features like atrophy and shrinkage of the brain are visualized. But as FDG-PET, MRI can not detect

cerebral A β plaques directly. Furthermore atrophy patterns are likely to overlap with other diseases. The development of ligands that are specific for fibrillar A β and suitable for PET, did enable direct visualization of A β plaques in the brain of living AD patients for the first time. The so called “amyloid PET” allows specific imaging of compact A β plaques with radioactive fluorine-18 labeled tracer agents, synthesized based on the structure of “Pittsburgh compound B” (PiB), an carbon-11-labeled radioactive analog of thioflavin T^{57,58} (ThT, Fig. 5). Over the last three decades PET imaging emerged as a robust marker of brain (dys-)function in AD, but not without certain limitations. The technique is relatively expensive, only available to a limited extent, it requires intravenous access and moreover involves an exposure to radioactivity⁵⁹.

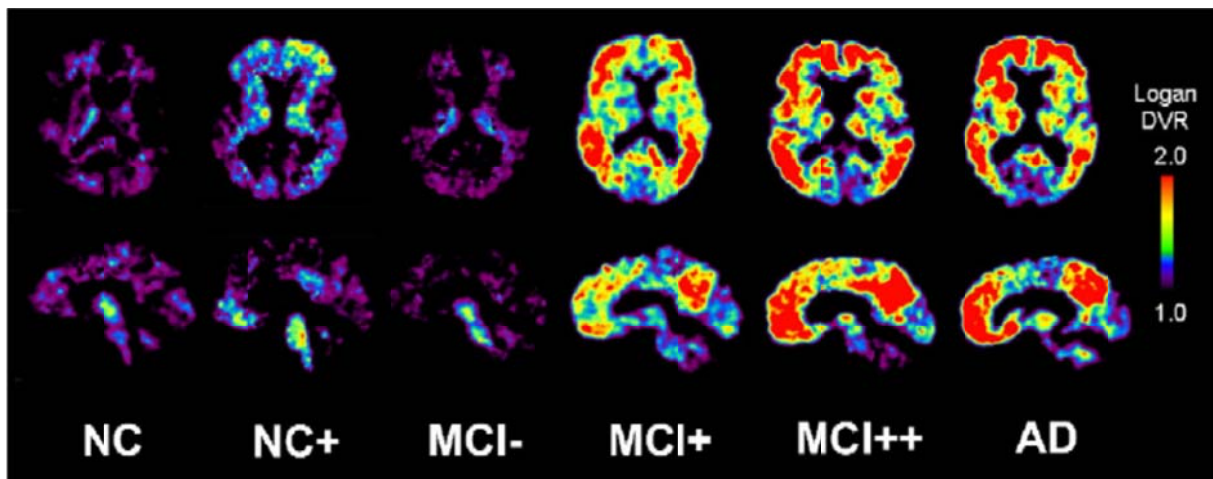


Figure 5: PiB PET imaging of several brains. Control (normal control (NC), [¹¹C]PiB-positive normal control (NC+)), MCI ([¹¹C]PiB-negative MCI subject (MCI-), [¹¹C]PiB-positive MCI subject (MCI+), highly [¹¹C]PiB-positive MCI subject (MCI++)) and [¹¹C]PiB-positive AD subjects reveal different ranges of cerebral A β deposition. Reprinted with permission from Mathis et al., *Nucl Med Biol*, 2007, 34(7), 809-22. Copyright © 2007, Elsevier.

Since distinct strengths and weaknesses of the currently available imaging techniques are largely complementary, the use of “multi-modal” imaging studies, provide the best diagnostic outcome so far. Those techniques are simultaneously or sequentially implemented to the same subject.

Finally, autopsy samples of suspected AD brains can be analyzed *postmortem* for a detailed neuropathological staging of Alzheimer-related changes⁶⁰ including the cerebral distribution of A β plaques and NFTs, investigated by semi-quantitative and stepwise analyses to be correlated with *in vivo* imaging and biomarker data.

The current knowledge on the pathogenesis of AD has been summed up in a model, that proposes the temporal evolution of AD biomarkers in relation to each other and to the onset

and progression of clinical AD symptoms⁶¹ (Fig. 6). Initially, years before the onset of symptoms, the atypical A β deposition may be detected by decreased CSF levels of A β ₄₂ and by using amyloid PET. Subsequently CSF tau amounts increase, probably induced by progressive A β deposition. Robust A β deposition causes neuronal loss and brain shrinkage, which then can be visualized by structural MRI. At this disease stage FDG-PET imaging can be utilized for clinical diagnostic as well. Finally MCI occurs, where worsening of symptoms is dependent on distinct risk profiles. At this time point, when symptoms are already evident, researchers assume, that due to the underlying substantial structural damage a curative treatment of AD might not be possible anymore⁶². Therefore a lot of effort is put into early, ideally pre-symptomatic detection of AD pathophysiology in subjects at risk.

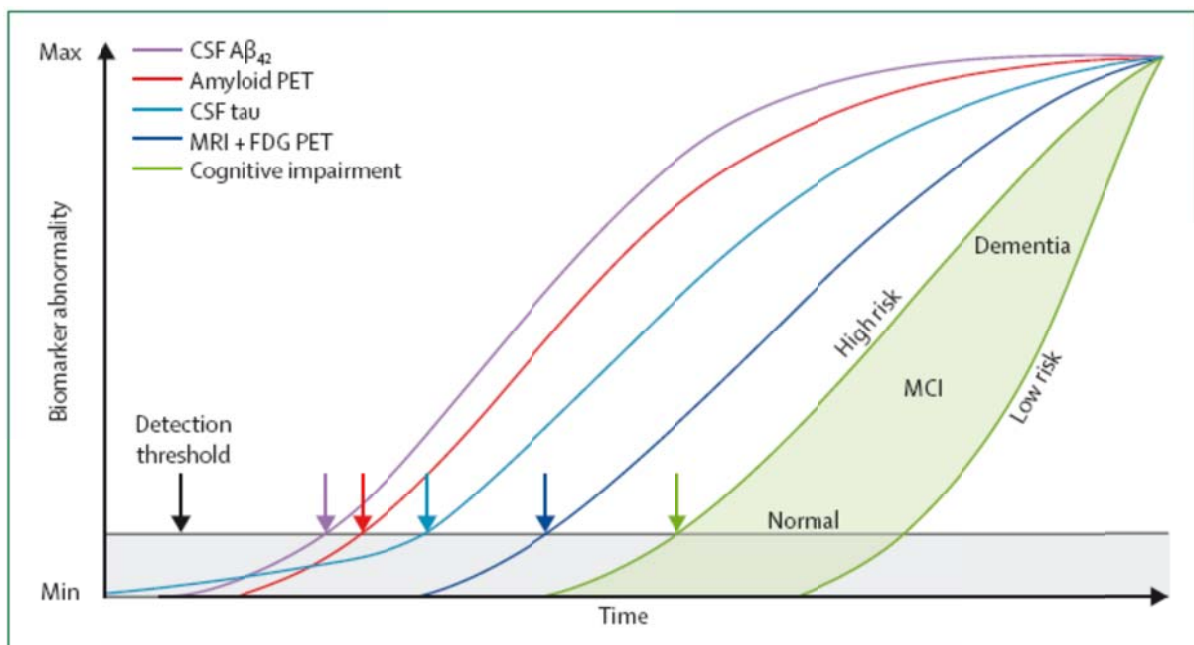


Figure 6: Model integrating AD immunohistology and distinct biomarkers. A time dependent change of biomarker abnormality ranges of CSF A β ₄₂ (purple), amyloid PET (red), CSF tau (light blue), MRI and FDG-PET (dark blue) as well as cognitive impairments (green) is shown. The black horizontal line represents the threshold for biomarker detection of pathophysiological changes. The grey area denotes the zone where these abnormal changes lie below the detection threshold of biomarkers. Reprinted with permission from Jack et al., *Lancet Neurol*, 2013, 12, 207-16. Copyright © 2013, Elsevier.

1.2.5 Alzheimer's disease mouse models

Based on several known mutations in genes associated with FAD, genetically modified animal models mimicking certain disease aspects have been generated and studied. Many transgenic AD mouse models overexpress a mutated form of the human *APP* gene in the brain and develop cerebral amyloidosis similar to that found in human AD brains, with A β accumulation

into extracellular A β plaques occurring in an age-dependent manner. Because the A β_{42} peptide is known to be the most aggregation prone species⁶³, cerebral A β plaque formation is accelerated in models of cerebral amyloidosis and leads to an earlier and more severe cognitive decline, when this peptide is preferentially cleaved from the precursor APP^{64,65} (for example the *APP^{PS1}* mouse model). In contrast, elevated levels of A β_{40} drive the formation of a cerebral A β pathology in the AD mouse models Tg2576 and APP23⁶⁶, leading to distinct properties of the pathological deposits. A β plaques in AD mouse models reveal a similar structure to those found in human brains – initially present diffuse plaques, consisting mainly of A β_{42} , develop to dense A β_{42} cores, surrounded by smaller A β assemblies and non-A β components like α -synuclein or ubiquitin⁶⁷. Tau pathology with NFTs containing hyperphosphorylated tau proteins, which is characteristic for human AD could be reproduced only in single mouse models. The majority of models develops only hyperphosphorylated tau containing dystrophic neurites and do not exhibit NFTs⁶⁸. But many AD mouse models reveal memory impairments and cognitive deficits as well. Although none of the current existing models fully reproduces the complete spectrum of the human disease, critical aspects of AD pathology and disease processes can be experimentally recapitulated⁶⁹. Experimental research in these mouse models has helped to better understand basic mechanisms of disease pathogenesis and has fueled novel treatment strategies, some of which are currently in late stages of clinical trials.

1.3 Luminescent conjugated oligothiophenes as novel amyloid binding agents

Luminescent conjugated oligothiophenes (LCOs) are a novel class of conformation-sensitive optical probes for the selective and specific staining of amyloids. LCOs emit fluorescent light after excitation and behave like structural chameleons – when a LCO molecule binds to amyloid, the structure of the molecular LCO backbone changes and simultaneously the wavelength of emitted light, as a direct indicator of structural properties of the detected amyloid species, alters³⁹. As derivatives of conventional amyloidotropic dyes like Congo red or ThT, which are sterically rigid, LCOs consist of a flexible thiophene backbone whose geometry modulates their emitted fluorescence. Emission spectra of distinct amyloid bound or unbound LCOs can be detected by various techniques (spectral imaging, two-photon imaging, fluorescence resonance energy transfer, PET) and used for identification, structural discrimination and characterization of different amyloid lesions.

Introduction

These molecular amyloid binding agents originate from conjugated polymers (CPs), which are in use as bioimaging tools or biosensors that provide a direct link between spectral signals and different biological processes⁷⁰. Besides to the detection of conformational changes of proteins, CPs are utilized as biosensors for the sensitive detection of genetic material (for example infectious diseases, single nucleotide polymorphisms) based i) on the effective energy transfer of CPs and/or ii) on conformational changes of CPs⁷⁰. Two important classes of CPs are luminescent conjugated polymers (LCPs) and LCOs, both described to be suitable for the detection and monitoring of conformational changes in proteins as well^{39,71}. In contrast to the smaller hydrophobic LCOs based on a pentameric thiophene scaffold (Fig. 7a), LCPs reveal high molecular weights (1500-11000 Da). They were proven useful for discrimination of morphologically distinct fibrillar deposits, but can not be utilized as *in vivo* amyloid imaging agents and do not detect pre-fibrillar amyloid assemblies³⁹. Smaller LCOs reveal molecular weights, which range between 530 and 650 Da and showed under physiological conditions striking specificity for amyloids. Enhanced selectivity and specificity for protein aggregates is associated with an increased exposure of the hydrophobic thiophene rings due to less ionic side chain substitutions than LCPs. Some LCOs even crossed the BBB rather efficiently after a peripheral administration in AD transgenic mice.

In numerous *in vitro* and *in vivo* studies analyzing amyloid, not only in the context of neurodegenerative diseases but also for example in the context of systemic amyloid deposition, LCPs and LCOs were described to be promising diagnostical tools. LCPs were shown to be a useful for the discrimination of several prion strains, causing for example bovine spongiform encephalopathy, sheep scrapie or chronic wasting disease. Besides the differentiation of several prion strains, which were not distinguishable immunohistologically, LCPs were shown to link PrP conformational features with distinct disease phenotypes in respect of clinical progression and infection rate. LCO spectroscopy was additionally shown to be a sensitive and powerful tool for the identification and characterization of distinct amyloid classes of systemic amyloidosis, which are described to be progressive and lethal, and which therapy depends on the identification of the deposited proteins⁷².

Furthermore, LCOs were shown to differentiate between distinct conformational states of A β assemblies during *in vitro* fibrillization, as well as between heterogeneous A β deposits on murine AD brain section by spectral imaging⁷¹. Two types of plaques were identified on tissue sections of transgenic mice. Compact-core plaques composed of rigid dense amyloid cores were visualized and more abundant A β plaques were detected, revealing a compact center with a protruding diffuse exterior. By the simultaneous use of two LCOs (qFTAA and

heptamer formyl thiophene acetic acid (hFTAA)) it was shown via spectral imaging, that conformational rearrangement within murine A β plaques occurs as the transgenic AD mice age⁷³. *APP/PS1* mice at different ages showed significant morphological differences in cerebral A β plaques. The center of individual A β plaques showed a relative increase in qFTAA fluorescence as *APP/PS1* mice aged (19 months), whereas plaques of young mice (six months) were labeled only by hFTAA, indicating structural differences in the detected amyloid species.

The pentameric formyl thiophene acetic acid (pFTAA, Fig. 7), one of the described LCOs, shows the unique property to detect soluble pre-fibrillar non-thioflavinophilic A β assemblies during *in vitro* fibrillization of A β peptides⁷⁴. In contrast, conventional amyloid probes identify only a subset of aggregates that are disease associated.

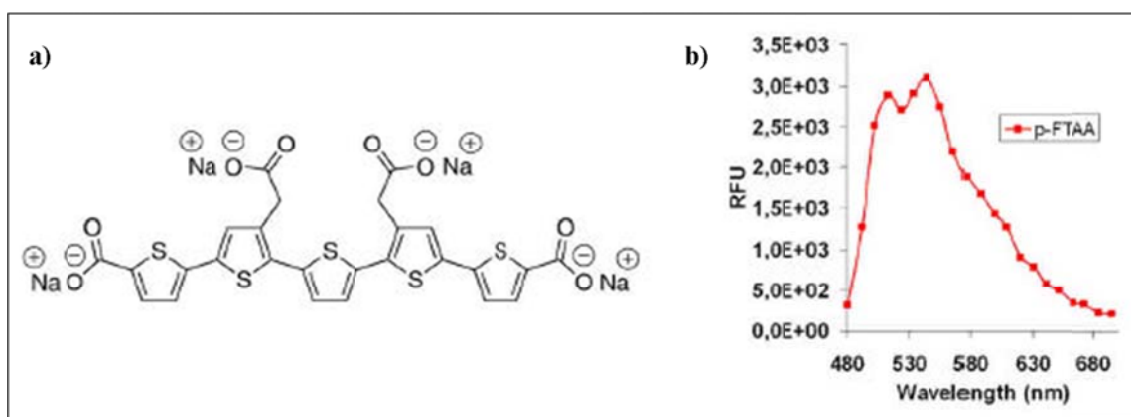


Figure 7: The pentameric LCO pFTAA. The chemical structure of pFTAA (a) and the emission curve highlighting the two distinct emission peaks at 520 nm and 545 nm of amyloid bound pFTAA (b) are depicted. RFU – relative fluorescence units. Adapted with permission from Aslund et al., *ACS Chem Biol*, 2009, 4(8), 673-684; Copyright © 2009, American Chemical Society.

On human brain tissue samples, A β deposits and NFTs were further differentiated by conformation-dependent emitted spectra of bound pFTAA (Fig. 8), and moreover pFTAA revealed complete co-localization with conventionally used antibodies for A β and p-tau staining. Also it has been demonstrated, that pFTAA is able to cross the BBB after injection into the tail vein of *APP/PS1* mice, which enabled *in vivo* monitoring of A β deposits using 2-Photon microscopy. 2-Photon microscopy could also be used to spectrally discriminate murine cerebral amyloid lesions after peripheral application of the heptameric derivative of pFTAA, the so called hFTAA. Similar to pFTAA, hFTAA crosses the murine BBB after systemic administration and specifically binds A β deposits in the brain parenchyma (A β plaques) and in the vasculature (CAA) as well as lesions of hyperphosphorylated tau protein (NFTs), described as characteristic pathological features of human AD⁷⁵.

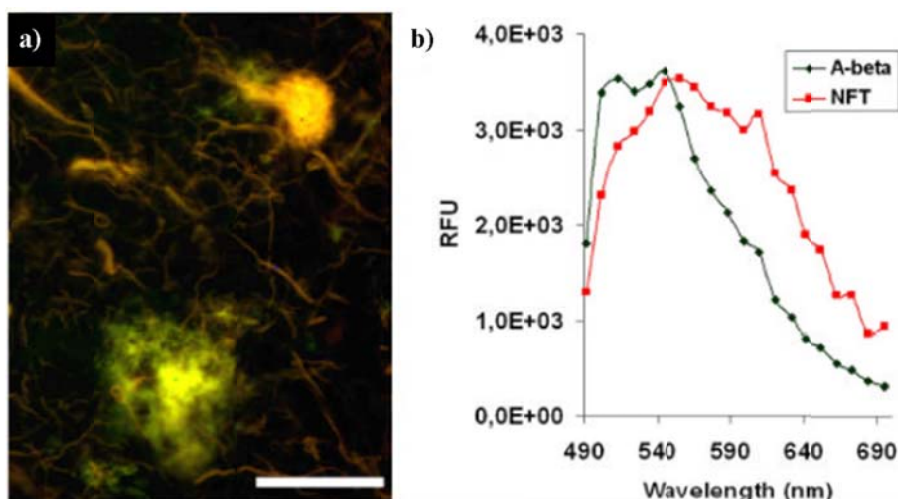


Figure 8: Using pFTAA for discrimination of A β plaques and NFTs in human AD brain tissue samples. The molecular amyloid marker pFTAA was shown to differentiate visually by a high resolution fluorescent image (a) and spectrally by measured emission spectra after binding of pFTAA (b), between A β plaques (green), NFTs and dystrophic neurites (yellow red). RFU – relative fluorescence units. Adapted with permission from Aslund et al., *ACS Chem Biol*, 2009, 4(8), 673-684; Copyright © 2009, American Chemical Society.

1.4 Aims and hypotheses of the thesis

LCOs represent a novel type of molecular imaging probe for detection and discrimination of amyloid deposits *in vitro* and *in vivo* and can therefore be supportive in early diagnosis of neurodegenerative diseases and in monitoring effects of therapeutic interventions in the context of systemic and cerebral amyloidosis such as AD³⁹. Since these conformation sensitive optical probes selectively label and remain bound to disease associated protein aggregates like A β deposits in AD transgenic mice, also a potential therapeutic effect of LCOs is conceivable. The present thesis focuses on the application of LCOs in the *APP/PS1* AD mouse model and investigates novel diagnostic and therapeutic implications of these molecular amyloid markers *in vivo*.

1.4.1 LCOs as *in vivo* imaging tracer for detecting cerebral A β deposits in Alzheimer's disease

Since the population worldwide continues to age, global prevalence rates of AD, the most common neurodegenerative disease in elderlies, are predicted to further rise. Diagnostically, neuroimaging of the pathological A β deposits in the brains of patients - the characteristic hallmarks of AD - reached a central position⁵⁹, however an optimized imaging technique for an efficient widespread usability is not available so far. To initiate an efficient treatment of

AD before progressive A β plaque pathology causes irreversible neuronal loss, a reliable method for pre-symptomatic detection of amyloid pathophysiology in subjects at risk is a prerequisite. But also for monitoring therapeutic effects of potential AD pharmacophores, appropriate imaging techniques as well as sensitive amyloid ligands are of high importance. The novel molecular amyloid binding agents LCOs were shown to label different A β assemblies with sensitivity and high specificity *in vitro*, on tissue sections and also *in vivo*. Interestingly LCOs readily crossed the BBB, which is known to limit the brain penetration of the majority of substances⁷⁶, after peripheral application with high efficacy and labeled characteristic cerebral amyloid lesions in AD transgenic mice³⁹. Here, the question arises if LCOs might also be utilized for *in vivo* diagnostic approaches in humans. Due to the flexible conformation and distinct optional side chain functionalities of the LCO backbone it is conceivable to couple these molecular amyloid markers to magnetic nanoparticles (MNPs) and thus enable amyloid imaging in humans using the non-invasive imaging technique MRI. Combined particles, consisting of an LCO and a MNP component (LCO-MNPs) would have the advantage to specifically bind cerebral A β plaques, which could be directly visualized by MRI. Therefore it was aimed to investigate within the present thesis, if LCO-MNPs show the same binding properties as uncoupled LCOs and still cross the BBB after peripheral administration in AD transgenic mice. Different facts argue that LCO-MNPs might pass the BBB after systemic administration. Several uncoupled, peripheral applied LCOs like pFTAA and hFTAA have been shown to cross the BBB readily and label cerebral A β plaques selectively and efficiently^{39,75}. Also, distinct nanoparticles (NPs) and MNPs were described to cross the BBB after a systemic administration. In cancer research NPs target brain tumors in context of MR imaging in transgenic mice⁷⁷, but also for drug delivery across the BBB, NPs are under investigation (Lockman et al., 2002). Due to these facts it is hypothesized in the present thesis that LCO-MNPs show the same binding properties as uncoupled LCOs and might pass the BBB following an intravenous (i.v.) injection in *APP/PS1* mice. LCO-MNPs could function as novel *in vivo* imaging tracer for the detection of cerebral A β deposits potentially also for human diagnostic AD approaches.

1.4.2 Effect of LCOs on Alzheimer's disease pathology in vivo

Most but not all neurodegenerative diseases are proteinopathies and are associated with the pathological deposition of distinct aggregated proteins in the brain. Characteristic extracellular fibrillar plaques, deposited in brains of AD patients, consist of aggregated A β

Introduction

peptides and are in accordance with the amyloid cascade hypothesis¹⁹ thought to be the driving force in AD pathology. Many therapeutic approaches of AD focus on inhibition of A β fibrillization and aggregation. Among other substances like small molecules or proteins as amyloid-binding agents⁴⁸, amyloid specific dyes like Congo red or methoxy-XO4 revealed anti-amyloidogenic properties directed against A β fibrillization and aggregation^{43,44,79}. Furthermore, LCPs, precursors of the conformation sensitive molecular amyloid dyes LCOs, were previously shown to reduce prion infectivity by binding and compacting PrP fibers *in vitro*. These PrP fibers are described to form characteristic pathological deposits in the brains of prion infected patients⁸⁰. As known for the PrP, which propagates through elongation and breakage of PrP aggregates, cerebral amyloid lesions in AD seems to spread partially autonomous, whereby new amyloid seeds may arise, possibly driving further A β aggregation and the progression of AD pathology^{9,81}. Since LCPs revealed preventive and therapeutic properties in prion diseases, and LCOs were discussed to possibly influence A β oligomer toxicity⁷⁴, a potential effect of LCOs on cerebral AD pathology is conceivable. But, besides a possible beneficial effect of LCOs on A β pathology in AD, the binding of pFTAA to A β fibrils could also cause a fibril breakage which would increase further seeding of broken A β fibrils and possibly enhance the progression of AD pathology.

It is hypothesized that a peripheral pFTAA treatment in the transgenic AD mouse model *APP^{PS1}* affects cerebral A β pathology in an either beneficial or detrimental manner. On the one hand an influence of peripheral applied pFTAA, which was shown to cross the BBB readily, on cerebral A β plaque pathology in *APP^{PS1}* mice *in vivo* was analyzed and on the other hand the impact of pFTAA on toxicity of pre-fibrillar A β species was investigated on a functional level *in vitro*. Besides the potential therapeutic usability, for a future diagnostic use, side effects of long-term administration of pFTAA in *APP^{PS1}* mice were determined simultaneously.

2. Material and Methods

2.1 LCOs, LCO derivatives and LCO-MNPs

LCOs (pFTAA, hFTAA) and LCO derivatives (4004, 4010, 4011, 4020, 4021) were kindly provided by the research group of K. Peter R. Nilsson, PhD (“Luminescent Conjugated oligothiophenes – Illuminating the Dark Matters of Biology and Pathology”), IFM-Department of Chemistry, Linköping University, Sweden. pFTAA and hFTAA have been synthesized as described previously^{39,70}. LCO-MNPs coupled to gadolinium fluoride (GdF₃; 4012, 4013, 5010, 5011, 5012) were kindly provided and synthesized in a collaboration with the Linköping University and the research group of Prof. Dr. Stéphane Parola (“Functional Materials and Photonics”) of the Laboratoire de Chimie ENS Lyon at the Ecole Normale Supérieure, Université Claude Bernard Lyon 1, France. Genovis AB, Sweden kindly provided the iron oxide (FeO) coupled LCO-MNP 4026 and the non-coupled control MNPs. In table 2 and 3 LCOs, LCO derivatives and LCO-MNPs are listed, which were used for stainings of tissue sections and *in vivo* labeling experiments described in this thesis.

Material and Methods

Table 2: Overview of LCOs and LCO derivatives

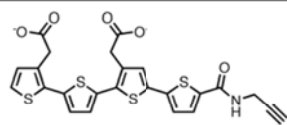
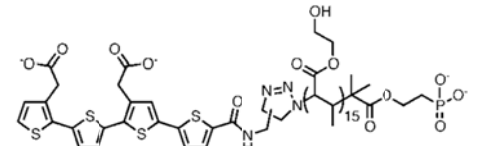
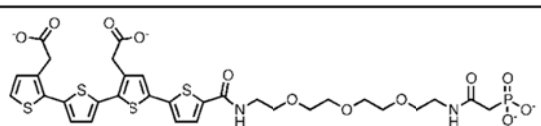
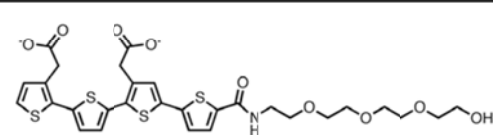
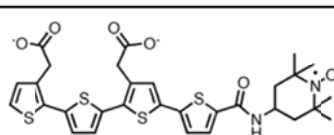
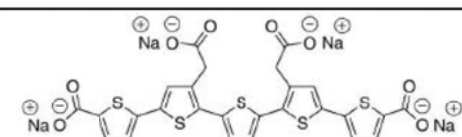
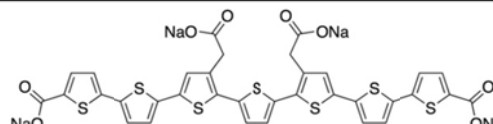
Nomenclature	Chemical structure	LCO concentration
4004 qFTAA-propargyl		1.53 mM
4010 phosphonate-Cyr15-qFTAA		0.52 mM
4011 phosphonate-TEG-qFTAA		1.36 mM
4020 OH-TEG-qFTAA		8.5 mM
4021 qFTAA-TEMPO		powder, dissolved in 1 ml ddH ₂ O
5001 pFTAA		variable (0.2 μM - 14 mM)
7001 hFTAA		1.15 mM

Table 3: Overview of LCO-MNPs

Nomenclature	Chemical structure	LCO concentration
4012 GdF3-PEG-NP-Cyr15-qFTAA		43 μ M
4013 GdF3-PEG-NP-TEG-qFTAA		150 μ M
4026 qFTAM-TEG-Succ-NHS amino PEG		1-190 μ M (not analyzed)
PEG coated iron oxide nanostructures		not analyzed
5010 GdF3-PEG-spcr26-2%-pFTAA		28.69 μ M
5011 GdF3-PEG-spcr26-10%-pFTAA		56.76 μ M
5012		4 mM

2.2 *In vivo* manipulations in mouse models

2.2.1 Alzheimer's disease mouse model *APP/PS1*

For all described approaches transgenic, heterozygous *APP/PS1* +/- mice (termed *APP/PS1* throughout this thesis) and age matched *APP/PS1* -/- littermate controls (termed wildtype (WT) throughout this thesis) were used. These mice were generated by co-injection of Thy1-APPKM670/671NL and Thy1-PS1L166P constructs into male pronuclei of C57BL/6J oocytes⁶⁴ and kindly provided by Prof. M. Jucker, PhD, Hertie-Institut für klinische Hirnforschung, Tübingen, Germany. In *APP/PS1* transgenic mice cerebral β -amyloidosis in the frontal cortex appears at two months of age by the onset of mostly small and compact amyloid

deposits. In the hippocampus, amyloidosis starts later at three to four months of age⁶⁴ (Fig. 9). Relating to cognitive functions and reversal learning, *APP/PS1* mice show impairment in a reversal task at eight month of age, whereas at earlier time points, no deficit is apparent⁶⁴. Equal amounts of female and male mice were analyzed. Mice were group housed under specific pathogen-free conditions on a 12 h light/dark cycle, and food and water were provided to the mice *ad libidum*. All animal experiments were approved by the regional offices for health and social services in Berlin (LAGeSo reference number G 0231/11).

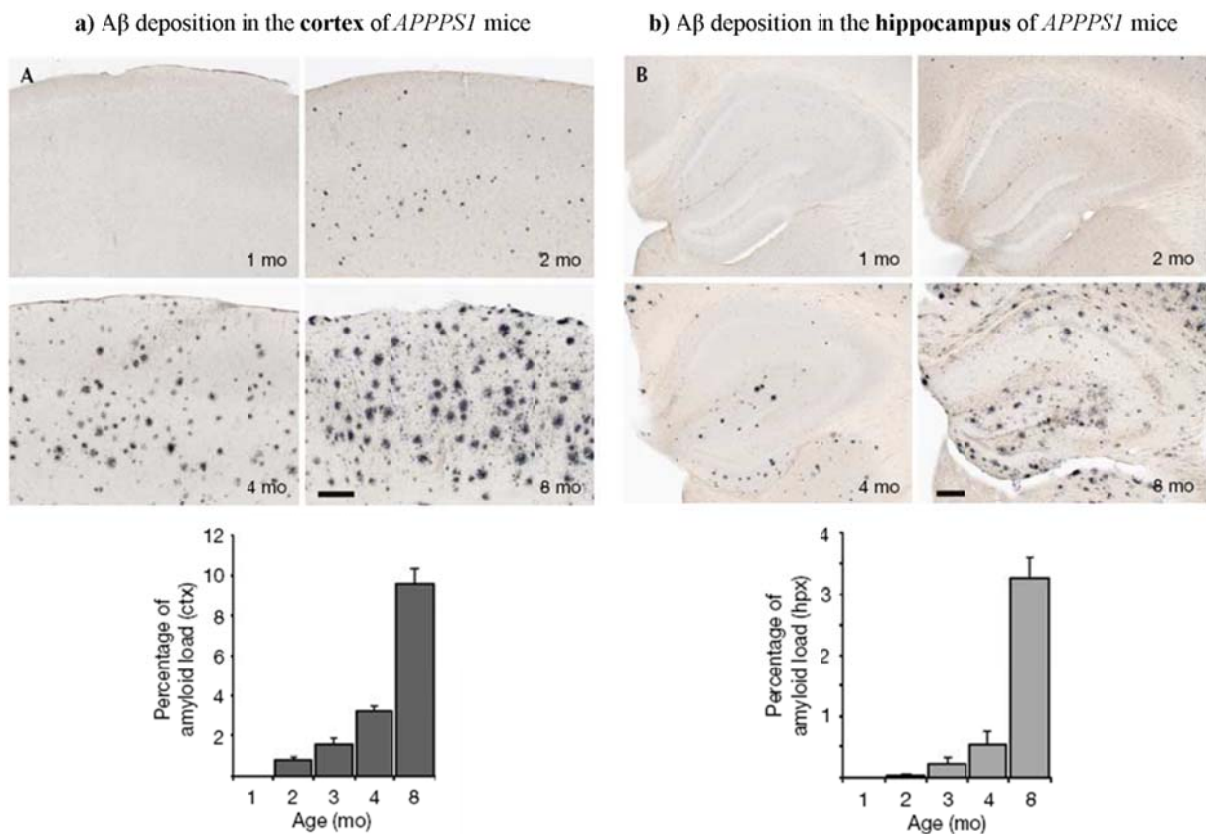


Figure 9: Age-related Aβ deposition in the brain of *APP/PS1* mice. Cortical (a) and hippocampal (b) Aβ deposition in *APP/PS1* mice is shown in an age dependent manner by an immunohistochemical Aβ staining (upper row). A quantitative analysis of the cortical (ctx) and hippocampal (hpx) Aβ load is depicted below. Adapted with permission from Radde et al., *EMBO Rep*, 2006, 7(9), 940-6. Copyright © 2006, John Wiley and Sons.

2.2.2 Genotyping of *APP/PS1* mice

Polymerase chain reaction (PCR) was used to determine the genotype of transgenic *APP/PS1* mice. Animals were ear-clipped at three weeks of age and biopsies served as templates for deoxyribonucleic acid (DNA) preparation.

Material and Methods

Lysis of biopsies

1x lysis buffer: 10 mM Tris(hydroxymethyl)-aminomethan (Tris) hydrochlorid (Merck; pH = 9 (adjusted with NaOH)), 50 mM potassium chloride, 0.5 % Nonidet P-40, 0.5 % Tween20

Proteinase K stock: 15.6 mg/ml in 10 mM Tris (pH = 7.5 (adjusted with HCl/NaOH); Roche)

Ear biopsies were incubated in 150 µl tail lysis buffer (1x) containing 0.1 mg/ml proteinase K overnight at 55 °C on a shaker. Next morning samples were incubated at 95 °C for 10 min to inactivate the proteinase K and subsequently centrifuged at 1,400 revolutions per minute (rpm) for 10 min. The supernatant was used for the PCR reaction.

PCR approach

Genotyping of transgenic mice was performed using primer pairs targeting a specific sequence of the *APP* transgene. The template DNA for the PCR approach was used undiluted from the lysis samples. The corresponding PCR reaction is listed in table 4 and was performed using a PCR cycler (Eppendorf) with PCR conditions depicted in table 5.

Table 4: PCR reaction

	[end] in 20 µl/tube	µl per sample
Template DNA		2
RED master mix (Invitek)		10
APP 5' – GAATCCGACATGACTCAGG [10 µM]	0.375 µM	0.75
APP 3' – GTTCTGCTGCTGCATCTTGACA [10 µM]	0.375 µM	0.75
Double-distilled water (ddH ₂ O)		6.5
Total		20

Table 5: PCR profile

	Temperatur	Time	Cycle
Initial denaturation	94 °C	2 min	1x
Denaturation	94 °C	30 s	35x
Annealing	58 °C	30 s	
Elongation	72 °C	30 s	
Final elongation	72 °C	5 min	1x
Storage	8 °C	unlimited	1x

Agarose gel electrophoresis

1x Tris-acetate-EDTA (TAE) buffer: 50x TAE buffer (Ultra Pur, DNA Typing Grade, Invitrogen) diluted in ddH₂O

2 % agarose gel: 2 % agarose (SeaKem® LE Agarose, Lonza) in 1x TAE buffer

10 µl of the PCR products were loaded onto 2 % agarose gels and PCR fragments were separated at 120 V. 1x TAE buffer was used as running buffer. Agarose gels containing the intercalant agent ethidium bromide (10 mg/ml, Roth) allow visualization of DNA bands via UV light. To document band profiles the G:Box system (Synoptics) was used. The band of the *APP* transgene is visible at 250 bp (Fig. 10).

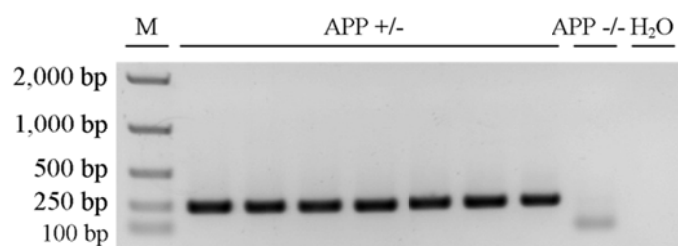


Figure 10: Detection of the *APP* gene by genotyping. Experimental mice were genotyped as heterozygous positive (*APP +/-*) or homozygous negative (*APP -/-*) for the *APP* gene before they were included in the *APPPS1* or WT groups of distinct experimental approaches. As marker (M) for the gel electrophoresis EasyLadder I (Bioline) was used. H₂O was used as negative control.

2.2.3 Intravenous and intraperitoneal applications in *APPPS1* mice

For the purpose of i.v. injections mice were anesthetized with isoflurane and placed on a heating surface. Before 100 µl of distinct solutions were i.v. injected to experimental animals, the tail was placed in warm water (30-35 °C). For the subsequent i.v. injection a 23 G cannula was used. Injected mice were monitored until recovery from anesthesia.

For the intraperitoneal (i.p.) injection mice were placed on the grid of the cage and the skin fold from the scruff of neck down the back was immediately gripped using the thumb and forefinger of the non-dominant hand. Before i.p. injection with a 30 G cannula, mice were tilted with the head slightly toward the ground to allow the abdominal viscera to shift cranially and minimize accidental puncture of abdominal organs at the injection site. Injected mice and the abdominal injection site were monitored three hours post injection and on the next day for possible side effects.

2.2.4 Blood sampling from *APPPS1* mice

For blood sampling from alive animals during an experiment about 300 µl blood were collected with the facial vein technique using a lancet⁸². The mouse was held by the skin between the shoulder blades in the air and the submandibular vein was punctured under tension by a quick insertion of a 5.0 mm lancet (Goldenrod, Animal Lancet, Fig. 11). The optimal puncture point was described to be at the back of the jaw, slightly behind the hinge of

the jawbones, toward the ear⁸². These lancets have the advantage to control the depth of the puncture. Furthermore the bleeding can be stopped as soon as the mouse is released.

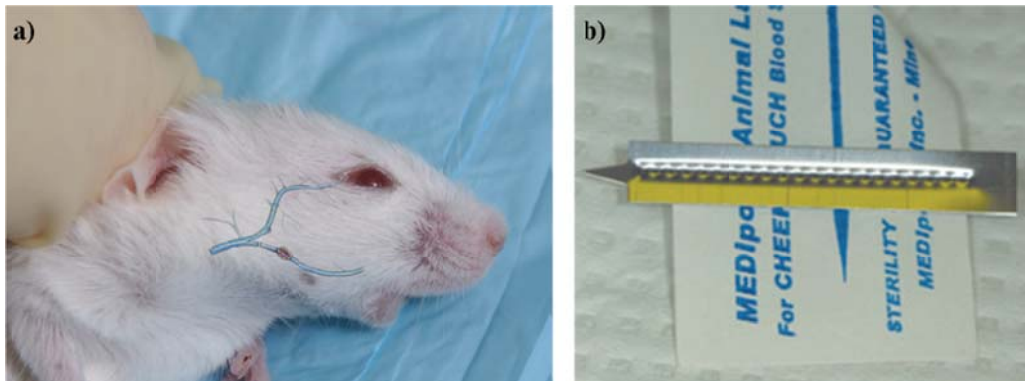


Figure 11: Blood sampling in alive mice using the facial vein technique. The optimal puncture point for submandibular vein puncture at the jaw of the experimental mouse is depicted (a). The submandibular vein is punctured using a 5.0 mm lancet (b). Adapted with permission from Golde et al., *Lab animal*, 2005, 34(9), 39-43. Copyright © 2005, Nature Publishing Group.

For the blood collection before euthanasia, mice were anesthetized using the following mixture of anesthetics: 0.24 ml 2 % Rompun (Bayer), 0.68 ml 10 % Ketamin (Actavis), 3.24 ml 0.9 % NaCl (B. Braun). 100 µl of the euthanasia mixture were i.p. injected per 10 g bodyweight of experimental mice. Reflexes of the narcotized mice were tested before the maximal volume of blood was sampled retro-orbital. Retro-orbital blood sampling was performed by puncturing the orbital sinus behind the eye of the experimental mouse using a glass pasteur pipette (Brand).

Blood collection tubes containing EDTA as anticoagulant were kept for 30 min at room temperature (RT), before samples were centrifuged for 5 min at 2,500 rpm. After centrifugation, the supernatant also termed EDTA-plasma was aliquoted and either analyzed by synlab, Berlin for differential blood counts and several hepatorenal parameters or stored at -80°C for subsequent biochemical A β measurements.

2.2.5 Euthanasia and organ sampling

30 % sucrose: 30 g sucrose (Roth) dissolved in 100 ml ddH₂O

Animals were euthanized with CO₂ and perfused transcardially with ice cold 1x phosphate buffered saline (PBS, pH = 7.4). The brain and several peripheral organs (peritoneal lymph nodes, heart, lung, kidney, liver, spleen) were sampled. One hemisphere and one part of each sampled organ were gently snap frozen by immersion in a 2-methylbutane (Merck) bath surrounded by liquid nitrogen and subsequently stored at -80°C until further use. The second

hemisphere and a part of each sampled organ were fixed for two hours in 4 % paraformaldehyde (PFA, Herbeta) before transferred to 30 % aqueous sucrose for dehydration. The remaining third part of sampled organs was fixed for one week in 4 % PFA before dehydration in an ascending alcohol series over night (Thermo Scientific, Excelsior™ ES Tissue Processor). Subsequently dehydrated tissue was embedded in liquid paraffin using the Shandon Histocentre 3 Embedding Center (Thermo Scientific, Electron Corporation). After cooling and hardening paraffin embedded tissue blocks were used for further analyses on paraffin sections.

2.3 Histology

2.3.1 Cutting of tissue

Free floating sections

Cryoprotectant: 150 ml ethylene glycol (4.6 M final concentration, Sigma-Aldrich), 125 ml glycerine (2.6 M final concentration, Roth), 250 ml 0.1 M PO₄ buffer
0.1 M PO₄ buffer: diluted from 0.4 M PO₄ buffer in ddH₂O
0.4 M PO₄ buffer: 76 mM disodium hydrogen phosphate (Merck), 316 mM monobasic sodium phosphate (Sigma-Aldrich) in ddH₂O

Tissue, which was dehydrated in 30 % sucrose, was subsequently embedded in tissue tec (Richard-Allan Scientific™ Neg-50™ Frozen Section medium, Thermo Scientific) and frozen down to -24 °C placed on a metal plate. Frozen tissue was cut via a cryostat (HM560, Microm) into 30 µm thick sections. Sections were stored at 4°C in 24-well plates until further processing, floating in cryoprotactant.

Frozen sections

Before frozen sections were cut using the cryostat, frozen tissue was transferred over night from -80 °C to -20 °C. 7 µm thick fresh frozen sections were mounted directly on glass cover slips (SuperFrost®, R. Langenbrinck) and stored at -20 °C until further use.

Paraffin sections

For generation of human paraffin sections, brain autopsies were performed following written consent for pathological examination according to the law of Berlin. Following routine diagnostic neuropathological examination parts of the frontal cortex were obtained and used for sectioning and conventional as well as immunohistochemical stainings. This procedure was approved by the Charité ethics commission (EA1/320/13).

PFA fixed and in paraffin embedded human and murine tissue was cut via a microtome (Microm) into 5 µm thick sections, which were mounted directly on glass cover slips. After drying overnight at 37 °C and fixation of sections at 55 °C for 30 min in an incubator, sections were stored at RT until further processing.

2.3.2 Staining of tissue

2.3.2.1 Hematoxylin and eosin staining

Matured hematoxylin: 3.3 mM hematoxylin (Merck); 1 mM sodium iodate (Merck, Germany); 0.12 M aluminium potassium sulfate dodecahydrate in ddH₂O
Addition of 0.3 M chloral hydrate and 4.8 mM citric acid monohydrate
Eosin: Eosin-Y (Brunschwig Chemie) 1:2 diluted in 70 % ethanol
Addition of 2-3 drops absolut acetic acid

Serial paraffin sections were cut from a paraffin block at 5 µm on a microtome and stained subsequently with hematoxylin and eosin (H&E). The hematoxylin staining colors nuclei of cells blue and is followed by a counterstaining with an alcoholic eosin solution, which stains eosinophilic structures (cytoplasm, keratin und erythrocytes) pink. Mounted paraffin sections were stained for 5 min with matured hematoxylin and differentiated subsequently for 10 min under running tap water. Afterwards sections were stained for 30 s in eosin and rinsed in ddH₂O. For dehydration an ascending alcohol series, including the steps 70 %, 80 %, 96 % and 100 % ethanol, was prepared and passed through. Before covering slides using Roti®-Histokitt II mounting medium (Roth), sections were treated twice with xylene (>98 %, Roth) for 1 min.

2.3.2.2 Amyloid stainings

pFTAA staining

For staining procedures 1 mg/ml (1.4 mM) stock solution of pFTAA (MW = 704.7) was prepared in ddH₂O and stored at -20 °C until needed. Working solutions were kept at 4 °C. Fresh staining solutions were made for each staining by diluting the working solution 1:500 in 1x PBS (Dulbecco's Phosphate Buffered Saline w/o Ca²⁺/Mg²⁺, Biochrom), resulting in a 2.8 µM staining solution. Free floating sections (30 µm), stored at 4 °C in cryoprotectant, were washed three times in 1x PBS and incubated for 30 min in the 2.8 µM pFTAA staining solution. Afterwards sections were rinsed again (3x), mounted on a glass slide and covered using an aqueous mounting agent (Microscopy Aquatex, Merck). pFTAA stained sections were analyzed on the day after.

pFTAA/hFTAA co-staining

For spectral imaging, performed at the Linköping University, Sweden, free floating sections were co-stained with pFTAA and hFTAA (MW = 868.9 MW). For both optical probes 1 mg/ml stock solutions were prepared in ddH₂O. Three serial free floating sections per transgene positive animal were mounted and rinsed (three times in 1x PBS), before being stained simultaneously for 30 min with pFTAA and hFTAA (1:2 (2.8 µM pFTAA staining solution : 2.3 µM hFTAA staining solution)). Sections were rinsed three times again, covered with aqueous mounting agent and analyzed on the day after.

Staining with LCO derivatives and LCO-MNPs

LCO derivatives and LCO-MNPs with known LCO concentrations were diluted in 1x PBS to a final concentration comparable to a pFTAA staining solution of equal concentration. Since fluorescent intensities of pFTAA labeled A β plaques are known, pFTAA was used as reference. If the LCO concentration of specific LCO derivatives or LCO-MNPs was not known, a dilution series (for example LCO derivative 4021 – available in powder form) was prepared and compared to stainings using a distinct pFTAA dilution. Labeled sections were analyzed on the day after using fluorescence microscopy.

Congo red staining

Stock solution I: 0.5 M sodium chlorid in 80 % ethanol – preparation 24 h before use
 Addition of 1 % sodium hydroxide before use
Stock solution II: Filtration of 8.6 mM Congo red in stock solution I
 Addition of 1 % sodium hydroxide before use

For the Congo red staining, free floating sections were rinsed three times with 1x PBS, mounted on a glass slide and differentiated under running tap water after counterstaining with matured hematoxylin (5 min, details see chapter 2.3.2.1). Afterwards sections were incubated for 20 min in stock solution I and subsequently for 45 min in stock solution II before rinsed two times in absolute ethanol, treated for 1 min with xylene and covered using Roti®-Histokitt II mounting medium.

2.3.2.3 Immunohistology

10 mM citrate buffer: 1.9 % citric acid (stock: 0.1 M) and 8.2 % potassium citrate dihydrate (stock: 0.1 M) in ddH₂O (pH = 6 (adjusted with HCl))

Cerebral free floating sections were used for immunohistological labeling of A β deposits, microglia, astrocytes, neurons and p-tau aggregates. Some stainings required a distinct pre-

Material and Methods

treatment of the tissue, which optimized subsequent stainings (details see Tab. 6). Before incubating sections with primary antibodies overnight at 4 °C, they were rinsed 3x in 1x PBS and blocked for 1 h at RT with 10 % normal goat serum (AdB Serotec) in 1x PBS containing 0.3 % triton X-100 (Sigma-Aldrich). To label A β deposits, sections were stained with two mouse anti-human A β antibodies: i) 4G8 - reactive to amino acid residues 17-24 in the mid region of the A β protein (Covance) or ii) 6E10 - reactive to N-terminal amino acid residues 1-16 (Covance). Microglia were stained by using antibody Anti Iba1 (Wako Chemicals) and astrocytes by antibody GFAP (Glial Fibrillary Acidic Protein, Dako). P-tau deposits were stained by the use of antibody AT8 (Thermo scientific) and for the neuronal staining antibody NeuN (Chemicon) was utilized. Primary antibodies were diluted with 5 % normal goat serum in 1x PBS containing 0.3 % triton X-100. After rinsing the sections three times with 1x PBS to wash off excessive primary antibodies, they were incubated with species specific peroxidase coupled (POD goat anti mouse/rabbit) or fluorescent secondary antibodies (Alexa Fluor®, see Tab. 6). Secondary antibodies were diluted with 5 % normal goat serum in 1x PBS containing 0.3 % triton X-100 and sections were incubated for 1 h on a shaker at RT. Incubations with fluorescent secondary antibodies were performed light protected. After rinsing the sections three times with 1x PBS to wash off the secondary antibody, stainings using peroxidase coupled secondary antibodies were developed with liquid DAB (Dako, K3647) and counterstained with matured hematoxylin. For dehydration an ascending alcohol series, including the steps 70 %, 80 %, 96 % and 100 % ethanol, was prepared and passed through. Before covering slides using Roti®-Histokitt II mounting medium, sections were treated twice with 98 % xylene for 1 min. Immunohistological stainings using fluorescent secondary antibodies were mounted after rinsing with 1x PBS (3x) and counterstained with DAPI containing aqueous mounting medium (Fluoroshiled Mounting Medium with DAPI, abcam®). Until further microscopic analyses, sections stained with fluorescent secondary antibodies were stored light protected at 4 °C.

Table 6: Overview of primary and secondary antibodies used for immunohistological stainings

Primary antibodies	Company /article no.	Dilution	Pre-treatment
4G8 (host: mouse)	Covance SIG-39220	1:1,000	None
6E10 (host: mouse)	Covance Sig39320	1:1,000	None
Anti Iba1 (host: rabbit)	Wako Chemicals 019-19741	1:500	10 mM citrate buffer (pH = 6) 30 min, 75 °C
GFAP (host: rabbit)	Dako Z0334	1:5,000	quenching 30 min, 1 % H ₂ O ₂ 30 min, 0.5 % H ₂ O ₂ 15 min, 1 % H ₂ O ₂
NeuN (host: mouse)	Chemicon MAB377	1:2,500	None
AT8 (host: mouse)	Thermo scientific MN1020	1:100	None
Secondary antibodies	Company/article no.	Dilution	
POD anti-mouse	Dianova 115-035-003	1:300	
POD anti-rabbit	Dianova 111-035-003	1:300	
Alexa Fluor® 568 Goat Anti-Mouse IgG (H+L)	abcam ab175473	1:300	
Alexa Fluor® 647 Goat Anti-Mouse IgG (H+L)	Invitrogen A-21235	1:300	

2.4 Quantitative analyses of cerebral free floating sections

2.4.1 Quantification of area covered by a specific staining

Quantitative analyses of distinct parameters on cerebral sections were done using the Stereo Investigator system including an Olympus microscope BX53, the QImaging camera COLOR 12 BIT, a stage controller MAC 6000 system and a Wide-Field Fluorescence Microscope Excitation Light Source (X-Cite® 120Q, Lumen Dynamics). For analyses the Stereo Investigator 64-bit software (MBF Bioscience) was used.

Cortical A β plaque burden (assessed by Congo red, pFTAA, 4G8 and 6E10 stainings) and cortical area covered by dystrophic neurites surrounding A β plaques (AT8 staining) were quantified with the Area Fraction Fractionator method of the Stereo Investigator software. 10-12 sections per staining were viewed on the Olympus BX53 microscope with a computer-controlled motorized stage at low magnification (4x/0.32 N.A. Plan-Apochromat) and the entire cortical region per section was contoured onto a live computer image using Stereo Investigator software. The measurement of plaque covered area was performed at a higher magnification (10x/1.4 N.A. Plan-Apochromat). Area covered by A β or p-tau staining was quantified by setting the counting frame to 100x100 μ m, the scan grid size to 300x500 μ m

and the Cavalieri grid spacing to 20 μm . Percentage of area covered was averaged of 10-12 sections to obtain a final estimate of cortical A β plaque burden for each transgene positive experimental animal. Quantitative analyses were done blinded.

2.4.2 Counting A β plaques

A β plaque count after specific stainings (Congo red, pFTAA, 4G8) was estimated on a set of serial sections ($n = 10-12$) of every 18th systematically sampled, 30 μm thick, coronal free floating section throughout the entire cortex. Plaque number was analyzed using the optical fractionator technique of the Stereo Investigator software. Stained free floating sections were viewed on the Olympus BX53 microscope at a low magnification (4x/0.32 N.A. Plan-Apochromat) and the entire cortical region per section was contoured. The A β plaque count was performed at a higher magnification (10x/1.4 N.A. Plan-Apochromat) by setting the counting frame and the scan grid size to 500x500 μm . The total plaque number per mm^3 cortex was determined subsequently as followed:

$$\text{Plaque number per mm}^3 \text{ cortex} = \frac{\text{Estimated total cortical plaque number}}{\text{Estimated total cortical volume } (\mu\text{m}^3)}$$

The coefficient of error (Gundersen), $m = 1$ was kept < 0.05 for the quantification of cortical A β plaque number per transgene positive experimental animal. Quantification was performed blinded.

2.4.3 A β plaque size distribution analysis

10-12 serial A β immunostained (4G8 staining) sections through the cortex (frontal to occipital) were used to assess the cortical plaque size distribution. Three defined cortical regions per section were recorded using an Olympus BX50 microscope and the Cell D software (Olympus). Individual plaques per image (in total 30-36 images) were classified by using the cellSens Dimension software (Olympus) into the following plaque size classes (adapted from Grathwohl et al., 2009): class 1: 10-500 μm , class 2: 500-1,000 μm , class 3: 1,000-1,500 μm , class 4: 1,500-2,000 μm , class 5: 2,000-2,500 μm , class 6: 2,500-3,000 μm , class 7: 3,000-6,500 μm . Objects smaller than 10 μm were excluded from the analysis. On sections with high staining background false-positive object detection was removed manually.

2.5 Biochemical analyses of cerebral A β burden

2.5.1 Extraction of cerebral A β by homogenization of frozen hemispheres

<i>TBS buffer:</i>	20 mM Tris, 137 mM NaCl (pH = 7.6) Addition of 1 pellet protease inhibitor (Roche) per 10 ml Tris-buffered saline (TBS) buffer
<i>TBS-T buffer:</i>	TBS buffer containing 1 % triton X-100
<i>SDS buffer:</i>	2 % Sodium dodecyl sulfate (SDS) in ddH ₂ O
<i>Formic acid:</i>	70 % formic acid (FA) in ddH ₂ O

Frozen hemispheres of experimental mice were homogenized (150 mg frozen tissue/1,500 μ l homogenization buffer) according to the publication of Kawarabayashi et al.⁸⁴ with slight modifications. Hemispheres were homogenized consecutively in i) TBS buffer containing protease inhibitors, ii) TBS-T buffer, iii) SDS buffer and iv) FA. Homogenization occurred mechanically by consecutive passing the solution through a 2 ml syringe and cannulas with decreasing diameter (G 23, G 27 and G 30). Brain extracts were incubated 30 min on ice (except FA homogenate, which was incubated at RT) and centrifuged at 100,000 g for 1 h at 4 °C. The supernatant was collected, aliquoted, snap frozen in liquid nitrogen and stored at -80°C until further use, the pellet was re-suspended in subsequent buffers. Protein concentrations of each fraction were determined using the Quantipro BCA Protein Assay Kit (Pierce) according to the manufacturer protocol using a TECAN fluorescence plate reader (Tecan).

2.5.2 Biochemical quantification of cerebral A β by an electroluminescence linked immunosorbent assay system

<i>1x Tris Wash Buffer:</i>	10x Tris Wash Buffer (supplied) diluted in ddH ₂ O
<i>1 % Blocker A Solution:</i>	1 % bovine serum albumin in 1x Tris Wash Buffer
<i>Detection Antibody Solution:</i>	2 % 50x SULFO-TAG 6E10 Detection Antibody and 1 % 100x Blocker G in 1 % Blocker A Solution
<i>2x MSD Read Buffer T:</i>	4x MSD Read Buffer T (supplied) diluted in ddH ₂ O

A β ₄₀ and A β ₄₂ concentrations in brain extracts of *APP/PS1* mice were determined with an electroluminescence linked immunosorbent assay system (MSD assay) using the MSD 96-Well MULTI-SPOT[®] Human (6E10) Abeta Triplex Assay (MSD, Meso Scale Discovery). 96-well plates, pre-spotted with A β peptide-specific capture antibodies against A β ₁₋₃₈, A β ₁₋₄₀ and A β ₁₋₄₂ were blocked for 1 h on a shaker (800 rpm) at RT with 1 % Blocker A Solution (150 μ l/well) and afterwards rinsed three times for 3 min with 1x Tris Wash Buffer (200 μ l/well). Subsequently 25 μ l of brain extracts (diluted 1:10 in 1 % Blocker A Solution) were incubated for 2 h on a shaker (800 rpm) at RT in a total volume of 50 μ l/well together with the Detection Antibody Solution on the MSD MULTI-SPOT[®] 96-well 4-spot plate. The plate was washed

three times (for 3 min) with 1x Tris Wash Buffer (200 µl/well). Afterwards 2x MSD Read Buffer T (150 µl/well) was added and the plate was read immediately on the Sector Imager 6000. In the detection process, the electrochemiluminescence of the SULFO-TAG[®] is captured by a CCD camera and quantified using the software MSD DISCOVERY WORKBENCH 2.0. Every sample was tested in duplicate and those with a coefficient of variance > 20 % were excluded from the analysis. Aβ concentrations were read from the standard curves.

To analyze Aβ amounts in the plasma of *APP/PS1* mice, the MSD 96-Well MULTI-SPOT[®] Human/Rodent (4G8) Abeta Triplex Ultra-Sensitive Assay (MSD) was utilized. Aβ detection was conducted according to the manufacturer's instruction, as described in detail above for the MULTI-SPOT[®] Human (6E10) Abeta Triplex Assay. For the Aβ measurement 25 µl of undiluted plasma were incubated together with the 4G8 detection antibody.

2.5.3 Biochemical quantification of cerebral Aβ by SDS-polyacrylamid gel electrophoresis and Western Blotting

<i>Tris buffer:</i>	<i>1M Tris (pH = 8)</i>
<i>Loading dye:</i>	<i>5 % β-Mercaptoethanol (Roth) in 4x LDS Sample Buffer (NuPAGE, novex)</i>
<i>10x Tris-Tricine-SDS running buffer:</i>	<i>1 M Tris, 1 M Tricine (Roth), 1 % SDS (pellets, Roth), (pH = 8.3)</i>
<i>10x Transfer buffer:</i>	<i>250 mM Tris(hydroxymethyl)-aminomethan, 1.92 M glycine (Roth)</i>
<i>Blocking buffer:</i>	<i>0.1% Tween-20 and 5% of skim milk in 1x PBS</i>

Tris/tricine SDS–polyacrylamide gel electrophoresis (SDS-PAGE) was performed to assess Aβ levels in different fractions after brain homogenization⁸⁵. To analyze Aβ amounts in the FA fractions, samples were diluted 2:3 in tris buffer to neutralize the pH. Since the supernatant of the FA fraction is too acidic, the protein concentration could not be estimated. Before electrophoresis appropriate samples (12 µl) of the TBS, TBS-T, SDS (20-30 µg protein, calculated based on sample with lowest protein concentration) and diluted FA fractions were mixed with 4 µl loading dye and subsequently boiled (5 min at 95 °C) to denature proteins. Boiled samples were loaded on a 10-20 % Novex[®] Tricine Gel and proteins were separated in 1x Tris/tricine SDS running buffer at initially 80 V (10 min) and subsequently at 120 V for about 60 min. For this purpose the CXell SureLock[™] Electrophoresis Cell (life technologies) was used according to manufacturer's instructions. To blot the tricine gels, 1x Western Blot (WB) transfer buffer was used for transfer of proteins on a nitrocellulose membrane (Hybond, Amersham Biosciences) at 100 V in the Mini-PROTEAN[®] Tetra Cell of BIO RAD. After blotting, membranes were boiled for 1 min in 1x PBS at 95 °C to fix blotted proteins on the nitrocellulose membrane and subsequently blocked in blocking buffer for 1 h. Aβ was

detected by incubating membranes with antibodies 6E10 or 4G8 (1:2,000, Covance) at 4 °C overnight. As internal control the monoclonal antibody against GAPDH (1:50,000, Biodesign, H86504M) was used. A HRP conjugated anti-mouse antibody (1:5,000, GE healthcare) was utilized as secondary antibody. The immunoreactive complexes of A β were visualized at 4 kDa by chemiluminescence using ECL™ Western Blotting kit according to manufacturers instructions (Fig. 12). The Syngene GeneGnome Bio Imaging System and the GeneTool Software (Syngene) were used to detect the signal, and data were quantified by using the Software Adobe Photoshop CS3 and Microsoft Excel. Loading variations between WB lanes were normalized according to the GAPDH signal.

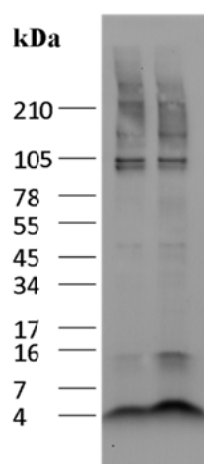


Figure 12: Example for A β detection after brain homogenization by WB (SDS fraction). Frozen hemispheres of two untreated 120 d old *APP^{PS1}* mice were homogenized by four-step extraction. 30 μ g proteins were loaded on a 10-20 % Novex® Tricine Gel and after blotting onto a nitrocellulose membrane A β was detected by antibody 6E10 at 4 kDa. Only two lanes of a whole WB membrane are depicted.

2.6 Spectral imaging of A β plaques after pFTAA and hFTAA co-staining

Spectral analyses of A β plaques after pFTAA and hFTAA co-staining were done at the IFM-Department of Chemistry, Linköping University, Sweden in the group of Prof. Per Hammarström, PhD.

2.6.1 Fluorescence microscopy

A 436 nm long pass excitation filter (436/10 (LP475)) was used for spectral imaging after pFTAA and hFTAA co-staining⁷³. Images of cerebral A β plaques co-stained with pFTAA and hFTAA (1 pFTAA:2 hFTAA, 10 mg/ml each) were collected using 10x and 40x magnification. At 10x magnification about eight representative cortical A β plaques of three serial sections per animal (in total 24 A β plaques) were analyzed, at 40x magnification

emission spectra of about 10 plaques (one to three plaques of five consecutive sections) were measured in total. The 509/589 ratio from the resulting 24 or 10 spectra per untreated, PBS or pFTAA treated *APPPSI* mouse were averaged and graphed.

2.6.2 Confocal microscopy

Spectra of A β plaques after pFTAA and hFTAA co-staining were recorded with an LSM 510 META (Zeiss) confocal laser scanning microscope through Plan-Neofluar 40L/0.75 objectives with an excitation at 458 nm. The selection of spectral regions and spectral processing was achieved with the standard software (LSM Image browser).

2.7 Electrophysiological measurements in the CA1 region of hippocampal slices

2.7.1 Generation of hippocampal slices

For slice preparation *APPPSI* mice were decapitated and their brains were quickly removed and bisected at the midsagittal plane. One brain hemisphere was used for electrophysiological measurements and the second hemisphere was gently snap frozen by immersion in a 2-methylbutane bath surrounded by liquid nitrogen and stored at -80 °C for further histological analyses. For electrophysiological measurements the cerebellum was cut off in an angle of about 45 ° and the hemisphere was glued onto that plane. Semicoronal slices of 400 μ m thickness were cut in ice-cold artificial cerebrospinal fluid (aCSF: 124 mM NaCl, 1,25 mM NaH₂PO₄, 10 mM glucose, 2 mM MgSO₄, 2 mM CaCl₂, 5 mM KCl, 26 mM NaHCO₃) using a vibratome (VT1000S, Leica Biosystems GmbH). After the preparation, slices were stored at RT and aerated with carbogen (95 % O₂, 5 % CO₂) for at least 45 min. Slices were transferred to a submerged perfusion chamber on an upright microscope (Axioskop FS, Zeiss), fixed in the chamber using an U-shaped platinum wire with a grid of nylon threads and superfused with aCSF at a flow rate of 4 to 6 ml/min at RT.

2.7.2 Long term potentiation in the hippocampal CA1 region

Field excitatory postsynaptic potentials (fEPSPs) were recorded with glass pipettes (1-1.5 M Ω , filled with 3 M NaCl) every 30 s in the hippocampal CA1 area and evoked by Schaffer collateral stimulation with an aCSF-filled glass electrode (Fig. 13). Baseline responses were collected using test pulses that yield about 30 % of the maximal fEPSP slope. Only slices with minimal fEPSP amplitude of 1 mV were recorded. Stable baseline response was measured for at least 10 min, before long term potentiation (LTP) was induced by theta-

burst stimulation. The theta-burst stimulation consisted of two stimulation trains at 100 Hz for 1 s with an interval of 1 min. After theta-burst stimulation, fEPSPs were observed for 60 min. The amount of LTP was described as percentage changes of fEPSP slopes after theta-burst stimulation normalized to baseline values (PatchMaster software, HEKA Elektronik).

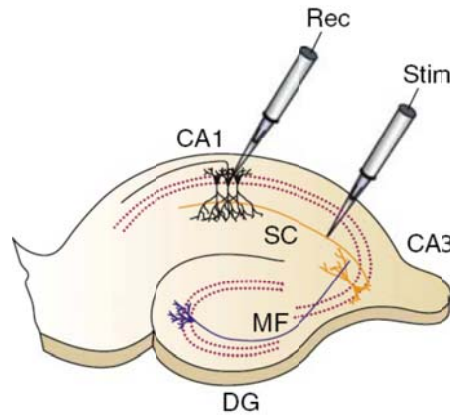


Figure 13: A schematic diagram of the rodent hippocampal slice preparation. The hippocampal CA1 and CA3 regions, the dentate gyrus (DG) as well as the mossy fibers (MF) are demonstrated. Typical electrode placements for studying synaptic plasticity at Schaffer collateral (SC) synapses onto CA1 neurons are indicated (Stim = stimulating electrode; Rec = recording electrode). Adapted with permission from Citri & Malenka, *Neuropsychopharmacology*, 2008, 33, 18-41. Copyright © 2007, Nature Publishing Group.

2.7.3 Paired pulse facilitation in the hippocampal CA1 region

fEPSP was recorded as described before. The inter-stimulus interval was changed from 25 ms to 50, 75, 100, 125, 150, 175 and 200 ms. Data were normalized by taking the first fEPSP value as 100 %.

2.8 Microscopy

Stained sections were analyzed by brightfield, fluorescence or confocal microscopy; distinct quantitative analyses after stainings were performed using the Stereo Investigator system. Unstained section after *in vivo* treatment of *APP/PS1* and WT mice with distinct LCOs, LCO derivatives and LCO-MNPs were screened for cortical A β plaque labeling by fluorescence microscopy (details see Tab. 7).

Table 7: Overview of utilized microscopy imaging techniques

	Stereo Investigator system	Brightfield microscopy	Fluorescence microscopy	Confocal-laser-scanning system
Microscope	Olympus BX53	Olympus BX50	Zeiss Observer Z1	Zeiss LSM 5 <i>Exciter</i>
Camera	QImaging Color 12 bit	Olympus DP25	Zeiss AxioCam MRm	-
Filter/laser	DAPI Dichroic mirror DM410 Excitation filter BP360-370 Barrier filter BA420IF FITC Dichroic mirror DM505 Excitation filter BP470-495 Barrier filter BA510IF Cy3 Dichroic mirror DM570 Excitation filter BP530-550 Barrier filter BA575IF Cy5 Dichroic mirror DM600 Excitation filter BP545-580 Barrier filter BA610IF	-	DAPI excitation G 365 emission BP 445/50 FITC excitation BP 470/40 emission BP 525/50 Cy3 excitation BP 545/25 emission BP 605/70 Cy5 excitation BP 640/30 emission BP 690/50	HeNe1 laser 543 nm HeNe2 laser 633 nm Laser Diode 405 405 nm Argon laser 458, 488, 514 nm
Software	Stereo Investigator (MBF BioScience)	Cell D (Olympus) cellSens Dimension (Olympus)	AxioVision 4 (Zeiss)	ZEN 2008 (Zeiss)

Transmission electron microscopy

TEM analyses were done in the Department of the Neuropathology, Charité – Universitätsmedizin Berlin with help of Hanna Plückhan (technician at the Department of Neuropathology). In brief, after euthanasia brains of experimental mice were sampled and the cortex of one hemisphere was cut into 2x2 mm large tissue blocks. Tissue was fixed over night in 2.5 % glutaraldehyd and for additional 4 h in 1 % osmium tetroxide. Subsequently cerebral tissue blocks were dehydrated in acetone and embedded in araldite. Semi-thin (0.5 µm) sections were generated using a Reichert ultramicrotome. To identify a tissue block containing Aβ plaques on the cut surface, these semi-thin sections were stained with Richardson solution and analyzed under a light microscope. From the original tissue block ultrathin sections (50-70 nm) were further cut with a diamond knife. Ultrathin sections were put on nickel grids and stained with uranyl acetate and lead citrate. Pictures were captured

using a Zeiss transmission electron microscope (model 902) and negatives were developed. Scanned images were inverted and processed in Adobe Photoshop CS3.

2.9 Magnetic resonance imaging and intracranial pressure measurement

Magnetic resonance imaging (MRI) and intracranial pressure (ICP) measurements were performed by the research group of Prof. Olav Haraldseth, Department of Circulation and Medical Imaging at the Norwegian University of Science and Technology (NTNU) in Trondheim, Norway.

2.10 Statistical analyses

Statistical analyses were performed using GraphPad Prism 5. Statistical significance is indicated as follows: * $p < 0.05$, ** $p < 0.01$ and *** $p < 0.001$. For the statistical analysis of pairwise comparisons of experimental groups, Student's t-test was used, whereas one-way ANOVA with Bonferroni's multiple comparison post-test was applied for comparison of more than two experimental groups.

3. Results

3.1 Efficient labeling of A β deposits with pFTAA on tissue sections and *in vivo*

3.1.1 Labeling of A β deposits in murine and human tissue samples

The pentameric LCO pFTAA is known to specifically bind and label amyloid deposits³⁹. Murine brain sections of aged *APPPSI* mice with robust cerebral A β plaque pathology and WT mice were stained with pFTAA (2.8 μ M) and compared. Analysis by fluorescence microscopy showed distinct staining of cerebral A β plaques in the *APPPSI* transgenic mouse brains but no staining was detectable in brains of WT mice (Fig. 14).

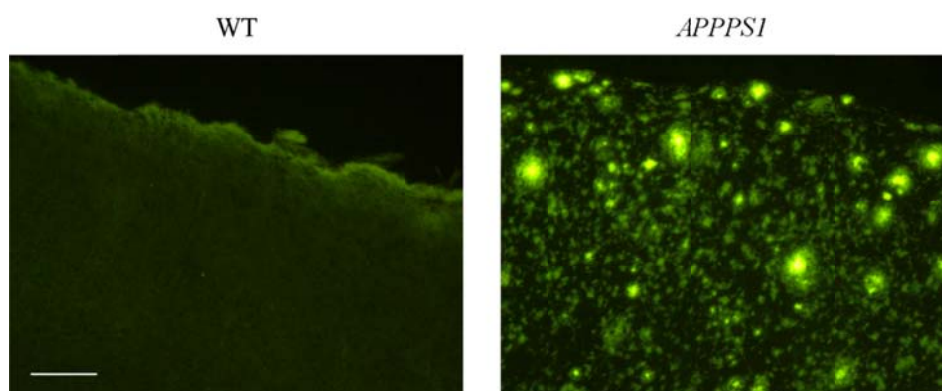


Figure 14: pFTAA staining of murine brain tissue. 30 μ m thick, cerebral free floating sections of an *APPPSI* and WT mouse were stained with pFTAA (2.8 μ M) and compared by fluorescence microscopy (FITC, Zeiss Observer Z1). Scale bar = 100 μ m.

To determine the detection qualities of pFTAA concentrations, cerebral sections of an aged *APPPSI* mouse were stained with different concentrations of pFTAA. As depicted in figure 15, even low pFTAA concentrations (as low as 0.56 μ M) stained A β deposits of cerebral *APPPSI* sections with high specificity. Based on these results the common pFTAA concentration of 2.8 μ M was used in subsequent experiments to keep staining results and staining intensities comparable between experiments.

Results

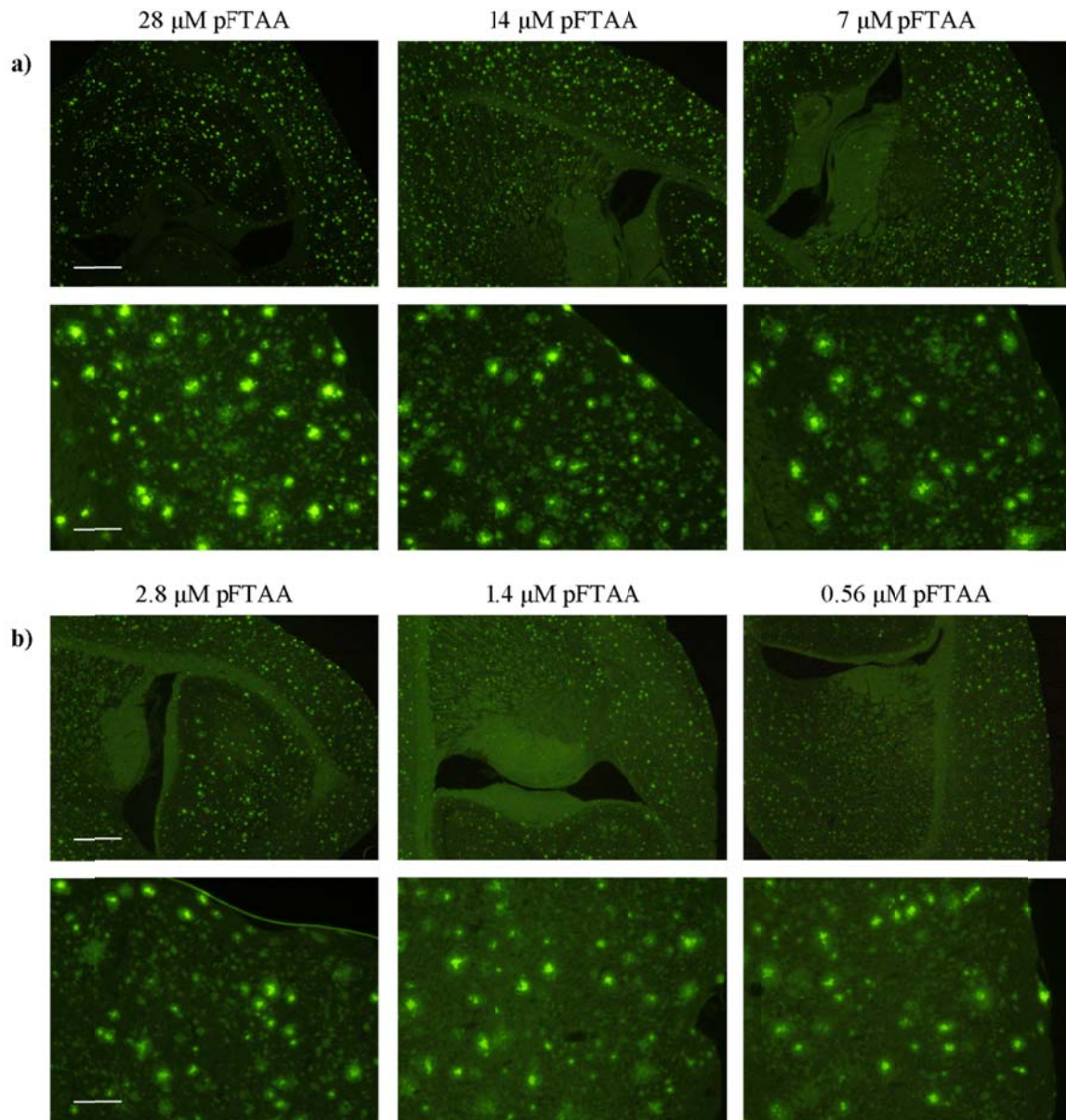


Figure 15: Dilution series of the pFTAA staining on *APPPS1* brain sections. Cerebral free floating sections of an aged *APPPS1* mouse were stained with six different pFTAA concentrations and analyzed by fluorescence microscopy (FITC, Zeiss Observer Z1). 1 μ l of the pFTAA stock dilution (1 mg/ml) was mixed with 1x PBS to achieve respective dilutions. Figure 15a shows stainings resulting from 28 μ M, 14 μ M and 7 μ M pFTAA dilutions; in Figure 15b are stainings with pFTAA concentrations of 2.8 μ M, 1.4 μ M and 0.56 μ M depicted. a), b) Scale bar = 500 μ m (upper row), Scale bar = 100 μ m (lower row).

pFTAA revealed specific staining of A β deposits on murine AD brain sections. In a next step it was tested if also A β plaques of human AD brain tissue can be detected by pFTAA. Cortical paraffin sections of two human autopsy brain tissue samples were stained with pFTAA: i) a non-AD case as control and ii) a case with neuropathologically confirmed AD. Analysis by fluorescence microscopy showed specific pFTAA labeling of A β plaques in the AD brain but no labeling of the control tissue (Fig. 16).

Results

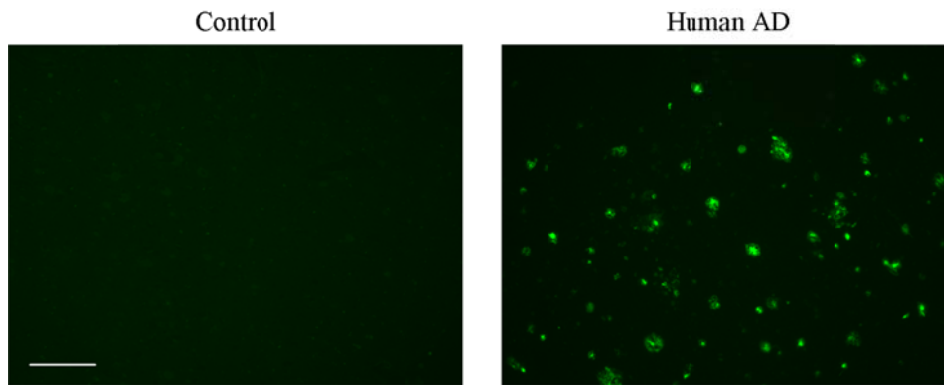


Figure 16: pFTAA staining of human brain tissue. Human cortical brain sections (5 μm thick paraffin sections) of an AD and a control case were stained with pFTAA (2.8 μM) and analyzed subsequently by fluorescence microscopy (FITC, Zeiss Observer Z1). Scale bar = 100 μm .

To determine pFTAA labeling is specific for $\text{A}\beta$ plaques, double stainings with $\text{A}\beta$ specific antibodies 4G8 and 6E10 were performed. Since LCOs are known to emit fluorescent light in a wide wavelength spectrum, it was necessary to initially check the channel specificity of pFTAA staining. To do so single stainings of the individual antibodies and pFTAA were analyzed in all channels used in the study. The immunofluorescent stainings of 4G8 and 6E10 were visualized with an Alexa Fluor® 647 Goat Anti-Mouse IgG (H+L) secondary antibody. Assessments of single stainings on the confocal microscope showed channel specificity and no overlapping emission spectra for pFTAA and Alexa Fluor® 647. pFTAA is only detected when excited with the Argon laser whilst Alexa Fluor® 647 is only detected with the HeNe2 laser (Fig. 17).

Results

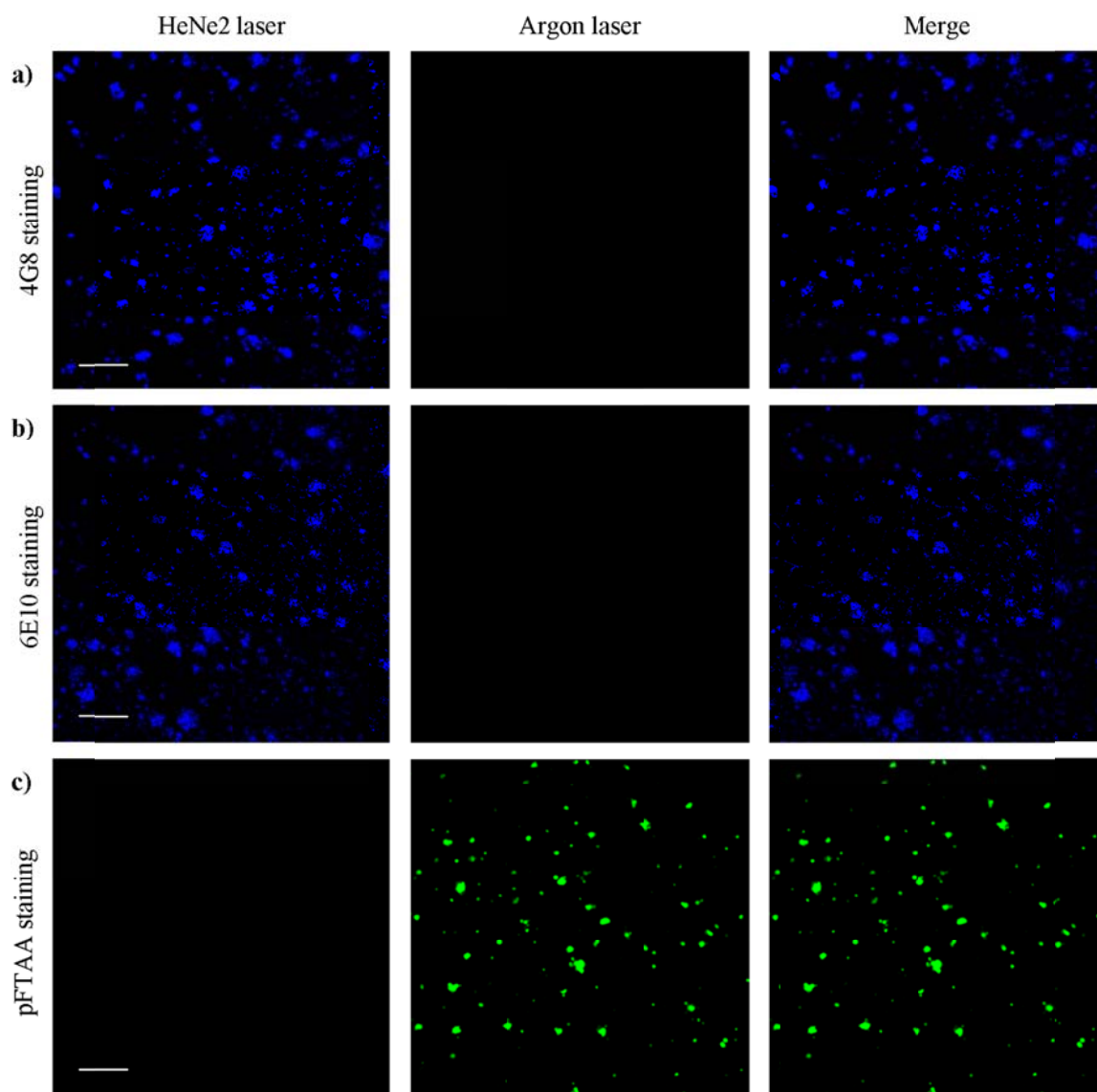


Figure 17: Single stainings of *APPPSI* brain sections with immunohistological antibodies (4G8, 6E10) and the amyloid binding agent pFTAA. Single stainings of *APPPSI* brain sections with A β specific immunohistological antibodies 4G8 (a) and 6E10 (b), and with the amyloid binding dye pFTAA (c) were assessed to analyze unspecific binding and possible bleed through of the fluorescent signal emitted by the secondary antibody Alexa Fluor® 647 Goat Anti-Mouse IgG (H+L) and pFTAA. The HeNe2 laser and the argon laser specificity of single stainings was analyzed by confocal microscopy (Zeiss LSM 5 *Exciter*). Images were subsequently merged using the software ZEN 2008. Scale bar = 100 μ m.

The channel specificity of pFTAA and antibody fluorochromes allowed the analysis of pFTAA specificity to cerebral A β deposits in double stainings. Cerebral sections of an aged *APPPSI* mouse were stained with pFTAA and 4G8 (reactive to A β amino acid residues 17-24) or 6E10 (reactive to A β amino acid residues 1-17) respectively and analyzed by confocal microscopy. This double-labeling study confirmed a co-localization of pFTAA staining with the respective antibody signals and confirmed the specificity of pFTAA to stain A β deposits (Fig. 18). The specific labeling was independent of the order the stainings were performed, indicating no major interference of LCOs with antibody binding to A β deposits and *vice*

Results

versa. However, it was observed that pFTAA detected less diffuse A β deposits than the specific antibodies. pFTAA revealed a precise overlay with compact congophilic A β plaques (Fig. 18).

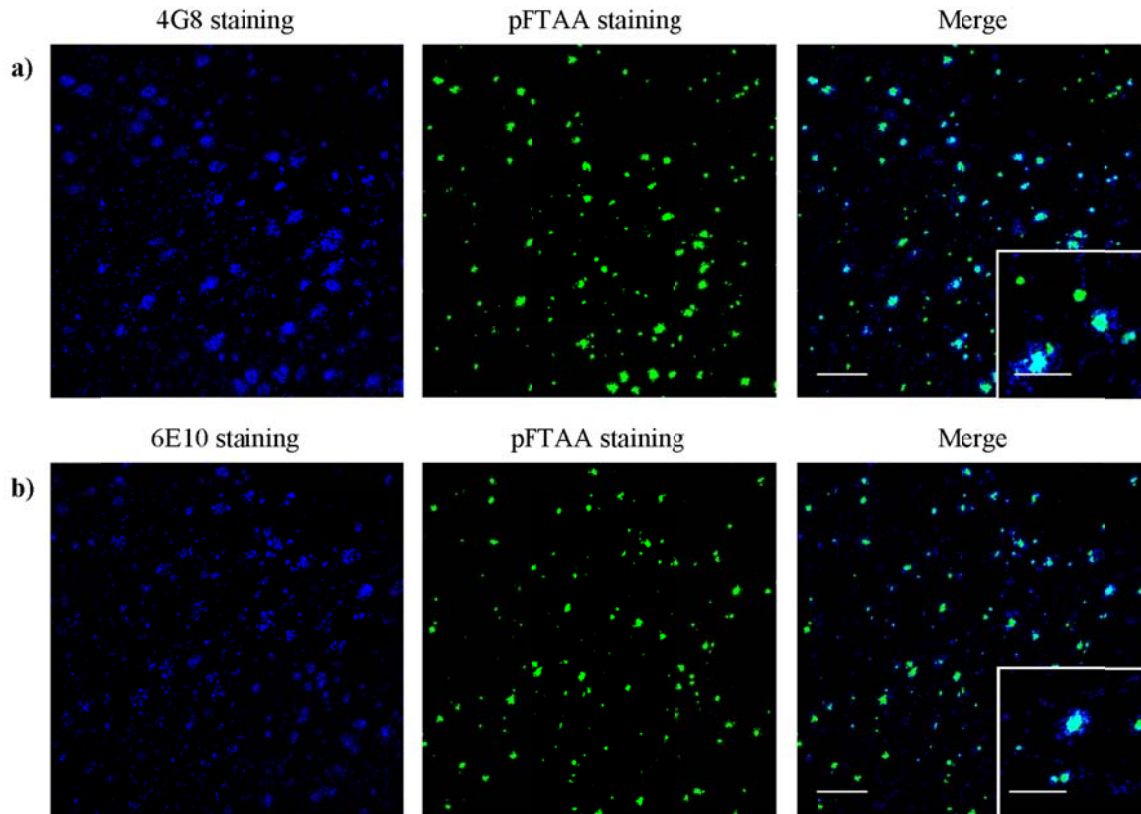


Figure 18: Co-staining of *APPPS1* brain sections with A β specific antibodies 4G8 or 6E10 and pFTAA. Cerebral free floating sections (30 μ m) of an aged *APPPS1* mouse were consecutively stained with the A β specific antibody 4G8 (a) or 6E10 (b) and pFTAA. For the depicted images the immunofluorescent staining was performed before labeling with pFTAA on the same sections. For the immunofluorescent stainings Alexa Fluor® 647 Goat Anti-Mouse IgG (H+L) was used as secondary antibody and both stainings were detected by the use of laser HeNe2. The pFTAA staining was detected by the argon laser. Images were taken with a confocal laser scanning microscope (Zeiss LSM 5 *Exciter*) and subsequently merged by using the software ZEN 2008. Scale bar = 100 μ m, Scale bar insert = 50 μ m.

To investigate the overlap of pFTAA with congophilic A β plaques, cerebral sections of an aged *APPPS1* mouse were co-stained with Congo red (Fig. 19a), a commonly used histological amyloid marker for diagnostic purposes which stains mainly the amyloid cores of compact A β plaques⁴⁴, and pFTAA (Fig. 19b). Microscopical analysis showed labeling of dense-core plaques as well as of diffuse A β deposits by pFTAA, while Congo red only labels the dense amyloid core of A β deposits. The different staining properties between Congo red and pFTAA were visualized by overlay images (Fig. 19c).

Results

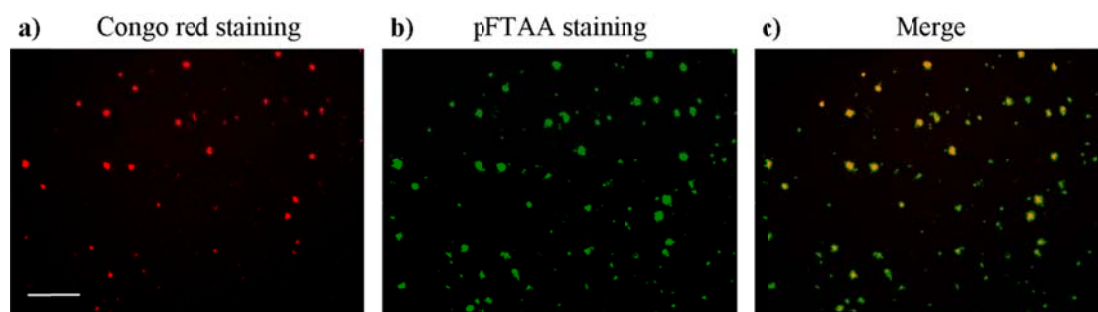


Figure 19: Co-staining of *APPPS1* brain sections with Congo red and pFTAA. Cerebral free floating sections (30 μm) of an aged *APPPS1* mouse with robust cerebral A β plaque pathology were consecutively stained with Congo red and pFTAA. For the depicted images the immunofluorescent staining was performed before labeling with pFTAA on the same sections. The Congo red staining was detected by the Cy3 filter, the pFTAA staining by using the FITC filter of the fluorescence microscope Observer Z1 (Zeiss). Images were subsequently merged using the software Axio Vision 4 of Zeiss. Scale bar = 100 μm .

3.1.2 *In vivo* labeling of cerebral A β deposits in the transgenic Alzheimer's disease mouse model *APPPS1*

3.1.2.1 Intravenous versus intraperitoneal pFTAA application

It was shown previously that pFTAA labels cerebral A β plaques 30 min after i.v. injection in *APPPS1* mice³⁹. To determine the cerebral A β plaque labeling efficacy of pFTAA by different injection routes, single i.v. and single i.p. pFTAA (10 mg/kg) injections in aged *APPPS1* mice with robust, cerebral A β deposits were performed. Mice were sacrificed one day later, cerebral free floating sections were prepared and A β plaque labeling was analyzed microscopically (Fig. 20). Experimental groups are depicted in table 8.

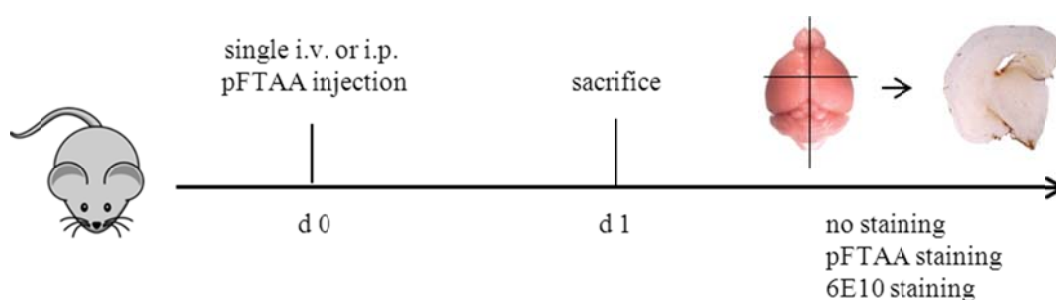


Figure 20: Experimental design of i.v. versus i.p. pFTAA injection in aged *APPPS1* mice. To compare cerebral A β plaque labeling after a single i.v. and i.p. pFTAA injection, aged *APPPS1* mice were treated once with pFTAA (10 mg/kg) and sacrificed one day later. Cerebral free floating sections (30 μm) were analyzed by fluorescence microscopy without any staining and after pFTAA staining (FITC, Zeiss Observer Z1). Consecutive sections were analyzed after 6E10 staining by brightfield microscopy (Olympus BX 50).

Results

Table 8: Experimental groups of i.v. versus i.p. pFTAA injection in aged *APPPS1* mice

Genotype	Age	Treatment
WT	534 d	i.v. pFTAA
<i>APPPS1</i>	588 d	no treatment
	588 d	i.v. pFTAA
	565 d	i.p. pFTAA

One day after a single i.v. and i.p. pFTAA application, peripheral cortical A β plaques showed fluorescent labeling with equal intensity (Fig. 21c, d). A β plaque labeling was detected mainly in the cortical periphery indicating an entry of pFTAA through meningeal blood vessels. Cerebral sections of the pFTAA injected WT animal and of the untreated *APPPS1* animal revealed no fluorescent signal (Fig. 21a, b).

Results

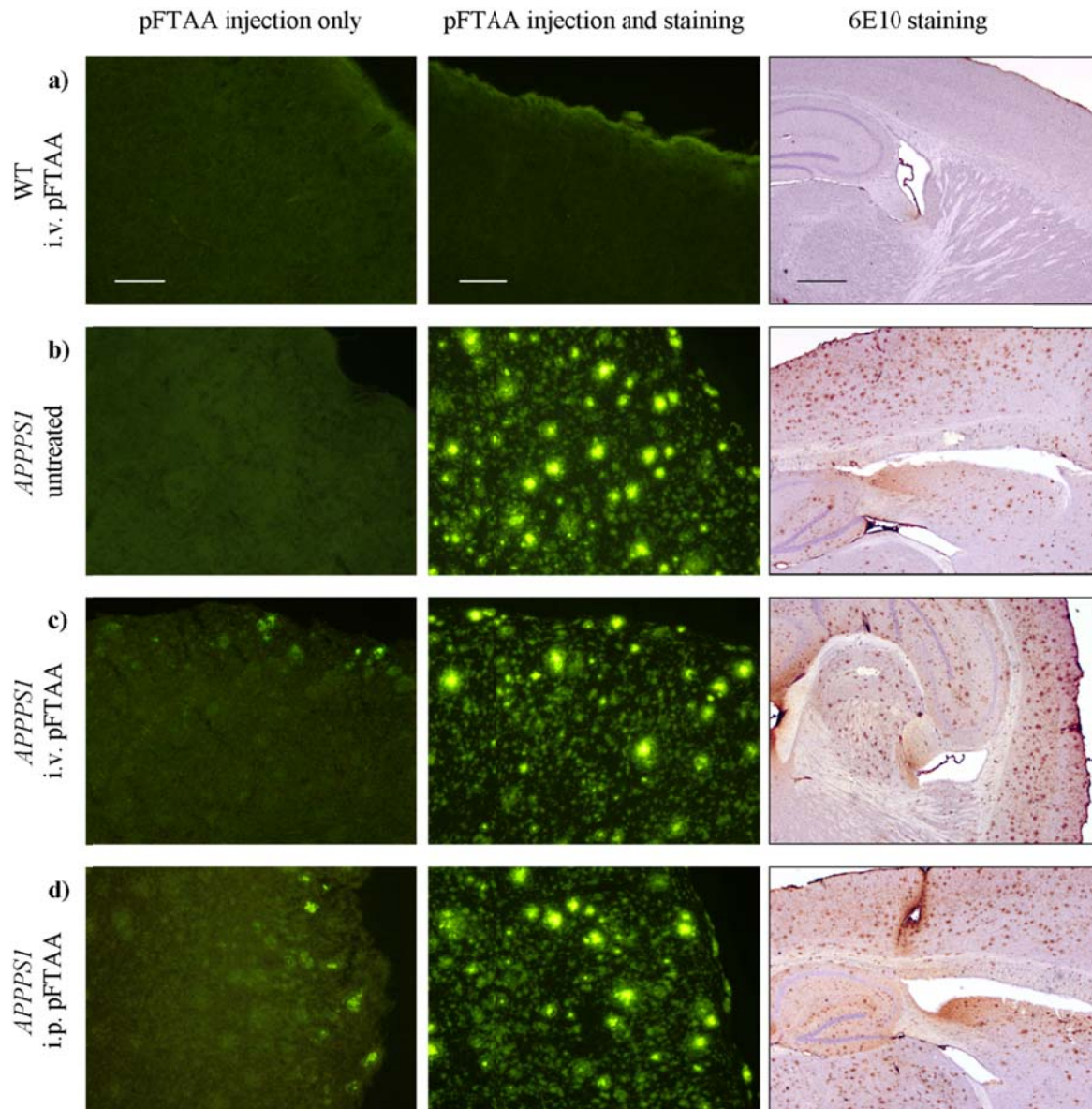


Figure 21: *In vivo* labeling of cerebral A β plaques in aged *APP*^{PS1} mice after a single i.v. and i.p. pFTAA injection. Aged *APP*^{PS1} mice were injected i.v. (c) and i.p. (d) with 10 mg/kg pFTAA. As controls a WT mouse (a) received a single i.v. injection of pFTAA. Sections of an untreated *APP*^{PS1} mouse (b) were added as further control. Treated mice were sacrificed one day after a single injection and cerebral free floating sections (30 μ m) were analyzed by fluorescence microscopy (FITC, Zeiss Observer Z1) for pFTAA labeled A β plaques. A pFTAA and immunohistochemical 6E10 staining (analyzed using FITC, Zeiss Observer Z1 and BF, Olympus BX50) of consecutive sections are shown for comparison in the middle and right column. Scale bar = 100 μ m (left and middle column), Scale bar = 500 μ m (right column).

To investigate the efficacy of serial i.p. injections of pFTAA to label A β plaques, four injections on consecutive days were performed and the cerebral tissue was analyzed (Fig. 22). Experimental groups are depicted in table 9.

Results

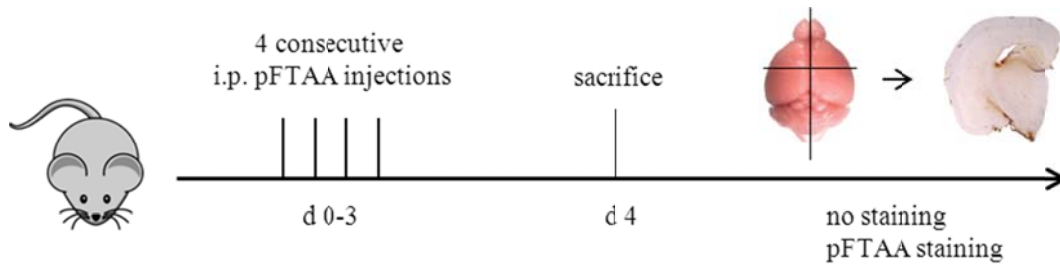


Figure 22: Experimental design of *in vivo* labeling of cerebral A β plaques in *APPPS1* mice after a single and four consecutive i.p. pFTAA applications. To compare four consecutive i.p. injections of pFTAA to a single i.p. application, aged *APPPS1* mice were treated on four consecutive days with 10 mg/kg pFTAA and sacrificed one day after the last injection. Cerebral free floating sections (30 μ m) were analyzed by fluorescence microscopy without any staining and after pFTAA staining (Zeiss, Observer Z1).

Table 9: Experimental groups of *in vivo* labeling of cerebral A β plaques in *APPPS1* mice after a single and four consecutive i.p. pFTAA applications

Genotype	Age	Treatment
WT	396 d	4x i.p. pFTAA
<i>APPPS1</i>	378 d	4x i.p. pFTAA
	565 d	1x i.p. pFTAA

In contrast to a single i.p. pFTAA injection, where only peripheral cortical A β plaques showed fluorescent labeling (Fig. 23c), analysis of *APPPS1* mice after serial i.p. injections of pFTAA showed labeling of A β plaques in the entire cortex (Fig. 23b). WT mice showed no specific cerebral fluorescent signals after four consecutive i.p. pFTAA injections (Fig. 23a).

Results

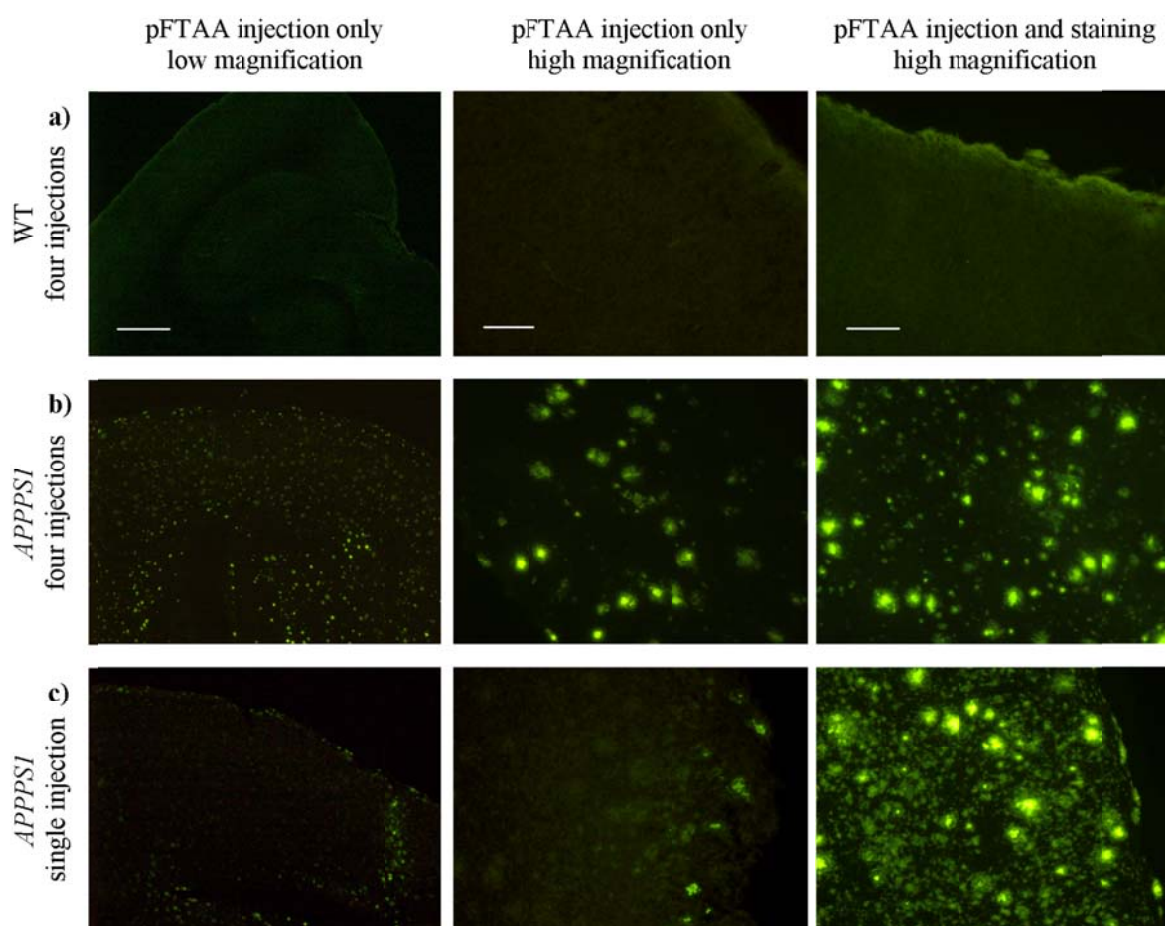


Figure 23: *In vivo* labeling of cerebral A β plaques in *APPPS1* mice after a single and four consecutive i.p. pFTAA applications. Aged *APPPS1* mice were injected once (c) and on four consecutive days (b) i.p. with 10 mg/kg pFTAA. As control a WT animal received four i.p. pFTAA injections (a). Mice were sacrificed one day after the single or last injection and unstained, cerebral free floating sections (“pFTAA injection only”) were analyzed for A β plaque labeling by fluorescence microscopy (left and middle column). A pFTAA staining of consecutive cerebral sections is shown for comparison in the right column. Sections were analyzed using the FITC filter of the fluorescence Zeiss Observer Z1 microscope. Scale bar = 500 μ m (left column), Scale bar = 100 μ m (middle and right column).

3.1.2.2 Titration of pFTAA dosage for *in vivo* application in *APPPS1* mice

Initial *in vivo* pFTAA applications were performed based on the published protocol where 10 mg/kg pFTAA were injected per single application³⁹. To determine if lower pFTAA concentrations and shorter treatment show a similar labeling efficacy of cerebral A β plaques in *APPPS1* mice, 2 and 5 mg/kg pFTAA were injected i.p. on two consecutive days and compared to two consecutive injections of 10 mg/kg pFTAA. Mice were sacrificed one day after the second injection, brain sections were prepared and analyzed by fluorescence microscopy (Fig. 24). Experimental groups are depicted in table 10.

Results

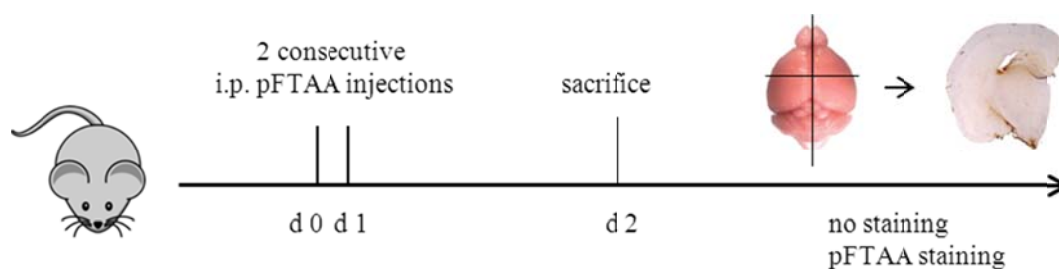


Figure 24: Experimental design of two consecutive i.p. injections with different pFTAA dosages in aged *APPPS1* mice. To compare the efficacy of cerebral A β plaque labeling after application of different pFTAA dosages, two consecutive i.p. injections in aged *APPPS1* mice were performed and experimental animals were sacrificed one day after the second injection. Cerebral free floating sections were analyzed without any staining and after pFTAA staining by fluorescence microscopy (FITC, Zeiss Observer Z1).

Table 10: Experimental group of titration of pFTAA dosage for *in vivo* application in aged *APPPS1* mice

Genotype	Age	Treatment
<i>APPPS1</i>	381 d	2x 2 mg/kg pFTAA (i.p.)
	369 d	2x 5 mg/kg pFTAA (i.p.)
	383 d	2x 10 mg/kg pFTAA (i.p.)

The comparison of 10 mg/kg pFTAA after two and four injections on consecutive days showed no differences in labeling intensity (Fig. 23b and 25c). Furthermore, it was observed, that lower pFTAA dosages were less efficient to label cerebral A β plaques after two consecutive i.p. injections compared to 10 mg/kg (Fig. 25d). After injection of 2 mg/kg and 5 mg/kg pFTAA cortical A β plaques were only weakly labeled as visualized by fluorescence microscopy (Fig. 25b, c). Based on these results pFTAA at 10 mg/kg was used for upcoming *in vivo* experiments.

Results

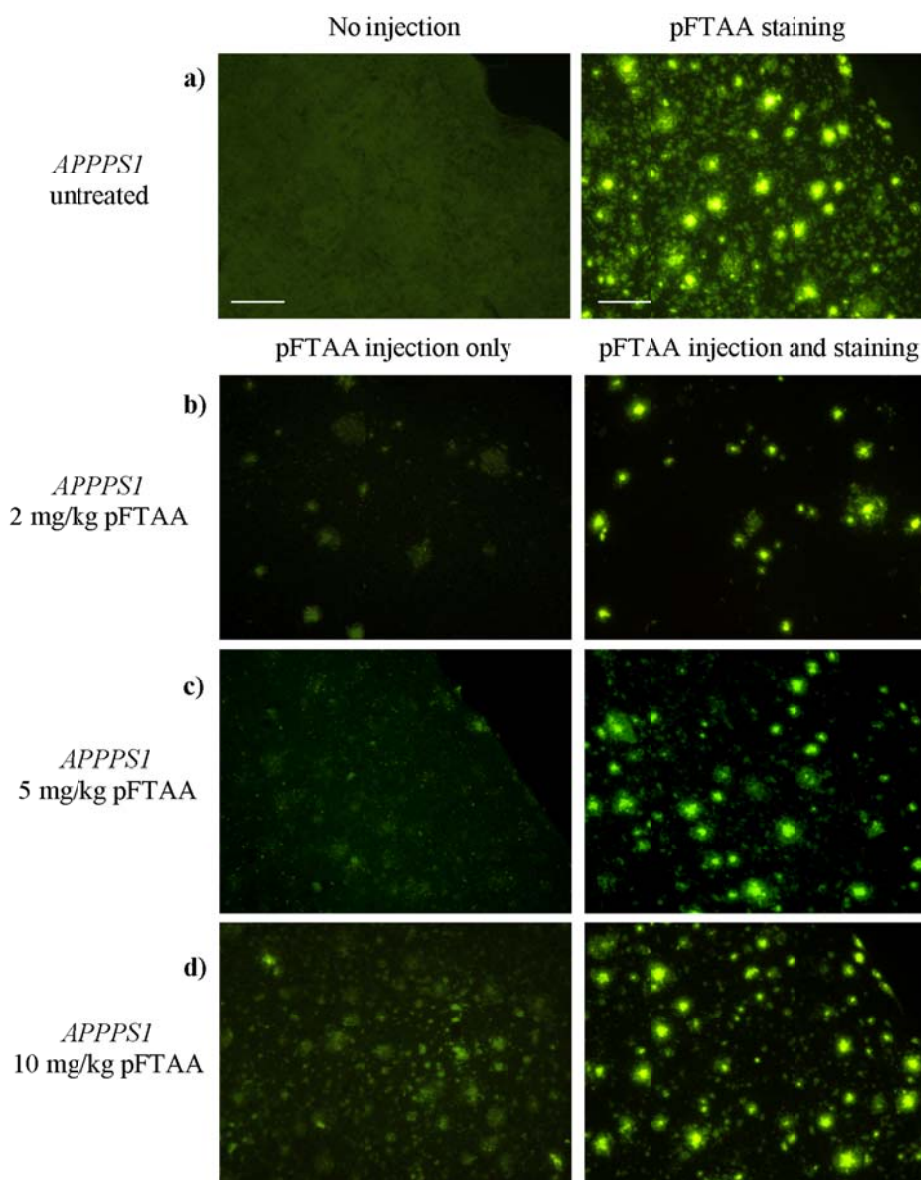


Figure 25: *In vivo* labeling of cerebral A β plaques in *APPPS1* mice after two consecutive i.p. injections of 2, 5 and 10 mg/kg pFTAA. Age matched *APPPS1* mice were i.p. injected with three different pFTAA dosages: i) 2 mg/kg (b), ii) 5 mg/kg (c), iii) 10 mg/kg (d) and *in vivo* pFTAA labeling of cerebral A β plaques was compared. As control cerebral sections of an untreated *APPPS1* mouse were analyzed simultaneously (a). pFTAA treated animals were sacrificed one day after the second pFTAA injection and 30 μ m thick cerebral free floating sections were prepared and analyzed. A pFTAA staining of consecutive cerebral sections is shown for comparison in the right column. Sections were analyzed using the FITC filter of the fluorescence Zeiss Observer Z1 microscope. Scale bar = 100 μ m.

3.1.2.3 Time course of pFTAA *in vivo* binding to cerebral A β plaques

In a further short-term pFTAA treatment approach the time course of pFTAA *in vivo* binding to cerebral A β plaques after two i.p. pFTAA applications was investigated. Therefore four age matched *APPPS1* mice were injected with 10 mg/kg pFTAA on two consecutive days and pFTAA labeling of cerebral A β plaques was analyzed one day, one week, three weeks and six weeks after the second injection using fluorescence microscopy (Fig. 26, Tab. 11).

Results

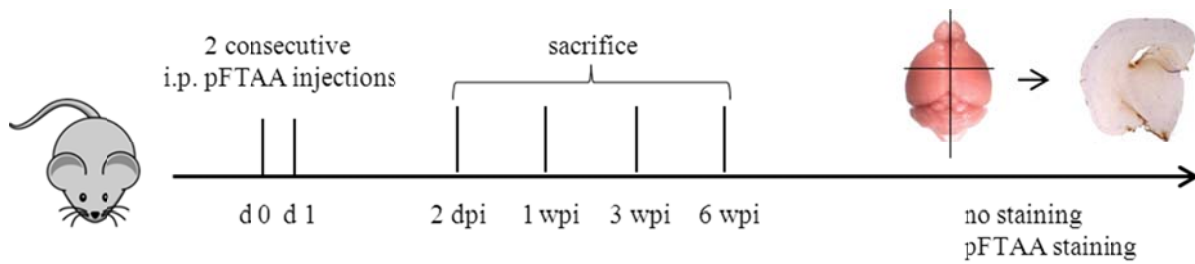


Figure 26: Experimental design of pFTAA *in vivo* binding time course after two i.p. applications in aged *APPPS1* mice. To analyze how long pFTAA remains bound to cerebral A β plaques in *APPPS1* mice, 10 mg/kg pFTAA were applied to aged animals on two consecutive days and brain sections were analyzed by fluorescence microscopy (FITC, Zeiss Observer Z1) at several time points (two days post initial injection (2 dpi); one, three and six weeks post initial injection (1, 3, 6 wpi)) after treatment.

Table 11: Experimental groups of pFTAA *in vivo* binding time course in aged *APPPS1* mice

Genotype	Age	Treatment
<i>APPPS1</i>	389 d	2x 10 mg/kg pFTAA (i.p.), sacrifice 2 dpi
	266 d	2x 10 mg/kg pFTAA (i.p.), sacrifice 1 wpi
	239 d	2x 10 mg/kg pFTAA (i.p.), sacrifice 3 wpi
	260 d	2x 10 mg/kg pFTAA (i.p.), sacrifice 6 wpi

Analyzed cerebral sections showed that even six weeks after injection pFTAA labeling of cerebral A β plaques was detectable (Fig. 27). In some cases the pFTAA signal appeared even stronger over time, with the unspecific background labeling of brain parenchyma reduced and a more specific labeling of cerebral A β plaques³⁹. These results suggest, that pFTAA remains in the circulation for a longer period of time and accumulates on A β deposits over time. Robust *in vivo* pFTAA labeling of A β plaques can be observed even three months after peripheral i.v. injection (Dr. Bettina Wegenast-Braun, Hertie-Institute, University of Tübingen, Germany, unpublished data).

Results

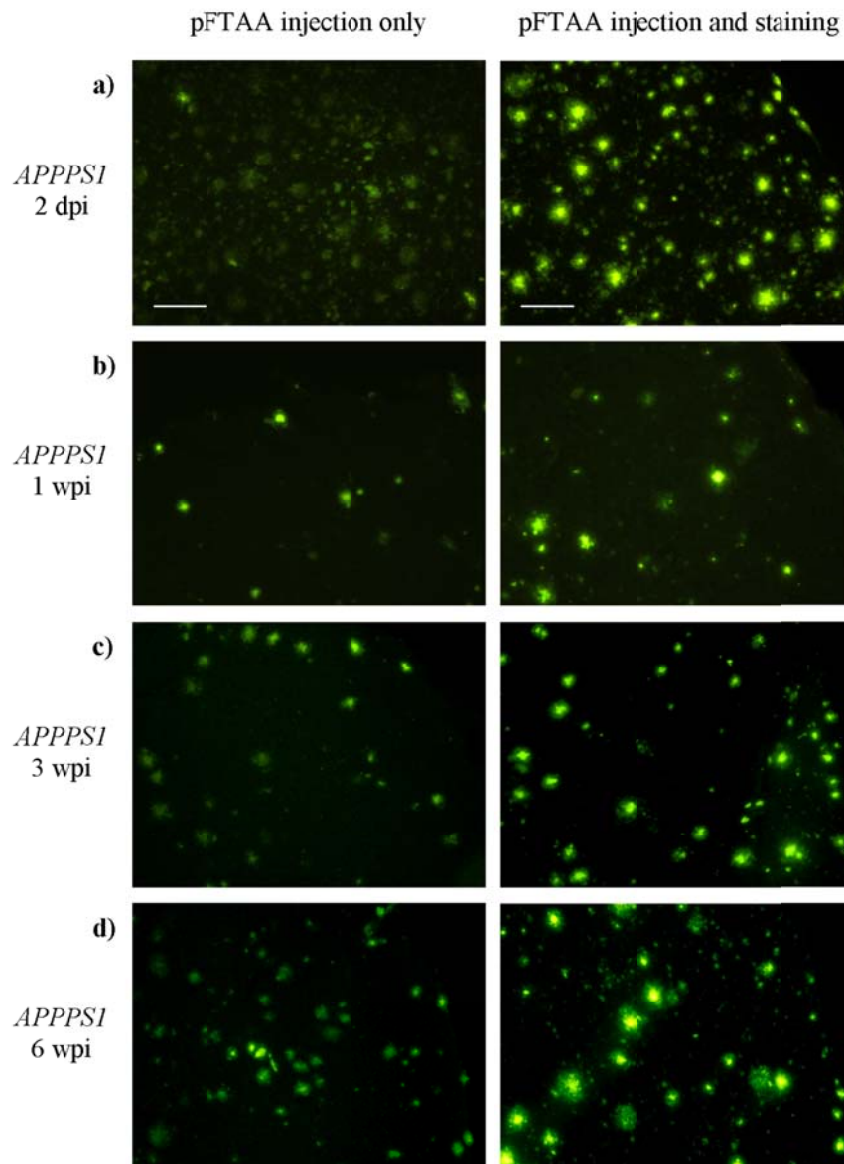


Figure 27: Timeline of pFTAA *in vivo* binding to cerebral A β plaques after two i.p. injections in aged *APPPS1* mice. Four age matched *APPPS1* mice were i.p. injected on two consecutive days with 10 mg/kg pFTAA. Single mice were consecutively sacrificed 2 dpi (a), 1 week (b), 3 weeks (c) and 6 weeks (d) after the initial pFTAA application and unstained, cerebral free floating sections (pFTAA injection only) were analyzed for pFTAA labeling (left column). A pFTAA staining of consecutive cerebral sections is shown for comparison in the right column. Sections were analyzed using the FITC filter of the fluorescence Zeiss Observer Z1 microscope. Scale bar = 100 μ m.

3.1.2.4 Histological analyses of peripheral organs after short term pFTAA application

Since it is not known how systemically administered pFTAA or LCOs affect peripheral organs in terms of metabolism, toxicity and potential deposition, distinct peripheral organs were screened for pathological alterations and pFTAA deposition i) two days and ii) six weeks after short term LCO application (two injections of 10 mg/kg pFTAA on two consecutive days).

Results

Unstained free floating sections (30 μm) of various organs were analyzed by fluorescence microscopy (FITC, Zeiss Observer Z1) for accumulation of pFTAA labeled aggregates and compared to sections of an untreated *APPPSI* mouse (Fig. 28-35 panel a). In parallel, H&E stained paraffin sections (5 μm) of various paraffin embedded organs were analyzed for pathological abnormalities by brightfield microscopy (BF, Olympus BX50) and compared to sections of an untreated *APPPSI* mouse (Fig. 28-35 panel b). Representative images of analyzed sections of peritoneal lymph nodes, heart, lung, kidney, liver, and spleen are depicted in figures 28–35.

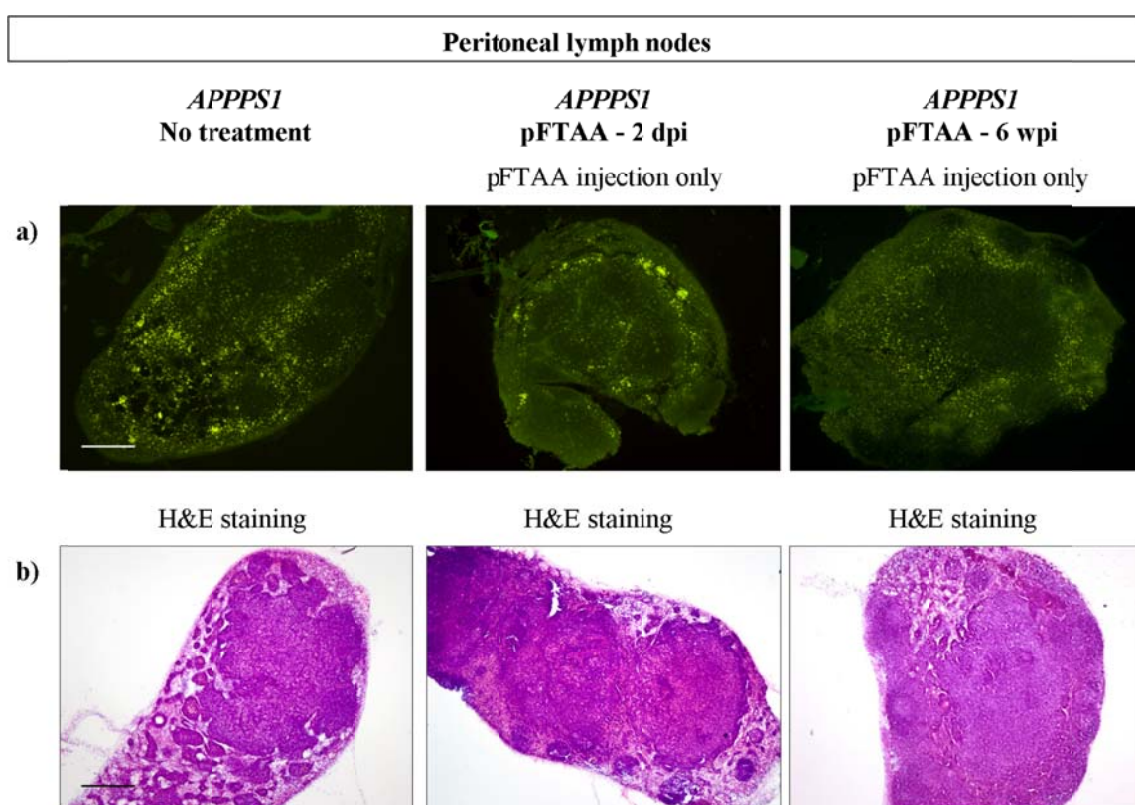


Figure 28: Postmortem histological analysis of peritoneal lymph nodes for systemic pFTAA deposition (a) and pathological abnormalities (b) after peripheral short term pFTAA treatment. Using fluorescence microscopy deposition of the “aging pigment” lipofuscin was visible in all analyzed peritoneal lymph nodes (a). Scale bar = 100 μm .

Results

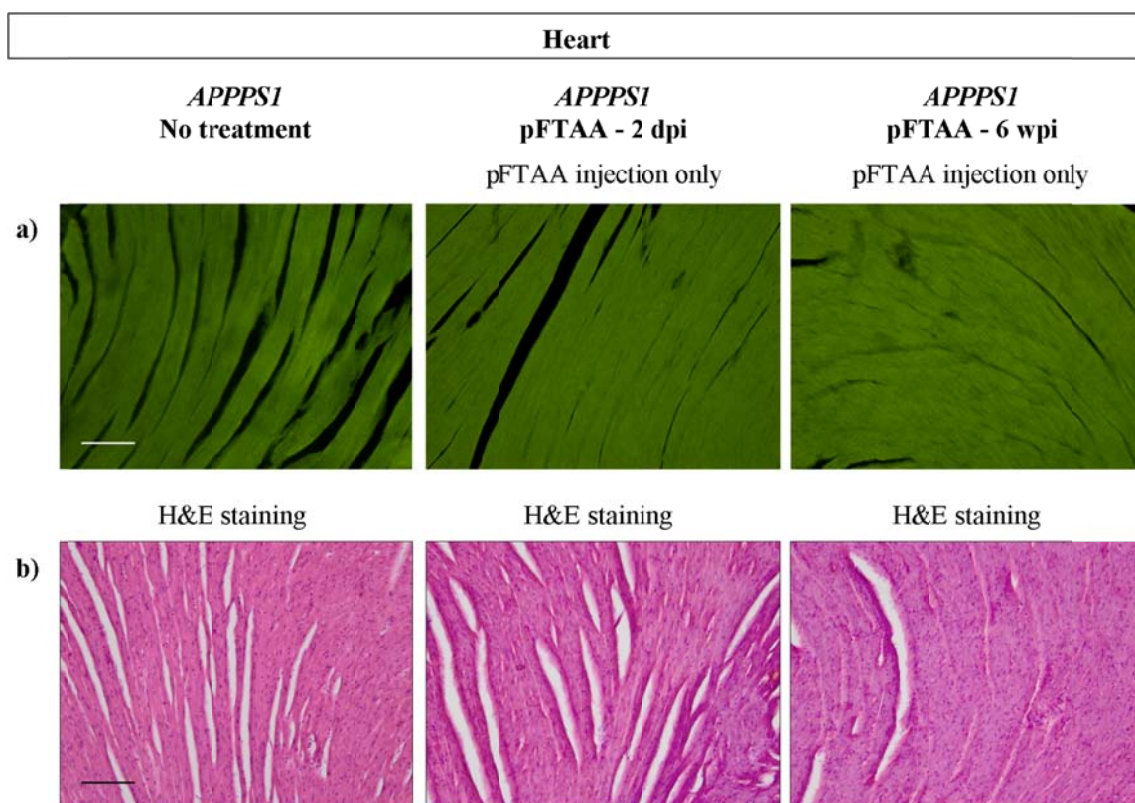


Figure 29: *Postmortem* histological analysis of heart muscle tissue for systemic pFTAA deposition (a) and pathological abnormalities (b) after peripheral short term pFTAA treatment. Scale bar = 100 μ m.

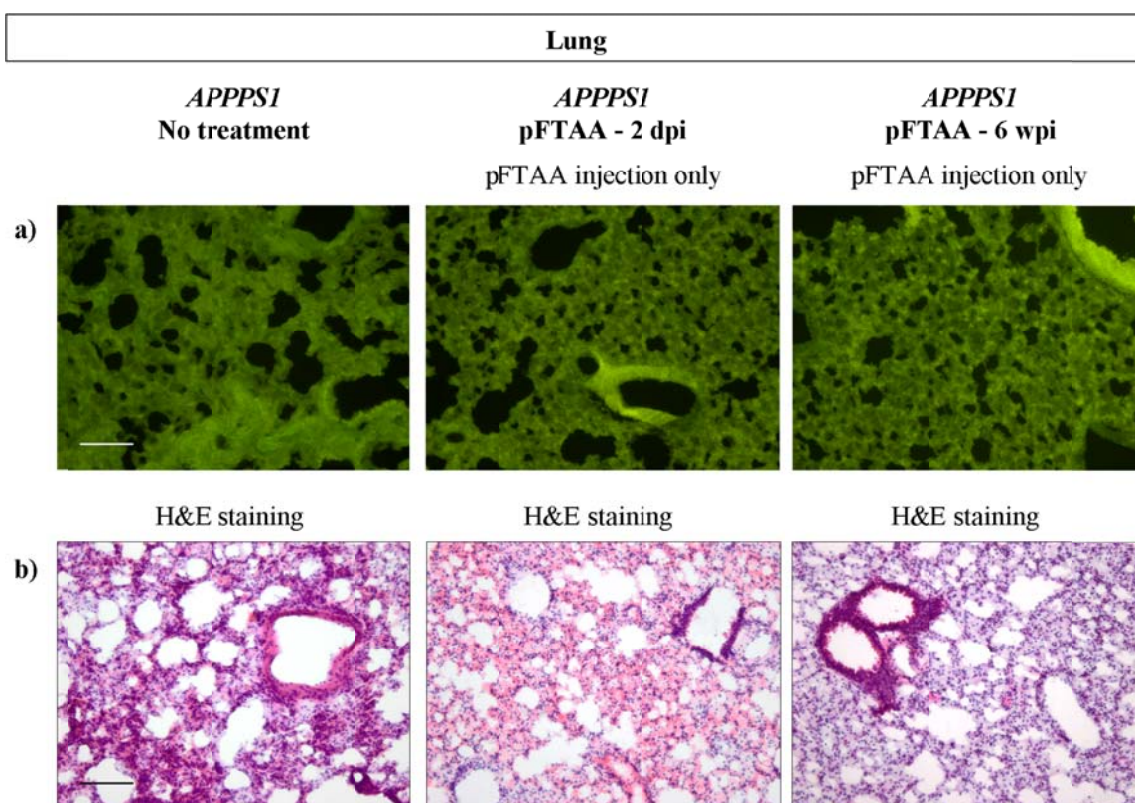


Figure 30: *Postmortem* histological analysis of lung tissue for systemic pFTAA deposition (a) and pathological abnormalities (b) after peripheral short term pFTAA treatment. Scale bar = 100 μ m.

Results

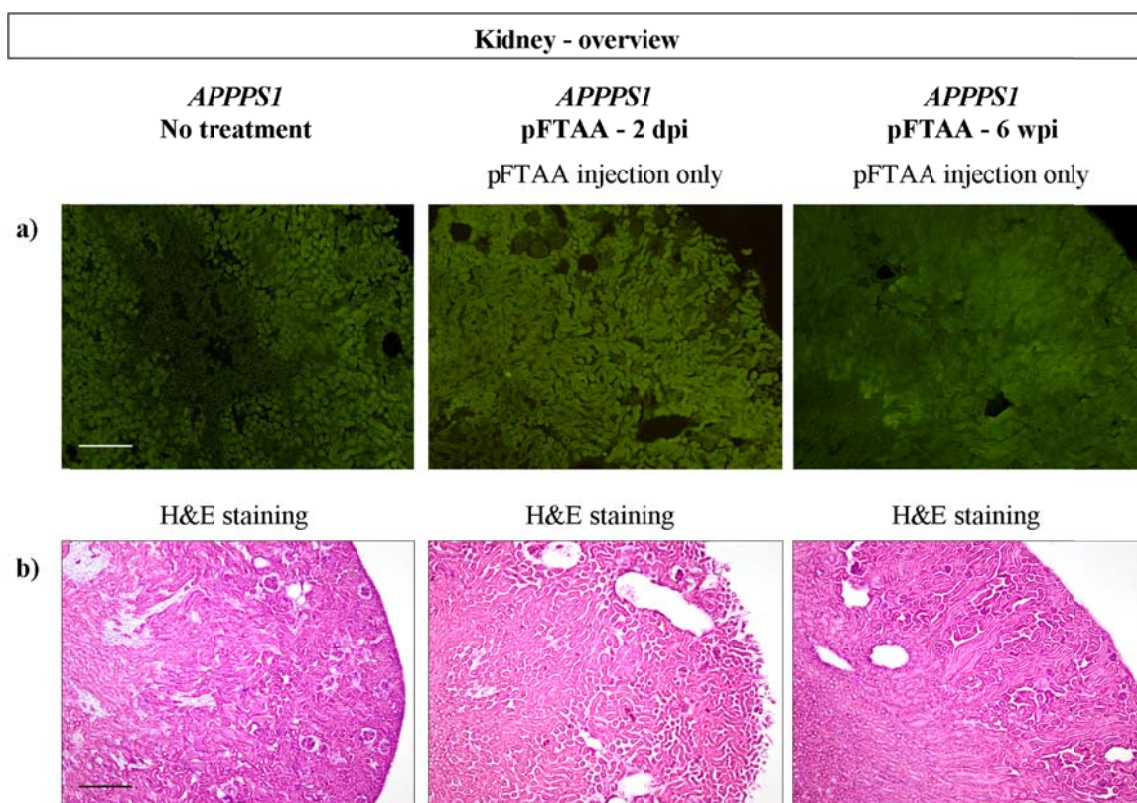


Figure 31: *Postmortem* histological analysis of the kidney for systemic pFTAA deposition (a) and pathological abnormalities (b) after peripheral short term pFTAA treatment. Scale bar = 400 μ m.

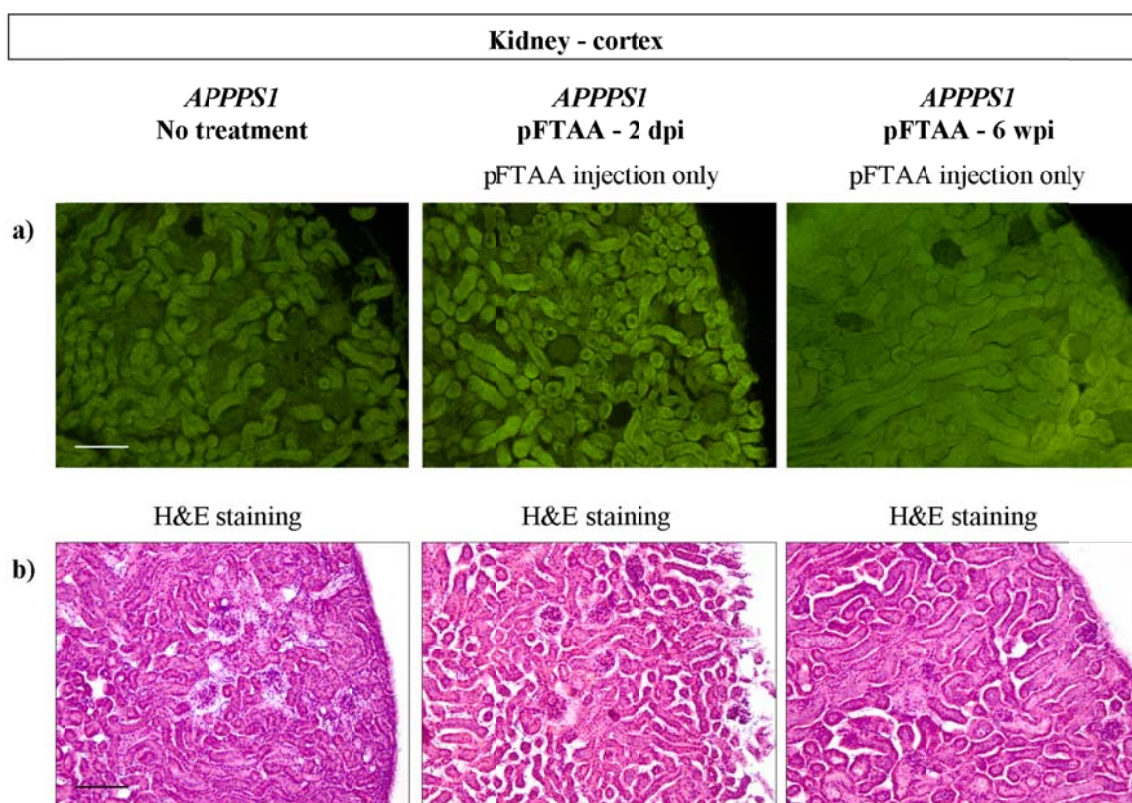


Figure 32: *Postmortem* histological analysis of the renal cortex for systemic pFTAA deposition (a) and pathological abnormalities (b) after peripheral short term pFTAA treatment. Scale bar = 100 μ m.

Results

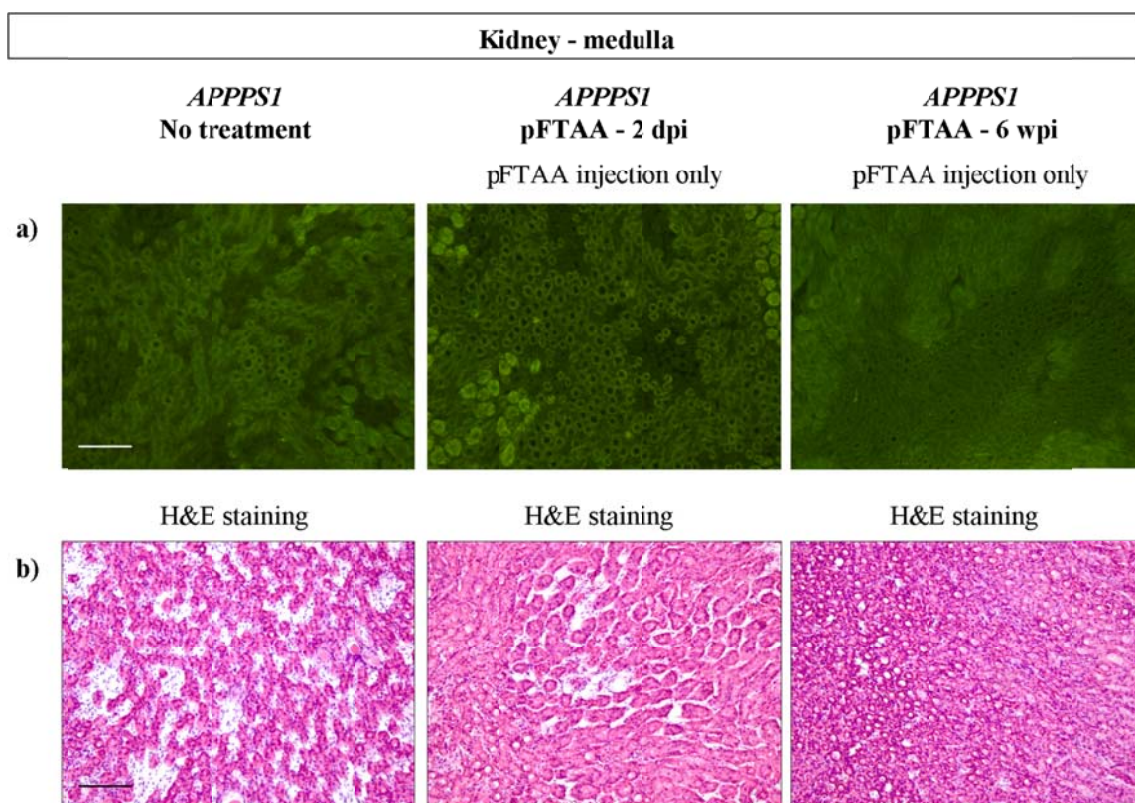


Figure 33: *Postmortem* histological analysis of the renal medulla for systemic pFTAA deposition (a) and pathological abnormalities (b) after peripheral short term pFTAA treatment. Scale bar = 100 μ m.

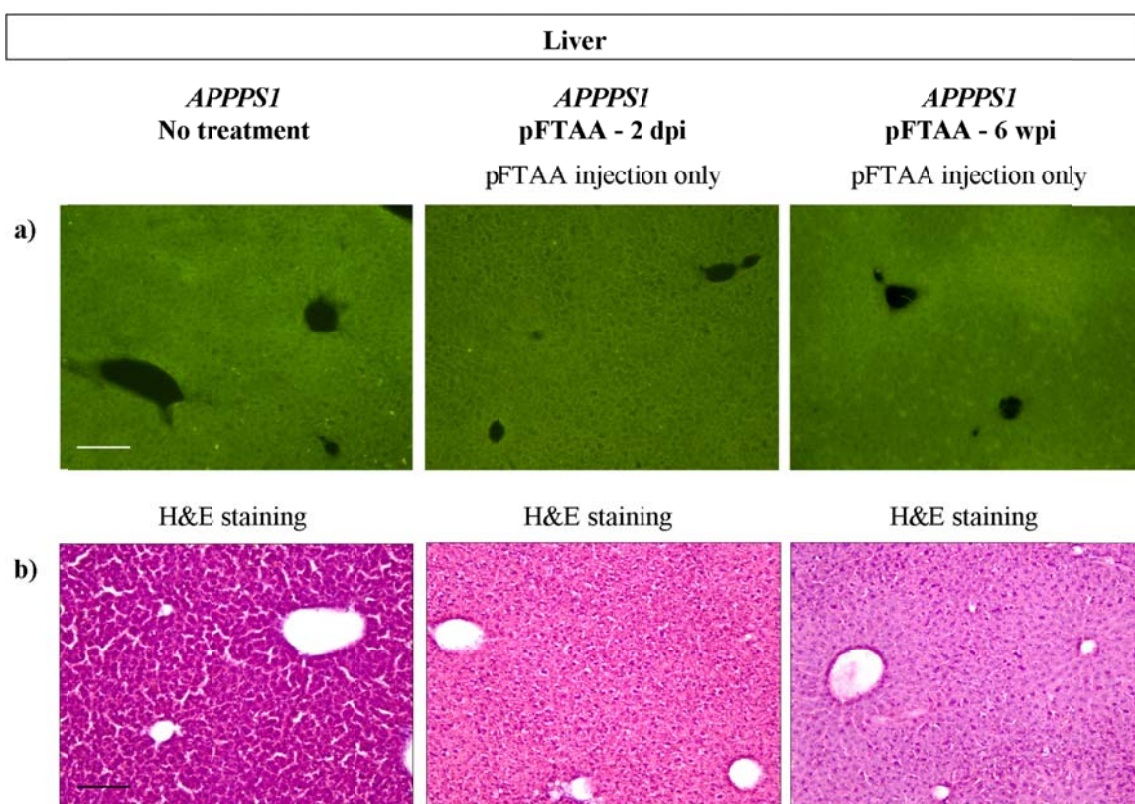


Figure 34: *Postmortem* histological analysis of the liver for systemic pFTAA deposition (a) and pathological abnormalities (b) after peripheral short term pFTAA treatment. Scale bar = 100 μ m.

Results

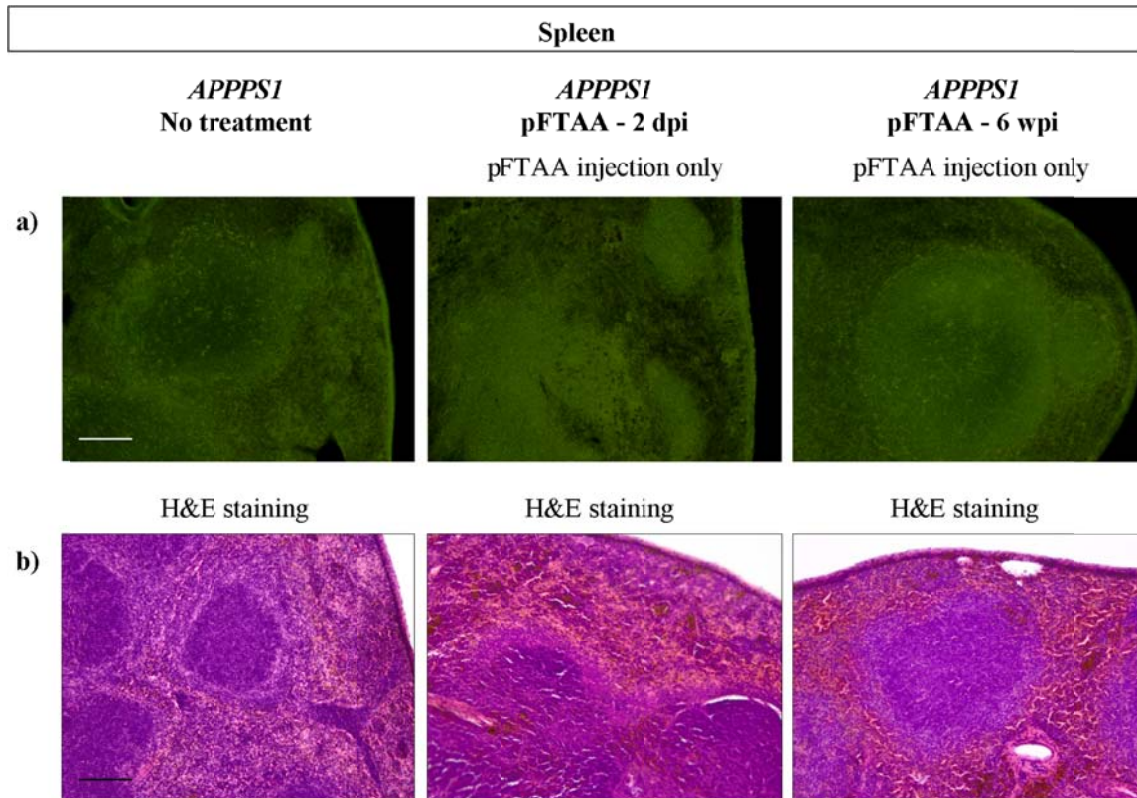


Figure 35: *Postmortem* histological analysis of the spleen for systemic pFTAA deposition (a) and pathological abnormalities (b) after peripheral short term pFTAA treatment. Scale bar = 100 μ m.

As shown in depicted figures above, apart from background signals (as visualized in renal tissue) no accumulation of pFTAA labeled aggregates was detected by fluorescence microscopy in the analyzed peripheral organs two days and six weeks after two consecutive pFTAA injections. Short term pFTAA treatment also caused no major pathological changes in analyzed peripheral organs. H&E stained paraffin sections of peripheral organs showed no difference between untreated and short term pFTAA treated, aged *APPPSI* mice. Histological analyses of peripheral organs indicate that a short term pFTAA treatment caused no abnormal deposition of pFTAA and no obvious pathological side effects in the murine system for up to six weeks after pFTAA injection.

3.2 LCOs coupled to magnetic nanoparticles as novel MRI contrast agents for diagnostics of Alzheimer's disease

LCOs as novel amyloid binding agents were shown to identify A β assemblies *in vitro* and A β deposits on tissue sections selectively and with high specificity. In addition, it was also shown that i.v. applied LCOs in transgenic AD mice passed the BBB readily and labeled cerebral A β plaques efficiently³⁹. Even after a peripheral i.p. application of the pentameric LCO pFTAA cerebral A β plaques revealed specific fluorescent labeling one day but also six weeks after injection (see chapter 3.1.2). In a next step, LCOs were investigated as potential *in vivo* amyloid tracers for human AD diagnostics. Since imaging of pathological A β deposition adopted a central role in AD diagnostics, specific and readily available amyloid binding agents are needed. For this purpose LCOs were coupled to MNPs with reactive groups and different spacer components. Optical imaging and the non-invasive MRI technique was used for A β plaque visualization in *APPPSI* mice.

The diagnostic utilization of LCOs coupled to reactive groups and different spacer components (termed LCO derivatives), and finally also of LCOs attached to MNPs (termed LCO-MNPs) was analyzed stepwise. When LCO labeling of cerebral A β plaques was detected after LCO-MNP injections, further MRI analyses were performed by collaborators from the group of Prof. Olav Haraldseth, Department of Circulation and Medical Imaging at the NTNU in Trondheim, Norway.

3.2.1 Staining of murine brain tissue with LCO derivatives and LCO-MNPs

Before distinct LCO derivatives and LCO-MNPs were tested *in vivo*, it was investigated if they are capable to label A β plaques on *APPPSI* brain sections. Brain sections were stained with the same concentration of LCO derivatives and LCO-MNPs and fluorescent intensities of labeled A β plaques were analyzed by fluorescence microscopy. Exposure times for picture capturing were kept constant and compared to pFTAA stainings as an internal reference. Only when the fluorescent signal emitted from labeled cerebral A β plaques on *APPPSI* brain sections lead to an overexposure with the given exposure time, the exposure time was manually adjusted.

LCO derivatives were synthesized based on the backbone of the LCO qFTAA. This quaternary LCO was attached to a reactive propyne group (4004 – qFTAA-propargyl), with short (4011 – phosphonate-TEG-qFTAA) and long (4010 – phosphonate-Cyr15-qFTAA)

Results

spacers with a terminal reactive group as well as with short spacers without a terminal reactive group (4020 – OH-TEG-qFTAA, 4021 – qFTAA-TEMPO).

At a LCO concentration of 14 μM LCO derivatives 4004, 4010, 4011 and 4020 demonstrated labeling of cerebral A β plaques on tissue sections, although with different efficacy. Despite the fact that all probes were used at same concentration, pFTAA revealed the highest fluorescent intensity signals (Fig. 36). Among the LCO derivatives probe 4010 showed the highest fluorescent intensity signal, followed by probe 4010, 4004, 4011 and 4020.

Results

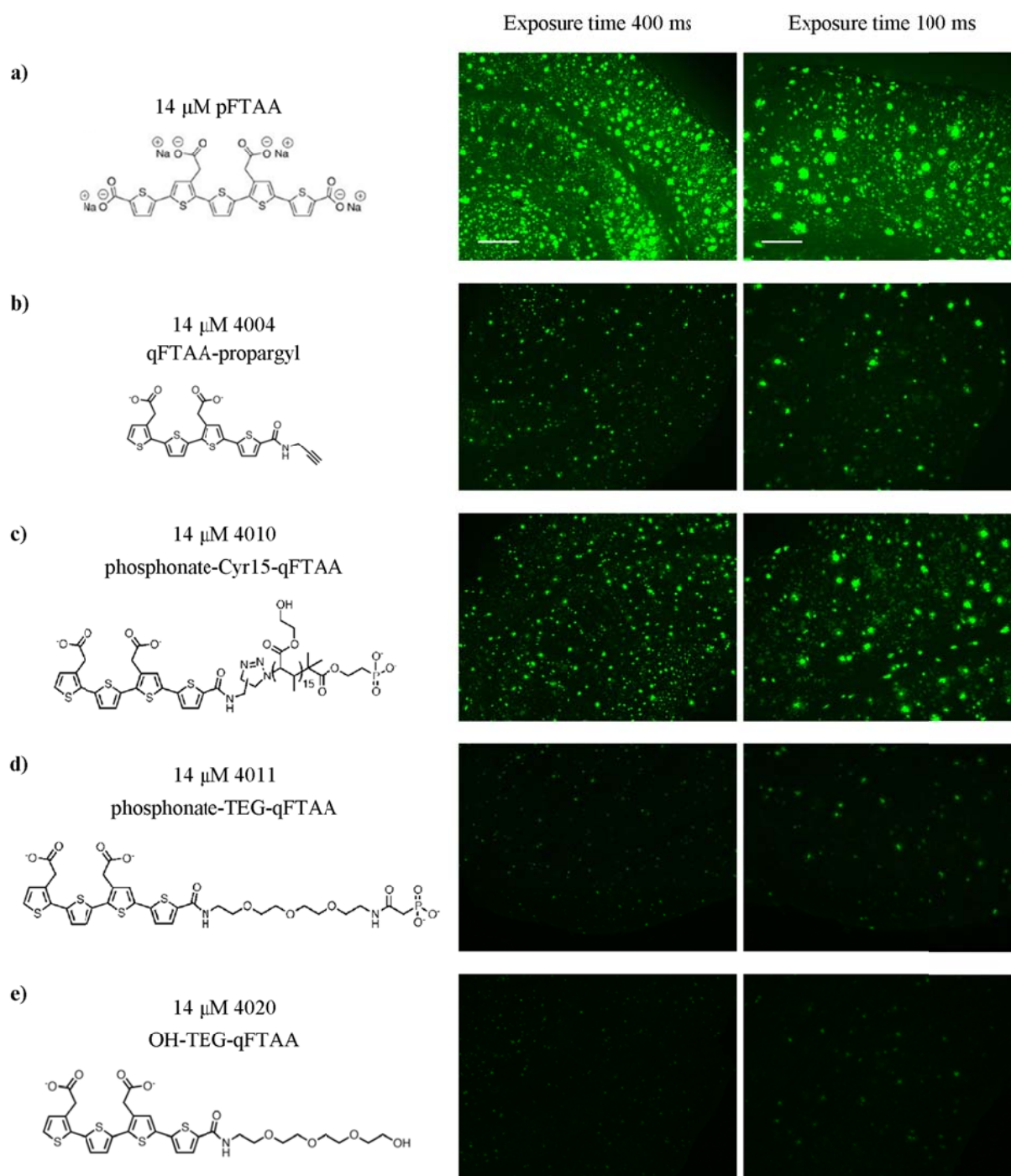


Figure 36: A β staining on *APPPS1* brain sections with 14 μ M pFTAA and LCO derivatives 4004 (qFTAA-propargyl), 4010 (phosphonate-Cyr15-qFTAA), 4011 (phosphonate-TEG-qFTAA) and 4020 (OH-TEG-qFTAA). pFTAA and LCO derivatives 4004, 4010, 4011 and 4020 were diluted in 1x PBS to a final LCO concentration of 14 μ M and used for A β plaque staining on *APPPS1* brain sections. Fluorescent intensities of LCO labeled, cerebral A β plaques after staining with distinct LCO derivatives were compared using fluorescence microscopy (FITC, Zeiss Observer Z1) to the fluorescent signals of plaques labeled by pFTAA (14 μ M) at an exposure time of 400 ms (Scale bar = 200 μ m) and 100 ms (Scale bar = 100 μ m).

Since the concentration of the LCO derivative 4021 (qFTAA-TEMPO), where qFTAA is attached to a short linker, was unknown, a dilution of 14 μ M could not be prepared. To evaluate the labeling capacity of LCO derivative 4021 to A β plaques on *APPPS1* brain

Results

sections, serial dilutions of probe 4021 were prepared and the fluorescent intensity was compared to pFTAA. The fluorescent images show, that even at high dilutions probe 4021 labeled A β plaque on cerebral sections (Fig. 37).

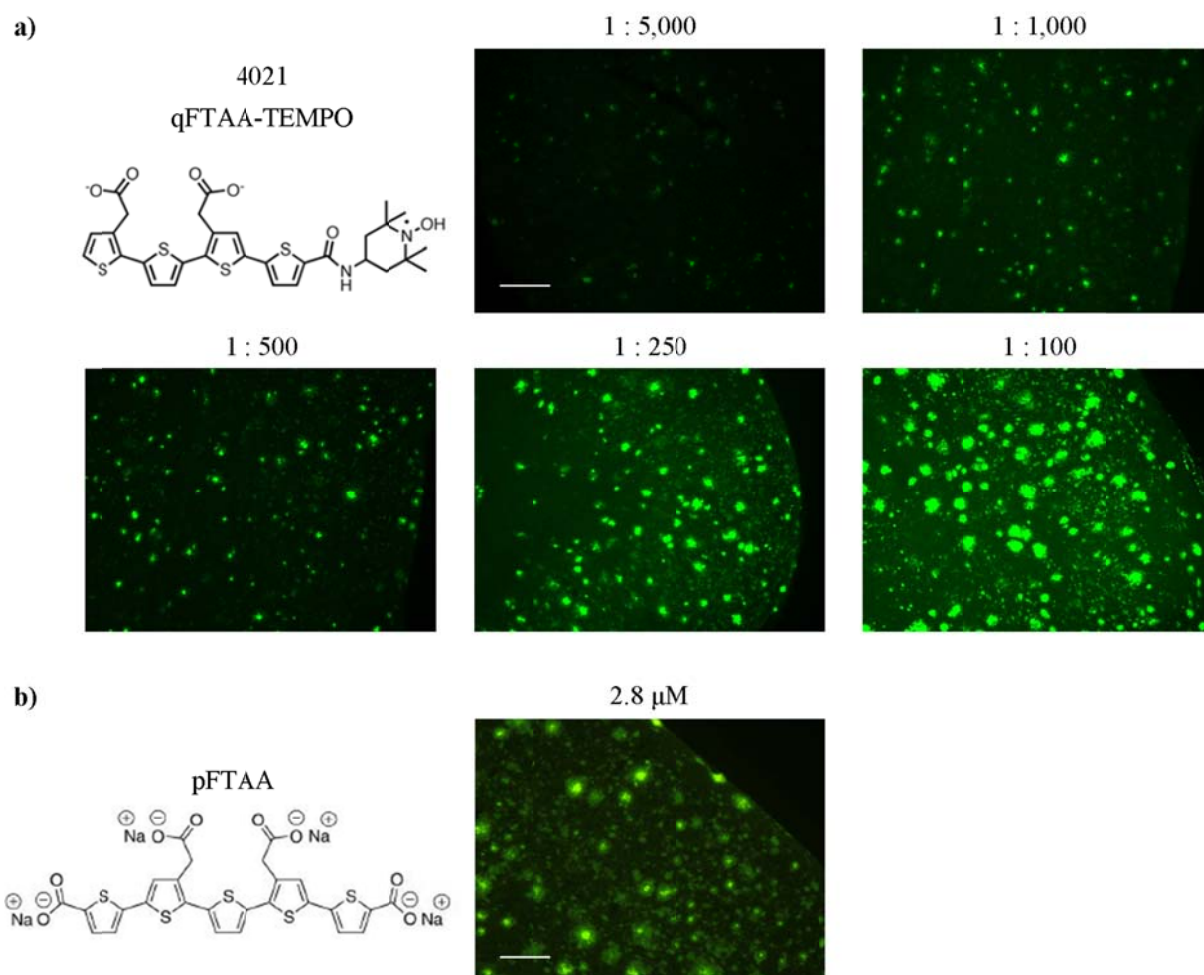


Figure 37: Staining of *APPPS1* brain sections with LCO derivative 4021 (qFTAA-TEMPO). For A β plaque staining on *APPPS1* brain sections, powdered LCO derivative 4021 was dissolved in 1 ml ddH₂O and a dilution series (1:5,000, 1:1,000, 1:500, 1:250, 1:100 in 1x PBS) was prepared. Subsequently the staining efficacy of labeled A β plaques on *APPPS1* tissue sections was analyzed at an exposure time of 100 ms (a) and compared to the fluorescent intensity of cerebral A β plaques using the common 2.8 μ M pFTAA dilution (b) by fluorescence microscopy (FITC, Zeiss Observer Z1). Scale bar = 100 μ m.

Probe 4012 (GdF3-PEG-NP-Cyr15-qFTAA) and 4013 (GdF3-PEG-NP-TEG-qFTAA) were investigated as representative LCO-MNPs for qFTAA linked to GdF3 with a long (4012) or short (4013) spacer. A β plaque labeling of *APPPS1* brain sections of both LCO-MNPs was compared to a pFTAA staining. All three probes were diluted to a final concentration of 0.4 μ M and A β plaque labeling of *APPPS1* mouse brain sections was analyzed by fluorescence microscopy. Homogeneous staining of cortical A β plaques was achieved with all three probes. However, A β labeling with MNP-LCO 4012 could only be visualized with a

Results

fourfold increase in exposure time (1,000 ms) compared to stainings with pFTAA and LCO-MNP 4013 (250 ms) as depicted in figure 38.

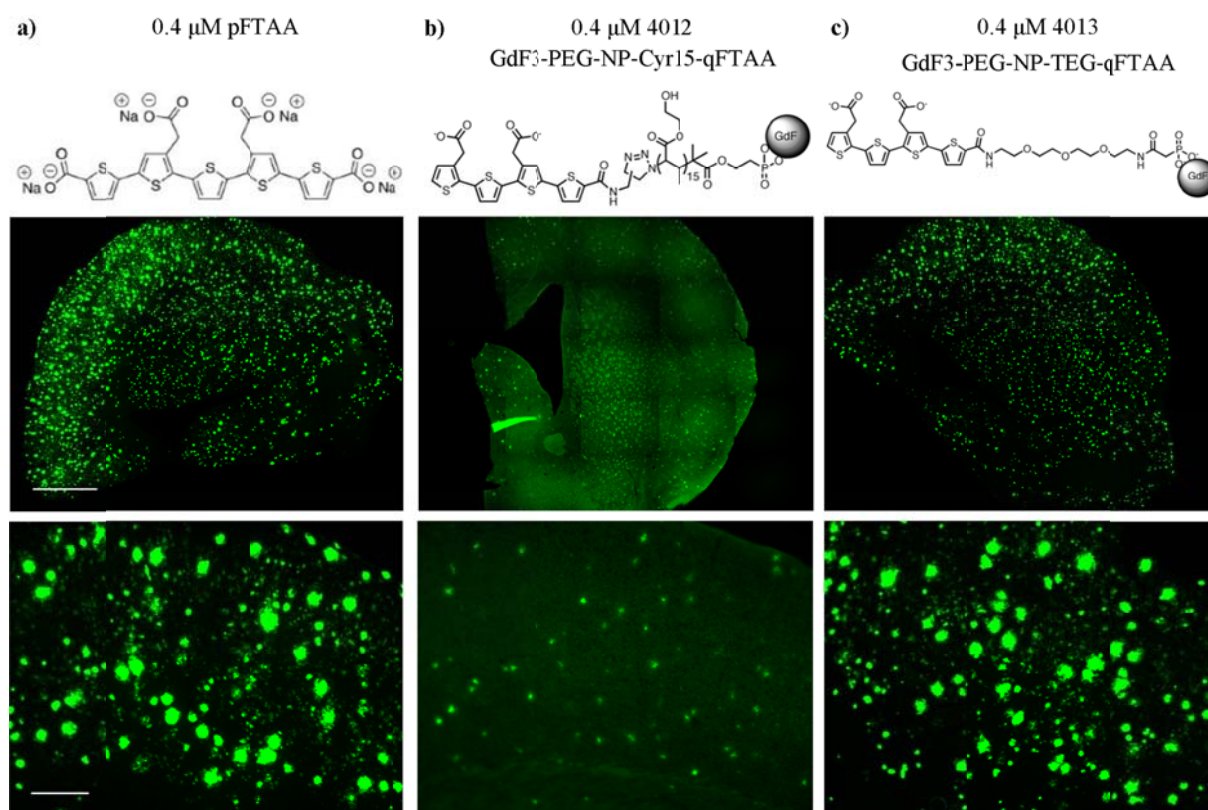


Figure 38: $A\beta$ staining on *APPPS1* brain sections with LCO-MNPs 4012 (GdF3-PEG-NP-Cyr15-qFTAA) and 4013 (GdF3-PEG-NP-TEG-qFTAA). Fluorescent signals after the $A\beta$ plaque staining of *APPPS1* brain sections with pFTAA (a) and LCO-MNPs 4012 (b) and 4013 (c), all diluted to a final LCO concentration of 0,4 μ M, were compared by fluorescence microscopy (FITC, Zeiss Observer Z1). The fluorescent signal of $A\beta$ plaque staining with LCO-MNPs 4012 was captured at an exposure time of 1000 ms (b), fluorescent signals of stainings with pFTAA (a) and LCO-MNP 4013 (c) required an exposure time of 250 ms. Scale bar (upper row) = 1,000 μ m. Scale bar (lower row) = 100 μ m.

Synthesized LCO-MNPs based on the pentameric LCO pFTAA coupled to GdF3 MNPs - 5010 (GdF3-PEG-spcr26-2%-pFTAA) and 5011 (GdF3-PEG-spcr26-10%-pFTAA) - were also tested for $A\beta$ plaque labeling on *APPPS1* brain sections. The difference between both pentameric LCO-MNPs is a 2 % (5010) and 10 % (5011) coating of the GdF3 MNP with pFTAA. At a LCO concentration of 0.2 μ M LCO-MNP 5010 and 5011 showed efficient labeling of cerebral $A\beta$ plaques on *APPPS1* brain sections comparable to the fluorescent intensity of plaque labeling achieved with a pFTAA staining solution of same LCO concentration (Fig. 39).

Results

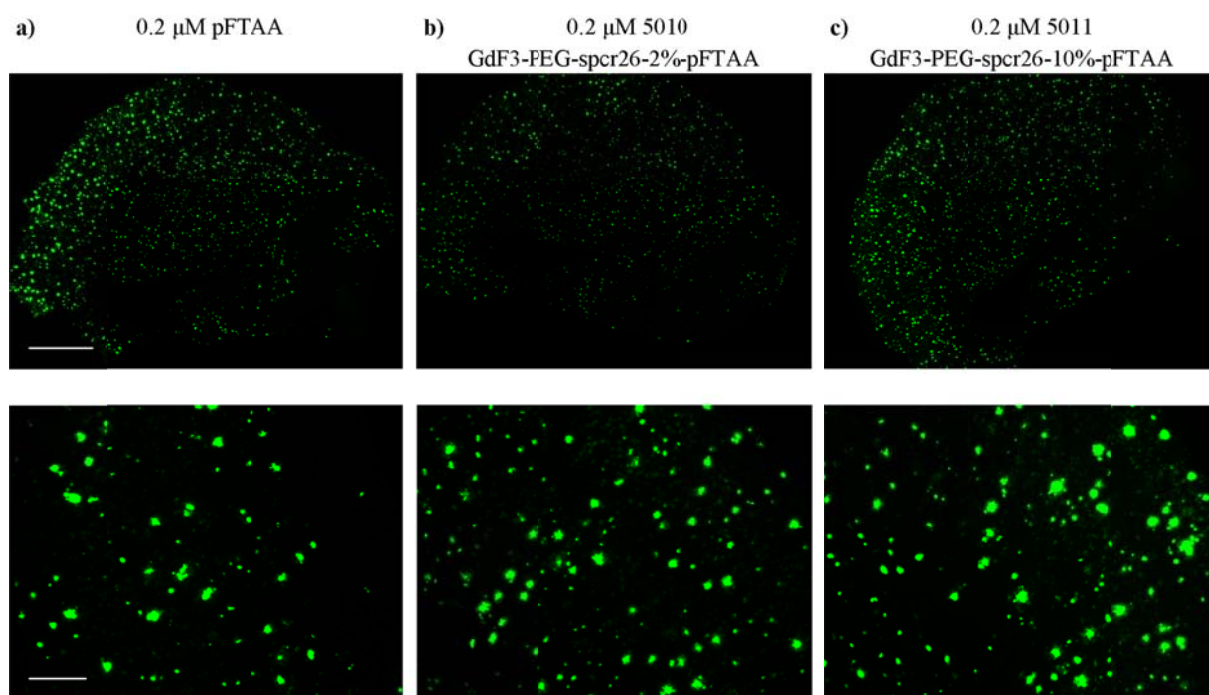


Figure 39: A β staining on *APPPS1* brain sections with pentameric LCO-MNPs 5010 (GdF3-PEG-spcr26-2%-pFTAA) and 5011 (GdF3-PEG-spcr26-10%-pFTAA). Brain sections of an aged *APPPS1* mouse were stained with 0.2 μ M dilutions of pFTAA (a) and LCO-MNPs 5010 (b) and 5011 (c). Fluorescent intensities of labeled A β plaques were detected and compared using fluorescence microscopy (FITC, Zeiss Observer Z1). An exposure time of 100 ms was used for detection of depicted images. Scale bar = 1,000 μ m (upper row), Scale bar = 100 μ m (lower row).

Probe 5012 is based on the pentameric LCO pFTAA and is attached to a single gadolinium molecule instead of a GdF3 MNP (Fig. 40, termed LCO-MNP derivative 5012 throughout this thesis).

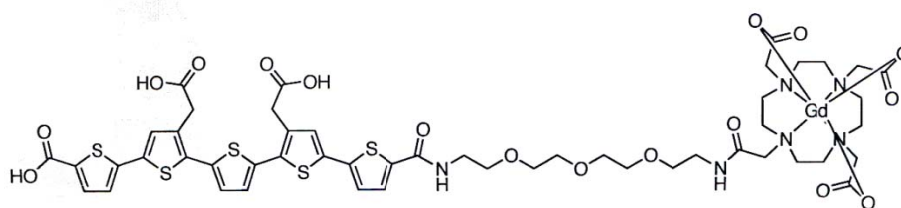


Figure 40: Chemical structure of LCO-MNP derivative 5012. LCO-MNP derivative 5012 represents a particle, where the pentameric LCO pFTAA is coupled to a gadolinium molecule instead of a GdF3 MNP.

For A β staining on *APPPS1* brain sections, LCO-MNP derivative 5012 was diluted to a LCO concentration of 16 μ M and fluorescent intensity of the cerebral A β plaque labeling was compared by fluorescence microscopy to a pFTAA staining of the same concentration. Both probes revealed homogenous labeling of cortical A β plaques at an exposure time of 100 ms. However, at the exposure time of 100 ms the pFTAA fluorescent signal was stronger than the signal of LCO-MNP derivative 5012 (Fig. 41).

Results

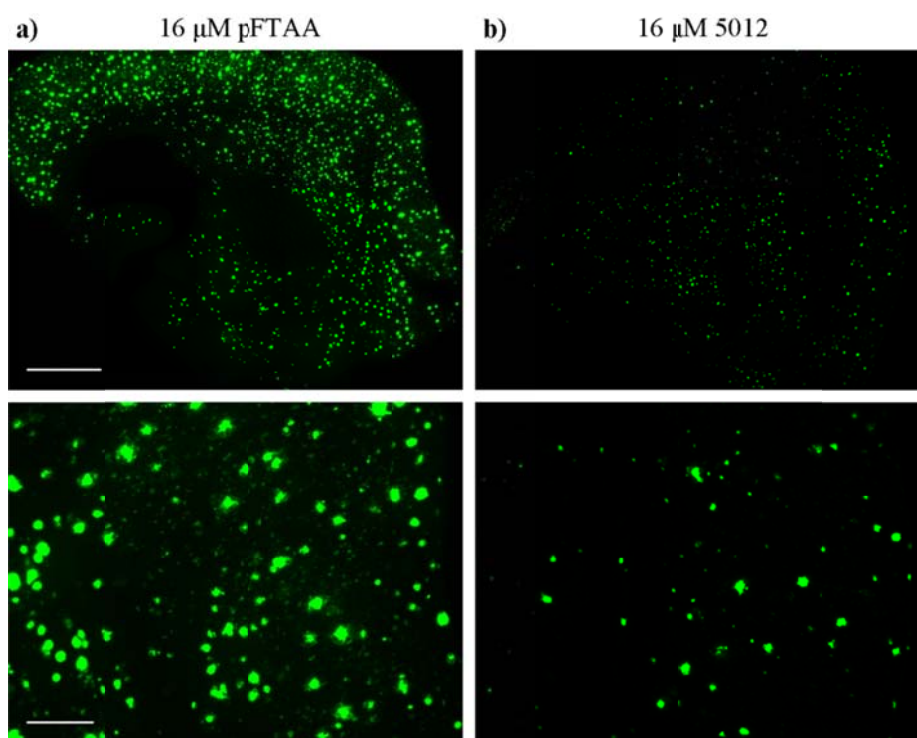


Figure 41: A β staining on *APPPS1* brain sections with LCO-MNP derivative 5012. LCO-MNP derivative 5012 is based on the pentameric LCO pFTAA and coupled through a short linker to a single magnetic gadolinium molecule. Fluorescent signals of the A β staining on *APPPS1* brain sections with LCO-MNP derivative 5012 (b) were analyzed by fluorescence microscopy (FITC, Zeiss Observer Z1) and compared to the fluorescent intensity of labeled A β plaques achieved with a pFTAA staining (a) of the same concentration (16 μ M). Images were taken at an exposure time of 100 ms. Scale bar = 1,000 μ m (upper row), Scale bar = 100 μ m (lower row).

Besides quaternary and pentameric LCO-MNPs coupled to GdF3 MNPs also an FeO MNP conjugated with qFTAM was tested for A β plaque labeling on *APPPS1* brain sections (Fig. 42). Superparamagnetic FeO particles present the currently preferred MRI contrast agents for *in vitro* and *in vivo* imaging, are biocompatible and can be reused or recycled by the organism for iron metabolism⁸⁷.

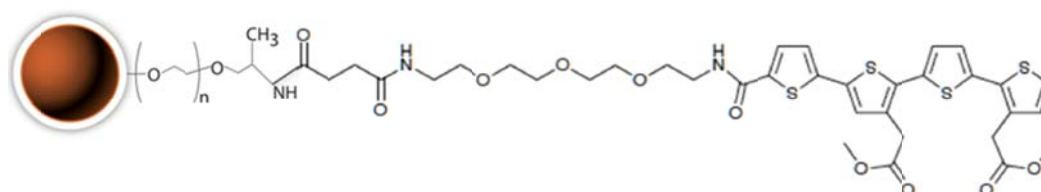


Figure 42: Chemical structure of LCO-MNP 4026 (qFTAM-TEG-Succ-NHS amino PEG). To synthesize the LCO-MNP 4026, 190 qFTAM molecules attached to a short linker (qFTAM-TEG-succ-NHS) were used to cover a PEG coated iron oxide nanostructure. Source: GENOVIS, Lund, Sweden.

Results

First the A β plaque labeling ability of LCO-MNP 4026 (qFTAM-TEG-Succ-NHS amino PEG) on *APPPSI* brain sections was investigated. The exact concentration of LCO-MNP 4026 was not determined after synthesis, but since 190 qFTAM molecules were attached per FeO MNP, the LCO concentration should be $\leq 190 \mu\text{M}$. Stock solutions of LCO-MNP 4026 and pFTAA were diluted to a final LCO concentration of $20 \mu\text{M}$. Staining of A β plaques on *APPPSI* brain sections with LCO-MNP 4026 showed a specific and homogenous, but compared to pFTAA, a much weaker fluorescent signal over the entire cortex. The exposure time for LCO-MNP 4026 was even increased eight times (800 ms) compared to the pFTAA control (100 ms; Fig. 43).

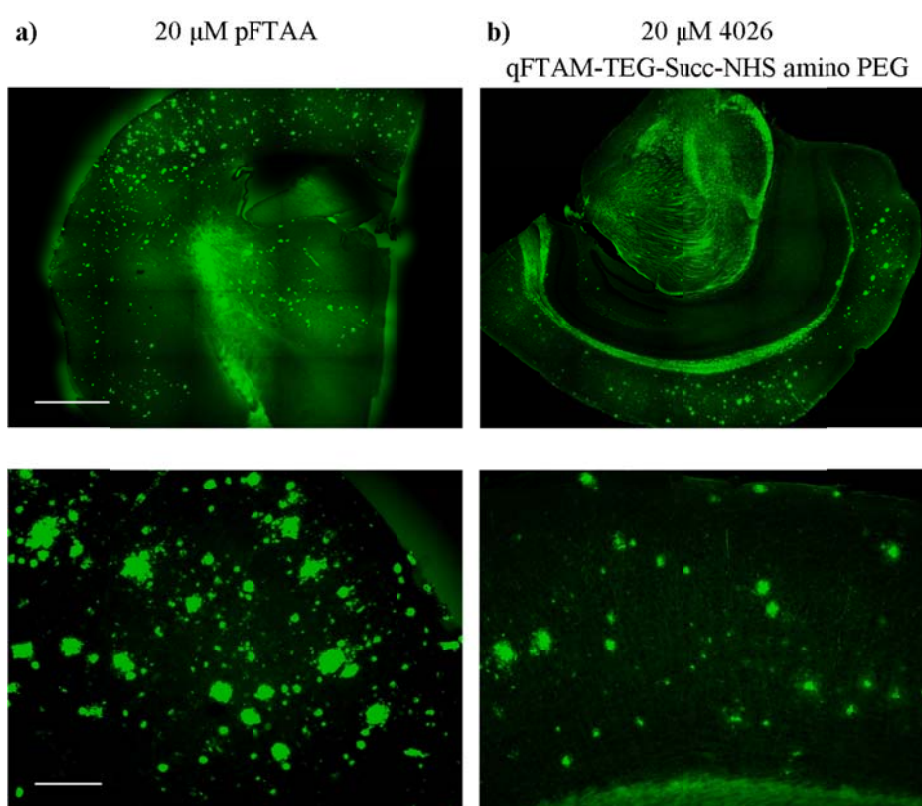


Figure 43: A β staining on *APPPSI* brain sections with LCO-MNP 4026 (qFTAM-TEG-Succ-NHS amino PEG). LCO-MNP 4026, where 190 qFTAM molecules were coupled to a FeO nanostructure, was tested for A β plaque labeling on *APPPSI* brain sections using fluorescence microscopy (FITC, Zeis Observer Z1, (b)). The fluorescent intensity after A β staining of cerebral *APPPSI* sections by LCO-MNP 4026 ($20 \mu\text{M}$) was compared to fluorescent signals achieved from pFTAA stained sections ($20 \mu\text{M}$ staining solution, (a)). Depicted images were taken at an exposure time of 800 ms (b) and 100 ms (a). Scale bar = $1,000 \mu\text{m}$ (upper row), Scale bar = $100 \mu\text{m}$ (lower row).

In summary all tested LCO derivatives independent of coupled reactive groups, short or long spacers and GdF3 or FeO based MNPs were capable to stain cerebral A β deposits on brain sections of aged *APPPSI* mice. Compared to pFTAA all LCO derivatives and LCO-MNPs showed weaker fluorescent intensity signals.

3.2.2 Investigation of LCO derivatives and LCO-MNPs for blood brain barrier crossing after peripheral application

LCO derivatives and LCO-MNPs showed efficient A β plaque labeling on *APPPSI* brain sections (see chapter 3.2.1), but it was not known, if these probes cross the BBB after peripheral i.v. injection and are able to efficiently label cerebral A β -plaques after peripheral application. To address these unknown parameters, aged *APPPSI* mice were treated i.v. on two consecutive days with previously described probes and fluorescent intensity of cerebral A β plaque labeling was analyzed on cerebral sections *postmortem* (Fig. 44). Since LCO derivatives and LCO-MNPs were only available at low concentrations, all probes were used at stock concentrations varying between 28.69 μ M and 8.5 mM (see chapter 2.1).

To control for the crossing of the BBB by the tested LCO derivative pFTAA was used in the same experimental set up as internal reference at concentrations ranging from 20 μ M, 0.5 mM, 7 mM and 14 mM pFTAA. Experimental groups are depicted in table 12.

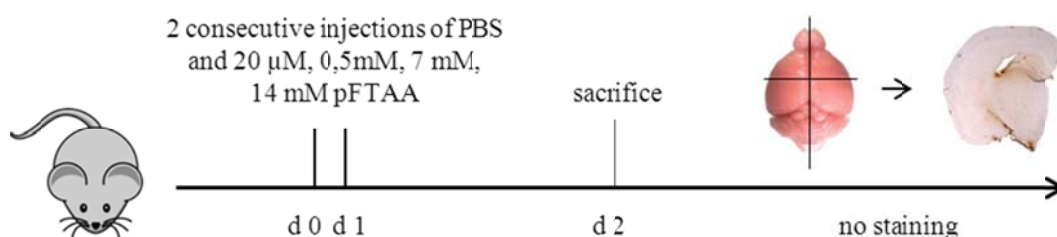


Figure 44: Experimental setup for i.v. injection of PBS and different pFTAA concentrations in aged *APPPSI* mice. To compare fluorescent intensities of cerebral A β plaque labeling after i.v. injection of different pFTAA concentrations, age matched *APPPSI* mice were treated with several pFTAA dilutions. As negative control PBS was injected to an *APPPSI* control mouse. Mice were treated on two consecutive days and sacrificed one day after the second injection. Unstained cerebral sections were analyzed for pFTAA labeling of cerebral A β deposits by fluorescence microscopy.

Table 12: Experimental mice for i.v. injections of PBS and different pFTAA concentrations in aged *APPPSI* mice

Genotype	Age	Treatment
<i>APPPSI</i>	390 d	2x PBS, i.v.
	382 d	2x 20 μ M pFTAA, i.v.
	398 d	2x 0.5 mM pFTAA, i.v.
	356 d	2x 7 mM pFTAA, i.v.
	374 d	2x 14 mM pFTAA, i.v.

Cerebral sections of PBS and pFTAA treated *APPPSI* mice were analyzed *postmortem* by fluorescence microscopy. Fluorescent intensity of cerebral A β plaque labeling after i.v. injection of different pFTAA concentrations was compared.

Results

Labeling of A β plaques with 20 μ M pFTAA showed extremely weak fluorescent intensity signals, which are barely distinguishable from autofluorescence of cerebral A β deposits. Specific labeling of cortical A β plaques was only visible after injections of 0.5 mM, 7 mM and 14 mM pFTAA (Fig. 45).

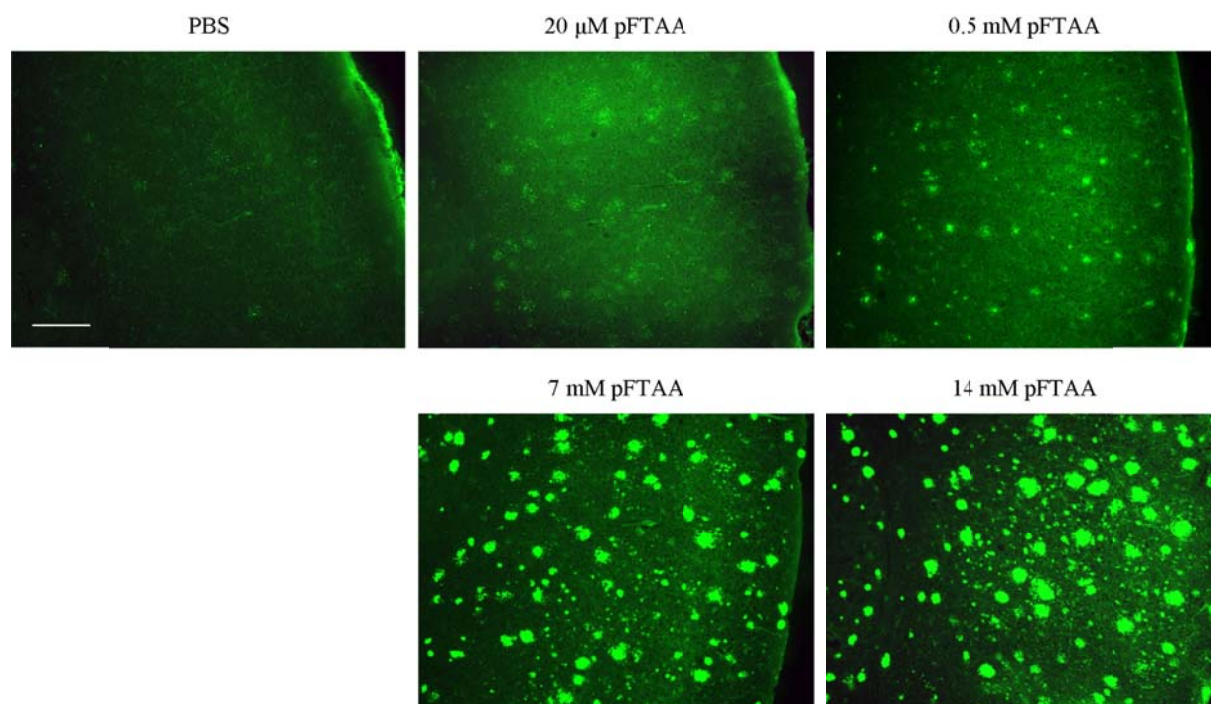


Figure 45: I.v. application of PBS and distinct pFTAA concentrations to aged *APPPS1* mice. Age matched *APPPS1* mice with robust plaque load were injected i.v. on two consecutive days with 1x PBS and four different pFTAA concentrations: i) 20 μ M, ii) 0.5 mM, iii) 7 mM, iv) 14 mM. Treated animals were sacrificed 24 h after the second application. Fluorescent intensity of cerebral A β plaque labeling was analyzed and compared on brain sections *postmortem* by fluorescence microscopy (FITC, Zeiss Observer Z1). All images were taken at an exposure time of 1,000 ms. Scale bar = 100 μ m.

In a next step aged *APPPS1* mice were i.v. injected on two consecutive days with i) different LCO derivatives attached to a reactive group (4004) or linked with short (4011, 4020, 4021) and long spacers (4010) as well as ii) GdF3 (4012, 4013, 5010, 5011, 5012) and iii) FeO (4026) based LCO-MNPs (Fig. 46). 100 μ l of the undiluted stock solution (Tab. 13) were applied per injection. LCO derivative treated mice were sacrificed one day after the second injection, in later experiments LCO-MNP treated *APPPS1* mice were sacrificed 1 week after the first injection (Fig. 46). The later time point for sacrifice was chosen since the time course of *in vivo* binding of pFTAA revealed reduced background labeling and a more restricted labeling of dense core plaques than diffuse A β deposits after longer incubation periods (see chapter 3.1.2.3). This phenomenon was observed and described also by our collaborators^{39,75}. *APPPS1* mice were not perfused before brains were taken to prevent eventual drainage of

Results

MNP-LCOs from the brain tissue. The right hemisphere was stored at $-80\text{ }^{\circ}\text{C}$ for subsequent spectral (Linköping University, Sweden) or MRI analyses (NTNU, Trondheim, Norway), whereas the left hemisphere was cut after formalin fixation and sucrose dehydration ($30\text{ }\mu\text{m}$ free floating sections) or fresh frozen ($7\text{ }\mu\text{m}$ sections) for immediate screening of efficient BBB crossing of the analyzed LCOs and derivatives.

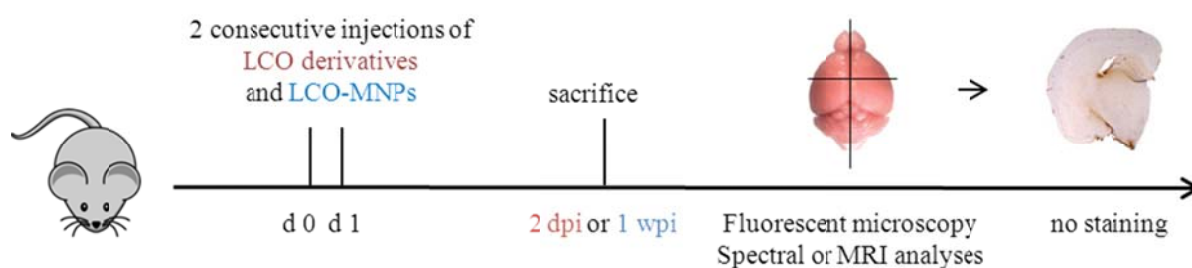


Figure 46: Experimental setup for i.v. injections with LCO derivatives and LCO-MNPs to aged *APPPS1* mice. To analyze if LCO derivatives and LCO-MNPs cross the BBB after peripheral injections, *APPPS1* mice were treated (i.v.) on two consecutive days with $100\text{ }\mu\text{l}$ of the undiluted stock solution (concentration see Tab. 13) of distinct probes. After treatment with LCO derivatives animals were sacrificed 2 dpi, after application with LCO-MNPs 1 wpi. Cerebral $\text{A}\beta$ plaque labeling on brain sections of LCO derivative and LCO-MNP treated mice was analyzed by fluorescence microscopy and compared to pFTAA injections with similar concentrations. The second hemisphere was used for subsequent spectral or MRI analyses.

Table 13: Concentrations of injected LCO derivative and LCO-MNP stock solutions

LCO derivatives	LCO concentration
4004 – qFTAA-propargyl	1.53 mM
4010 – phosphonate-Cyr15-qFTAA	0.52 mM
4011 – phosphonate-TEG-qFTAA	1.36 mM
4020 – OH-TEG-qFTAA	8.5 mM
4021 – qFTAA-TEMPO	not analyzed (powder dissolved in 1 ml ddH ₂ O)
LCO-MNPs	LCO concentration
4012 – GdF3-PEG-NP-Cyr15-qFTAA	43 μM
4013 – GdF3-PEG-NP-TEG-qFTAA	150 μM
4026 – qFTAM-TEG-Succ-NHS amino PEG	$\leq 190\text{ }\mu\text{M}$
5010 – GdF3-PEG-spcr26-2%-pFTAA	28.69 μM
5011 – GdF3-PEG-spcr26-10%-pFTAA	56.76 μM
5012	4.0 mM

Results

Fluorescent labeled A β plaques on brain sections of LCO derivative treated *APP^{PS1}* mice were analyzed *postmortem* using fluorescence microscopy. In comparison to control PBS and pFTAA injections (Fig. 45, 47a) only LCO derivative 4011 (Fig. 47d) led to specific labeling of cerebral A β plaques at high magnification, indicating to reveal best BBB crossing properties among tested LCO derivatives (Fig. 47).

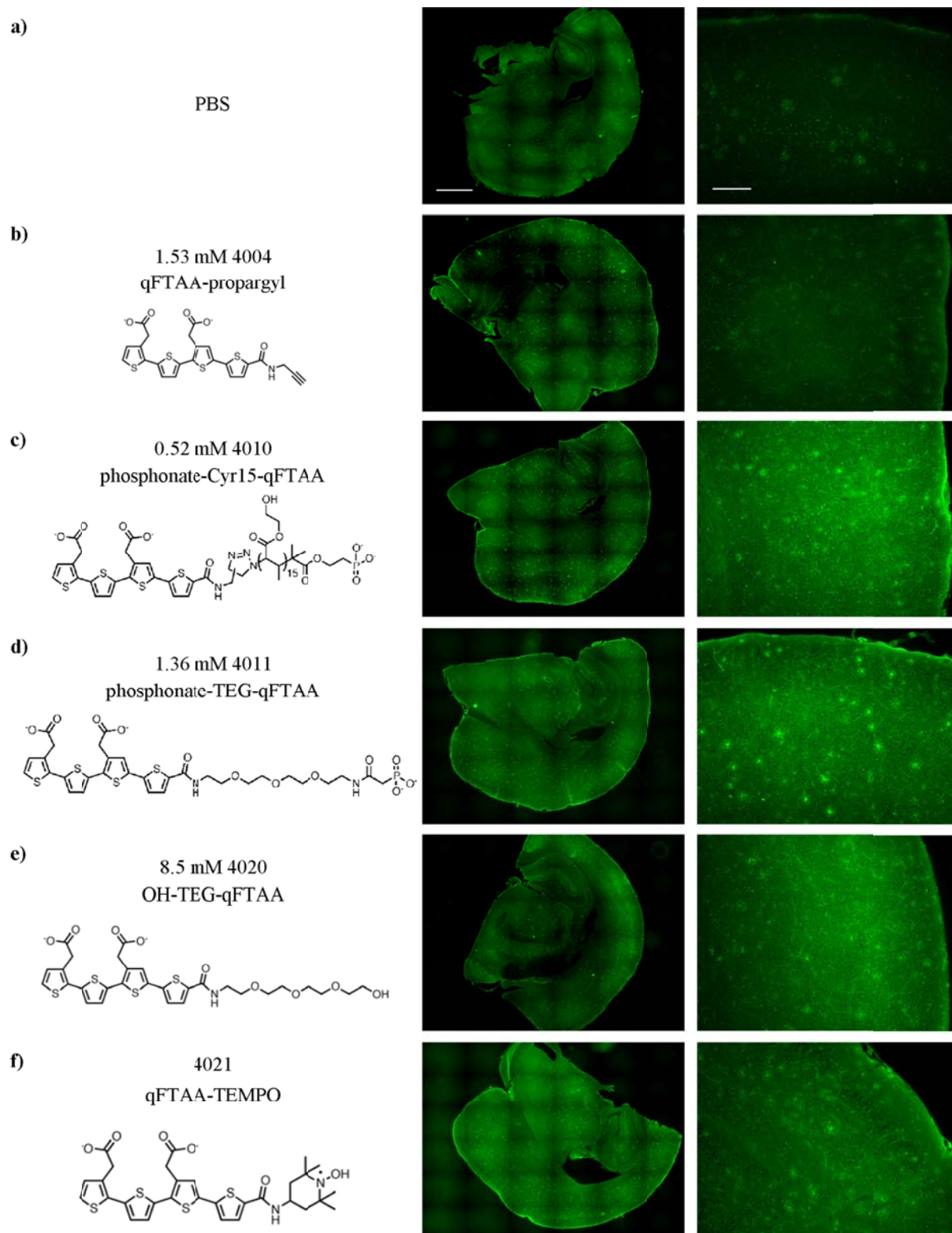


Figure 47: *In vivo* labeling of cerebral A β plaques after two consecutive i.v. injections of distinct LCO derivatives in aged *APP/PS1* mice. Cerebral sections of *APP/PS1* mice, treated on two consecutive days with LCO derivatives 4004 (b), 4010 (c), 4011 (d), 4020 (e) and 4021 (f) were analyzed *postmortem* by fluorescence microscopy (FITC, Zeiss Observer Z1) for A β plaque labeling. Fluorescent intensity of labeled cerebral A β plaques was compared to sections of animals, which were treated in parallel with PBS (a) and pFTAA (Fig. 45). Cortical A β plaques were analyzed using whole mount overview pictures (left row) and detailed pictures at higher magnification (right row). All images were taken at an exposure time of 2,000 ms. Scale bar = 1,000 μ m (left row), Scale bar = 100 μ m (right row).

Results

In a next step BBB crossing and cerebral A β plaque labeling in *APP/PS1* mice after peripheral i.v. injection of GdF3 based LCO-MNPs 4012 (GdF-PEG-NP-Cyr15-qFTAA; 43 μ M), 4013 (GdF-PEG-NP-TEG-qFTAA; 150 μ M), 5010 (GdF3-PEG-spcr26-2%-pFTAA; 28,7 μ M) and 5011 (GdF3-PEG-spcr26-10%-pFTAA, 56,8 μ M) was investigated.

Compared to A β plaques on brain sections of a PBS (Fig. 48a) treated *APP/PS1* mouse, LCO-MNP 4012 (Fig. 48b) achieved no specific A β plaque labeling but LCO-MNP 4013 (Fig. 48c) specifically labeled cerebral A β plaques at high magnification after two peripheral i.v. applications in aged *APP/PS1* mice.

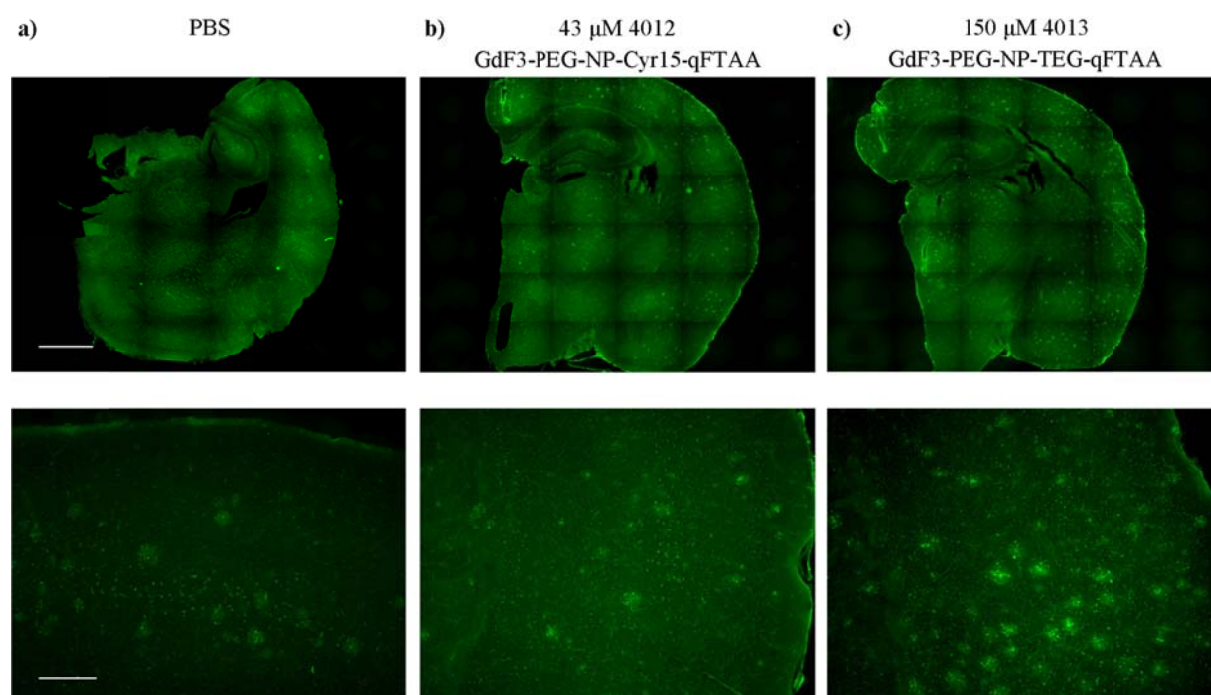


Figure 48: *In vivo* labeling of cerebral A β plaques after two consecutive i.v. injections of LCO-MNP 4012 (GdF3-PEG-NP-Cyr15-qFTAA) and 4013 (GdF3-PEG-NP-TEG-qFTAA) in aged *APP/PS1* mice. Cerebral A β plaque labeling on brain sections of *APP/PS1* mice, treated with LCO derivative 4012 (43 μ M, b) and 4013 (c) were analyzed *postmortem* by fluorescence microscopy (FITC, Zeiss Observer Z1). Fluorescence labeling of cerebral A β plaques was compared to plaques on sections of *APP/PS1* mice treated twice with PBS (a). A β plaques were analyzed by whole mount overview pictures (upper row) and in detail at higher cortical magnification (lower row). All images were taken at an exposure time of 2,000 ms. Scale bar = 1,000 μ m (upper row), Scale bar = 100 μ m (lower row).

As depicted above, efficient brain penetration of LCO-MNP 4013 was indicated after i.v. injection. Additional TEM analyses were performed to investigate, if the detected fluorescent labeling by LCO-MNP 4013 coincided with deposition of GdF3 MNPs around or within cerebral A β plaques. For this purpose, single cortical A β plaques and meningeal vessels were analyzed by TEM after two i.v. injections of PBS, LCO-MNP 4012 and 4013. Compared to PBS treated *APP/PS1* mice (Fig. 49a), no GdF3 MNPs were visible around and within cerebral

Results

A β plaques on ultrathin cerebral sections of LCO-MNP 4012 (Fig. 49b) and 4013 (Fig. 49c) injected mice.

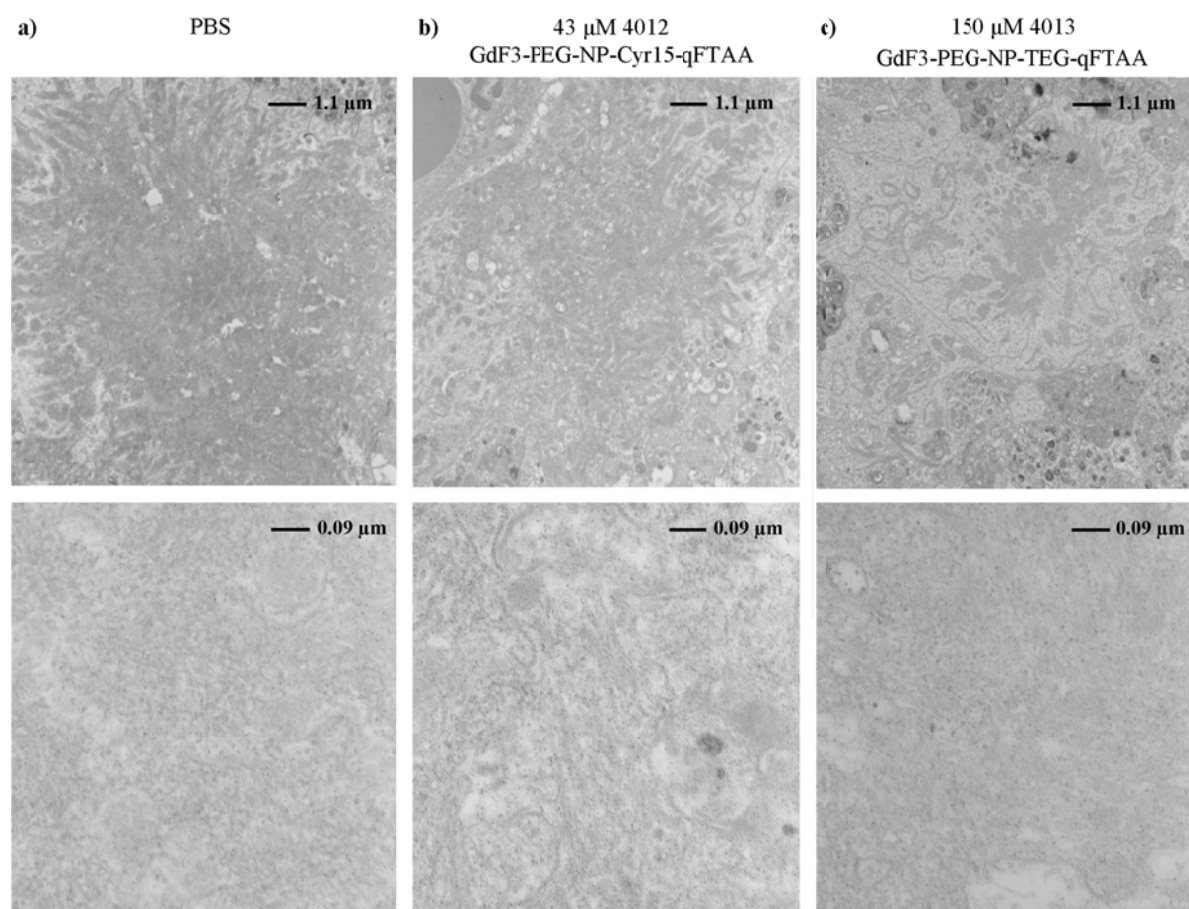


Figure 49: TEM images of single cerebral A β plaques after two consecutive i.v. injections of PBS, LCO-MNP 4012 (GdF3-PEG-NP-Cyr15-qFTAA) and 4013 (GdF3-PEG-NP-TEG-qFTAA) in *APP/PS1* mice. Left hemisphere of aged *APP/PS1* mice i.v. injected on two consecutive days with PBS and stock solutions of LCO-MNPs 4012 (43 μ M) and 4013 (150 μ M) were fixed in glutaraldehyde for subsequent TEM analyses. Single cerebral A β plaques on ultrathin brain sections of PBS (a), LCO-MNP 4012 (b) and LCO-MNP 4013 (c) treated *APP/PS1* mice are depicted in the 7,000 fold magnification (upper row). The 85,000 fold magnification (lower row) shows A β fibrils in detail.

Since no GdF3 MNPs have been detected around and within cerebral A β plaques by TEM (Fig. 49) and previous investigations showed that A β plaques close to the ventricles and the meninges are labeled first after peripheral injection of several probes, single meningeal vessels were further analyzed for GdF3 MNPs using TEM.

However, TEM analysis of meningeal vessels showed no immobilized GdF3 MNPs on vessel walls after two i.v. injections of LCO-MNPs 4012 (Fig. 50b) and 4013 (Fig. 50c). These results were confirmed by analysis of ultrathin cerebral sections from PBS treated *APP/PS1* mice (Fig. 50a) and indicate that LCO-MNPs 4012 and 4013 might not have passed the BBB.

Results

Especially for LCO-MNP 4013 this result is surprising since an efficient fluorescent cerebral A β plaque labeling was observed previously (Fig. 48c).

Since TEM analyses visualize a limited cerebral area it is imaginable that MNPs could not be captured. A small number of cerebral A β plaques in the cortical periphery and close to ventricles as well as cerebral vessels were analyzed. Thus it is conceivable that LCO-MNPs were not detected.

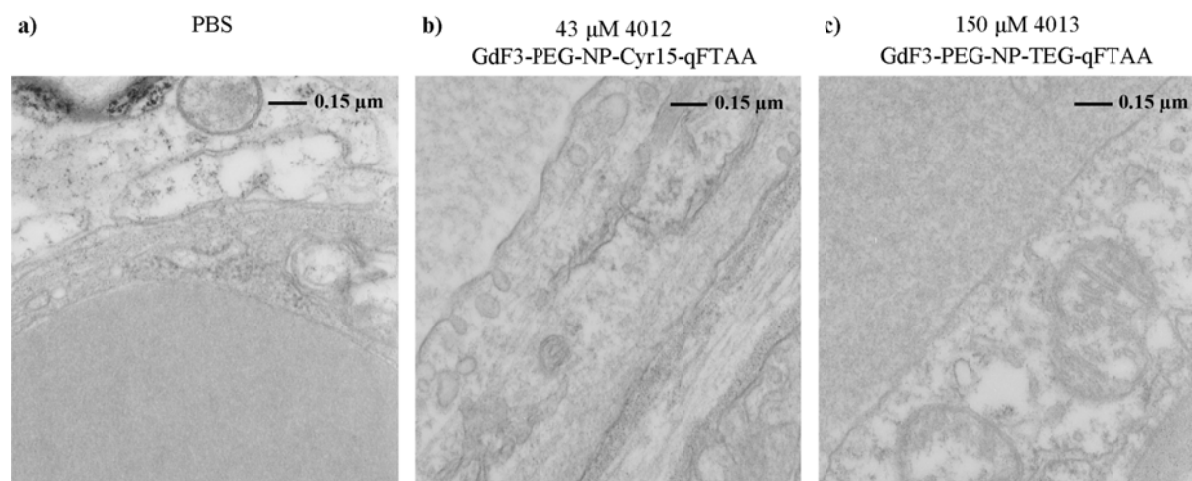


Figure 50: TEM images of single meningeal vessels after two consecutive i.v. injections of PBS, LCO-MNP 4012 (GdF3-PEG-NP-Cyr15-qFTAA) and 4013 (GdF3-PEG-NP-TEG-qFTAA) in *APPPS1* mice. For TEM analyses of GdF3 MNPs in vessel walls, the left hemisphere of PBS, LCO-MNP 4012 and 4013 treated aged *APPPS1* mice was fixed without previous perfusion in glutaraldehyd. The 85,000 fold magnification of single vessel walls on ultrathin cerebral sections is depicted.

As further LCO-MNPs the pentameric probes 5010 and 5011 were analyzed for BBB passing. Whole mount overview images revealed a weak labeling of cerebral A β plaques in aged *APPPS1* mice after two consecutive injections of 50 μM pFTAA (control injection), 29.7 μM 5010 and 56.8 μM 5011 (Fig. 51, upper row). In contrast, a more detailed analysis at a higher magnification showed efficient and specific pFTAA labeled A β plaques one week after two consecutive i.v. injections of 50 μM pFTAA, MNP-LCOs 5010 and 5011, whereby a slightly higher fluorescent intensity was detected after the injection of 50 μM pFTAA (Fig. 51, lower row).

Results

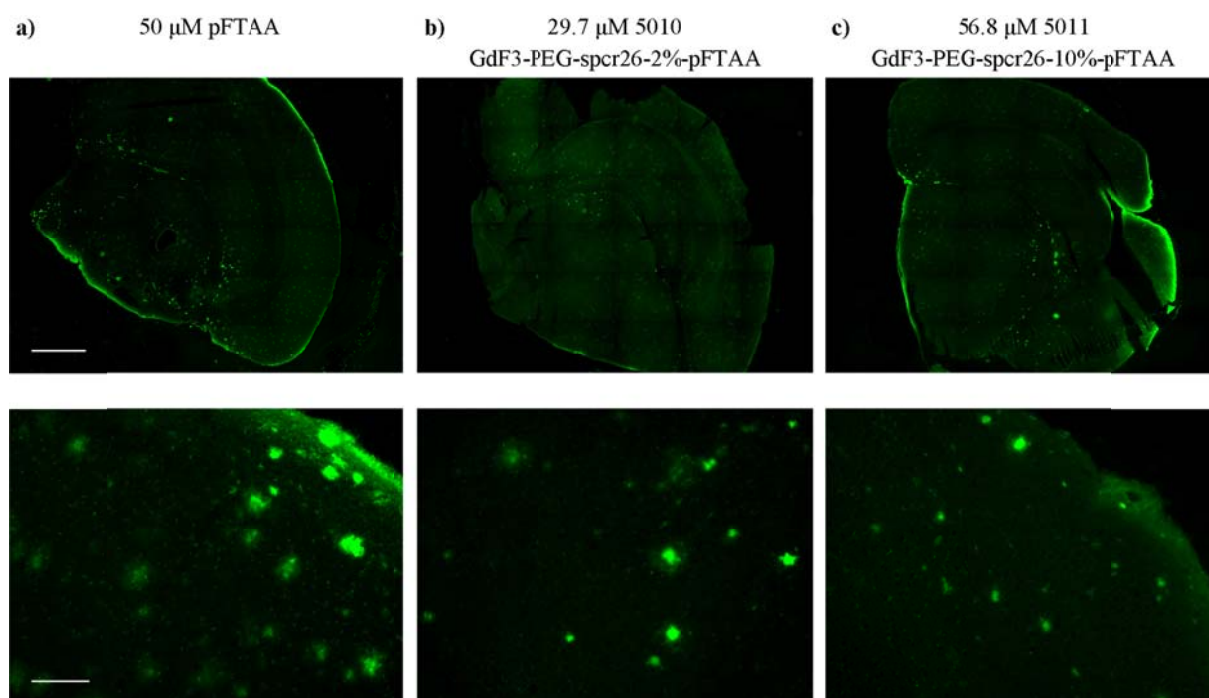


Figure 51: *In vivo* labeling of cerebral A β plaques after two consecutive i.v. injections of LCO-MNPs 5010 (GdF3-PEG-spcr26-2%-pFTAA) and 5011 (GdF3-PEG-spcr26-10%-pFTAA) in aged *APP/PS1* mice. Depicted are cerebral sections of 50 μ M pFTAA (a), LCO-MNPs 5010 (29.7 μ M, b) and 5011 (56.8 μ M, c) treated (two i.v. injections on consecutive days) *APP/PS1* mice, which were analyzed *postmortem* for cerebral A β plaque labeling using fluorescence microscopy (FITC, Zeiss Observer Z1). Cortical A β plaques were analyzed using whole mount overview pictures (upper row, exposure time at 1,500ms) and in detail at higher cortical magnification (lower row, exposure time at 500 ms). Scale bar = 1,000 μ m (upper row), Scale bar = 100 μ m (lower row).

Specific labeling of cerebral A β plaques by LCO-MNPs 5010 (GdF3-PEG-spcr26-2%-pFTAA) and 5011 (GdF3-PEG-spcr26-10%-pFTAA) was observed by fluorescence microscopy indicating efficient transfer of these two probes across the BBB. To determine if the fluorescent properties of the LCO-MNPs 5010 and 5011 are maintained after i.v. injection and BBB crossing, spectral analysis of emitted fluorescence was performed. Sections of *APP/PS1* mice treated twice with LCO-MNPs 5010 and 5011 were analyzed and emission spectra of single cortical A β plaques labeled by LCO-MNPs recorded at the Linköping University, Sweden.

The assessment of the spectral analysis of cortical A β plaques after LCO-MNP 5010 and 5011 application showed two pFTAA characteristic emission peaks at 520 and 545 nm (Fig. 52).

Results

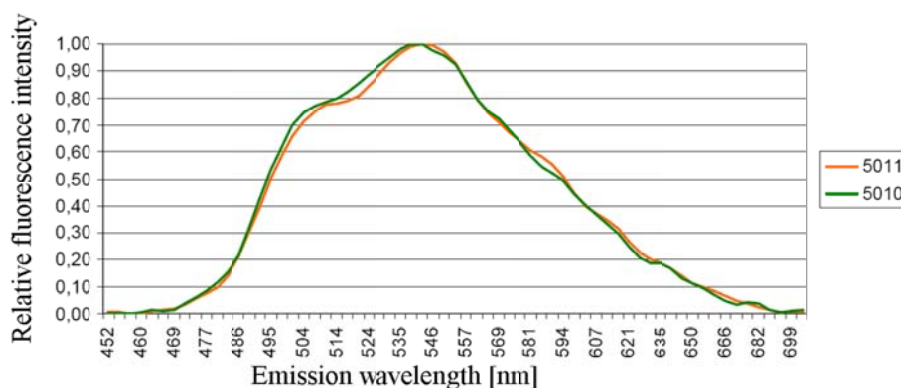


Figure 52: Emission curve of fluorescent labeled A β plaques on *APPPS1* brain sections after i.v. injection of LCO-MNP 5010 and 5011. Emitted fluorescence of labeled A β plaques was analyzed on cerebral sections by spectral imaging after peripheral treatment of *APPPS1* mice with LCO-MNPs 5010 (green) and 5011 (orange). Data of the present figure are presented with permission from Sofie Nyström, PhD, Linköping University, Sweden.

Since these are characteristic peaks for pFTAA, when bound to protein aggregates in tissue samples³⁹, it can be concluded, that at least the pFTAA component of both LCO-MNPs possesses the capacity to cross the BBB after peripheral application without changes of its emission profile. Microscopical and spectral analysis revealed a higher fluorescent intensity for A β plaques located close to the ventricle compared to central cortical plaques indicating cerebral penetration of peripheral applied LCO-MNPs through meningeal vessels (Fig. 53a, b).

Additionally, A β plaques with different fluorescent intensities, bright and dim emission, after treatment with LCO-MNP 5011 were compared to autofluorescent A β plaques after a PBS control treatment. The comparison shows clear differences of emission curves and peaks for LCO-MNP 5011 labelled and autofluorescent plaques in PBS treated mice (Fig. 53c). This comparative control measurement confirmed the specificity of A β plaque bound pFTAA after peripheral injection of LCO-MNP 5011 in an aged *APPPS1* mouse.

Results

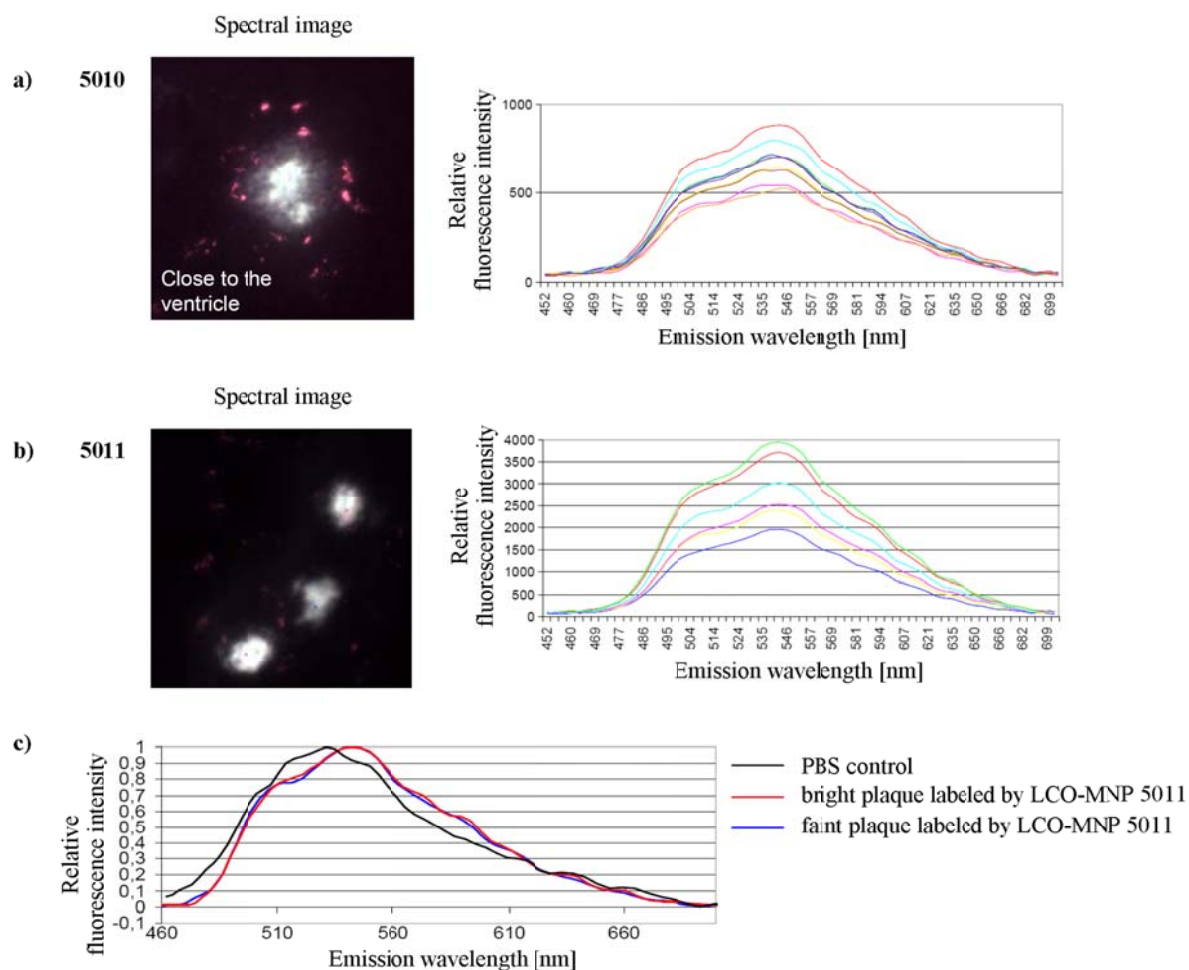


Figure 53: Spectral analyses of cerebral A β plaques after two consecutive i.v. injections of LCO-MNP 5010 (GdF3-PEG-spcr26-2%-pFTAA) and 5011 (GdF3-PEG-spcr26-10%-pFTAA) in aged *APP/PS1* mice. Aged *APP/PS1* mice were injected on two consecutive days with LCO-MNP 5010 and 5011 and cerebral sections were analyzed *postmortem* for specific A β plaque labeling by spectral imaging. Representative spectral images with pFTAA labeled A β plaques after treatment with LCO-MNP 5010 (a) and 5011 (b) are depicted and associated emission spectra of several cortical A β plaques graphed. Various colours of depicted emission curves represent various fluorescent intensities of different analyzed A β plaques. Emitted fluorescence intensity of bright and faint pFTAA labeled A β plaques after treatment with LCO-MNP 5011 was further compared to plaques on brain sections of a PBS injected control animal (c). Data assembly of the present figure is presented with permission from Sofie Nyström, PhD, Linköping University, Sweden.

Additionally, cerebral ultrathin sections of the LCO-MNP 5011 treated mouse were analyzed by TEM to determine if MNPs were also capable to cross the BBB. Analysis of the sections at 12,000x magnification (Fig. 54 upper row) showed no obvious differences between mouse brains of pFTAA (Fig. 54a) and LCO-MNP 5011 (Fig. 54b) injected animals. Even at 85,000x (Fig. 54 lower row) magnification, no MNPs could be detected within A β fibrils after peripheral application of LCO-MNP 5011 when compared to the pFTAA injection.

Since fluorescence and spectral analyses revealed LCO labeled cerebral A β plaques but no GdF3 MNPs could be visualized by TEM the question arises, if LCO-MNPs crossed the BBB

Results

as intact, coupled molecules or if the MNPs deattached from the probes in the circulation and only the LCO component passed the BBB and labeled cerebral A β plaques. However, since TEM is limited to the analysis of a small cerebral area and A β plaque number, it cannot be excluded that possibly MNPs were not detected.

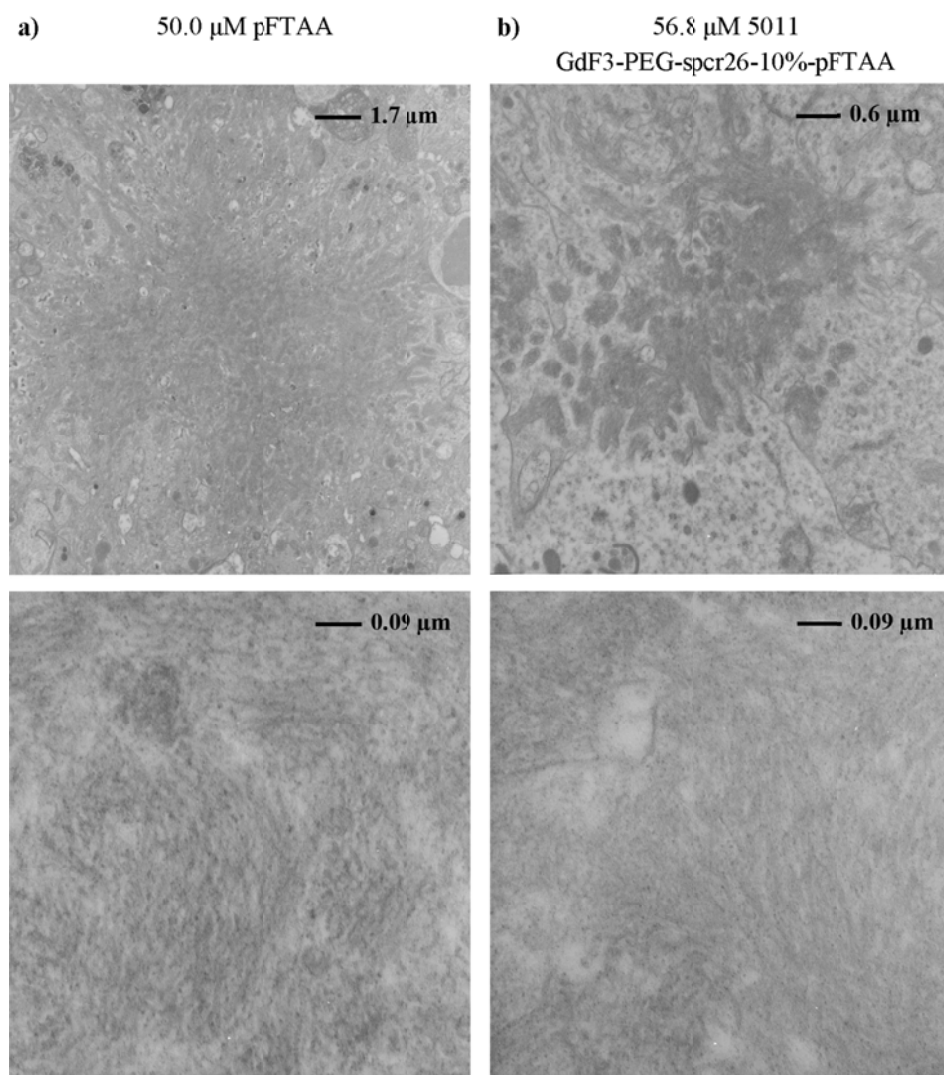


Figure 54: TEM images of single cerebral A β plaques and A β fibers after peripheral pFTAA and LCO-MNP 5011 i.v. injection in aged *APPPS1* mice. After two consecutive i.v. injections of aged *APPPS1* mice with pFTAA (50.0 μ M) and LCO-MNP 5011 (56.8 μ M), animals were sacrificed without previous perfusion one week later. Glutaraldehyd fixed cerebral ultrathin sections were analyzed by TEM for GdF3 MNPs. Initially single cerebral A β plaques (upper row) were screened and subsequently A β fibers (lower row) were analyzed in detail at higher magnification.

LCO-MNP derivative 5012 represents the attachment of pFTAA to a single gadolinium molecule instead of a GdF3 MNP. Since this probe is much smaller than all already tested LCO-MNPs, its ability to cross the BBB was assumed to be best.

After it was shown by our collaborators at the Linköping University in Sweden, that spectral imaging was reproducible best on unfixed fresh frozen sections, the protocol was changed and

Results

cerebral hemispheres for fluorescence and spectral microscopy were no longer fixed in formalin but cut fresh frozen. After short term treatment of an aged *APP/PS1* mouse with LCO-MNP derivative 5012 fresh frozen sections (30 μm) were screened unstained for pFTAA labeled cortical A β plaques by fluorescence microscopy.

Equivalent to injection of 1 mM pFTAA (Fig. 55a), cerebral A β plaques of the entire cortex were specifically labeled by LCO-MNP derivative 5012 after two peripheral i.v. injections in aged *APP/PS1* mice (Fig. 55b). This result indicates efficient crossing of the BBB of injected LCO-MNP derivative 5012. Since probe 5012 was synthesized based on the pFTAA backbone, the detected fluorescent intensity was comparable to the application of 1 mM uncoupled pFTAA (Fig. 55).

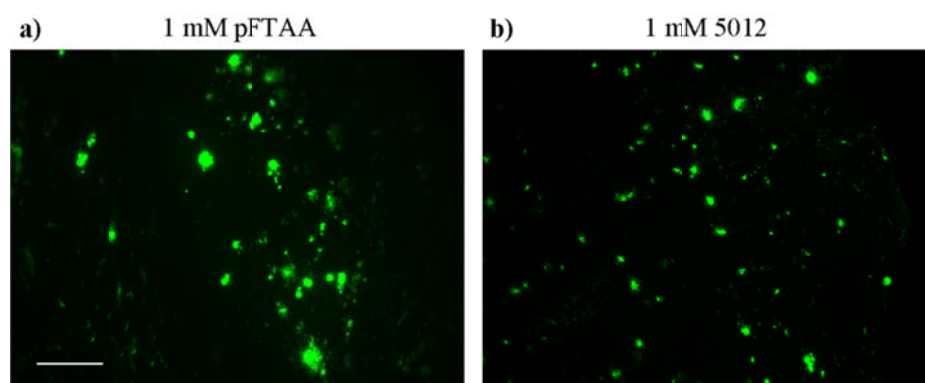


Figure 55: *In vivo* labeling of cerebral A β plaques after two consecutive i.v. injections of LCO-MNP derivative 5012 in aged *APP/PS1* mice. Aged *APP/PS1* mice were i.v. treated on two consecutive days with LCO-MNP derivative 5012 (1 mM, b) and 1 mM pFTAA (a). One week after the first injection animals were sacrificed and fluorescent intensity of cerebral A β plaque labeling was compared on fresh frozen sections using fluorescence microscopy (FITC, zeiss Observer Z1). Both images were taken at an exposure time of 50 ms. Scale bar = 100 μm .

In a next step an LCO-MNP with FeO as the MNP-component attached to the quaternary LCO qFTAM was tested for crossing of the BBB and cerebral A β plaque labeling after peripheral injection. The exact LCO concentration of probe 4026 (qFTAM-TEG-Succ-NHS amino PEG) was not analyzed, but since the reaction ratio was set to 190 qFTAM molecules per FeO MNP, the LCO concentration should be $\leq 190 \mu\text{M}$. As controls PBS and the FeO MNP only (amino PEG) were applied to aged *APP/PS1* mice. Microscopical analysis of cerebral tissue showed a homogeneous and specific A β plaque labeling after two injections of LCO-MNP 4026 (Fig. 56c). In contrast, control injections of PBS (Fig. 56a) and amino PEG (Fig. 56b) showed no A β plaque labeling.

Results

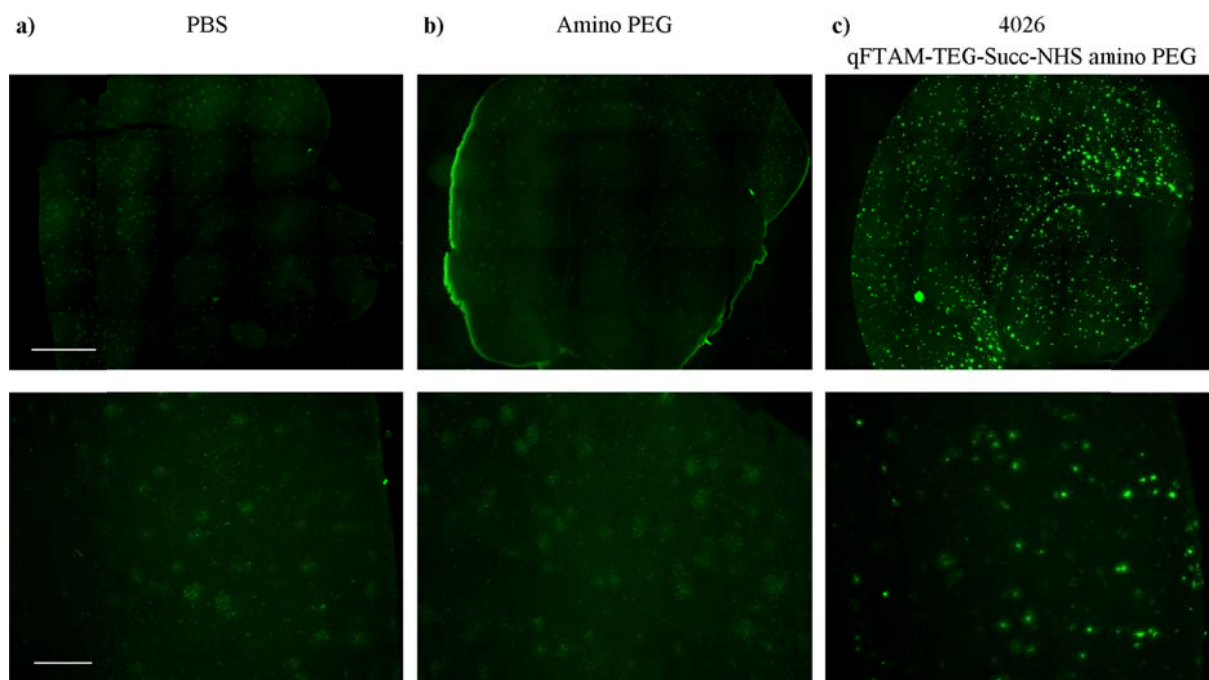


Figure 56: *In vivo* labeling of cerebral A β plaques after two consecutive i.v. injections of LCO-MNP 4026 (qFTAM-TEG-Succ-NHS amino PEG) in aged *APP/PS1* mice. Aged *APP/PS1* mice were injected i.v. on two consecutive days with LCO-MNP 4026 and fluorescent intensity of labeled cerebral A β plaques (c) was compared to sections of *APP/PS1* mice treated simultaneously with PBS (a) and pure FeO MNPs (amino PEG, (b)). Images were taken at an exposure time of 1,000 ms. Scale bar = 1,000 μ m (upper row - overview), Scale bar = 100 μ m (lower row – higher magnification).

Additionally to the fluorescence analyses of cerebral sections after peripheral application of LCO-MNP 4026, brain sections were analyzed for the presence of iron to assess whether iron containing FeO MNPs are detectable within the tissue. No specific iron staining was achieved (data not shown). These data indicate that after peripheral injection of LCO-MNP 4026 the LCO component penetrated into the brain and labeled A β plaques, but similar to the other analyzed LCO-MNP particles BBB crossing of the MNP component could not be demonstrated.

3.2.3 Summary of MRI results after short term application of LCO-MNPs to APP/PS1 mice

LCO-MNPs were developed and synthesized for *in vivo* detection of amyloid deposits by MRI. Since the efficient labeling of cerebral A β plaques after i.v. injection of LCO-MNPs indicated efficient passing of these probes across the BBB, MRI analyses were performed. Initially frozen, right hemispheres of LCO-MNP injected *APP/PS1* mice described above were analyzed by MRI, but no significant MRI signals could be detected in hemispheres of LCO-MNP injected *APP/PS1* mice compared to hemispheres of untreated animals. Since the

Results

analyzed frozen hemispheres revealed *postmortem* artefacts and no significant MRI signals could be detected, subsequent MRI analyses were performed on live animals after i.v. injection directly at the NTNU in Trondheim, Norway. The following summarized results of the MRI measurements were generated by and are presented in the present thesis with permission of the research group of Prof. Olav Haraldseth, Department of Circulation and Medical Imaging at the NTNU in Trondheim, Norway.

First study protocols and MRI sequence protocols for detecting changes in tissue relaxation times were established. T1 and T2 mapping was chosen to enable quantification of changes in tissue relaxation time due to A β plaque bound LCO-MNPs. MRI studies after i.v. injections of LCO-MNP 4013 (GdF3-PEG-NP-TEG-qFTAA), 4026 (FeO-PEG-qFTAM) and 5011 (GdF3-PEG-spcr26-10%-pFTAA) showed in live *APP/PS1* mice no significant changes in T2 mapping. Also by TEM no MNPs could be detected around or within cerebral A β plaques; also MNPs stuck in meningeal vessels were also not visible. Since it could not be proven, that MNPs reached the brain or cerebral A β plaques after systemic administration, it has to be assumed that possibly only the LCO component of LCO-MNPs crosses the BBB and labeled fluorescent detected A β plaques.

ICP measurements with the same injection protocol showed that MNPs are present at such low concentrations that measurable changes in T1 and T2 relaxation times could not be induced. The conclusion from this result was, that the LCO-MNPs did not cross the BBB and did not remain in the brain parenchyma at detectable levels, in contrast to what was initially assumed based on the fluorescent imaging alone.

Subsequently a new study protocol with an intracranial (i.c.) injection of the LCO-MNP derivative 5012 into the *cisterna magna* was developed, in order to bypass the BBB. Particle 5012 was assumed to have best tissue penetration properties due to the pFTAA coupled gadolinium molecule instead of before utilized GdF3 MNPs. Since particle 5012 showed primarily T1 effects, T1 mapping was performed in this study. The MRI results showed a change in T1 in several brain regions of several animals, however without reaching statistical significance in contrast to untreated animals. ICP measurements confirmed that the injection of particle 5012 revealed high enough gadolinium concentrations in the brain to measure a theoretical reduction of T1. For this reason it was proven, that the i.c. application worked and injected LCO-MNPs bypass the BBB and remained in the brain. Further improvements of the MRI and study protocols need to be established in order to detect a significant MRI signal.

To sum up, peripheral i.v. administration of distinct LCO-MNPs led only to a weak penetrance of injected particles over the BBB. Measurable MRI signals could be achieved following direct administration of LCO-MNPs into the CSF, indicating that for establishing a more generalized applicability, MRI protocols for the peripheral administration of LCO-MNPs need to be optimized.

3.2.4 Summary of LCOs as novel MRI contrast agents for diagnostics of Alzheimer's disease

LCOs as potential novel tool for *in vivo* amyloid detection were coupled to MNPs and BBB crossing and cerebral A β plaque labeling of LCO-MNPs was investigated in aged *APP/PS1* mice after peripheral i.v. application. First it was shown *in vitro* by tissue stainings and spectral imaging (Linköping University, Sweden) that A β specific properties of LCOs are retained when LCOs were coupled to MNPs. LCO derivatives and LCO-MNPs efficiently and specifically labeled A β deposits *in vitro*. After peripheral i.v. injection of aged *APP/PS1* mice, only LCO derivative 4011, where qFTAA was attached to a short linker with a terminal reactive phosphate group, achieved efficient cerebral A β plaque labeling. Otherwise, besides probe 4012 all applied LCO-MNPs showed efficient labeling of cerebral A β plaques after peripheral i.v. injection of *APP/PS1* mice. Compared to LCO derivatives, LCO-MNPs showed stronger fluorescent A β labeling of cerebral plaques after peripheral application despite their larger size, even at lower LCO concentrations. Among different LCO-MNPs, the FeO nanostructure coupled to the quaternary LCO qFTAM revealed the highest fluorescent intensity of labeled A β plaques after peripheral injection. However, probe 5012, which represents a gadolinium molecule coupled to pFTAA and is known to be a very small probe (not detectable by TEM), led also to a strong and homogenous A β plaque labeling after two i.v. injections. Since injected stock solutions of these two probes revealed the highest possible LCO concentrations among injected LCO-MNPs, it was assumed that the fluorescent intensity of labeled A β plaques after peripheral i.v. injection in *APP/PS1* mice correlates with the LCO concentration of the applied stock solution.

Subsequent experimental results showed, that the attachment of different spacers (terminal reactive groups, short or long spacers) to LCOs led to no efficient cerebral A β plaque labeling after peripheral i.v. injection, indicating poor abilities to pass the BBB. Since systemic administered LCO-MNPs in general led to an efficient and specific fluorescent labeling of cerebral A β plaques after peripheral application, BBB crossing of coupled probes was

assumed. However, MRI measurements and TEM have not confirmed BBB crossing of LCO-MNPs, no significant magnetic signal was detected and GdF3 MNPs could also not be visualized by TEM after peripheral injection of coupled probes.

3.3 Long term pFTAA treatment of young experimental animals

3.3.1 *Experimental setup of long term pFTAA treatment of young experimental animals*

pFTAA as novel molecular amyloid marker was shown to cross the BBB of *APP/PS1* mice after peripheral i.p. injection and to efficiently label cerebral A β plaques of treated animals (see chapter 3.1.2). Several amyloid binding dyes like Congo red or methoxy-XO4 were described to influence A β aggregation and fibrilization^{43,44}, hence the question arises if pFTAA has the same properties. To analyze, whether a long term pFTAA application influences AD pathology *in vivo*, a 12 week long pFTAA treatment of young *APP/PS1* mice was assessed. Within that approach young *APP/PS1* and WT mice were injected weekly with 10 mg/kg pFTAA (*APP/PS1* n = 11, WT n = 6) or PBS (*APP/PS1* n = 4) up to a final age of 120 d. The treatment was initiated at an age of 6-8 weeks, before cerebral plaque deposition starts in *APP/PS1* mice⁶⁴, with repetitive i.p. pFTAA or PBS injections on four consecutive days. Re-injections of 10 mg/kg pFTAA or PBS were applied to animals weekly. Untreated *APP/PS1* (n = 5) and WT mice (n = 2) were used as further controls (Fig. 57, Tab. 14).

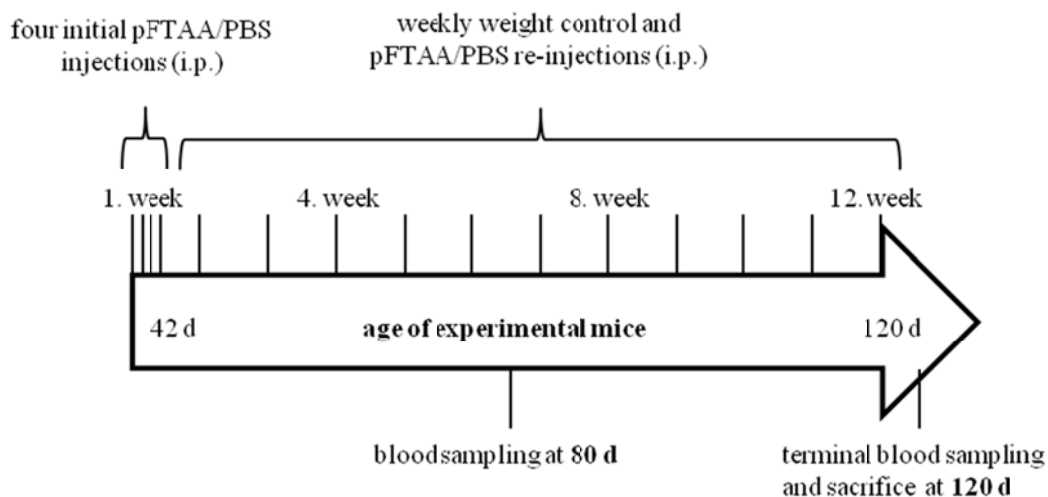


Figure 57: Experimental setup of long term pFTAA treatment in young *APPPS1* and WT mice. Young *APPPS1* and WT mice (6-8 weeks of age) were treated over 12 weeks with 10 mg/kg pFTAA or PBS. Initially mice were injected on four consecutive days, subsequent applications were performed weekly. Weight gain of young *APPPS1* and WT mice was controlled weekly and blood of experimental animals was taken to determine differential blood count and to analyze several hepatorenal parameters within the treatment period at 80 d of age and finally at 120 d, when mice were sacrificed.

Table 14: Experimental groups of long term pFTAA treatment in young *APPPS1* and WT mice

Genotype	Number (n)	Treatment
<i>APPPS1</i>	5	none
	4	PBS
	11	pFTAA
WT	2	none
	6	pFTAA

3.3.2 Monitoring toxic side effects during and after long term pFTAA treatment of young experimental animals

3.3.2.1 Weight gain of young experimental animals during long term pFTAA treatment

During the long term pFTAA treatment, young *APPPS1* mice were weighed before every single injection of 10 mg/kg pFTAA or PBS. No obvious toxic side effects of the long term pFTAA application were observed – treated experimental animals developed and behaved normally and gained weight constantly as seen in mice of respective age groups. Furthermore, no statistical significant difference of weight gaining between treated experimental groups was detected (Fig. 58).

Results

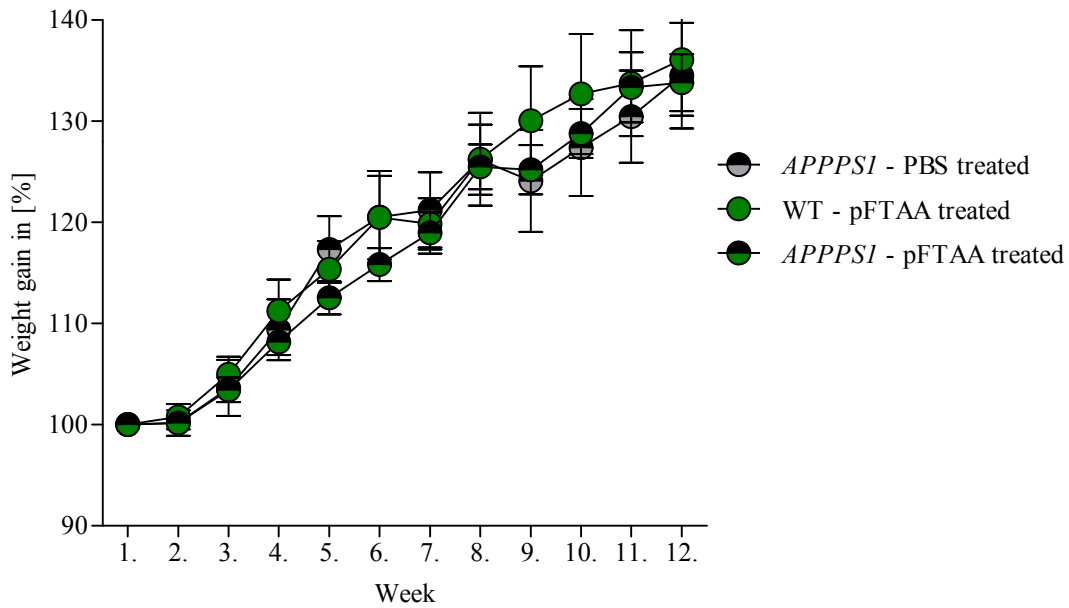


Figure 58: Weight gain of young *APPPSI* and WT mice during long term treatment. 6-8 weeks old *APPPSI* mice and age matched WT controls were treated over 12 weeks with 10 mg/kg pFTAA or PBS. Before every single injection mice were weighted. Weight gain [%] of experimental groups i) *APPPSI* – PBS treated (n = 4), ii) WT – pFTAA treated (n = 6) and iii) *APPPSI* – pFTAA treated (n = 11) over 12 weeks is graphed. For statistical analyses one-way ANOVA with Bonferroni’s post test was used.

Since transgenic *APPPSI* mice were generated on the C57BL/6J background, weight development of experimental mice was compared to available basic physiology data on C57BL/6J mice (The Jackson Laboratory, Body weight information, JAX[®] mice strain C57BL/6J). Weight measurements of experimental *APPPSI* and WT mice at 6-8 weeks and 120 d (17 weeks) of age were comparable to published weight data of C57BL/6J mice (Tab. 15), indicating no treatment specific effect on weight gain of young experimental mice.

Table 15: Mean weights of experimental mice and C57BL/6J mice at 6-8 weeks and 120 d of age

Source: The Jackson Laboratory, Body weight information, JAX[®] mice strain C57BL/6J.

Animals	Gender	Weight at 6-8 weeks of age	Weight at 120 d of age
C57BL/6J JAX[®] mice strain	male	22.6 ± 1.5 g	30.,7 ± 2.2 g
	female	18.1 ± 1.1 g	22.6 ± 2.0 g
<i>APPPSI</i> PBS treated	male	19.0 ± 2.0 g	27.5 ± 0.8 g
	female	16.1 ± 0.5 g	20.9 ± 1.3 g
WT pFTAA treated	male	20.6 ± 2.5 g	28.9 ± 2.1 g
	female	17.1 ± 1.3 g	21.5 ± 0.5 g
<i>APPPSI</i> pFTAA treated	male	19.7 ± 0.6 g	26.7 ± 0.1g
	female	16.9 ± 0.4 g	21.4 ± 0.3 g

3.3.2.2 Blood analyses during and after long term pFTAA treatment of young experimental animals

At two different time points (80 and 120 d of age) of the long term treatment of young *APPPSI* and WT mice, blood was sampled and a differential blood count (erythrocytes; hemoglobin; hematocrit; mean corpuscular volume (MCV); mean corpuscular hemoglobin (MCH); mean corpuscular hemoglobin concentration (MCHC); leucocytes: granulocytes (neutrophils, basophiles, eosinophils), monocytes, lymphocytes; thrombocytes) was assessed to check the general health state of pFTAA and PBS treated experimental animals. At the age of 120 d also several hepatorenal parameters were measured. Blood analyses using EDTA-plasma were performed by synlab, Berlin.

In comparison to the specific reference ranges of synlab, Berlin, erythrocyte numbers, hemoglobin and hematocrit amounts slightly increased in all experimental groups at 80 d of age, however no statistical significant difference was detectable between the individual groups (Fig. 59a). The three red blood cell indices MCV, MCH and MCHC showed also no statistical significant differences between experimental groups (Fig. 59b).

Results

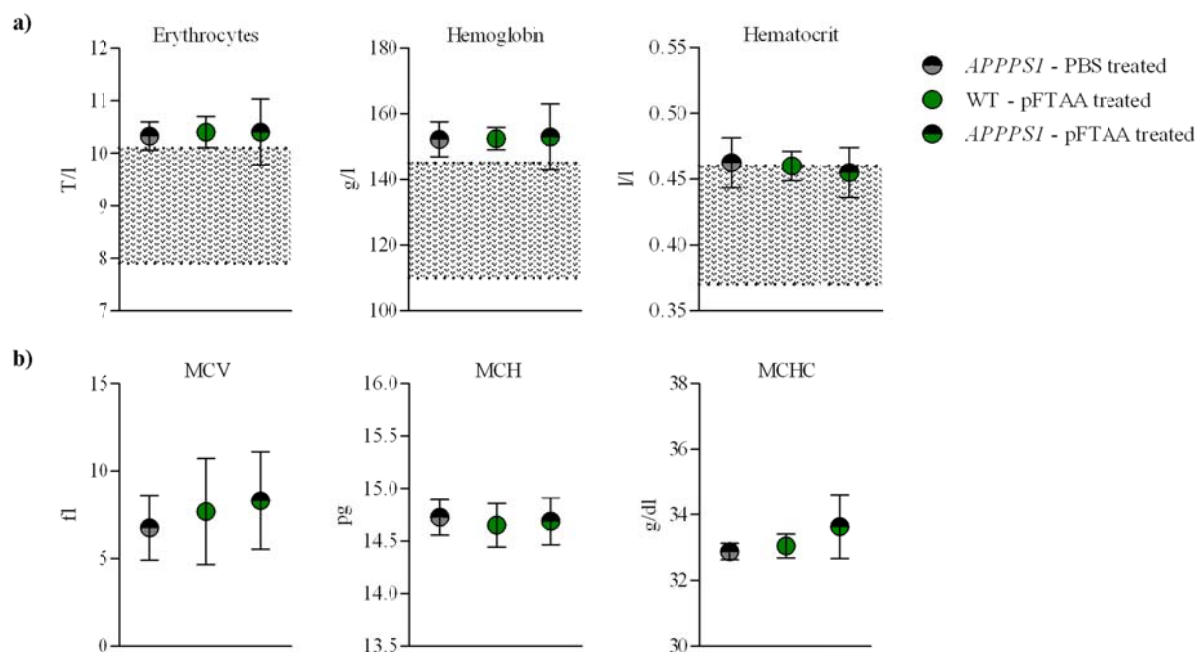


Figure 59: Detection of erythrocyte number, hemoglobin, hematocrit, MCV, MCH and MCHC values in the EDTA-plasma of long term treated *APPPSI* and WT mice at 80 d of age. Blood of treated *APPPSI* mice and age matched WT animals of the long term treatment was sampled with the facial vein technique and EDTA-plasma was analyzed at 80 d of age. Erythrocyte numbers, hemoglobin and hematocrit amounts (a) as well as MCV, MCH and MCHC amounts (b) were measured by synlab Berlin, whose specific reference range is defined as grey area in the graphs. Experimental groups i) *APPPSI* – PBS treated (n = 4), ii) WT – pFTAA treated (n = 6) and iii) *APPPSI* – pFTAA treated (n = 8) are depicted and were compared. For statistical analyses one-way ANOVA with Bonferroni’s post test was used.

EDTA-plasma of pFTAA and PBS treated *APPPSI* and WT mice revealed no statistical significant differences in total leucocyte number (Fig. 60a) and in amounts of differentiated subpopulations monocytes and lymphocytes (Fig. 60a), as well as granulocytes (neutrophils and eosinophils, Fig. 60b) between experimental groups at 80 d. All values were determined in given reference ranges of synlab Berlin (Fig. 60a, b). The thrombocyte number in pFTAA treated *APPPSI* and WT mice was slightly increased compared to PBS treated *APPPSI* mice at 80 d, but this difference did not reach statistical significance (Fig. 60c). Mean thrombocyte numbers of pFTAA treated *APPPSI* and WT mice were higher (*APPPSI*: $1,204 \pm 139$ G/l; WT: $1,218 \pm 87$ G/l) than the given reference range (600 – 1,200 G/l).

Results

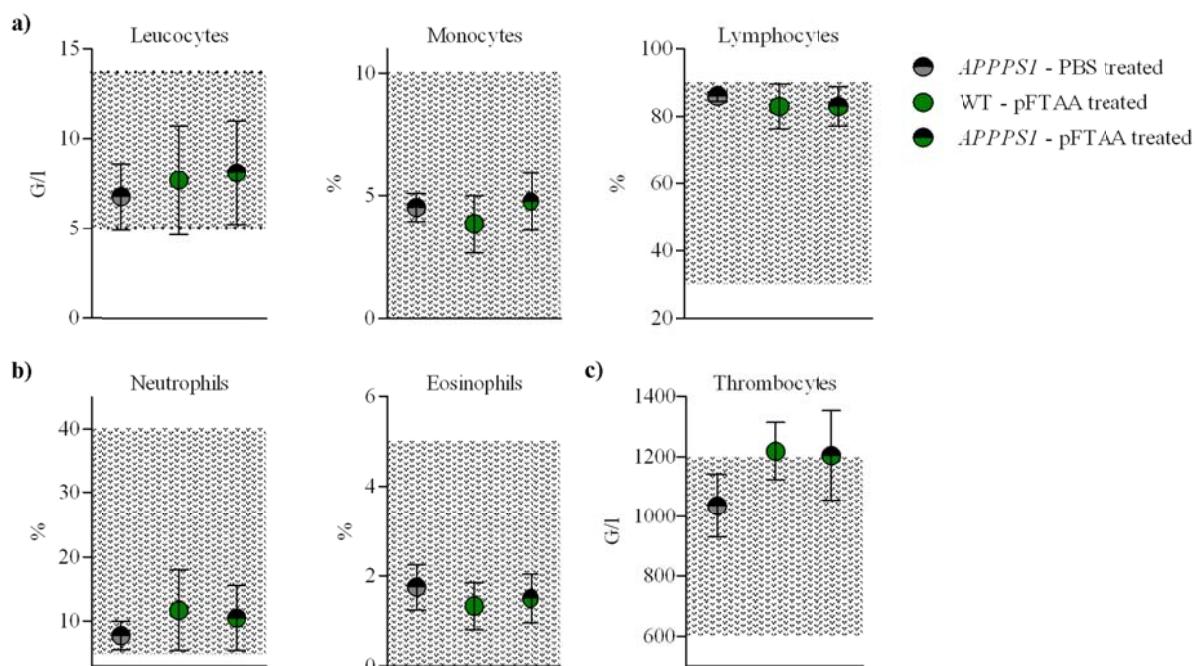


Figure 60: Detection of leucocyte and thrombocyte numbers in the EDTA-plasma of long term treated *APPPSI* and WT mice at 80 d of age. Blood of treated *APPPSI* and WT mice was sampled with the facial vein technique and EDTA-plasma was analyzed at 80 d of age. The number of leucocytes (a) and differentiated subpopulations (monocytes and lymphocytes, (a)), granulocytes (neutrophils and eosinophils, (b)) as well as the amount of thrombocytes (c) in the EDTA-plasma of experimental mice was detected and is graphed related to the given reference range (synlab Berlin, defined as grey area in graphs). Experimental groups i) *APPPSI* – PBS treated (n = 4), ii) WT – pFTAA treated (n = 6) and iii) *APPPSI* – pFTAA treated (n = 8) were compared after long term pFTAA or PBS treatment. At 80 d of age no band neutrophils (stab cells) and basophiles were detected in the EDTA-plasma of any of the experimental groups. For statistical analyses one-way ANOVA with Bonferroni's post test was used.

In contrast to differential blood count results at 80 d of age, nearly all erythrocyte, hemoglobin and hematocrit values of the differential blood count at 120 d were detected in the given reference range of synlab Berlin. The hemoglobin value of *APPPSI* mice after PBS treatment was slightly increased. However, no statistical significant difference between experimental groups was detected (Fig. 61a). Also no statistical significant differences of the MCV, MCH and MCHC values were observed between pFTAA or PBS treated *APPPSI* and WT mice (Fig. 61b).

Results

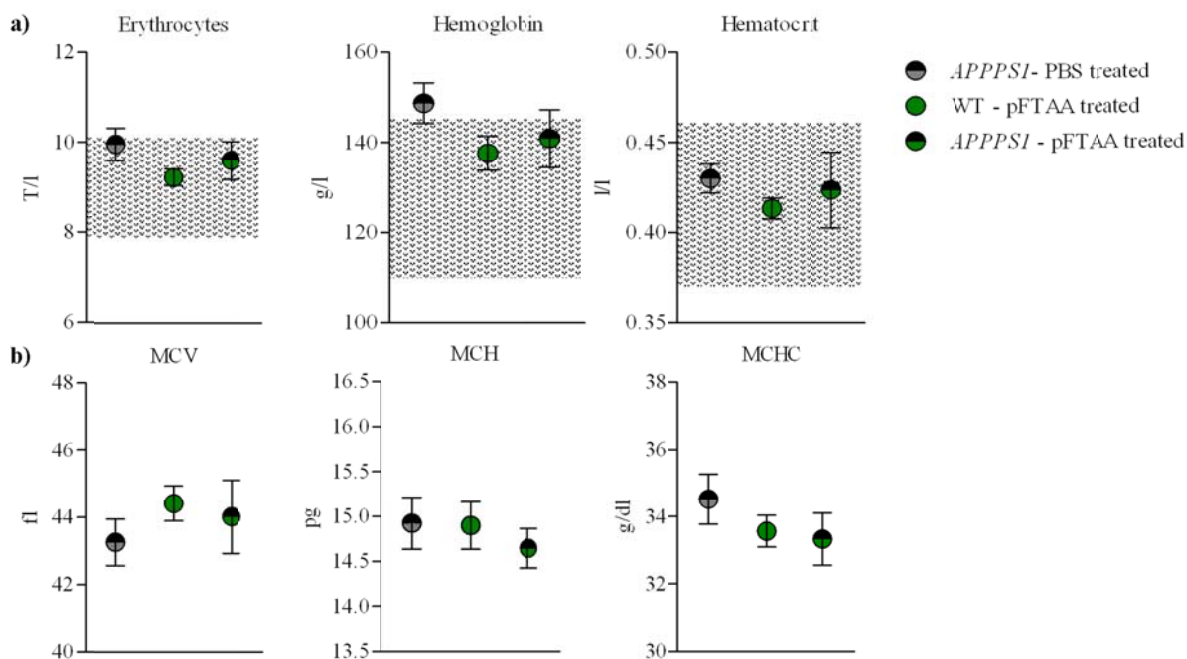


Figure 61: Detection of erythrocyte number, hemoglobin, hematocrit, MCV, MCH and MCHC values in the EDTA-plasma of long term treated *APPPSI* and WT mice at 120 d of age. At 120 days of age a terminal blood sampling was performed before experimental animals were perfused. The EDTA-plasma was used to assess a differential blood count. Erythrocyte numbers, hemoglobin and hematocrit values (a), as well as MCV, MCH, and MCHC values (b) of the three main experimental groups i) *APPPSI* – PBS treated (n = 4), ii) WT – pFTAA treated (n = 3) and iii) *APPPSI* - pFTAA treated (n = 11, a) were analyzed. The grey area defines the reference range given by synlab Berlin. For statistical analyses one-way ANOVA with Bonferroni's post test was used.

Leucocytes and relative amounts of their differentiated subpopulations were also measured in the EDTA plasma of experimental animals at 120 d of age. All values were detected in the given reference range of synlab Berlin and no statistical significant difference between experimental groups i) *APPPSI* – PBS treated, ii) WT – pFTAA treated and iii) *APPPSI* – pFTAA treated was detected (Fig. 62a, b). The same was observed for the measurement of thrombocyte numbers at 120 d of age (Fig. 62c).

Results

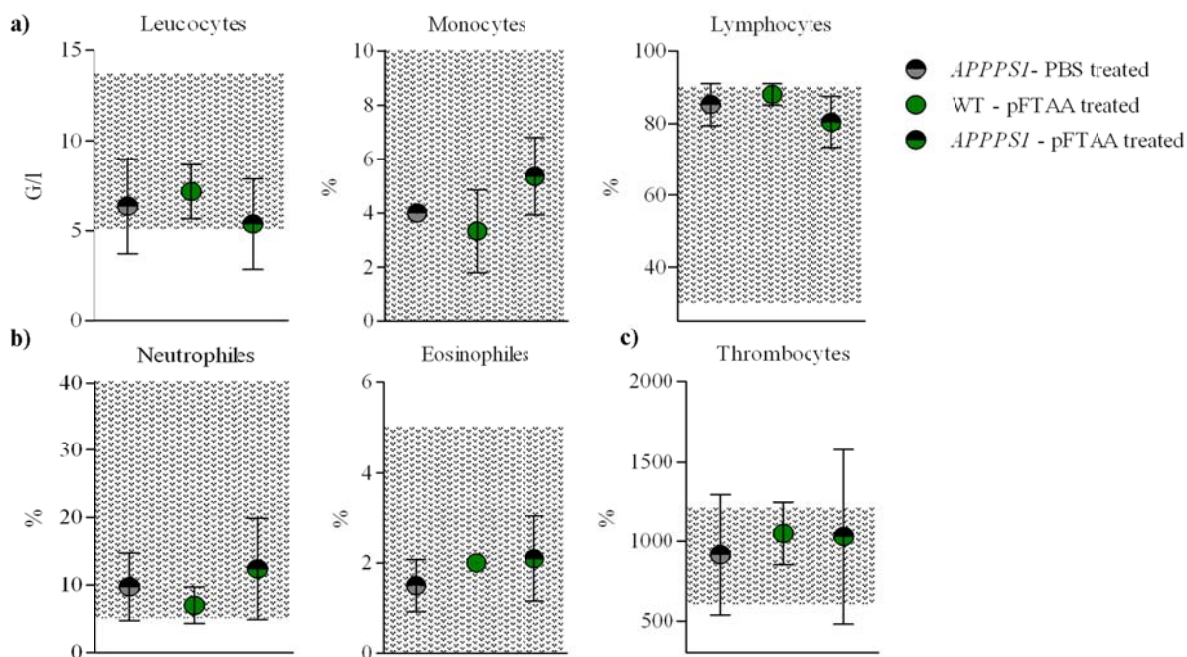


Figure 62: Detection of leucocyte and thrombocyte numbers in the EDTA-plasma of long term treated *APPPSI* and WT mice at 120 d of age. After the long term treatment of young *APPPSI* and WT mice, blood was sampled before animals were perfused at 120 d. Leucocyte numbers (a) and relative amounts of its differentiated subpopulations (monocytes and lymphocytes (a), granulocytes (neutrophils and eosinophils, (b)) as well as thrombocyte amounts (c) were detected in EDTA-plasma related to the defined reference range of synlab Berlin (defined as grey area in graphs a–c). Results of the three experimental groups i) *APPPSI* – PBS treated (leucocytes n = 4, thrombocytes n = 3), ii) WT – pFTAA treated (n = 3) and iii) *APPPSI* – pFTAA treated (n = 11) are graphed and were compared. For statistical analyses one-way ANOVA with Bonferroni's post test was used.

For the blood analysis at 120 d, several hepatorenal parameters (alkaline phosphatase, aspartat aminotransferase (AST) and alanine aminotransferase (ALT) - Fig. 63a; glutamate dehydrogenase (GLDH) and creatinine - Fig. 63b) were measured in the EDTA-plasma of experimental *APPPSI* and WT mice. Those parameters could not be assessed for all experimental mice, since not enough EDTA-plasma was available. No differences of hepatorenal parameters between experimental groups were detected after long term treatment of young *APPPSI* and WT mice (Fig. 63).

Results

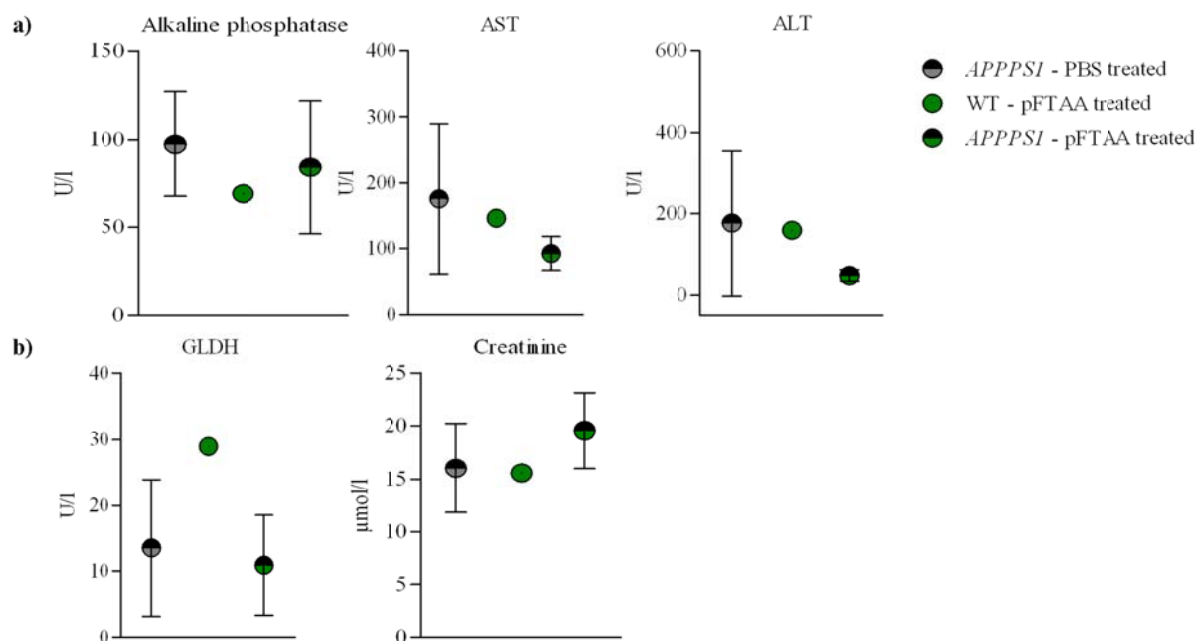


Figure 63: Detection of hepatorenal parameters in the EDTA-plasma of long term treated *APPPSI* and WT mice at 120 d of age. After the long term treatment of young *APPPSI* and WT mice, blood was sampled before animals were perfused at 120 d. Hepatorenal parameters alkaline phosphatase, AST, ALT, GLDH and creatinine were assessed in EDTA-plasma and compared between experimental groups i) *APPPSI* – PBS treated (n = 3), ii) WT – pFTAA treated (n = 1) and iii) *APPPSI* – pFTAA treated (n = 7, alkaline phosphatase n = 5, creatinine n = 3). The value of the gamma glutamyl transferase (U/l) was for all analyzed animals < 3. A statistical analysis was not performed since only one value for pFTAA treated WT mice was determined.

Differential blood counts at 80 and 120 d, and analyses of hepatorenal parameters at 120 d of long term pFTAA or PBS treated *APPPSI* and WT mice revealed no statistical significant differences between experimental groups at 80 and 120 d of age. The observed results indicate that pFTAA treatment did not cause toxic effects on hematopoiesis or distinct blood related values. Also no obvious signs for inflammation or liver and kidney related side effects were detected by analyses of the EDTA-plasma of experimental mice.

3.3.2.3 Postmortem screening of peripheral organs after long term pFTAA treatment of young experimental animals

To analyze potential side effects of the long term pFTAA or PBS treatment of young *APPPSI* and WT mice in more detail, histopathological *postmortem* analyses of several peripheral organs (heart, lung, kidney, liver, spleen) were performed. First it was investigated if unbound pFTAA accumulated in the murine system (Fig. 64-68) and secondly H&E stained organ sections were screened for pathological alterations using bright field microscopy (Fig. 69-74). Since it is not known, how LCOs (for example pFTAA) are metabolized in the murine system, it was of interest, if pFTAA accumulates in the periphery of experimental mice after long term

Results

treatment. This was relevant especially for pFTAA treated WT mice, because these mice do not develop significant amyloid deposition and therefore do not provide a specific target for binding of pFTAA. Fluorescence microscopy (FITC, Zeiss Observer Z1) was used to analyze free floating sections of peripheral organs for accumulations of pFTAA labeled aggregates after long term pFTAA treatment of young *APP/PS1* and WT mice, and to compare them with organs of untreated and PBS treated animals.

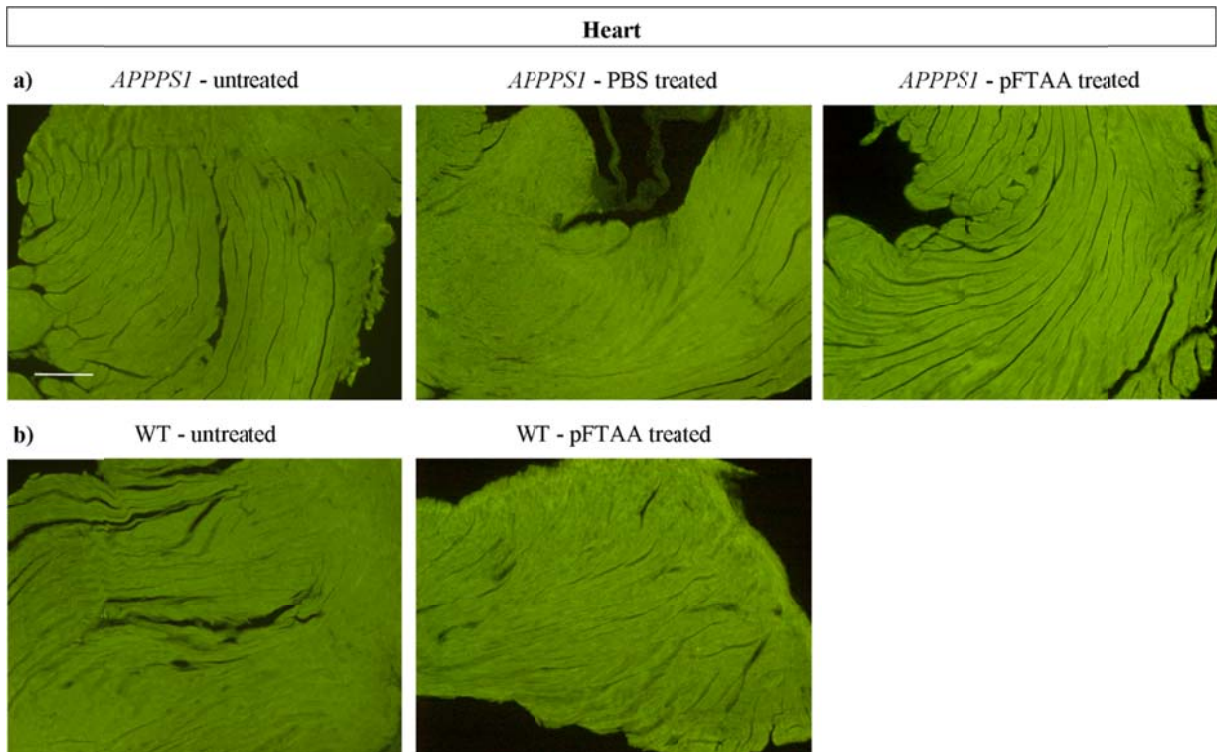


Figure 64: *Postmortem* screening of heart muscle tissue for pFTAA deposition after long term treatment of 120 d old *APP/PS1* and WT mice. Scale bar = 100 μ m.

Results

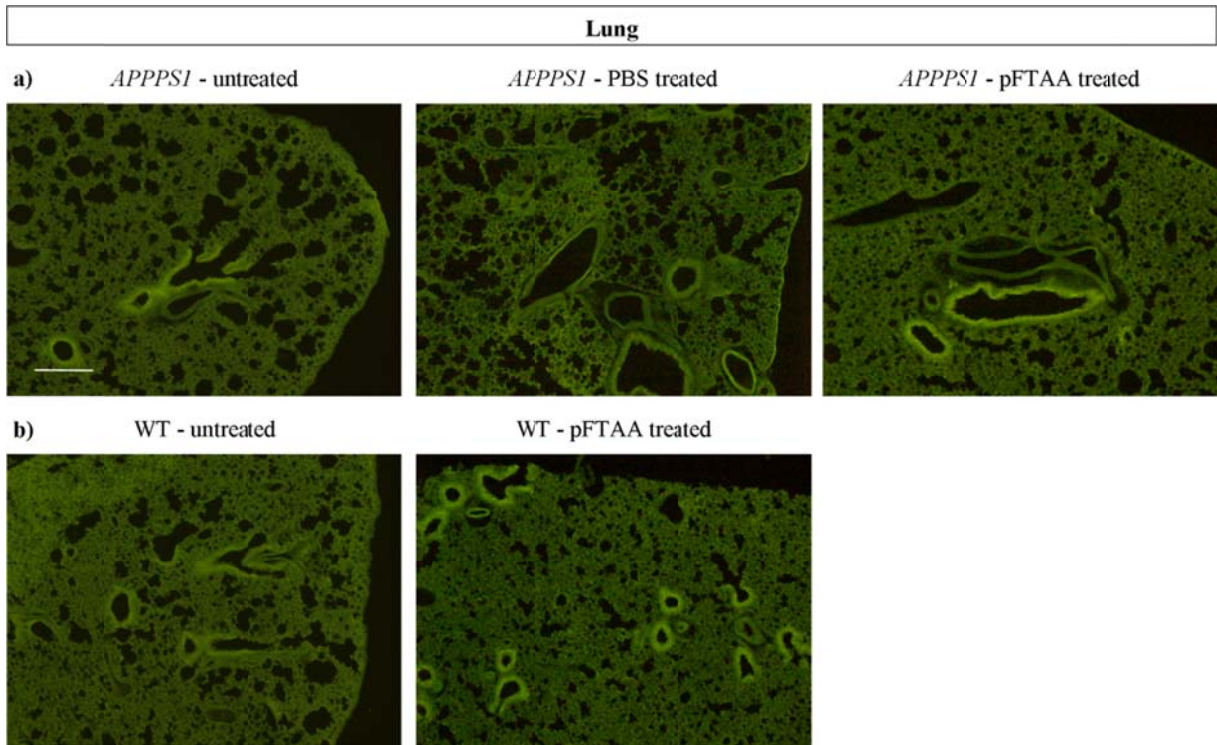


Figure 65: *Postmortem* screening of lung tissue for pFTAA deposition after long term treatment of 120 d old *APPSI* and WT mice. Scale bar = 100 μ m.

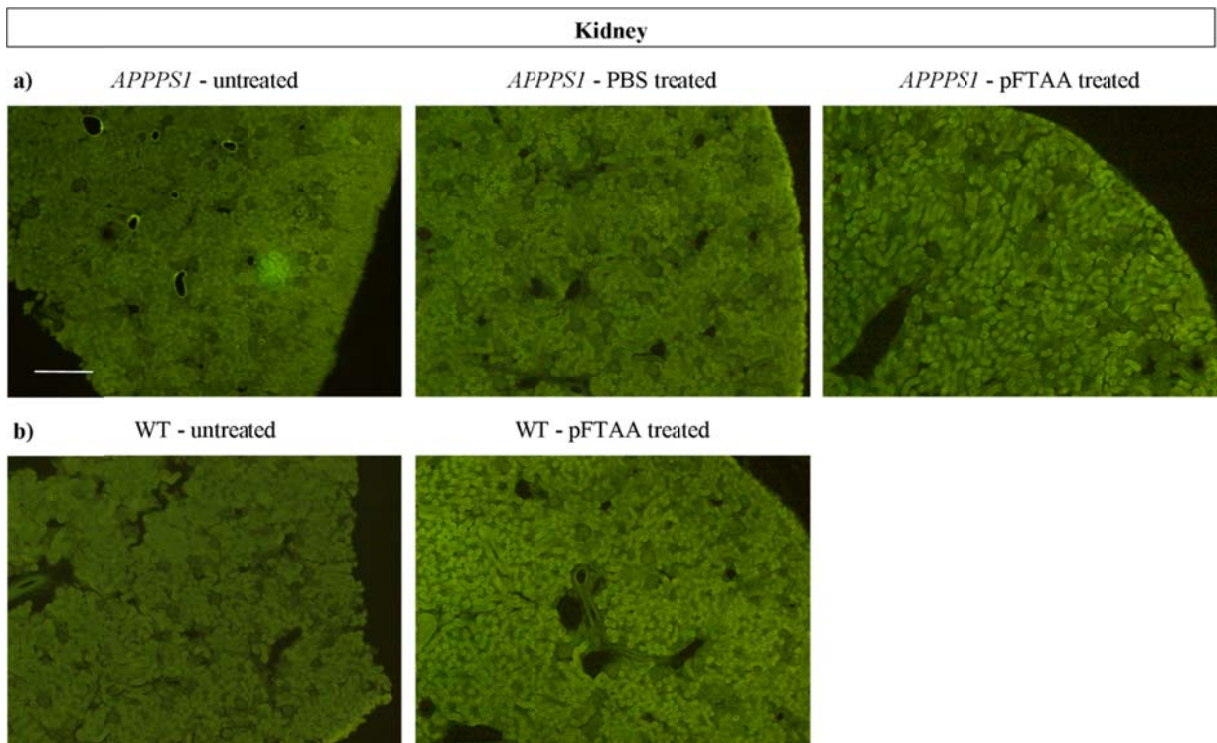


Figure 66: *Postmortem* screening of renal tissue for pFTAA deposition after long term treatment of 120 d old *APPSI* and WT mice. Scale bar = 100 μ m.

Results

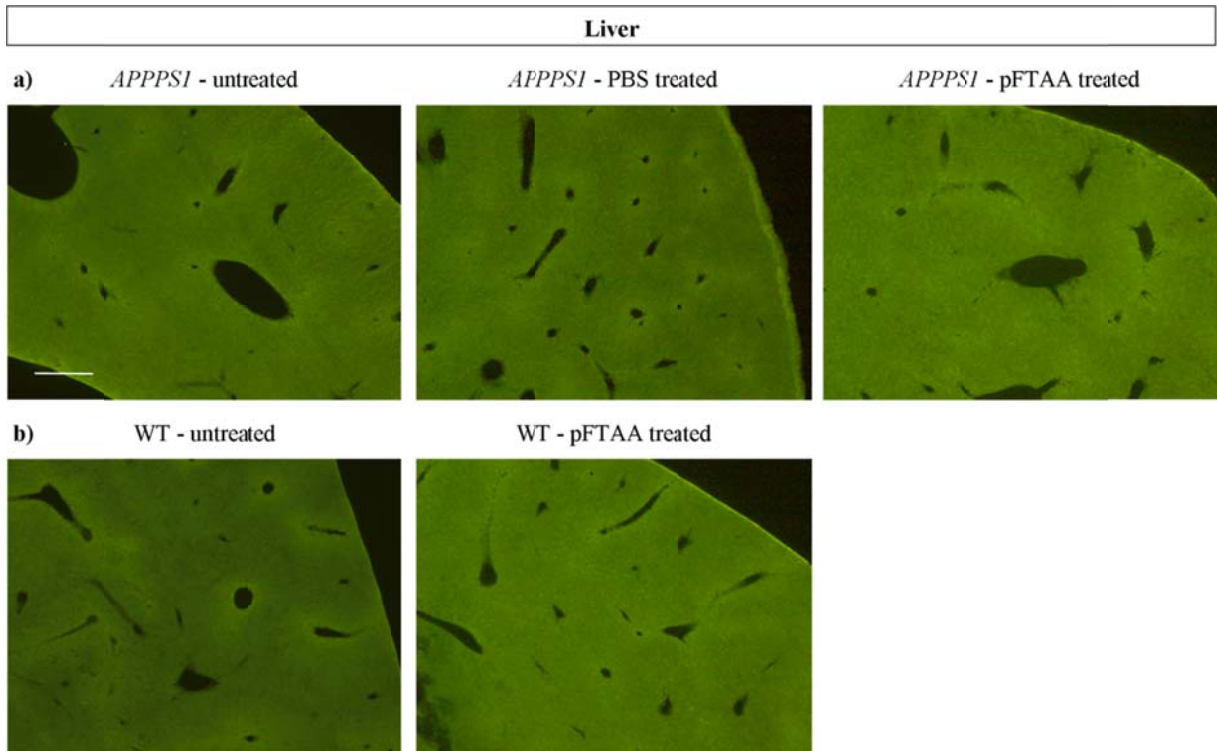


Figure 67: *Postmortem* screening of liver sections for pFTAA deposition after long term treatment of 120 d old *APPSI* and WT mice. Scale bar = 100 μ m.

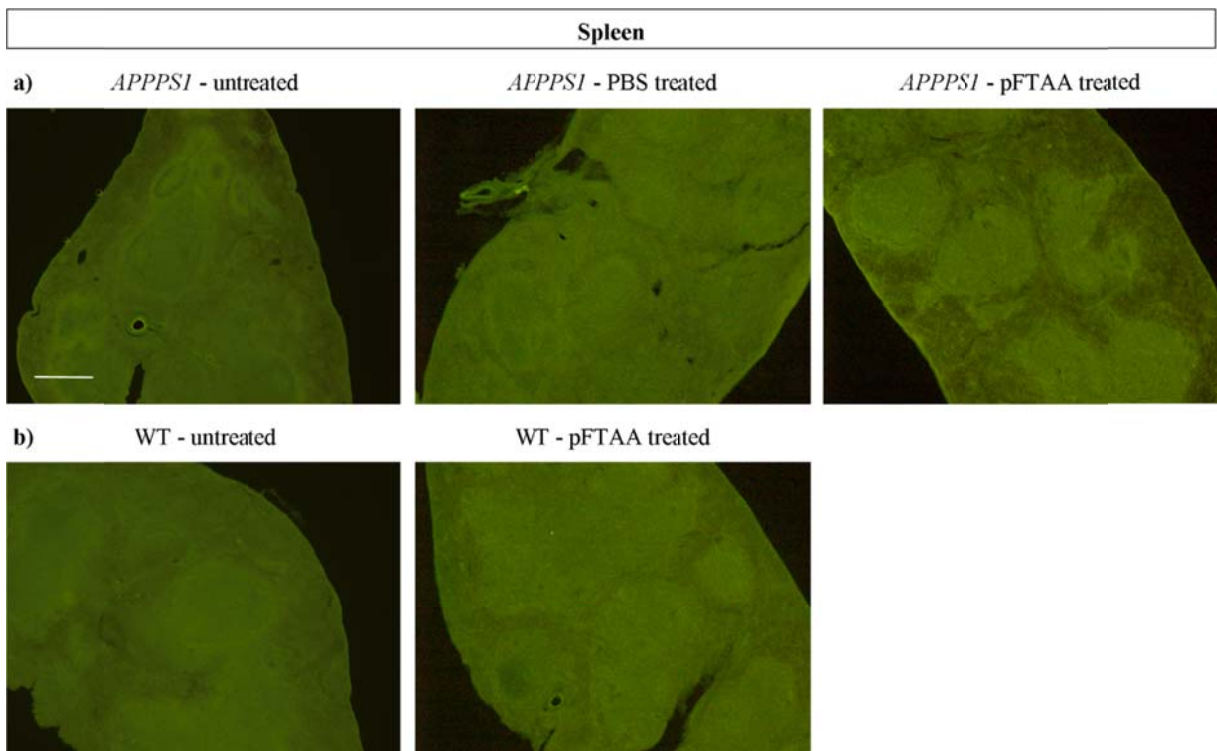


Figure 68: *Postmortem* screening of splenic sections for pFTAA deposition after long term treatment of 120 d old *APPSI* and WT mice. Scale bar = 100 μ m.

Results

In summary, none of the analyzed peripheral organs revealed systemic pFTAA deposition in *APPPSI* and WT mice after long term treatment. Furthermore no differences to PBS and untreated *APPPSI* and WT mice were observed.

The standard histological H&E staining method was used to screen peripheral organs for pathological structural alterations as an indication of toxicity after the long term pFTAA treatment of young *APPPSI* and WT mice. Serial paraffin sections (5 μm) of sampled organs were stained with H&E and analyzed by bright field microscopy (Olympus BX50). The following figures (Fig. 69-74) provide a histopathological overview of the analyzed organs. Sections of untreated *APPPSI* and WT mice were used as controls.

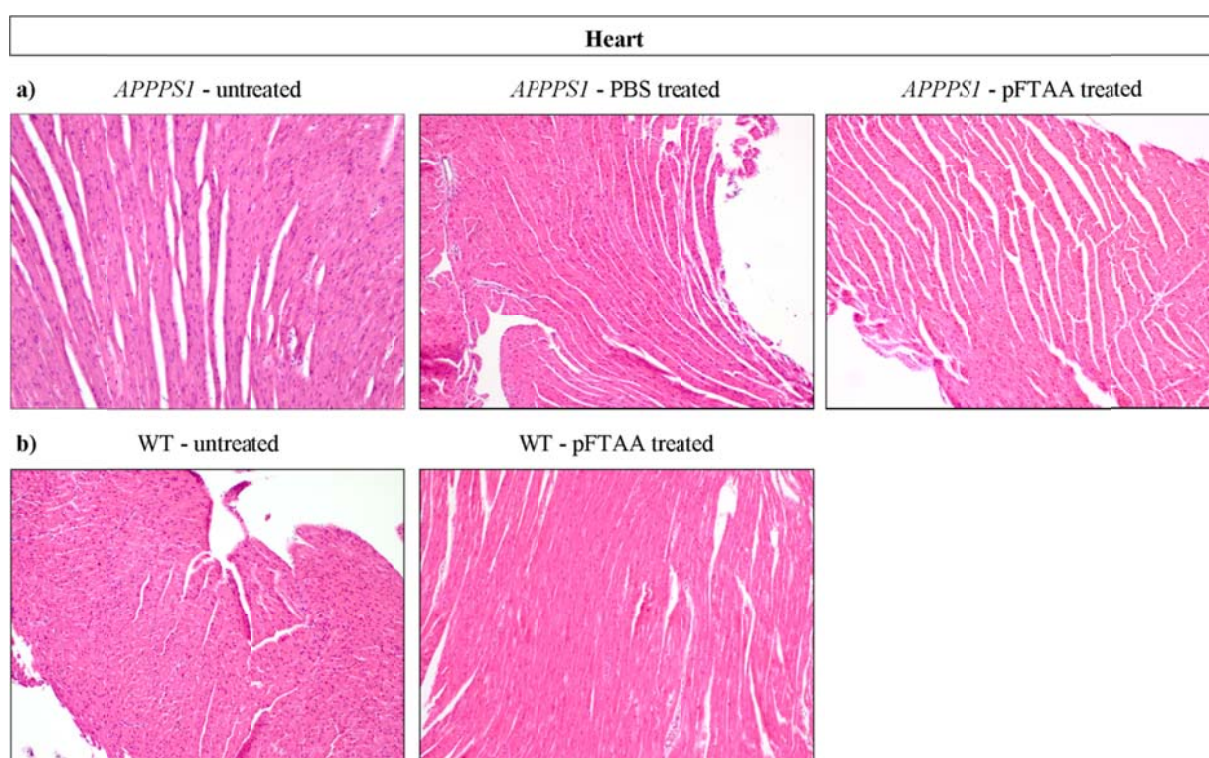


Figure 69: Histopathological analysis of cardiac muscle tissue by H&E staining after long term treatment of young *APPPSI* and WT mice. Scale bar = 100 μm .

Results

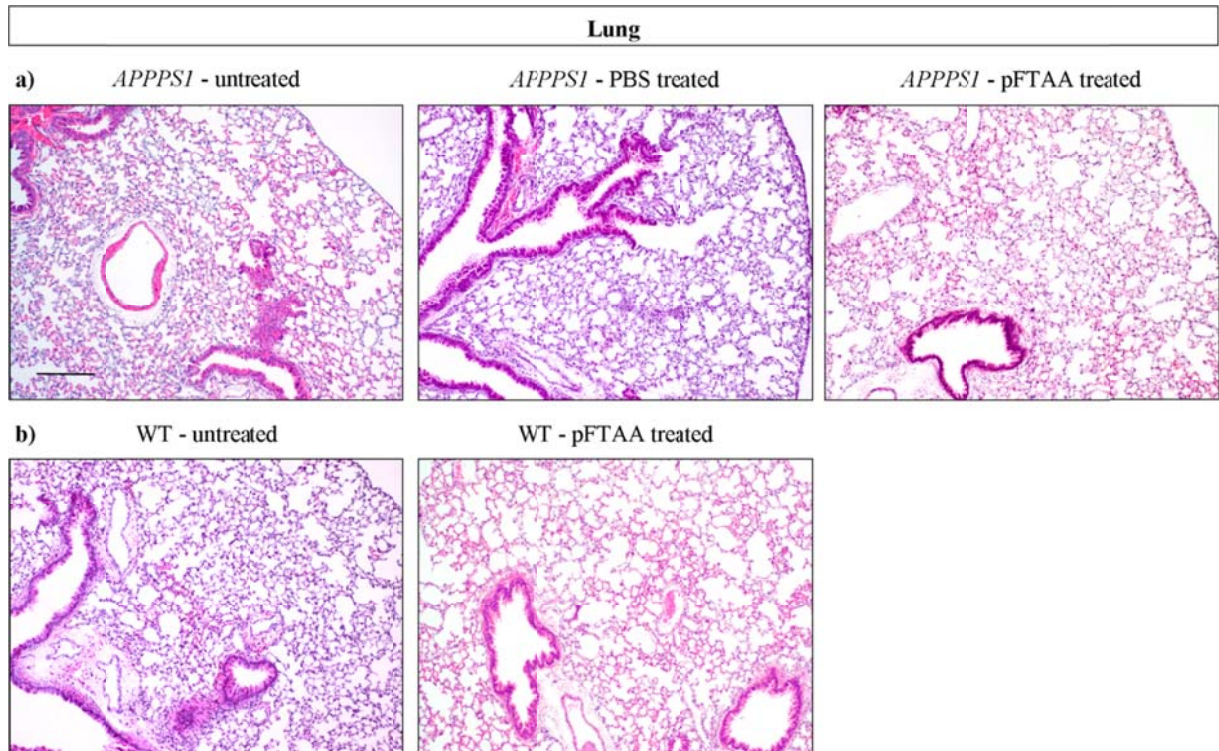


Figure 70: Histopathological analysis of lung tissue by H&E staining after long term treatment of young *APPSI* and WT mice. Scale bar = 100 μ m.

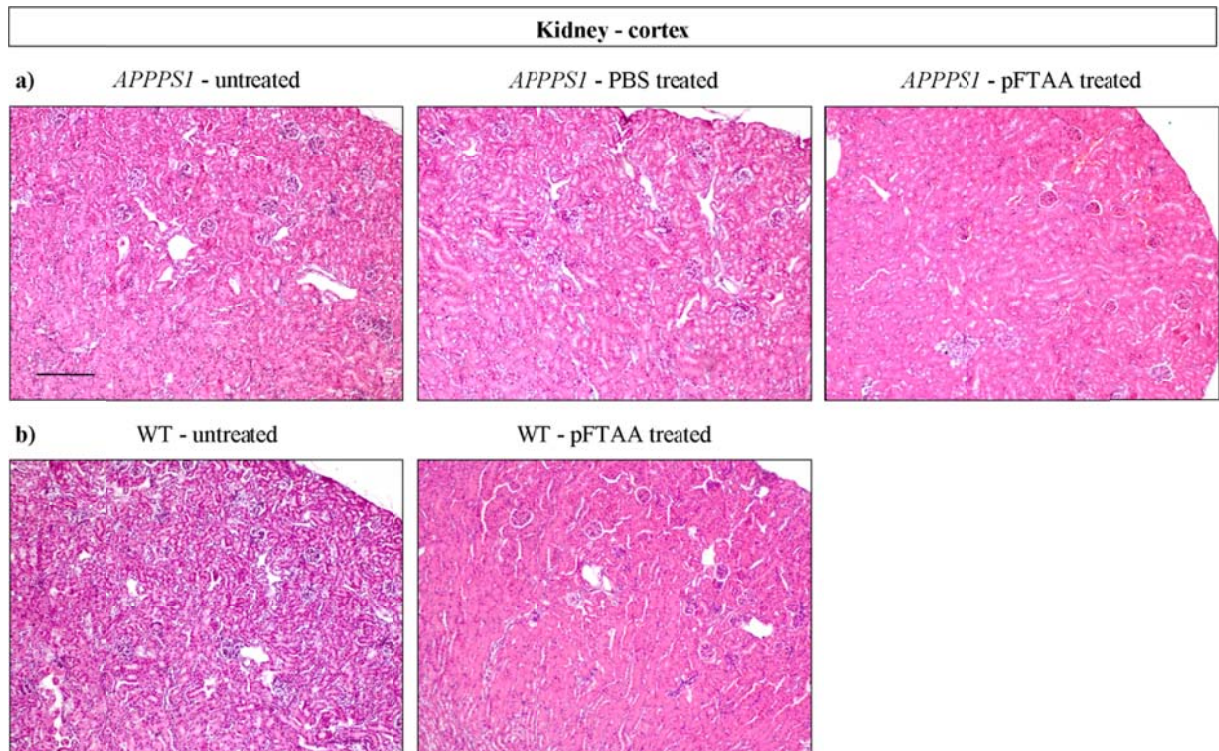


Figure 71: Histopathological analysis of cortical renal tissue by H&E staining after long term treatment of young *APPSI* and WT mice. Scale bar = 100 μ m.

Results

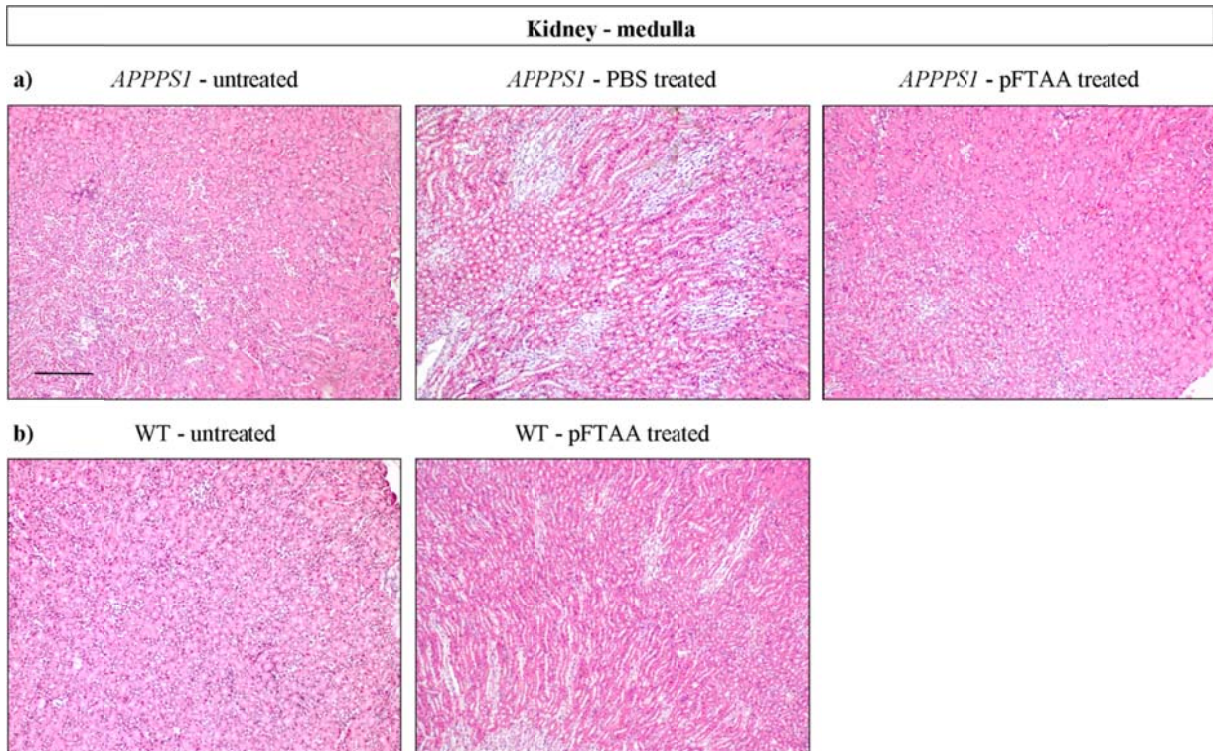


Figure 72: Histopathological *postmortem* analysis of renal medulla by H&E staining after long term treatment of young *APPPSI* and WT mice. Scale bar = 100 μ m.

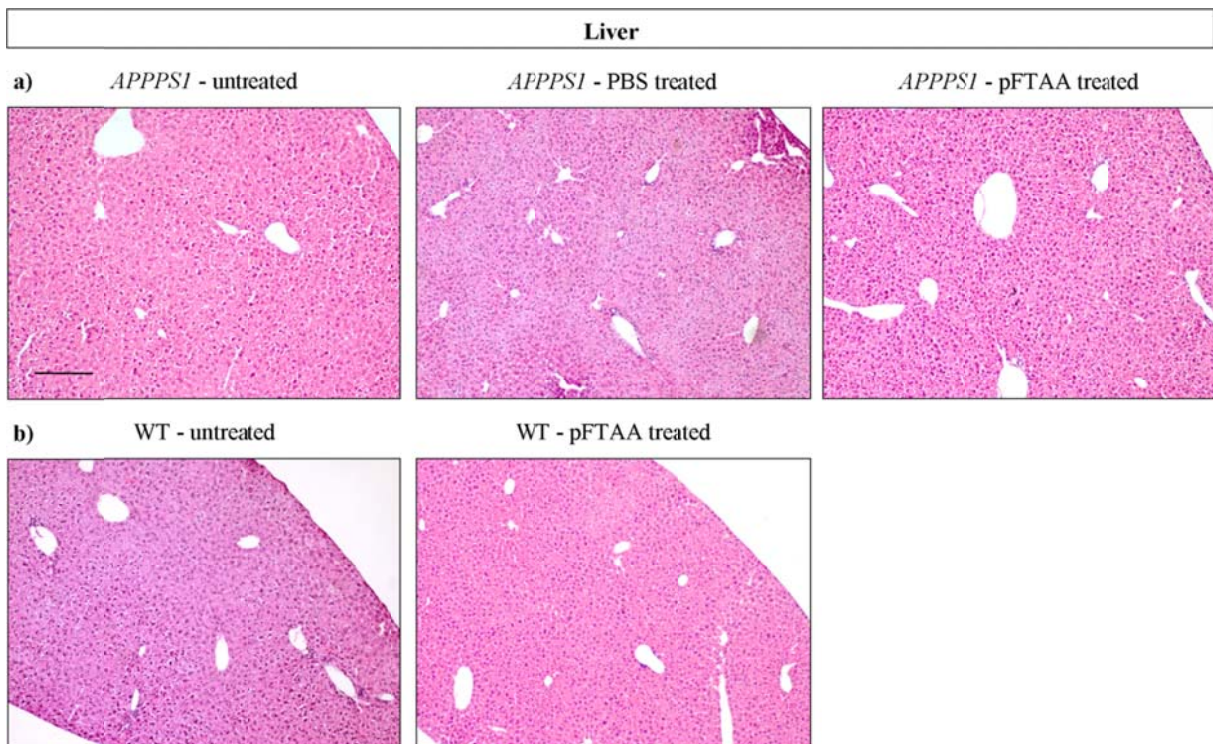


Figure 73: Histopathological analysis of liver tissue by H&E staining after long term treatment of young *APPPSI* and WT mice. Scale bar = 100 μ m.

Results

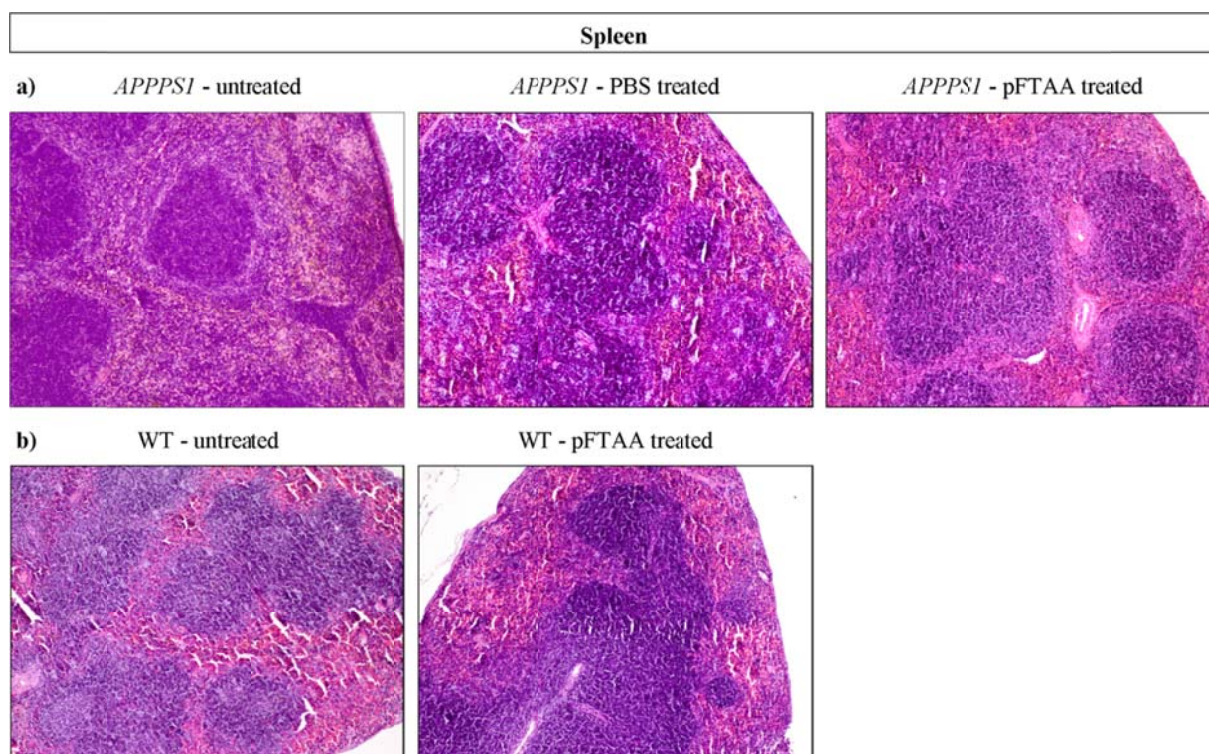


Figure 74: Histopathological analysis of splenic tissue by H&E staining after long term treatment of young *APPPSI* and WT mice. Scale bar = 100 μm.

As seen in figures 69-74 no obvious pathological alterations on H&E stained organ sections (heart, lung, kidney, liver, spleen) were detected after the 12 week long pFTAA treatment of *APPPSI* and WT mice. By comparing sections of pFTAA treated *APPPSI* and WT mice to PBS treated and untreated control animals, also no obvious pathological changes were found.

In conclusion, no obvious side effects of the peripheral pFTAA treatment were observed in analyzed mice. In comparison to PBS treated or untreated *APPPSI* and WT mice, no pFTAA treatment specific effect on weight gain of young experimental animals, blood count or functionality of peripheral organs was detected. Also no systemic deposition of pFTAA and pathological alternations were found after 12 weeks. This indicates no obvious and severe toxic side effects of long-term pFTAA presence in the murine system.

3.3.3 Histological analyses of cerebral sections after long term pFTAA treatment of young experimental animals

The most important question to answer after the long term pFTAA treatment of young *APPPSI* and WT mice was, if the treatment and the *in vivo* binding of pFTAA to A β aggregates affect AD pathology at 120 d of age. Therefore cerebral sections of i) untreated, ii) PBS treated and iii) pFTAA treated *APPPSI* mice were stained for A β deposits with

conventional amyloid dyes Congo red and pFTAA and immunohistochemically using A β specific antibodies 4G8 and 6E10. Afterwards cortical A β plaque burden was quantified. A β plaque burden was assessed by analysis of area covered by the specific staining as well as by counting the total number of A β plaques. For both analyses 10 to 12 serial cerebral sections were quantified using the Stereo Investigator system. For the antibody staining with 4G8 an additional plaque size distribution analysis was done using the cellSens Dimension software. Three cortical pictures per section were taken using the Olympus BX50 brightfield microscope and subsequently cortical A β plaques per image were classified into seven different plaque size classes by the software cellSens Dimension.

3.3.3.1 Quantification of cerebral A β plaque burden by conventional amyloid stainings

Congo red is a commonly used histological dye for amyloid detection. It stains the compact core of A β plaques, the so called congophilic plaques consisting of dense aggregated A β fibrils. pFTAA, as one of the available LCOs, in contrast also labels diffuse A β deposits.

After the long term pFTAA or PBS treatment of young *APP/PS1* mice the area covered by Congo red staining (Fig. 75b) and the number of cortical congophilic A β plaques of cerebral sections was quantified using the Stereo Investigator system (Fig. 75c). Also there was a trend of an increase in A β burden in pFTAA treated *APP/PS1* mice when assessed by Congo red staining, the analysis showed no statistically significant difference between groups in A β covered area by Congo red staining between untreated, PBS and pFTAA treated *APP/PS1* mice (Fig. 75b). However, a significant difference in A β plaque number, i.e. the cortical amount of A β plaques, was detected. pFTAA treated *APP/PS1* mice revealed significantly ($p < 0,05$) more congophilic A β plaques in comparison to PBS treated *APP/PS1* mice (Fig. 75c). No statistically significant difference in plaque number was observed between untreated and PBS treated as well as between untreated and pFTAA treated *APP/PS1* mice (Fig. 75c).

Results

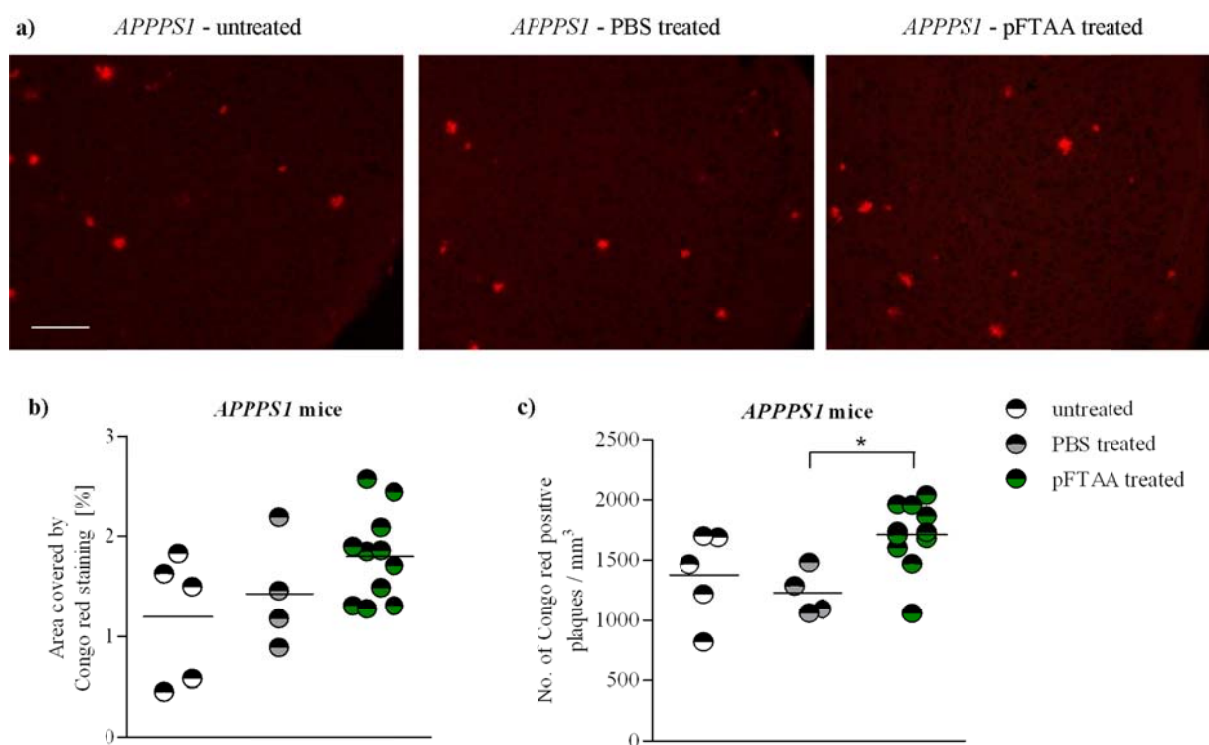


Figure 75: Quantification of cerebral A β burden by Congo red staining in 120 d old *APPPSI* mice after long term pFTAA treatment. After a peripheral pFTAA or PBS treatment of *APPPSI* mice, cerebral A β plaque burden was assessed and compared to untreated animals. Representative images of each transgene positive experimental group (*APPPSI* – untreated, PBS and pFTAA treated) are depicted (a, Scale bar = 50 μ m). 10-12 serial coronal sections of *APPPSI* mice were quantified by assessing the area covered by Congo red staining using the Stereo Investigator system (b). Additionally an A β plaque count in the cortex of untreated, PBS and pFTAA treated *APPPSI* mice was performed (c). For statistical analyses one-way ANOVA with Bonferroni's post test was used.

Cerebral A β plaque burden was additionally analyzed by a pFTAA staining of *APPPSI* brain sections after long term treatment. The quantification of the cortical A β plaque covered area by pFTAA staining revealed no statistical significant difference of overall A β burden between untreated, PBS and pFTAA treated *APPPSI* mice (Fig. 76b). However, pFTAA treated *APPPSI* mice revealed a statistically significant increase ($p < 0.01$) of pFTAA labeled A β plaque number in contrast to PBS treated animals (Fig. 76c). This statistical significant increase in pFTAA positive plaque number after pFTAA treatment is similar to what was observed for the Congo red staining (Fig. 75c). This indicates that long term pFTAA treatment leads to smaller individual plaques without affecting overall A β plaque covered area substantially. Again no difference in plaque number between untreated and PBS treated as well as between untreated and pFTAA treated *APPPSI* mice was observed (Fig. 76c).

Results

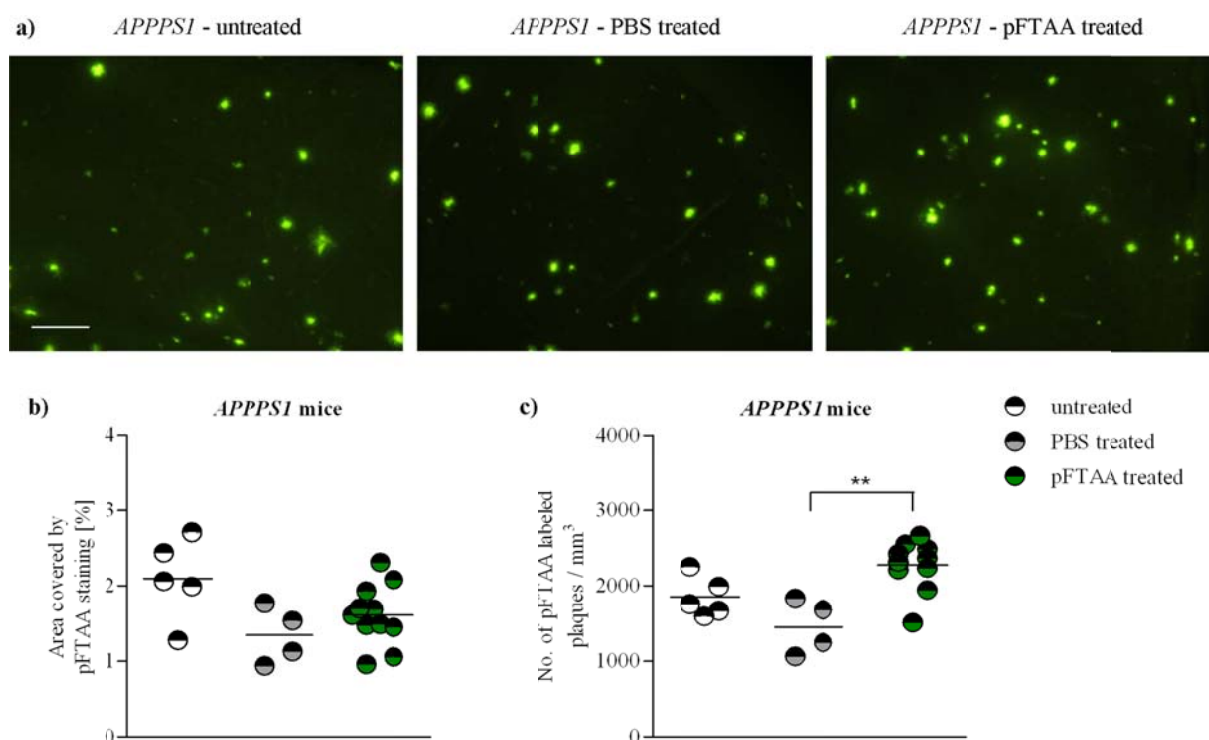


Figure 76: Quantification of cerebral A β burden by pFTAA staining in 120 d old *APPPS1* mice after long term treatment. After a peripheral pFTAA or PBS long term treatment of young *APPPS1* mice, cerebral A β burden was assessed using a pFTAA staining and compared to untreated animals. Representative images of the pFTAA staining for each transgene positive experimental group (*APPPS1* – untreated, PBS and pFTAA treated) are shown (a, Scale bar = 100 μ m). The cortical area (b) covered by pFTAA staining [%] as well as a cortical A β plaque count (c) was analyzed using the Stereo Investigator software. For statistical analyses one-way ANOVA with Bonferroni's post test was used.

3.3.3.2 Quantification of cerebral A β plaque burden by immunohistological stainings

The two A β specific antibodies 4G8 (binds to amino acids residues 1-16) and 6E10 (binds to amino acid residues 17-24), which bind to different epitopes of the A β peptides, have been used for immunohistological quantification of cerebral A β plaque burden after long term treatment of young *APPPS1* mice. In contrast to Congo red and pFTAA, these specific antibodies label beside A β plaque cores also diffuse A β deposits (see chapter 3.1.1).

No statistical significant difference of area covered by 4G8 staining was observed between untreated, PBS and pFTAA treated *APPPS1* mice (Fig. 77b). In comparison to PBS treated animals, the stereological count of 4G8 labeled cortical A β plaques revealed a statistical significant ($p < 0.05$) increase of plaque number after pFTAA treatment of young *APPPS1* mice (Fig. 77c). No difference of the A β plaque count was measured when cerebral plaque number of untreated and PBS treated or untreated and pFTAA treated *APPPS1* mice was compared. The increased cortical A β plaque number after pFTAA treatment of young *APPPS1* mice was observed also by Congo red and pFTAA staining (see chapter 3.3.3.1), indicating

Results

that the pFTAA treatment caused the occurrence of an increased number of smaller individual A β plaques while the overall A β covered area remained unchanged.

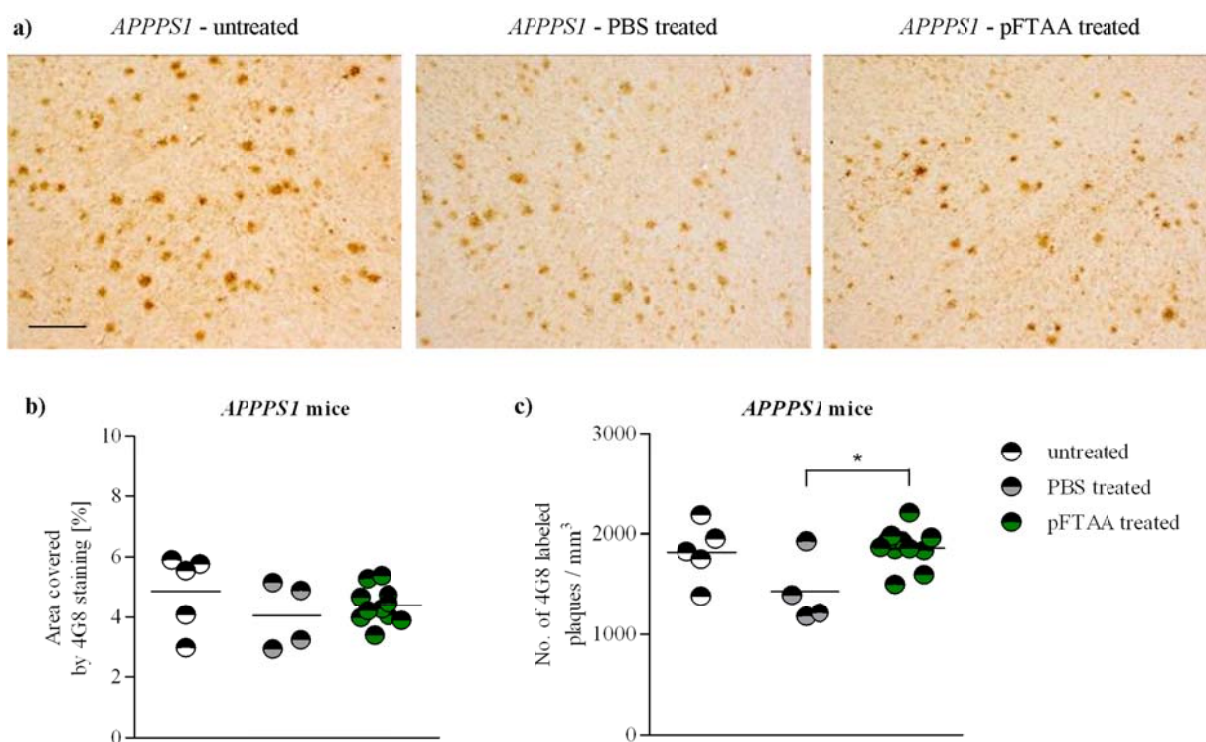


Figure 77: Quantification of cerebral A β burden by immunohistochemical 4G8 staining in 120 d old *APPPS1* mice after long term treatment. To investigate if peripheral applied pFTAA has an effect on cerebral A β burden, young *APPPS1* and WT mice were treated over 12 weeks with pFTAA or PBS and plaque burden was quantified and compared to untreated *APPPS1* mice *postmortem* on coronal brain sections. Initially a visual screening of cortical A β plaques was performed. Representative images are depicted in Fig. 84a (Scale bar = 100 μ m). Furthermore the Stereo Investigator system was used to quantify the area covered (b) by 4G8 staining [%] and the number (c) of 4G8 labeled A β plaques. For statistical analyses one-way ANOVA with Bonferroni's post test was used.

Since the quantification of cortical A β plaque number analyzed by Congo red, pFTAA and 4G8 staining revealed the presence of smaller individual plaques after pFTAA treatment of young *APPPS1* mice, a detailed size analysis of cerebral plaques was performed. Using the cellSens Dimension software, cortical A β plaques were classified into seven different size classes: class 1: 10-500 μ m, class 2: 500-1,000 μ m, class 3: 1,000-1,500 μ m, class 4: 1,500-2,000 μ m, class 5: 2,000-2,500 μ m, class 6: 2,500-3,000 μ m and class 7: 3,000-6,500 μ m. It was observed, that pFTAA treated *APPPS1* mice have significantly more small A β plaques in size class 1 in contrast to PBS ($p < 0.01$) and untreated ($p < 0.001$) animals (Fig. 78). PBS treated animals showed in comparison to untreated mice a statistical significant increase ($p < 0.01$) in plaque number of class 1. Furthermore pFTAA treated *APPPS1* mice revealed in comparison to PBS and untreated mice significant less plaques in classes 2-5 (Fig. 78). For

Results

PBS treated *APP/PS1* mice a statistical significant decrease in A β plaque number of classes 2 and 3 was detected when compared to untreated animals. Taken together the size distribution analysis revealed, that a 12 week long pFTAA treatment in young *APP/PS1* mice led to the development of more small cerebral A β plaques (class 1) and less medium and very large plaques (class 2-5).

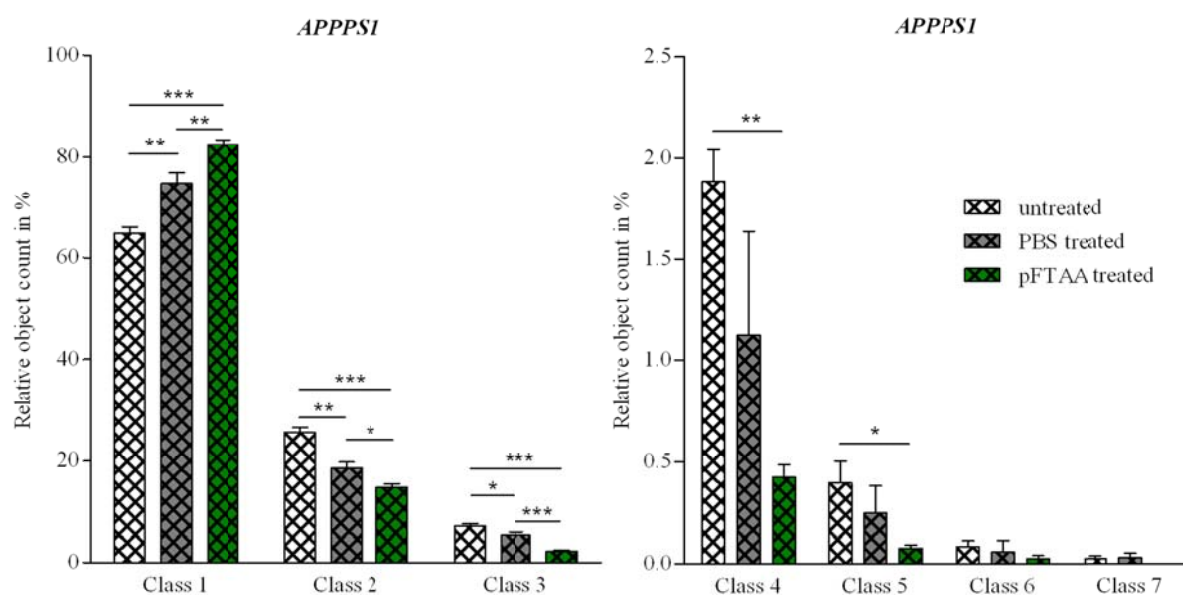


Figure 78: Plaques size distribution analysis of 4G8 labeled A β plaques in 120 d old *APP/PS1* mice after long term treatment. 4G8 labeled cortical A β plaques of three transgene positive experimental groups (*APP/PS1*: i) untreated (n = 3), ii) PBS treated (n = 4), iii) pFTAA treated (n = 11) were classified after long term treatment into seven different plaque size classes: class 1: 10-500 μ m, class 2: 500-1,000 μ m, class 3: 1,000-1,500 μ m, class 4: 1,500-2,000 μ m, class 5: 2,000-2,500 μ m, class 6: 2,500-3,000 μ m and class 7: 3,000-6,500 μ m. Three images per section, in total 10-12 coronal free floating sections per *APP/PS1* mouse, were analyzed using the cellSens Dimension software of Olympus. For statistical analyses one-way ANOVA with Bonferroni's post test was used.

The plaque size distribution analysis showed that the mean area per cortical A β plaque was statistically significantly decreased in *APP/PS1* mice after long term pFTAA treatment in contrast to PBS treated ($p < 0.05$) and untreated ($p < 0.001$) animals (Fig. 79). PBS treated *APP/PS1* mice showed a mild but also significant reduction ($p < 0.01$) in mean area per cortical A β plaque, when compared to untreated animals (Fig. 79). The minor difference in mean plaque area in PBS treated animals compared to untreated animals is most likely due to the impact of the weekly injections on neuroinflammation⁸⁸ and thus A β deposition⁸⁹⁻⁹¹.

Results

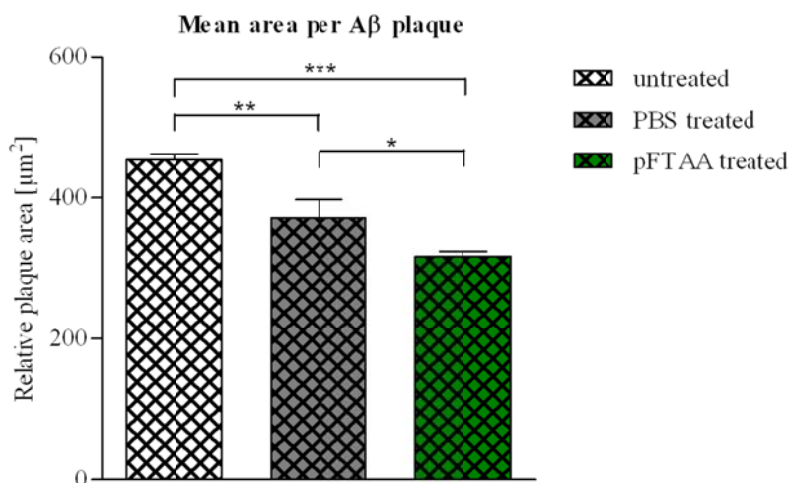


Figure 79: Mean area per 4G8 labeled cortical A β plaque in 120 d old *APPPS1* mice after long term treatment. The mean area per cortical A β plaque was assessed by plaque size distribution analysis (cellSens Dimension software, Olympus) of 4G8 labeled cerebral free floating sections (30 μm) after long term pFTAA treatment of *APPPS1* mice and compared to PBS treated and untreated animals. For statistical analyses one-way ANOVA with Bonferroni's post test was used.

Overall the plaque size distribution analysis revealed more numerous small and less large cortical A β plaques as well as a decreased mean area per plaque after systemic pFTAA treatment in young *APPPS1* mice. The higher number of small A β plaques in pFTAA treated animals may point to an increase in seeding of amyloid deposits⁹². In addition the decreased mean area per cortical A β plaque of pFTAA treated *APPPS1* mice indicates a slower plaque growth and maturation. It is conceivable that simultaneously to inducing more cerebral amyloid seeds, pFTAA slows the maturation of cerebral A β plaques leading to a comparable overall A β plaque burden in pFTAA treated animals when compared to PBS treated animals.

An additional immunohistochemical staining of cerebral A β plaques was performed with antibody 6E10 (Fig. 80a). Although it was shown previously that pFTAA labeling of cerebral A β plaques does not interfere with immunohistochemical A β stainings (see chapter 3.1.1), it is possible that a long term pFTAA treatment caused epitope-masking for specific antibody binding sites. To exclude epitope-masking, a second immunohistochemical staining for A β quantification was performed.

The quantification of the area covered by 6E10 staining revealed also no significant difference in A β plaque burden of untreated, PBS and pFTAA treated *APPPS1* mice (Fig. 80b). This result was in line with the A β quantifications performed after Congo red, pFTAA and 4G8 staining – no significant differences of overall A β plaque covered were observed between the three experimental groups. Immunohistochemical A β quantifications using antibodies 4G8

Results

and 6E10 revealed identical results (Fig. 77b, Fig. 80b), which indicates no relevant epitope masking effect of pFTAA binding to A β plaques.

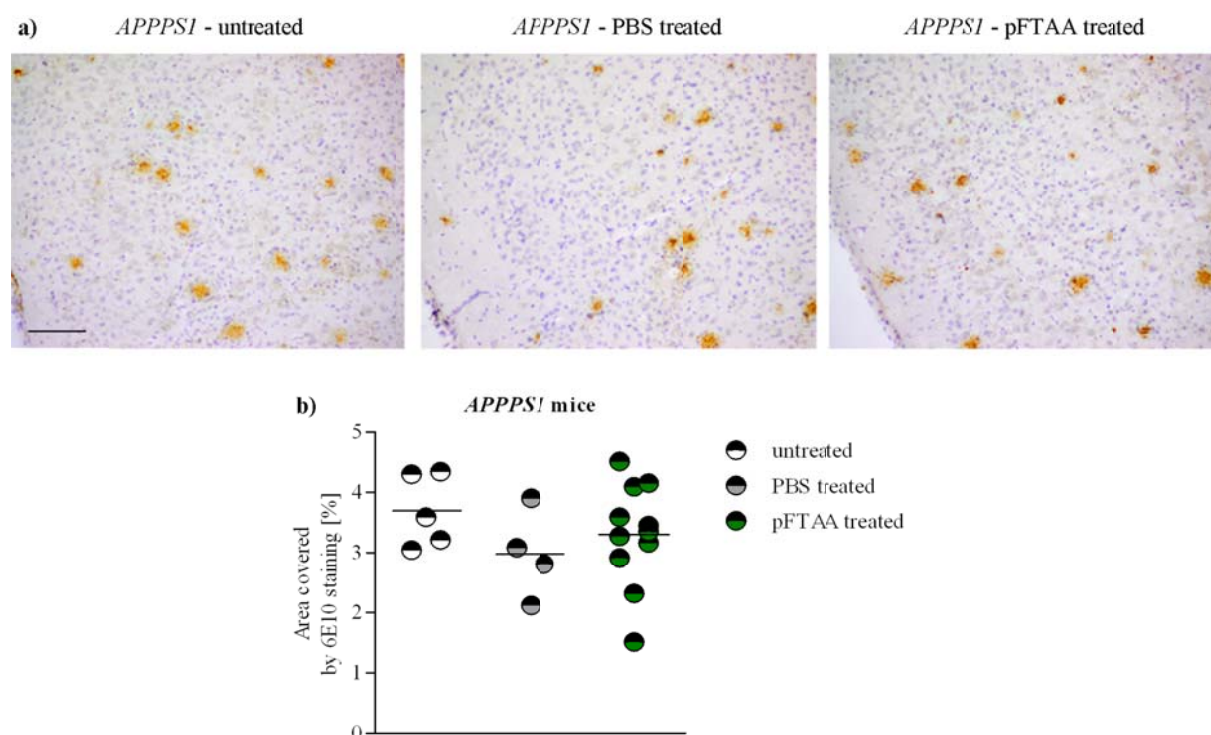


Figure 80: Quantification of A β burden in 120 days old APPPS1 mice by immunohistochemical 6E10 staining after long term pFTAA treatment. Representative images of 6E10 stained, cerebral free floating sections (30 μ m) for each transgene positive experimental group (APPPS1 – untreated, PBS and pFTAA treated) are shown (a, Scale bar = 50 μ m). The quantification of the area covered by 6E10 staining [%] was assessed and compared subsequently for untreated, PBS and pFTAA treated APPPS1 mice using the Stereo Investigator system (b). For statistical analyses one-way ANOVA with Bonferroni's post test was used.

The long term pFTAA treatment of initially 6-8 weeks old APPPS1 mice revealed no effect on overall cerebral A β burden as assessed by different staining methods (Fig. 75-77b, 80b). However detailed analysis showed an impact of the pFTAA treatment in young APPPS1 mice on plaque number (Fig. 75-77c) and size (Fig. 78). In comparison to PBS treated and untreated APPPS1 mice, pFTAA treated animals revealed more numerous and smaller plaques (Fig. 78, 79). These results indicate structural changes of cerebral A β depositions after systemic pFTAA treatment of young APPPS1 mice.

3.3.3.3 Spectral analyses of A β plaques after long term pFTAA treatment

A detailed histological quantification of the cerebral A β burden after pFTAA treatment of young APPPS1 mice (see chapter 3.3.3.2) revealed treatment specific changes of cerebral amyloid deposition. In contrast to PBS treated and untreated animals, pFTAA treated APPPS1

Results

mice showed more numerous and smaller A β plaques, indicating structural changes in amyloid deposition after treatment. To further investigate the structure of deposited A β in pFTAA treated *APP/PS1* mice, a spectral analysis of A β plaques in these mice was performed. For this purpose, cerebral sections of untreated, PBS and pFTAA treated, 120 d old *APP/PS1* mice were co-stained with two structurally distinct, but related LCOs, hFTAA and pFTAA, to analyze plaque conformation. In a similar fashion double labeling was used previously to perform an age dependent analysis of cerebral A β deposits in *APP/PS1* mice⁷³. Three serial, coronal free floating sections of untreated, PBS and pFTAA treated *APP/PS1* mice were co-stained with hFTAA and pFTAA (1 mg/ml each) and fluorescence and confocal microscopy was used for spectral imaging of co-stained A β plaques.

Analyses by confocal microscopy revealed that core and periphery of A β plaques on cerebral sections of PBS treated and untreated *APP/PS1* mice could be distinguished by an hFTAA/pFTAA co-staining. Plaque cores were labeled by pFTAA and emitted green fluorescent light. These dense cores could easily be differentiated from the hFTAA labeled plaque periphery, which comprise diffuse A β plaques emitting red light (Fig. 81a, b). In contrast, pFTAA treated *APP/PS1* mice did not show a well-defined pFTAA labeled plaque core, which can be separated from the plaque periphery. A β plaques of pFTAA treated animals were mainly stained by hFTAA (Fig. 81c).

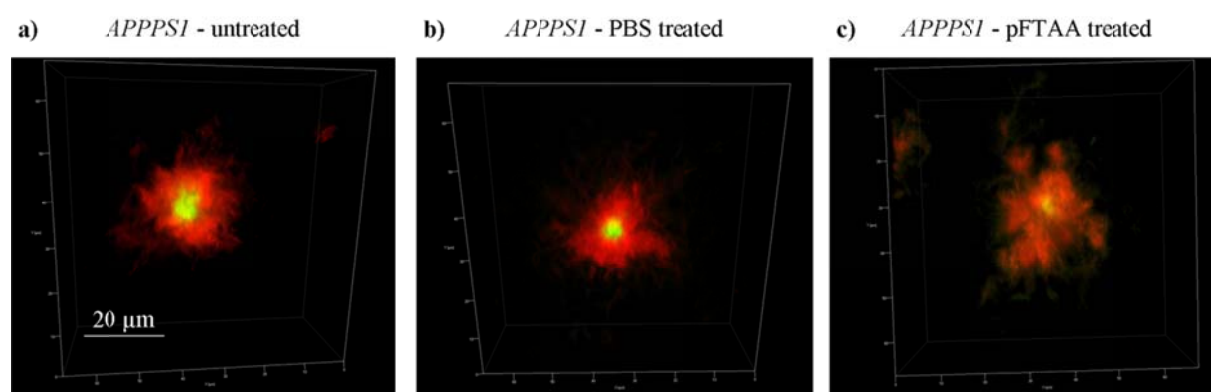


Figure 81: Spectral imaging of cerebral A β plaques after long term treatment of young *APP/PS1* mice by confocal microscopy. Confocal microscopy (LSM 510 META, Zeiss) was used to image hFTAA/pFTAA co-stained cerebral A β plaques on brain sections of untreated, PBS and pFTAA treated 120 d old *APP/PS1* mice. Staining differences related to a distinct A β plaque morphology are visualized. Scale bar = 20 μ m.

Since morphological differences between pFTAA and PBS treated or untreated *APP/PS1* mice were observed using spectral confocal imaging, a detailed spectral analysis of cerebral A β plaques after pFTAA/hFTAA co-staining was assessed by spectral fluorescence imaging.

Results

Therefore a 436 nm long pass excitation filter was used. Single A β plaques were imaged using the 10x and 40x objective and emitted spectra of monitored plaques were recorded. Analysis of spectra of A β plaques showed, that cores of untreated and PBS treated animals emitted blue light achieved by pFTAA binding. The plaque periphery emitted yellow light representing bound hFTAA (Fig. 82a, b). In contrast, A β plaques of pFTAA treated animals showed no staining specific difference between core and periphery, pFTAA/hFTAA co-stained plaques emitted an almost homogenous yellow light as seen for hFTAA staining (Fig. 82c). Since the largest changes in the emission spectra of pFTAA/hFTAA co-stained A β plaques on brain sections of untreated, PBS and pFTAA treated *APP/PS1* mice were recorded at 509 nm and 589 nm, the ratio of the associated emission values was calculated and confirmed the differences achieved by the spectral confocal analysis. A statistically significant difference ($p < 0.001$) of the 509/589 nm ratio between pFTAA treated animals and untreated/PBS treated 120 d old *APP/PS1* mice was detected (Fig. 82d).

Results

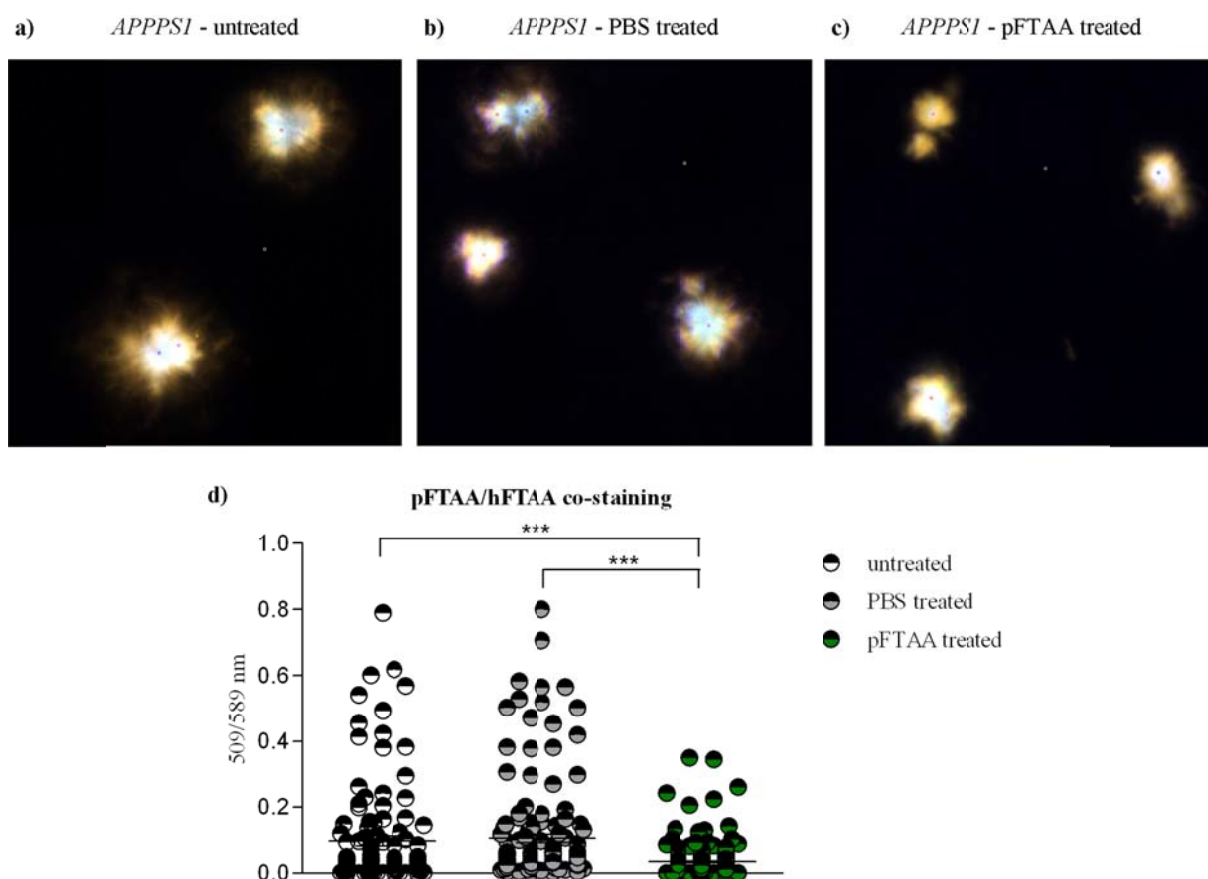


Figure 82: Spectral imaging of cortical A β plaques after no, PBS and pFTAA treatment of initially 6-8 weeks old *APPPSI* mice using fluorescence microscopy. Single cortical A β plaques of untreated ($n = 3$), PBS ($n = 4$) and pFTAA treated ($n = 6$), 120 d old *APPPSI* mice were analyzed spectrally using a 436 nm long pass excitation filter (436/10 (LP475)) after an LCO co-staining by hFTAA and pFTAA. 38 randomly selected A β plaques per animal were analyzed with the 40x magnification of the objective. Fig. 88a-c give a visual overview of spectrally analyzed, cortical A β plaques after no treatment and a long term PBS and pFTAA treatment in young *APPPSI* mice. The ratio of measured emission values at 509 nm and 589 nm was calculated for single A β plaques of each experimental, *APPPSI* positive group (b). For statistical analyses one-way ANOVA with Bonferroni's post test was used.

These differences in LCO staining provide evidence for structural differences between distinct A β deposits after long term pFTAA treatment of young *APPPSI* mice, which were already indicated by quantifications of cerebral A β burden by immunohistological and conventional staining methods (see chapter 3.3.3.1 and 3.3.3.2). Changes of spectrally measured emission spectra confirmed this notion further. The ratio of emission values at 509 nm and 589 nm showed significant differences between pFTAA and untreated or PBS treated *APPPSI* mice. These results indicate structural differences between cerebral A β deposits in young *APPPSI* mice after long term treatment, comparable to what was observed previously for cerebral A β deposits of *APPPSI* mice as the animals age⁷³.

3.3.3.4 Quantification of dystrophic neurites around cerebral A β plaques

Since structural differences of cerebral A β plaques on brain sections of pFTAA treated *APP/PS1* mice compared to PBS and untreated *APP/PS1* mice were detected by immunohistological as well as by spectral analyses, an influence of the long term pFTAA treatment on A β plaque associated cellular pathology was investigated next. *APP/PS1* mice reveal no classical NFT formation as it is described for human AD brains, however dystrophic neurites containing hyperphosphorylated tau aggregates can be detected in the vicinity of cerebral A β plaques⁶⁴. The area covered by dystrophic neurites, stained by the antibody AT8, surrounding A β plaques was quantified using the Stereo Investigator system. The histological quantification of AT8 covered area around cortical A β plaques showed a trend towards less dystrophic neurites around plaques in 120 d old, pFTAA treated *APP/PS1* mice when compared to controls. However, this tendency did not reach statistical significance (Fig. 83).

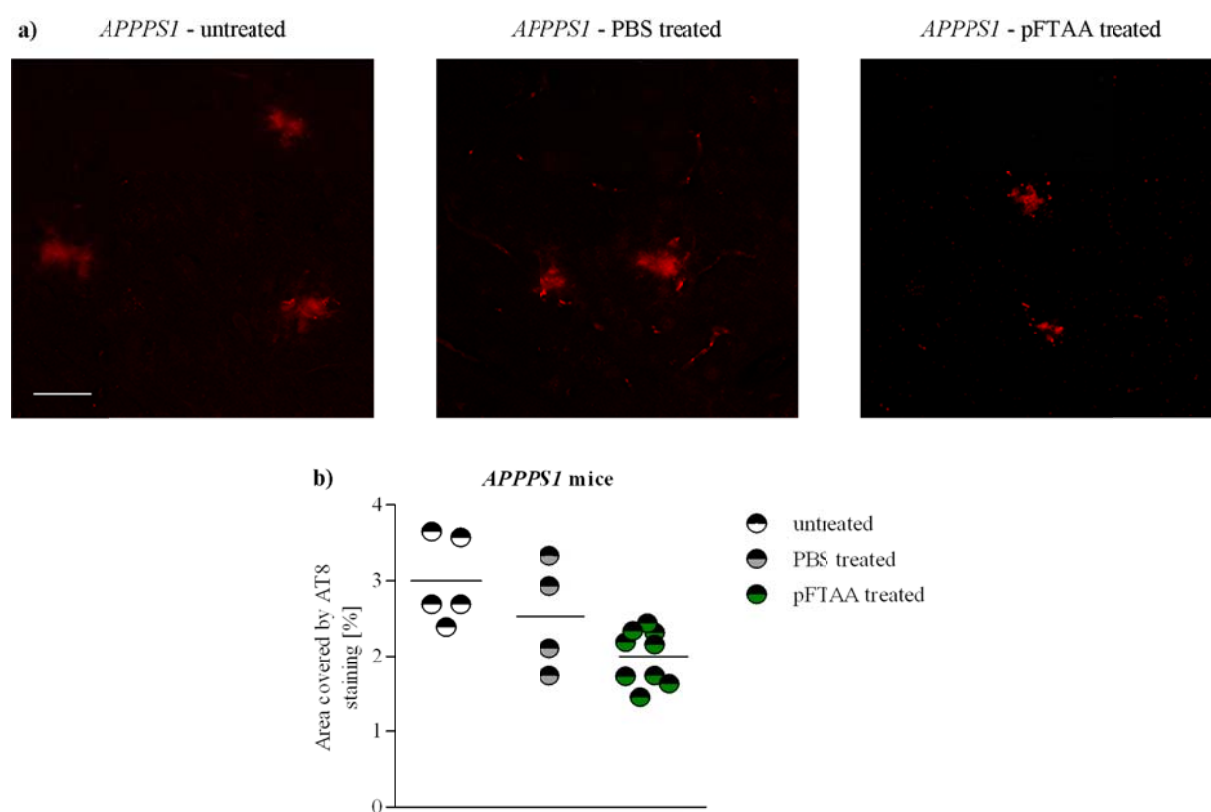


Figure 83: Quantification of dystrophic neurites surrounding cortical A β plaques by AT8 staining in 120 d old *APP/PS1* mice after long term pFTAA treatment. After a peripheral pFTAA or PBS treatment of young *APP/PS1* mice, the area of dystrophic neurites surrounding cortical A β plaques was assessed and compared to untreated animals. Representative images of the AT8 staining for each transgene positive experimental group (*APP/PS1* – untreated, PBS and pFTAA treated) were taken using fluorescence microscopy (Cy5, Zeiss Observer Z1) and are depicted (a, Scale bar = 25 μ m). A quantification of the A β plaque surrounding area, covered by AT8 staining [%], was analyzed subsequently using the Stereo Investigator system (b). 10-12 coronal free floating sections (30 μ m) were analyzed by fluorescence microscopy (Cy5, Olympus BX53). For statistical analyses one-way ANOVA with Bonferroni's post test was used.

3.3.3.5 Histological analyses of neuronal loss in distinct cerebral regions

The analysis of dystrophic neurites around cerebral A β plaques on brain sections of long term treated *APP/PS1* mice revealed a trend towards decreased dystrophic neurites around cerebral A β plaques after long term pFTAA application compared to control animals. Because neuronal loss is a characteristic hallmark of AD, an immunohistochemical neuron staining of cerebral sections using the monoclonal antibody NeuN was assessed in a next step and neurons in distinct A β plaque affected regions were analyzed on *APP/PS1* brain sections after long term treatment by brightfield microscopy. Untreated, PBS and pFTAA treated *APP/PS1* and WT mice were compared. No overt neuronal loss on analyzed brain sections of 120 d old *APP/PS1* mice was detected independent of treatment and genotype of screened animals when NeuN labeled brain sections were compared (Fig. 84). Especially detailed microscopic analyses of the cortex (Fig. 84b), the hippocampal CA1 region (Fig. 84c) and the dentate gyrus (Fig. 84d) revealed no obvious differences in experimental groups, either. It was shown before, that 17 month old *APP/PS1* mice with robust cerebral A β plaques pathology did not show neuronal loss in the cortex but exhibited a thinned neuronal layer in the hippocampal dentate gyrus formation⁹³. Since *APP/PS1* mice in the present study were 13 months younger than the animals, which revealed neuronal loss in the hippocampus in this previous study⁹³, the results presented here are in line with the reported properties of the *APP/PS1* animal model, where no overt neuronal loss is expected at 4 months of age.

Results

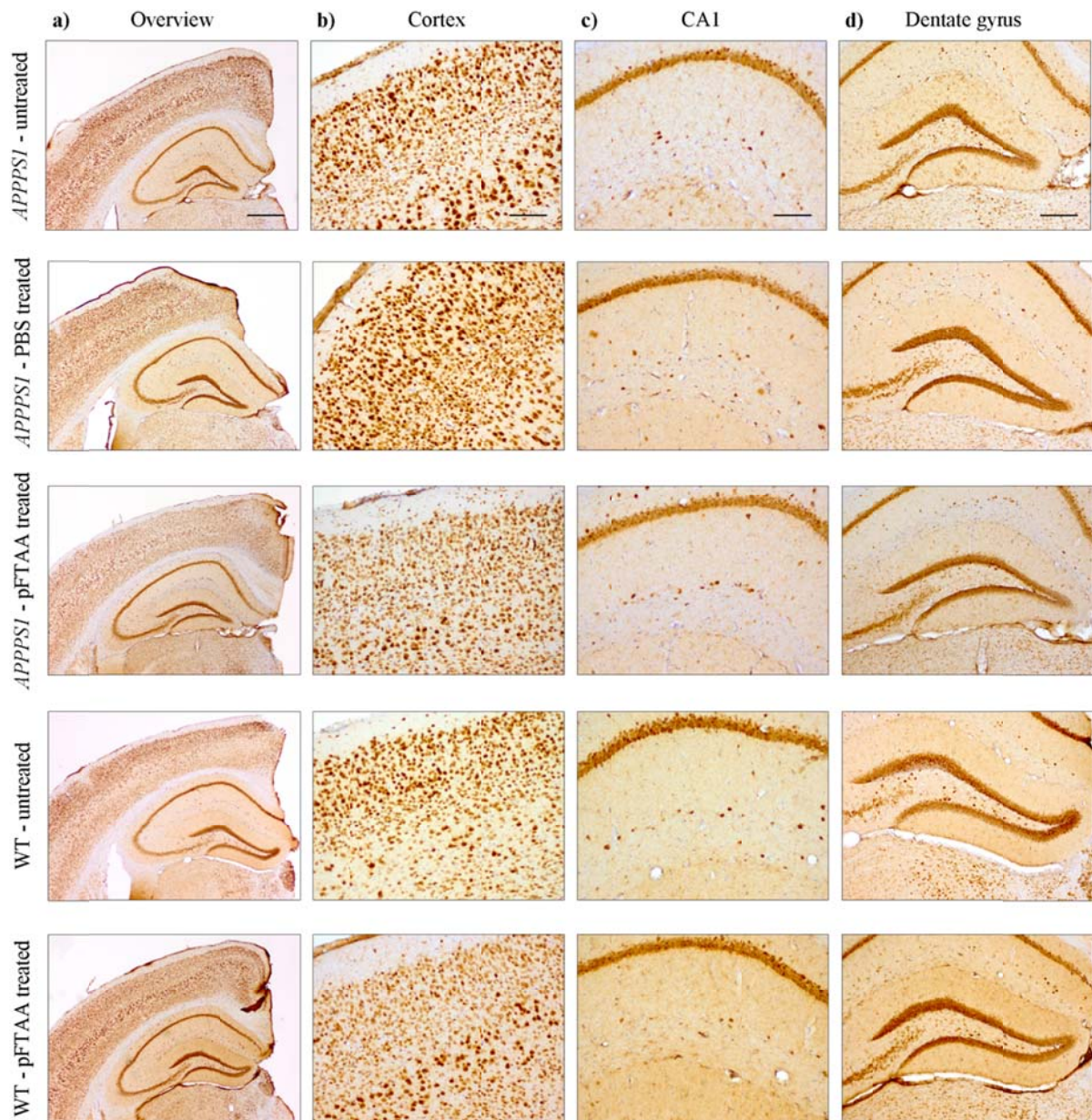


Figure 84: Histological analysis of neurons in distinct cerebral regions using NeuN staining in 120 d old *APPPS1* mice after long term treatment. 6-8 weeks old *APPPS1* and WT mice were treated over 12 weeks with pFTAA or PBS to investigate the influence of pFTAA on cerebral A β plaque pathology. As controls untreated *APPPS1* and WT mice were added for *postmortem* analyses. Neurons on cerebral free floating sections (30 μ m) were stained using antibody NeuN and distinct cerebral regions were analyzed by brightfield microscopy (Olympus BX50). Cortex and hippocampus were monitored at a low magnification (a, Scale bar = 500 μ m). A cortical region (b, Scale bar = 100 μ m), the hippocampal CA1 region (cm, Scale bar = 100 μ m) and the dentate gyrus (d, Scale = 200 μ m) were screened for neuronal loss in detail at higher magnification.

3.3.3.6 Histological analyses of cortical gliosis

Cerebral A β plaque deposition in AD is significantly associated with microglia and astrocyte mediated inflammation, which leads to microgliosis and astrogliosis⁹⁴. Coronal brain sections were stained with the microglia marker Iba1 and astrocytic marker GFAP and assessed to screen for cerebral gliosis after pFTAA or PBS treatment in *APPPS1* and WT mice.

Results

Antibodies targeting Iba1 and GFAP, were used for a systematic qualitative analysis of A β plaque associated cerebral gliosis in young *APP/PS1* mice and a possible treatment related gliosis in WT mice after long term treatment.

The antibody detecting Iba1 was used to label cerebral microglia, the brain's intrinsic phagocytes on brains sections of experimental *APP/PS1* and WT mice. As shown before^{64,95}, activated and hypertrophic microglia tightly clustered around A β plaques in 120 d old *APP/PS1* mice. This reaction was observed irrespective of treatment – on cerebral sections of untreated, PBS and pFTAA treated *APP/PS1* mice Iba1-positive microglia clustered around A β plaques and revealed characteristic morphological features including hypertrophic cytoplasm, shortened and highly branched processes (Fig. 85a). Since WT mice exhibit no cerebral A β deposition, no plaque associated microgliosis was detected in untreated WT mice. Furthermore no pFTAA treatment specific activation of microglia was observed in aged pFTAA treated WT mice, when compared to untreated WT mice (Fig. 85b).

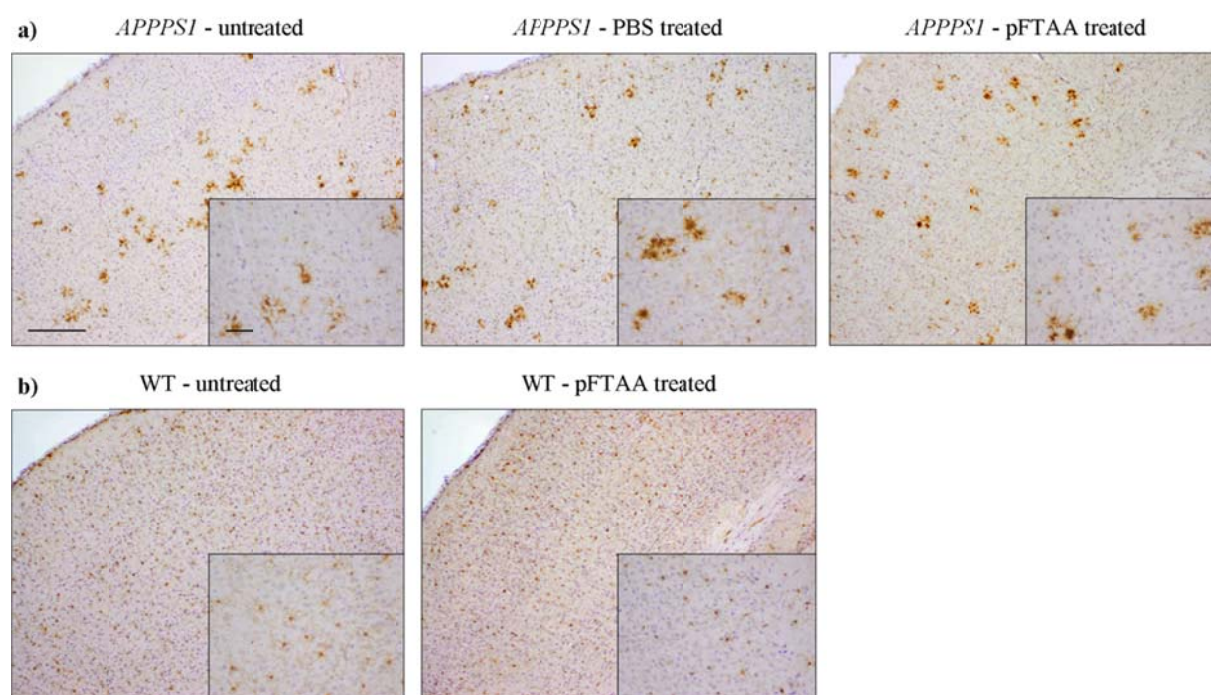


Figure 85: Iba1-positive microglia in the cortex of 120 d old *APP/PS1* and WT mice after no treatment, and long term PBS and pFTAA treatment. To investigate if pFTAA affect A β plaque associated pathology in young *APP/PS1* (a) and WT (b) mice, which were treated over 12 weeks with 10 mg/kg pFTAA or PBS, a microglial staining of brain sections was assessed. Cerebral free floating sections were stained immunohistochemically with an antibody detecting Iba1 and subsequently a systematic qualitative analysis for cerebral microgliosis was performed using brightfield microscopy (Olympus BX50). As additional control, sections of untreated *APP/PS1* and WT mice were added. Scale bar overview = 100 μ m, Scale bar insert = 25 μ m.

Results

Activated astrocytes in the brains of untreated, PBS or pFTAA treated young (initially 6-8 weeks old) *APP/PS1* and WT mice after long term treatment were visualized by an immunohistochemical staining with an antibody detecting GFAP. No difference in astroglial reaction towards A β plaques in *APP/PS1* mice was observed (Fig. 86a) – GFAP-positive, activated astrocytes clustered around A β plaques, as described in previous publications⁶⁴, independent if mice were untreated, PBS or pFTAA treated. No significant astrogliosis was detected in untreated or pFTAA treated WT mice (Fig. 86b).

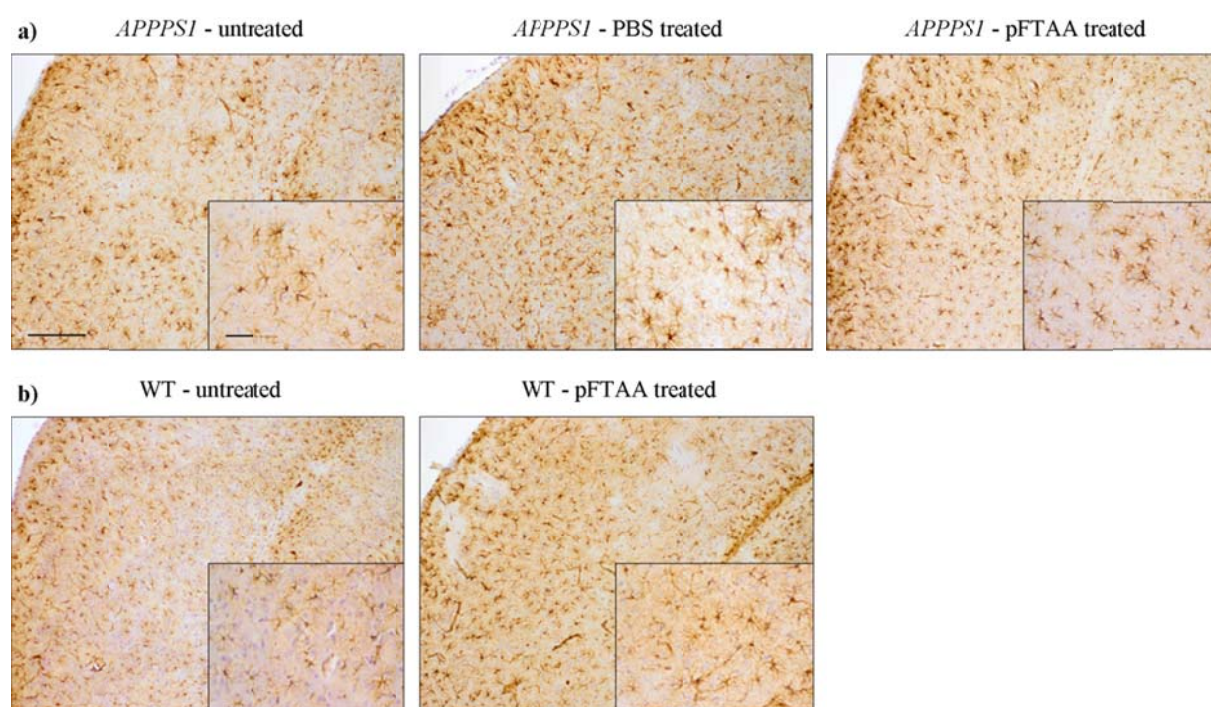


Figure 86: GFAP-positive astrocytes in the cortex of 120 d old *APP/PS1* and WT mice after no treatment, and PBS and pFTAA treatment. Young *APP/PS1* and WT (6-8 weeks old) mice were treated over 12 weeks with pFTAA or PBS and cerebral free floating sections (30 μ m), labeled with an antibody detecting GFAP, were used for a systematic qualitative analysis for cerebral astrocytosis. A pFTAA treatment related astrocytosis was investigated in WT animals (b) and a cerebral A β plaque associated astrogliosis in *APP/PS1* mice (a) using brightfield microscopy (Olympus BX50). As additional control sections of untreated *APP/PS1* and WT mice were added. Scale bar overview = 100 μ m, Scale bar insert = 25 μ m.

pFTAA treatment did not alter microgliosis and astrogliosis in *APP/PS1* mice and also did not induce significant activation of microglia and astrocytes, indicating no major effect of pFTAA on the glial reaction in *APP/PS1* and WT mice.

3.3.4 Biochemical analysis of cerebral A β burden after long term treatment of young *APPPSI* mice

3.3.4.1 Detection of cerebral A β amounts by MSD 6E10 assay and by SDS-polyacrylamid gel electrophoresis and Western Blotting

Immunohistological analysis of overall cerebral A β plaque burden revealed no significant difference between untreated, PBS and pFTAA treated *APPPSI* mice after long term treatment, while indicating a structural change of A β deposits (see chapter 3.3.3.1 and 3.3.3.2). To confirm the immunohistological results, the second hemisphere of long term treated experimental *APPPSI* mice was used for biochemical analysis of cerebral A β amounts. For this purpose soluble and insoluble A β of frozen hemispheres was extracted in a stepwise fashion in TBS, TBS-T, SDS and FA-buffer according to previously published protocols⁸⁴ and A β amounts of single fractions were measured by the MSD 6E10 assay and by SDS-PAGE and WB.

First, A β concentrations in the TBS fraction, which contains soluble A β from the cerebral parenchyma after brain homogenization were determined using the MSD 6E10 assay. A statistically significant difference of A β_{40} amounts between untreated, PBS and pFTAA treated *APPPSI* mice (Fig. 87a) was not detected. However, the cerebral A β_{42} amount in the TBS fraction of pFTAA treated *APPPSI* mice was statistically significantly increased ($p < 0.05$) when compared to PBS treated animals. There was no statistical significant change of the A β_{42} amount between untreated and PBS treated as well as between untreated and pFTAA treated *APPPSI* mice (Fig. 87b).

Results

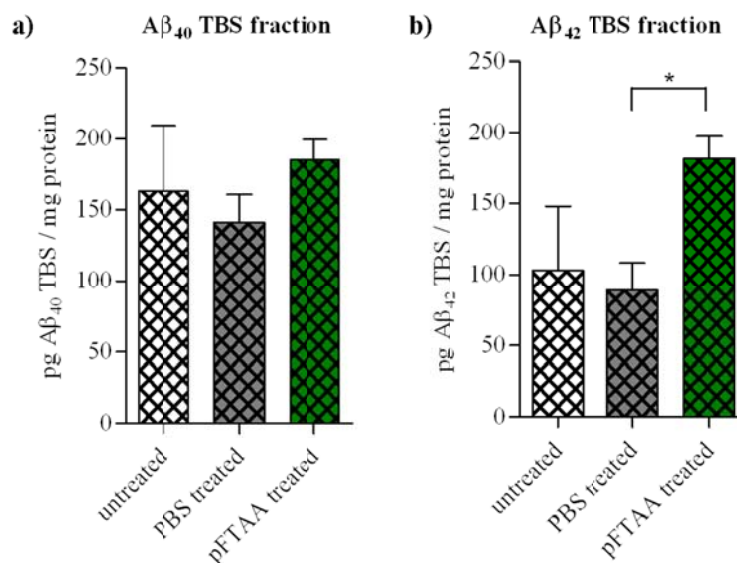


Figure 87: Cerebral Aβ₄₀ and Aβ₄₂ amounts in the supernatant of TBS fractions after brain homogenization of 120 d old *APPPS1* mice. The frozen second hemisphere of 120 d old untreated mice and *APPPS1* mice, long term treated with pFTAA or PBS, was used for biochemical Aβ analyses. Cerebral Aβ₄₀ (a) and Aβ₄₂ amounts (b) in the supernatant of the TBS fraction were measured after homogenization by the MSD 6E10 assay and compared between transgene positive experimental groups (*APPPS1*: i) untreated (n = 2), ii) PBS treated (n = 4), iii) pFTAA treated (n = 10)). For statistical analyses one-way ANOVA with Bonferroni's post test was used.

Total Aβ amounts in the supernatant of the TBS fractions were further determined by SDS-PAGE and WB, to confirm the results of the MSD 6E10 assay. A representative Western Blot showing soluble Aβ of the TBS fraction at 4 kDa is depicted in figure 88a, the quantification of Aβ amounts in TBS fractions (n = 2 gels) of untreated, PBS and pFTAA treated *APPPS1* mice using Adobe Photoshop software is shown in figure 88b. In contrast to the results of the MSD 6E10 assay (Fig. 87b), no statistical significant difference of cerebral Aβ amounts in TBS fractions using SDS-PAGE and WB analysis were observed between the analyzed experimental groups (Fig. 88b). This is most likely due to the lower sensitivity of the Western Blot, compared to the MSD assay, since only low amounts of Aβ were detected in the TBS fraction.

Results

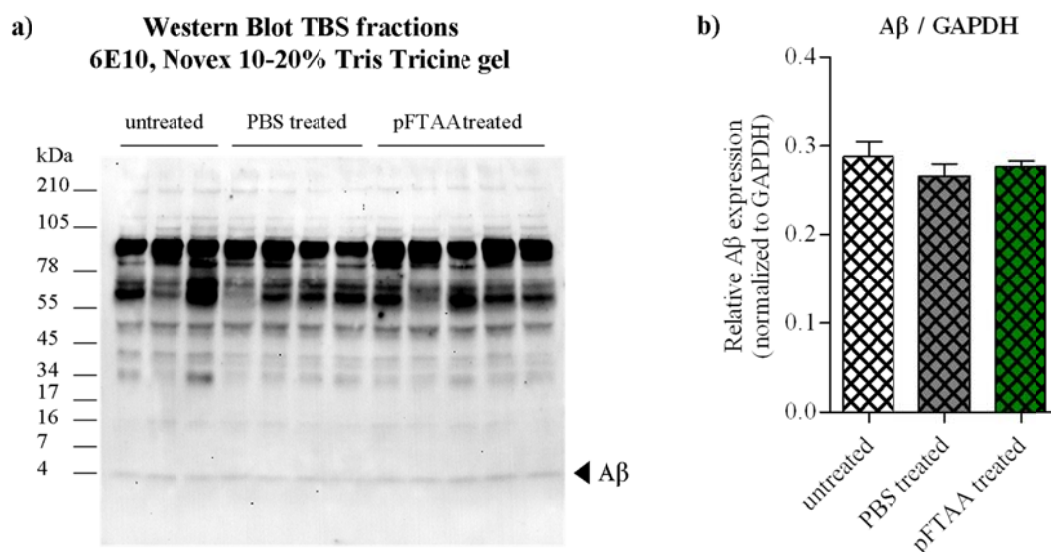


Figure 88: Detection of A β in TBS fractions by SDS-PAGE and WB after homogenization of 120 d old *APPPSI* hemispheres after long term treatment. Frozen hemispheres of 120 d old, untreated (n = 3), PBS (n = 4) or pFTAA (n = 5) treated *APPPSI* mice were homogenized after long term treatment by four-step extraction and A β in the supernatant of TBS fractions was detected using SDS-PAGE and WB. A representative WB showing soluble A β amounts of untreated, PBS and pFTAA treated *APPPSI* mice at 4 kDa is depicted (a). Relative 6E10 expression of two WB gels was analyzed and normalized to GAPDH (b). For statistical analyses one-way ANOVA with Bonferroni's post test was used.

Next A β amounts in the TBS-T fraction, containing cell membrane bound and soluble A β were measured by MSD 6E10 assay and SDS-PAGE and WB. The MSD assay revealed no statistical significant differences of A β_{40} and A β_{42} amounts in the TBS-T fraction between untreated, PBS and pFTAA treated *APPPSI* mice (Fig. 89). Using the SDS-PAGE and subsequent WB, membrane bound A β of the TBS-T fraction could not be detected (Fig. 90) and further quantified, possibly due to low total A β amounts in this fraction.

Results

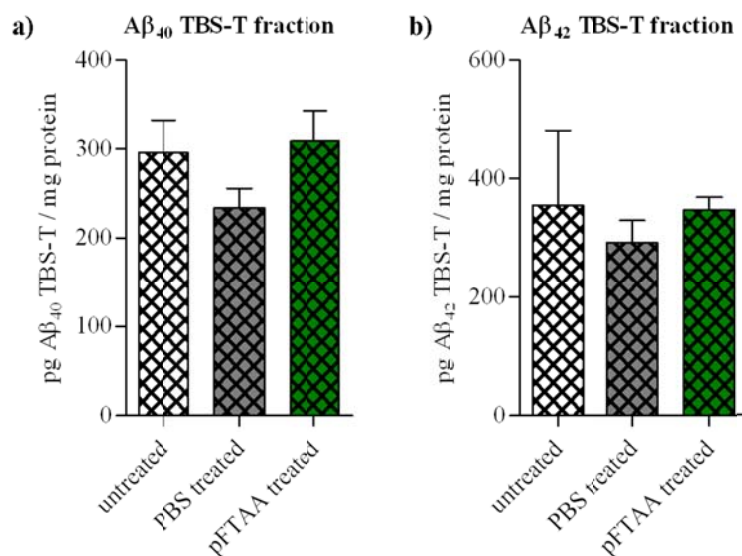


Figure 89: Cerebral Aβ₄₀ and Aβ₄₂ amounts determined in TBS-T fractions after brain homogenization of 120 d old *APP^{PS1}* mice using the MSD 6E10 assay. Frozen hemispheres of 120 d old, transgene positive experimental mice (*APP^{PS1}*) long term treated with pFTAA (n = 10) or PBS (n = 4) were homogenized for biochemical Aβ detection. Two hemispheres of untreated, age matched *APP^{PS1}* mice (n = 2) were analyzed as additional controls. Cerebral Aβ₄₀ (a) and Aβ₄₂ (b) amounts in the supernatant of TBS-T fractions were determined after four-step extraction by the MSD 6E10 assay. For statistical analyses one-way ANOVA with Bonferroni's post test was used.

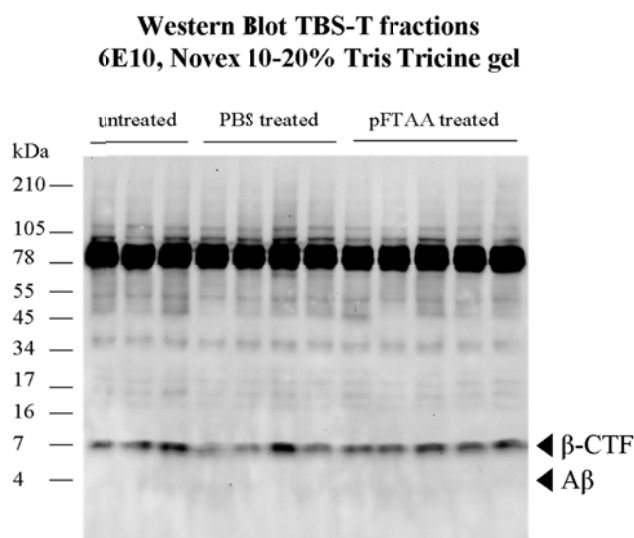


Figure 90: Detection of Aβ in the TBS-T fractions by SDS-PAGE and WB after homogenization of 120 d old *APP^{PS1}* hemispheres. Hemispheres of 120 d old *APP^{PS1}* mice (untreated (n = 2), PBS (n = 5) and pFTAA (n = 5) treated) were homogenized by four-step extraction and Aβ amounts in the supernatant of the TBS-T fraction were detected by SDS-PAGE and WB. A representative WB showing membrane bound Aβ amounts of untreated, PBS and pFTAA treated *APP^{PS1}* mice at 4 kDa is depicted.

Aβ₄₀ and Aβ₄₂ amounts of the SDS fraction, which consists mainly of aggregated Aβ, were determined using the MSD 6E10 assay. Aβ₄₀ and Aβ₄₂ levels in the SDS fraction showed a

Results

significant reduction after pFTAA treatment of young *APP/PS1* mice when cerebral A β amounts were compared to untreated and PBS treated *APP/PS1* mice after long term treatment (Fig. 91). SDS-PAGE and subsequent WB as further biochemical analyses confirmed this finding and showed in contrast to untreated and PBS treated animals a statistically significant reduction ($p < 0.01$) of cerebral aggregated A β levels in hemispheres of pFTAA treated *APP/PS1* mice (Fig. 92). In contrast to untreated and PBS treated *APP/PS1* mice, pFTAA treated animals revealed reductions of about 80 % (Fig. 92b).

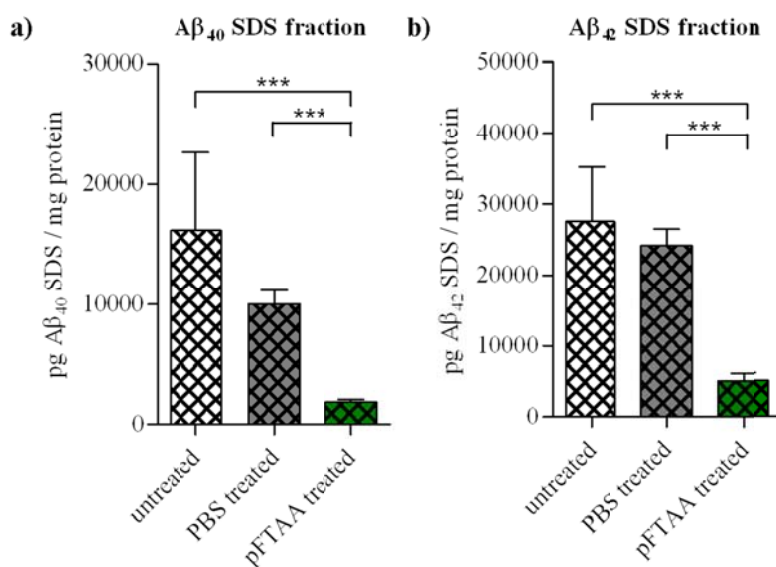


Figure 91: Cerebral A β_{40} and A β_{42} amounts determined in SDS fractions after brain homogenization of 120 d old *APP/PS1* mice using the MSD 6E10 assay. Frozen hemispheres of untreated ($n = 2$) and over 12 weeks with PBS ($n = 4$) or pFTAA ($n = 10$) treated young *APP/PS1* mice (initially 6-8 weeks) were homogenized and cerebral A β levels of the SDS fraction were detected biochemically. Cerebral A β_{40} (a) and A β_{42} (b) amounts in the supernatant of SDS fractions were measured after the stepwise A β extraction of hemispheres after long term treatment by the MSD 6E10 assay. For statistical analyses one-way ANOVA with Bonferroni's post test was used.

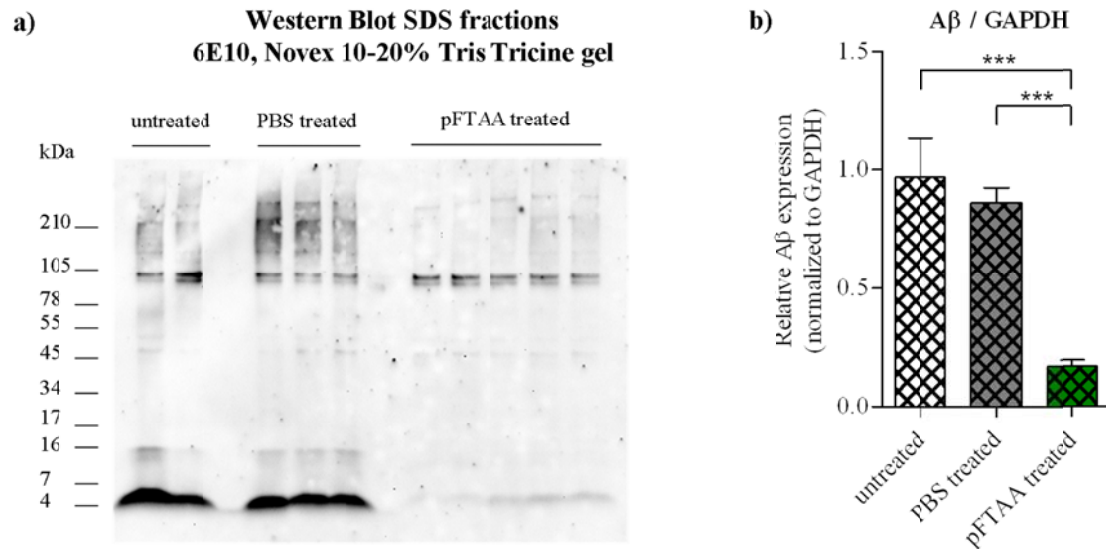


Figure 92: Detection of A β in SDS fractions by SDS-PAGE and subsequent WB analysis after homogenization of 120 d old *APPPS1* hemispheres. Frozen hemispheres of 120 d old *APPPS1* mice (untreated (n = 2), PBS (n = 3) and pFTAA treated (n = 5)) were homogenized after peripheral long term treatment by four-step extraction and A β in the supernatant of SDS fractions was detected by SDS-PAGE and WB. A representative WB showing intracellular A β levels of untreated, PBS and pFTAA treated *APPPS1* mice at 4 kDa is depicted (a). Relative 6E10 expression of three WBs was quantified and normalized to GAPDH expression (b). For statistical analyses one-way ANOVA with Bonferroni's post test was used.

During the second and third step of brain extraction the membrane-bound APP protein is solubilized and subsequently detectable in the TBS-T and SDS fraction. To determine if the peripheral pFTAA treatment in young *APPPS1* mice affected the APP transgene expression, APP amounts in these two fractions were quantified additionally. However, SDS-PAGE and WB revealed no significant differences in APP transgene expression between untreated, PBS and pFTAA treated young *APPPS1* mice (Fig. 93).

Results

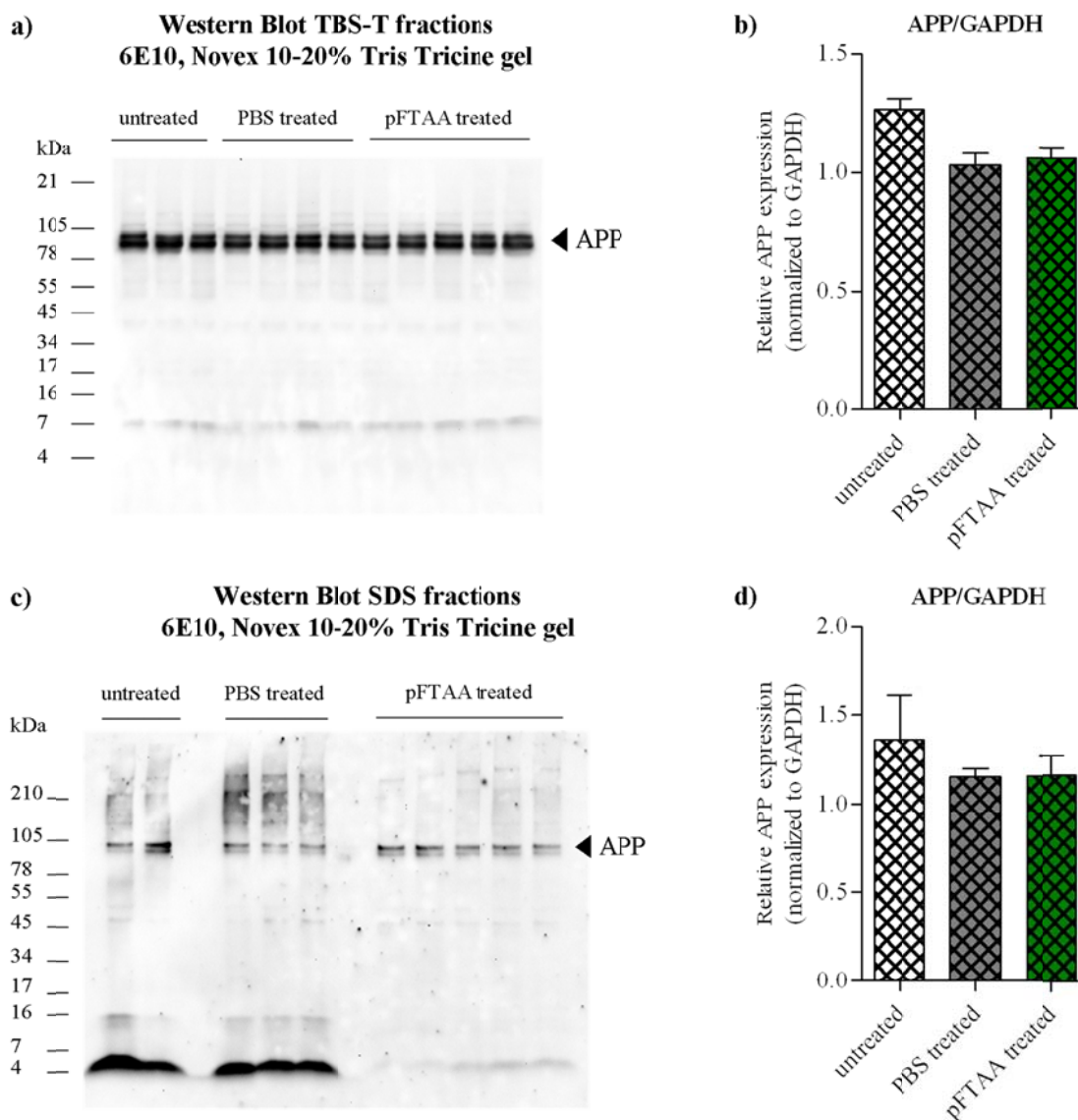


Figure 93: Detection of APP in the TBS-T and SDS fraction by SDS-PAGE and subsequent WB analysis after homogenization of 120 d old *APPPS1* hemispheres. Frozen hemispheres of 120 d old *APPPS1* mice (untreated (n = 2), PBS (n = 3) and pFTAA treated (n = 5)) were homogenized after peripheral long term treatment by four-step extraction and APP was detected by SDS-PAGE and WB in the supernatant of TBS-T and SDS fractions. Representative WB showing APP levels in TBS-T (a) and SDS fractions (c) of untreated, PBS and pFTAA treated *APPPS1* mice at 4 kDa are depicted. Relative 6E10 expression of two (TBS-T fraction, b) and four (SDS fraction, d) WBs was quantified and normalized to GAPDH expression. For statistical analyses one-way ANOVA with Bonferroni's post test was used.

In contrast to untreated and PBS treated mice, significantly reduced insoluble $A\beta_{40}$ and $A\beta_{42}$ amounts in the FA fraction, extracted from hemispheres of pFTAA treated *APPPS1* mice were detected using the MSD 6E10 assay (Fig. 94). Insoluble $A\beta_{40}$ levels were significantly decreased ($p < 0.05$) in pFTAA treated animals compared to untreated mice (Fig. 94a). In contrast, there was a statistical significant decrease ($p < 0.05$) of $A\beta_{42}$ in pFTAA treated *APPPS1* mice, when compared to PBS treated animals (Fig. 94b).

Results

The decrease of aggregated, insoluble A β in FA fractions of pFTAA treated *APP/PS1* mice could be semi-quantitatively confirmed by SDS-PAGE and WB. Due to the low pH of the FA fractions, running behavior of FA samples in the 10-20 % Novex® Tricine gel was influenced. However, since samples were diluted in Tris (pH = 8) and neutralized, proteins run in the gel in a wavelike manner and in contrast to untreated and PBS treated *APP/PS1* mice, pFTAA treated animals showed significantly less insoluble A β on a representative WB (Fig. 95). Since no housekeeping proteins can be detected in the FA-fraction, a quantitative analysis of A β -levels was not performed.

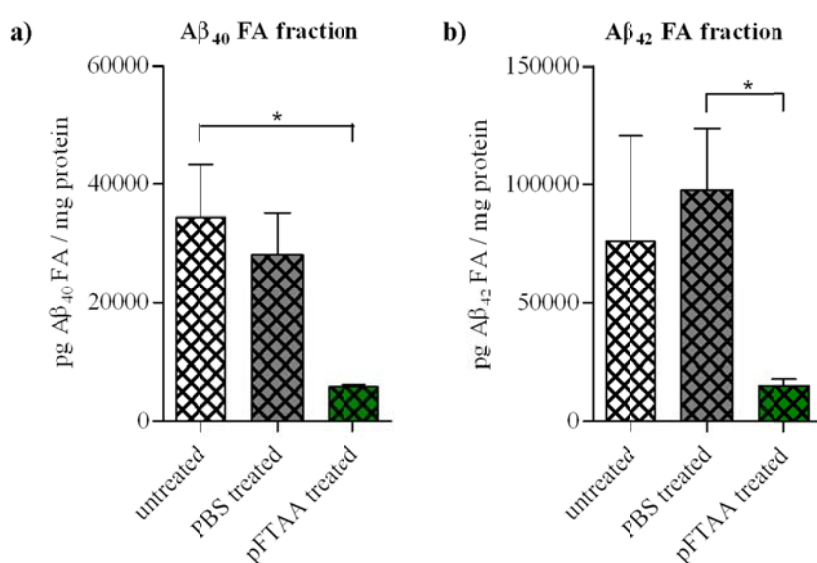


Figure 94: Cerebral A β_{40} and A β_{42} amounts determined in FA fractions after brain homogenization of 120 d old *APP/PS1* mice using the MSD 6E10 assay. Frozen hemispheres of untreated (n = 2), PBS (n = 4) or pFTAA (n = 10) treated *APP/PS1* mice after long term treatment were homogenized by four-step extraction and cerebral A β_{40} (a) and A β_{42} (b) amounts of FA fractions were detected biochemically using the MSD 6E10 assay. For statistical analyses one-way ANOVA with Bonferroni's post test was used.

Results

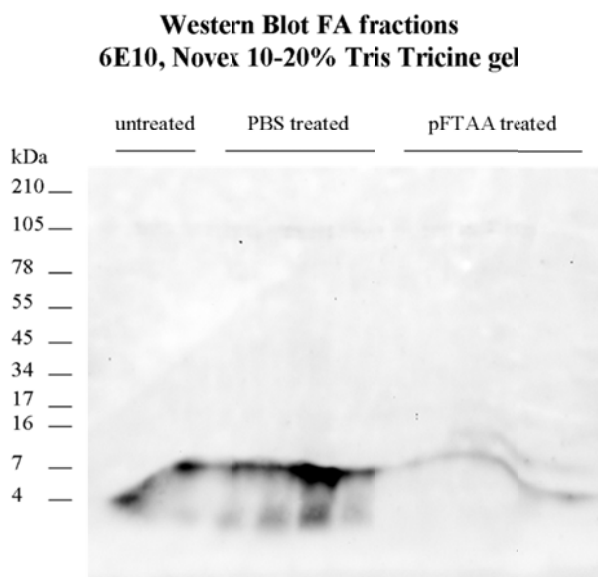


Figure 95: Detection of A β in FA fractions by SDS-PAGE and subsequent WB analysis after homogenization of 120 d old *APPPSI* hemispheres. Frozen hemispheres of 120 d old *APPPSI* mice (i) untreated (n = 2), ii) PBS (n = 3) and iii) pFTAA treated (n = 5) were homogenized after long term treatment by four-step extraction and total A β in the diluted supernatant (1:10 in 1 M Tris (pH = 8)) of the FA fractions was detected by SDS-PAGE and WB analysis. A representative WB showing intracellular A β levels of untreated, PBS and pFTAA treated *APPPSI* mice at 4 kDa is depicted (a).

Biochemical analysis of cerebral A β amounts after brain homogenization revealed a controversial result to the previously shown histological A β quantification (see chapter 3.3.3.1 and 3.3.3.2). While the histological analysis of total cerebral A β burden of untreated, PBS and pFTAA treated *APPPSI* mice showed no major difference between experimental groups, the biochemical analyses revealed significant reductions of A β levels and an increase of soluble A β_{42} amounts in pFTAA treated animals. Due to this observation the question arose, if the overall distribution of cerebral A β in distinct fractions is altered after a long term pFTAA *in vivo* treatment. For the A β distribution analysis results of the MSD 6E10 assay were used. As depicted in figure 96, the distribution of total A β_{40} and A β_{42} was not changed when TBS, TBS-T, SDS and FA fractions of transgene positive experimental mice (*APPPSI*: untreated (a), PBS treated (b), pFTAA treated (c)) were compared. Highest amounts (67-73 %) of A β_{40} and A β_{42} were detected in FA fractions, followed by 23-32 % in SDS fractions. Only minor amounts of soluble A β_{40} and A β_{42} assemblies were present in the TBS (0-2 %) and TBS-T (0.8-4 %) fraction. *APPPSI* mice were shown to reveal small amounts of soluble and high amounts of insoluble cerebral A β_{40} and A β_{42} levels before⁸³. Conclusively, a change of cerebral A β distribution, for example from less insoluble to more soluble A β assemblies, does not explain the controversial results achieved by histological and biochemical A β measurements in long term treated *APPPSI* mice.

Results

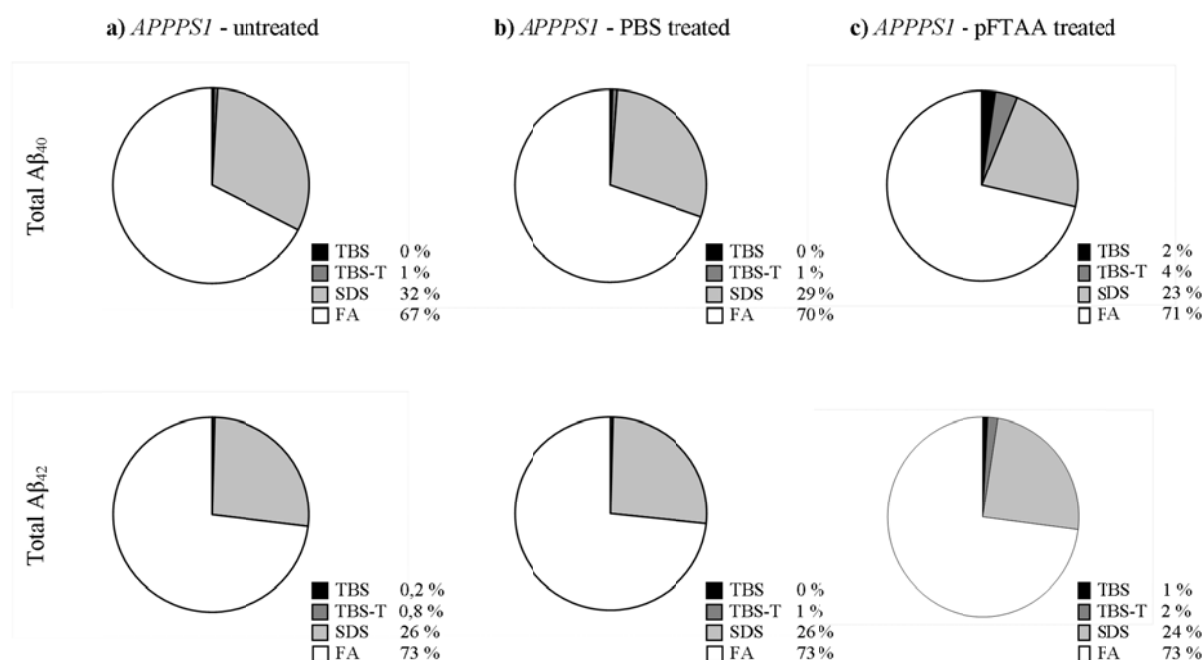


Figure 96: Total Aβ distribution in TBS, TBS-T, SDS and FA fractions after brain homogenization of 120 d old APPPS1 mice of long term treatment. The overall distribution of Aβ₄₀ (upper row) and Aβ₄₂ (lower row) amounts in TBS, TBS-T, SDS and FA fractions after brain homogenization of 120 d old, long term treated APPPS1 mice (a) untreated (n = 2), b) PBS (n = 3) and c) pFTAA (n = 10) treated) are depicted. The Aβ distribution analysis was assessed using results of distinct MSD 6E10 assays shown above.

Since no difference of Aβ₄₀ and Aβ₄₂ distribution in distinct fractions was observed after brain homogenization between transgene positive experimental groups, total Aβ amounts for untreated, PBS and pFTAA treated APPPS1 mice were calculated. Total cerebral Aβ levels were assessed by results of the the MSD 6E10 assay, which was used to detect Aβ₄₀ and Aβ₄₂ amounts in distinct fractions after brain homogenization. Compared to untreated and PBS treated control mice, Aβ₄₀ (Fig. 97a, p < 0.05), Aβ₄₂ (Fig. 97b, p < 0.01) and total Aβ levels (Fig. 97c, p < 0.05) were significantly decreased after pFTAA treatment.

Since the overall distribution of soluble and insoluble cerebral Aβ was not changed after pFTAA treatment of young APPPS1 mice and total Aβ amounts were shown to be significantly reduced by biochemical Aβ measurements but were not changed by histological Aβ quantification when compared to untreated and PBS treated animals, it was assumed that the presence of pFTAA might influence Aβ extraction *in vitro*.

Results

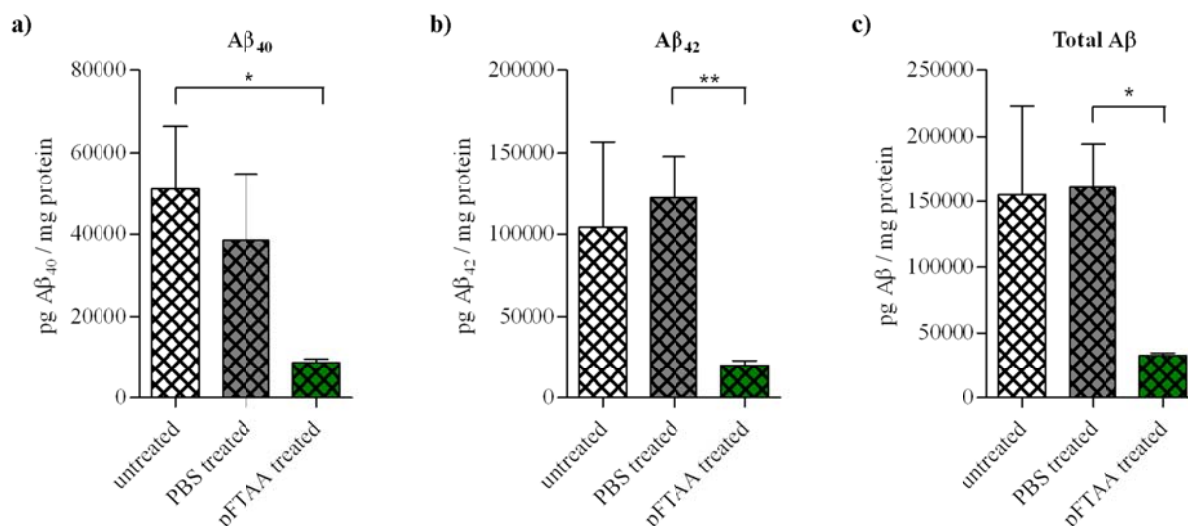


Figure 97: Total cerebral A β amounts determined by the MSD 6E10 assay after brain homogenization of 120 d old, long term treated *APPPSI* mice. Total A β_{40} (a), A β_{42} (b) and A β levels (c) of untreated (n = 2), PBS (n = 4) and pFTAA (n = 4) treated, young *APPPSI* mice were calculated by summing A β amounts of single fractions after brain homogenization, which were previously determined by the MSD 6E10 assay.

3.3.4.2 Impact of pFTAA on A β extraction from brain tissue

After observing a massive reduction of total cerebral A β in pFTAA treated *APPPSI* mice by biochemical analyses (see chapter 3.4.1), which was in contrast to results of the histological quantification of A β plaque burden, it was investigated if the presence of pFTAA influences A β extraction. For this purpose A β of two aged *APPPSI* brains (150 d old) was extracted in four steps⁸⁴. One hemisphere of each brain was homogenized in TBS buffer containing protease inhibitors and the other hemisphere was homogenized in TBS buffer with protease inhibitors and pFTAA (10 mg/kg). Subsequently extraction buffers were used as described before (see chapter 2.5.1). A β was detected in the supernatant of all four fractions by the MSD 610E assay and by SDS-PAGE and subsequent WB analyses. In the supernatant of the TBS fraction, A β_{40} amount, measured by the MSD 6E10 assay, was slightly increased after homogenization in the presence of pFTAA, for A β_{42} equal amounts were detected independent of pFTAA presence in the first extraction buffer (Fig. 98a). Supernatants of TBS-T, SDS and FA fractions revealed a strong reduction of A β_{40} and A β_{42} amounts after brain homogenization in presence of pFTAA in the first extraction buffer (TBS buffer) when compared to amounts achieved after homogenization without the presence of pFTAA (Fig. 98b-d). These results are in line with achieved results after brain homogenization of untreated, PBS and pFTAA treated finally 120 d old *APPPSI* mice (see chapter 3.3.4.1), indicating an influence of pFTAA on A β extraction *in vitro*.

Results

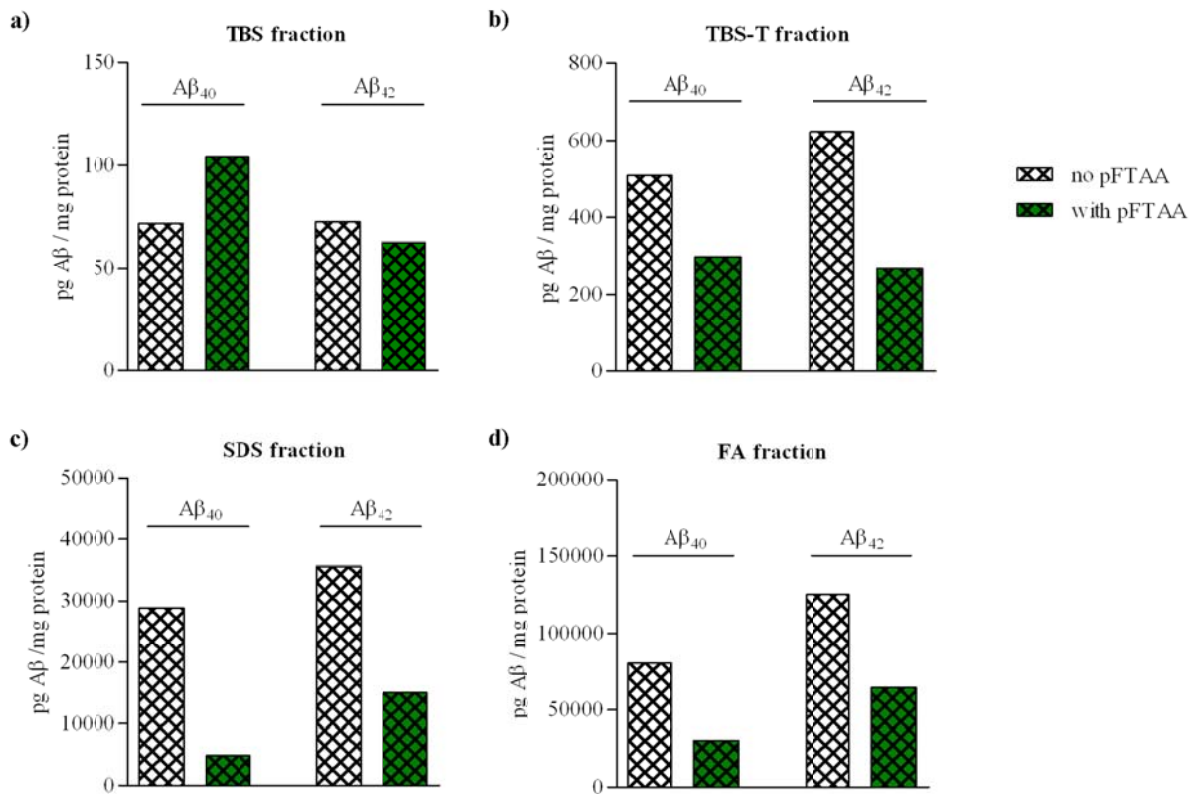


Figure 98: Cerebral Aβ₄₀ and Aβ₄₂ amounts after brain homogenization in the absence and presence of pFTAA *in vitro* determined by the MSD 6E10 assay. To analyze if pFTAA affects Aβ extraction *in vitro*, hemispheres of aged *APP^{PS1}* mice were homogenized by four-step extraction in the absence (n = 1) and presence (n = 1) of pFTAA (10 mg/kg) in the first extraction buffer (TBS buffer). Aβ₄₀ and Aβ₄₂ levels in the TBS (a), TBS-T (b), SDS (c) and FA (d) fraction were biochemically measured in absence and presence of pFTAA during the first extraction step using the MSD 6E10 assay. A statistical analysis was not performed since Aβ amounts of only two brains were determined.

Total Aβ levels of the first three extraction fractions (TBS, TBS-T and SDS) were simultaneously measured by SDS-PAGE and WB after brain homogenization in absence and presence of pFTAA in the first extraction buffer. In the TBS fractions no difference of total Aβ amounts between both extraction approaches was detected. But as seen previously by the MSD 6E10 assay, WB revealed also a reduction in Aβ levels of the TBS-T and SDS fractions (Fig. 99a), which was confirmed by quantification (Fig. 99b).

Results

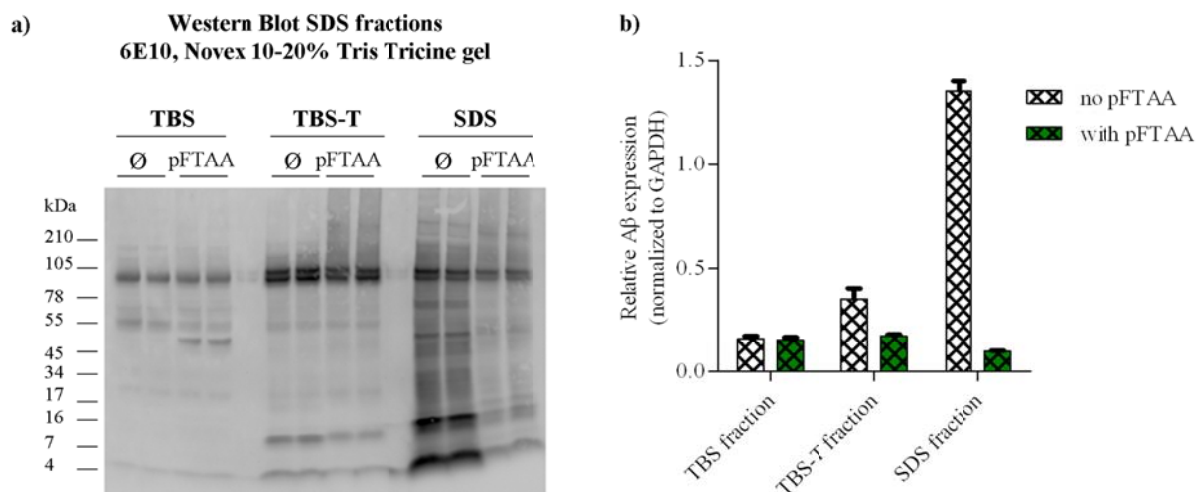


Figure 99: Cerebral A β amounts after brain homogenization in the absence and presence of pFTAA *in vitro* using SDS-PAGE and WB analysis. Brains of two aged *APPPSI* mice were used to analyze if pFTAA has an effect on A β extraction *in vitro*. One hemisphere each was homogenized in the presence of 10 mg/kg pFTAA in the first extraction buffer (TBS) and the second hemisphere in absence of pFTAA. Total A β amounts of the first three fractions (TBS, TBS-T, SDS) were detected by SDS-PAGE and WB (a) and subsequently quantified (b). A statistical analysis was not performed since A β amounts of only two brains were determined.

By calculating total A β amounts, the same picture after brain homogenization *in vitro* as before *in vivo* after long term pFTAA treatment of young *APPPSI* mice was received (see chapter 3.4.3). In the presence of pFTAA total A β_{40} (Fig. 100a), A β_{42} (Fig. 100b) and A β (Fig. 100c) amounts were significantly reduced as measured by the MSD 6E10 assay. Compared and normalized to total A β amounts in fractions homogenized in pure TBS buffer, A β_{40} was reduced by 77 %, A β_{42} by 66 % and total A β by 71 %.

Results

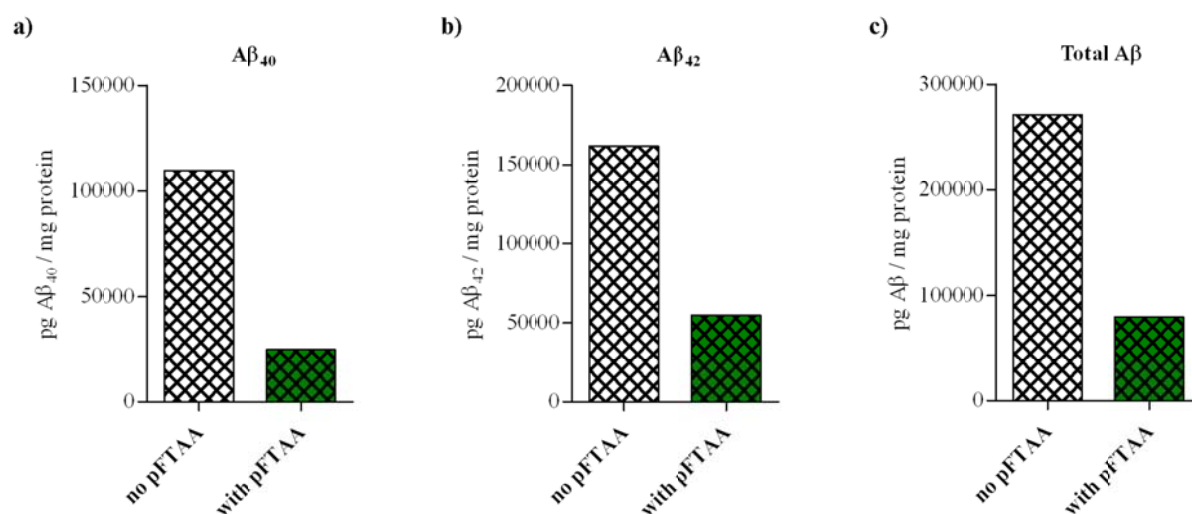


Figure 100: Total Aβ amounts after homogenization of aged *APP/PS1* hemispheres in absence and presence of pFTAA *in vitro*. During homogenization of two aged *APP/PS1* brains using the four-step extraction protocol, one hemisphere was homogenized in the absence and the other hemisphere in the presence of 10 mg/kg pFTAA. Total Aβ₄₀ (a), Aβ₄₂ (b) and Aβ (c) amounts measured in the supernatants of TBS, TBS-T, SDS and FA fraction by MSD 6E10 assay were calculated. A statistical analysis was not performed since Aβ amounts of only one brain of each group were determined.

It was shown that the presence of pFTAA, independent of *in vivo* or *in vitro* application, causes a reduction of Aβ levels during brain homogenization. Next it was aimed to answer, if the presence of pFTAA during brain homogenization induces a precipitation of Aβ *in vitro*. Therefore again two aged *APP/PS1* brains (180 d old) were homogenized, one hemisphere in the absence, the other in the presence of pFTAA. A two-step extraction was performed, because earlier studies detected highest Aβ amounts in SDS and FA fractions (see chapter 3.4.2). Aβ of one hemisphere of each brain was extracted in 2 % SDS buffer containing protease inhibitors, Aβ of the other hemisphere in 2 % SDS buffer containing protease inhibitors and pFTAA (10 mg/kg). Aβ levels were determined in the pellet of the SDS and FA fraction by WB after extraction. Aβ amounts in the pellet of the SDS fraction showed no differences between absence and presence of pFTAA during homogenization (data not shown). In contrast, a difference of Aβ amounts in the pellet of the FA fractions was observed – when hemispheres were homogenized in the presence of pFTAA, higher Aβ amounts were detected in the FA pellet, i.e. the FA insoluble pool of proteins, by SDS-PAGE and WB analyses. The FA pellet was serially diluted (1:100, 1:250, 1:500, 1:1,000) in 1 M Tris (pH = 8) and for every single dilution step higher Aβ levels were revealed in that pellet, where extraction took place in presence of pFTAA (Fig. 101a). The Aβ quantification of the depicted WB (Fig. 101b) confirmed the finding. These results showed that the presence of pFTAA

during brain homogenization caused a precipitation of A β since A β precipitates were detected in the pellet of the FA fraction.

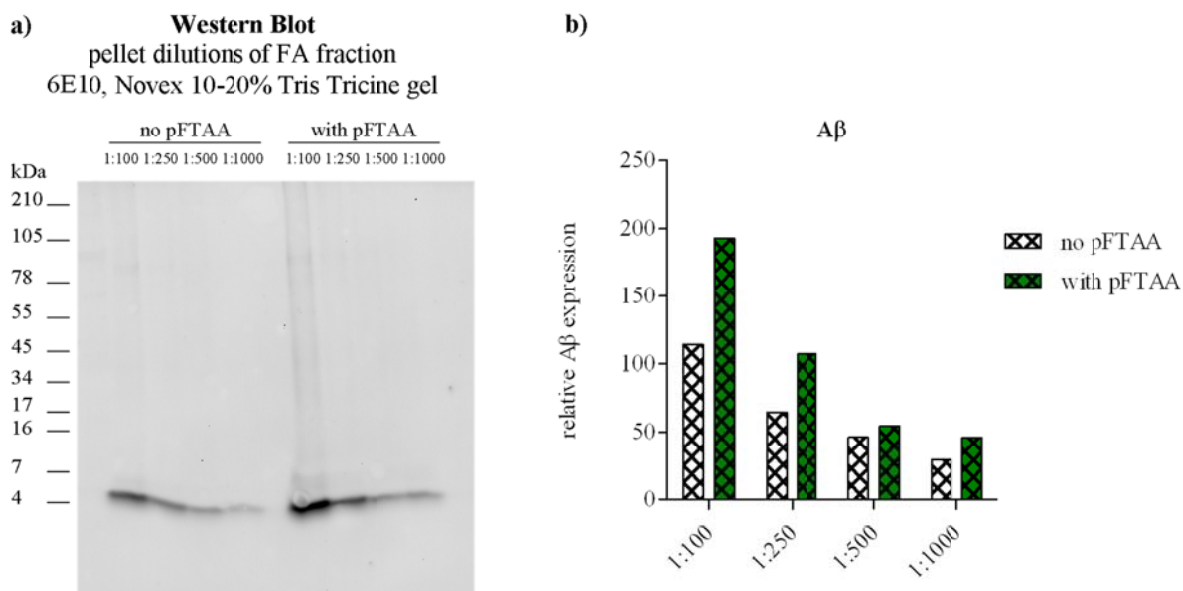


Figure 101: A β amounts of serial dilutions of the FA pellet after brain homogenization in absence and presence of pFTAA *in vitro*. To proof if the presence of pFTAA during homogenization leads to A β precipitation *in vitro*, brains of two aged *APPPSI* mice were homogenized by a 2-step extraction – one hemisphere in the absence, the other in the presence of 10 mg/kg pFTAA in the first extraction buffer (2 % SDS). A β amounts were analyzed in the pellet (diluted 1:100, 1:250, 1:500, 1:1,000 in 1M Tris (pH = 8)) of the FA fractions by SDS-PAGE and WB using the detection antibody 6E10 (a). Relative 6E10 expression of the samples of the depicted WB was subsequently quantified (b). A statistical analysis was not performed since A β amounts of only two brains group were determined.

Biochemical analyses of cerebral A β amounts after long term treatment of young *APPPSI* mice revealed a significant reduction of cerebral A β levels after pFTAA treatment when compared to A β levels of untreated and PBS treated animals. This finding was controversial to the determined A β quantification by histological analyses of serial cerebral brain sections, where no difference of overall A β plaque burden was detected between experimental groups (see chapter 3.3.3). By analyzing the impact of pFTAA on A β extraction *in vitro*, it was detected that pFTAA causes a precipitation of A β . Increased precipitated A β amounts were detected in the pellet of FA fractions when pFTAA was present during brain homogenization. The observed effect of pFTAA on A β extraction precludes a biochemical quantification of cerebral A β in the presence of pFTAA.

3.3.5 Summary of long term pFTAA treatment in young experimental animals

The peripheral long term treatment of young *APP/PS1* mice with the molecular amyloid marker pFTAA, which readily crosses the BBB and labels cerebral A β plaques, caused no obvious side effects in treated animals and did not alter the overall cerebral A β plaque pathology, as assessed by *postmortem* histological A β quantification. However, more detailed histological analyses of cerebral A β plaques revealed that pFTAA treated *APP/PS1* mice have more numerous but smaller cortical A β plaques than untreated and PBS treated animals. Furthermore structural changes of cerebral amyloid deposits were observed after pFTAA treatment by spectral analysis – A β plaques appeared to grow and mature more slowly, as seen by a less developed dense-core of A β plaques in contrast to control mice. The observed higher number of cerebral A β plaques in pFTAA treated *APP/PS1* mice could be caused by increased seeding amyloid deposits induced by pFTAA. In conclusion, the peripheral pFTAA treatment influenced the structure of cerebral A β deposits, while having no significant impact on overall plaque burden and plaque associated pathology.

3.4 Functional impact of short term pFTAA treatment in aged experimental animals

It was described that besides A β aggregates, pFTAA as novel molecular amyloid marker also binds oligomeric, soluble, non-fibrillar A β assemblies *in vitro*³⁹. These species have been shown to be the most toxic ones, causing synaptic loss and cognitive impairment in Alzheimer's disease⁹⁶. In the present thesis long term potentiation (LTP) and paired pulse facilitation (PPF) measurements in the hippocampal CA1 region at the Schaffer Collateral synapses were used, to analyze if a peripheral pFTAA treatment over 8 weeks influences synaptic long and short term plasticity in aged *APP/PS1* mice. Aged *APP/PS1* mice were chosen for the present approach because it is described, that the murine AD strain *APP/PS1* reveal first impairments relating to cognitive functions and synaptic plasticity in the hippocampus at 8 month of age^{64,97}. Since no significant change in overall cerebral A β plaque burden was visible after a 12 week long pFTAA treatment of young *APP/PS1* mice (see chapter 3.3), it was of interest to know if peripheral pFTAA applications affect mice with robust cerebral A β plaque burden i) on a functional level and ii) on cerebral A β plaque pathology.

3.4.1 Hippocampal long term potentiation measurements in young and aged *APPPSI* versus WT mice

Before aged *APPPSI* mice were treated with pFTAA or PBS to analyze if a pFTAA application affects hippocampal long and short term plasticity by binding oligomeric A β species, it was analyzed if hippocampal LTP of *APPPSI* mice can be distinguished from that of WT mice. In the present experiment hippocampal LTP in 4 and 10-15 month old *APPPSI* and WT mice was measured and compared. No statistical significant difference ($p = 0.47$) in field excitatory post-synaptic potentials (fEPSP) between 4 month old *APPPSI* and WT mice was assessed (Fig. 102a). After recording a stable baseline potentiation and theta-burst stimulation (high frequent stimulation (HFS)) of hippocampal slices, fEPSP in the CA1 region of 4 month old *APPPSI* mice increased in average up to 202 %, slices of WT animals revealed a mean potentiation of 174 % 30 min after the HFS that induces potentiation of synaptic transmission. A different result was recorded for *APPPSI* and WT mice at an age of 10-15 month. Hippocampal slices of aged *APPPSI* mice were hardly potentiable at all and showed only a weak mean potentiation of 115 % 30 min after HFS, whereas slices of WT mice exhibited a mean potentiation of about 145 % (Fig. 102b). Despite this observed difference between 10-15 month old *APPPSI* and WT mice, the result was statistically not significant ($p = 0.16$). However, it was confirmed that there are no measurable differences in hippocampal LTP between young *APPPSI* mice and WT controls, while there was a difference in aged (≥ 8 month old) animals⁹⁷.

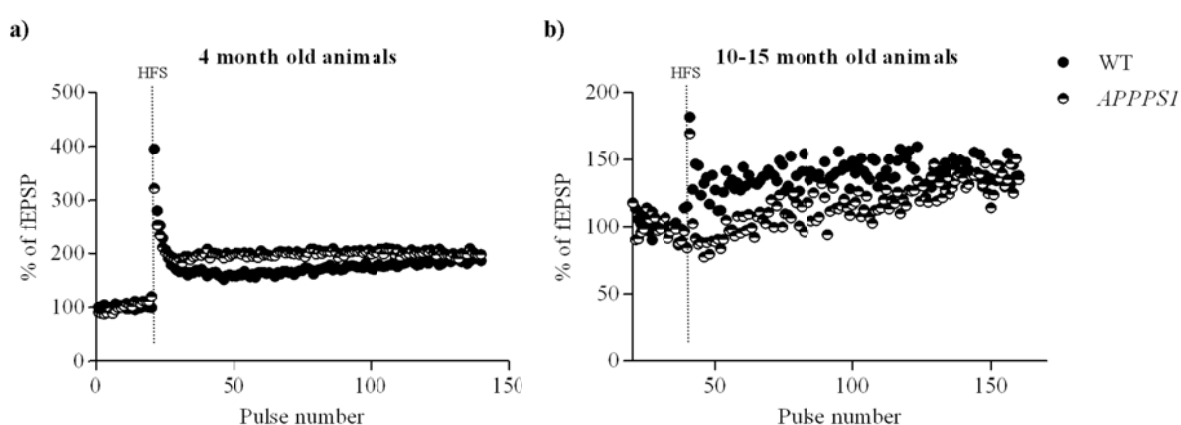


Figure 102: LTP measurement in the CA1 region of hippocampal slices of 4 and 10-15 month old *APPPSI* and WT mice. Hippocampal slices of 4 (a) and 10-15 month (b) old *APPPSI* and WT mice were prepared directly after decapitation of experimental mice and LTP was measured in the hippocampal CA1 region. 4 months: WT ($n = 5$), *APPPSI* mice ($n = 4$). 10-15 month: WT ($n = 7$), *APPPSI* mice ($n = 9$). For statistical analyses Student's t test was used.

3.4.2 Short term pFTAA treatment of aged experimental animals

To analyze if peripherally applied pFTAA affects toxicity of oligomeric A β species in the brain, aged *APPPSI* mice were treated for 8 weeks with pFTAA or PBS and hippocampal LTP measurements were assessed subsequently. Initially, at 7.5 month of age, *APPPSI* mice (n = 8) were i.p. injected with 10 mg/kg pFTAA on four consecutive days to label present cerebral A β plaques. An aged matched *APPPSI* control group (n = 7) was treated simultaneously with PBS (Tab. 16). Treatment was continued for 2 month with two injections weekly. At an age of 9.5 month animals were sacrificed and the brain was harvested for hippocampal slice preparation as well as for further biochemical and immunohistological analyses. Additionally plasma of experimental animals was taken to detect peripheral A β .

Table 16: Experimental groups of pFTAA treatment in aged *APPPSI* mice

	Number (n)	Treatment
<i>APPPSI</i>	7	PBS (control)
<i>APPPSI</i>	8	pFTAA

7.5 month old *APPPSI* mice were treated over two month with PBS (n = 7) or pFTAA (n = 8) before i) electrophysiological measurements in the hippocampal CA1 region and ii) quantifications of cerebral and peripheral A β amounts were performed.

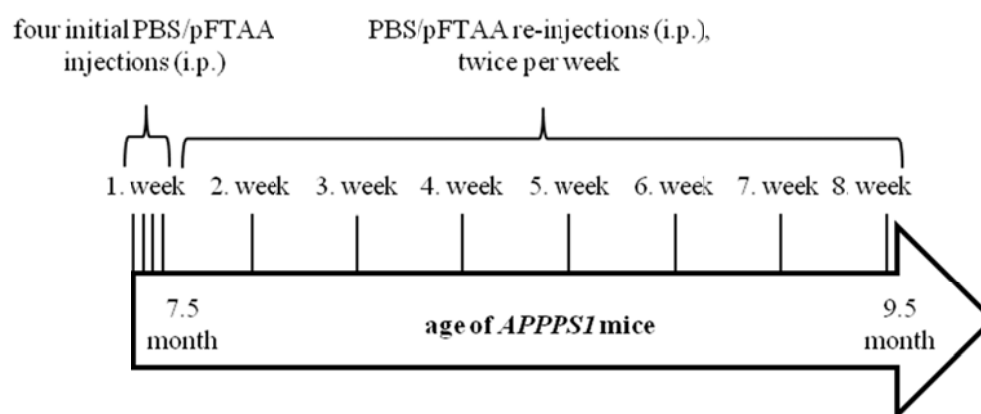


Figure 103: Timeline of pFTAA treatment in aged *APPPSI* mice. pFTAA or PBS treatment in aged *APPPSI* mice was initiated at 7.5 month of age and after 4 initial applications of 10 mg/kg pFTAA or PBS on consecutive days, animals were further i.p. injected biweekly. *APPPSI* mice were weighted before every single injection. Experimental animals were sacrificed at an age of 9.5 month and the brain and plasma were harvested.

To monitor side effects of the pFTAA treatment in aged *APPPSI* mice, experimental animals were weighted before every single pFTAA or PBS injection. Stable weight curves with slight deviations for both experimental groups (i) *APPPSI* – PBS treated and ii) *APPPSI* – pFTAA treated) were observed over eight weeks, indicating no obvious toxic side effects of the

treatment in older mice (Fig. 104). For statistical analysis Student's t-test was used and revealed no significant difference between pFTAA or PBS treated *APPPSI* mice. As the short term treatment was initiated at 7.5 months of age, where *APPPSI* mice were already adult, no major weight change over the treatment period was expected.

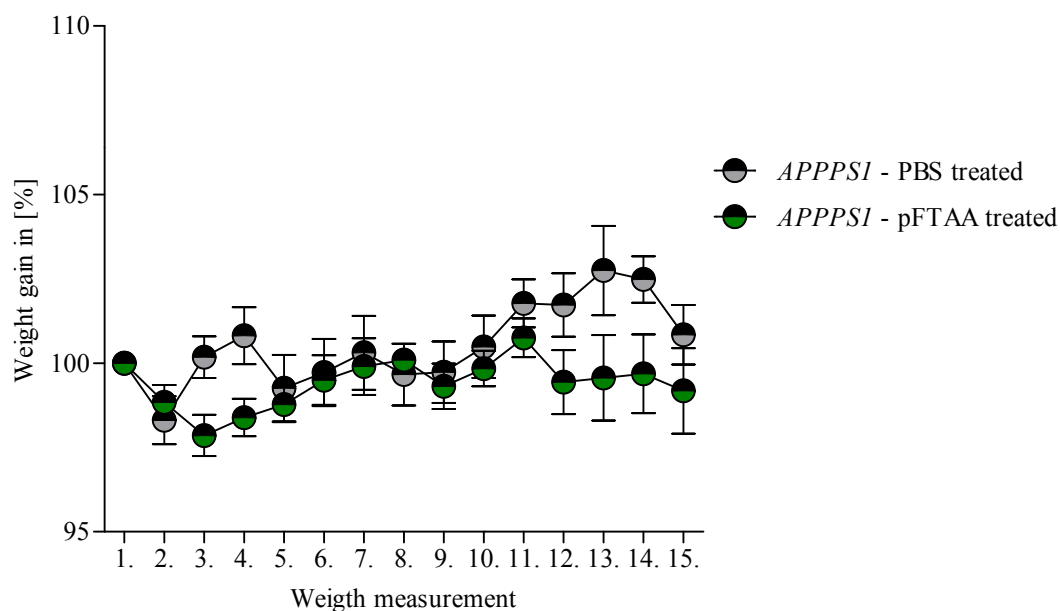


Figure 104: Weight curves of aged *APPPSI* mice included into the short term treatment approach. To analyze possible toxic side effects of a short term pFTAA treatment in aged *APPPSI* mice, 7.5 month old animals were treated with PBS (n = 7) or pFTAA (n = 8) and the body weight was measured before every single injection. Student's t-test was used for statistical analysis.

After sacrificing pFTAA and PBS treated *APPPSI* mice at 9.5 month of age, hippocampal slices were prepared for subsequent electrophysiological measurements, where LTP and PPF in the hippocampal CA1 region have been assessed. Since pFTAA is known to bind A β oligomers, which were described to cause synaptic dysfunction in AD brains⁷, it was investigated if changes in synaptic transmission can be measured by hippocampal LTP after an eight week long peripheral PBS or pFTAA treatment of aged *APPPSI* mice. A stable synaptic baseline transmission (fEPSP) was measured for 10 min before slices were stimulated at high frequency and fEPSPs were assessed for the subsequent hour. No statistical significant difference between PBS and pFTAA treated, aged *APPPSI* mice was observed 30 min after HFS (Fig. 105), synaptic transmission of experimental, aged *APPPSI* mice showed a mean potentiation of about 158 % after PBS and 161% after pFTAA treatment.

Results

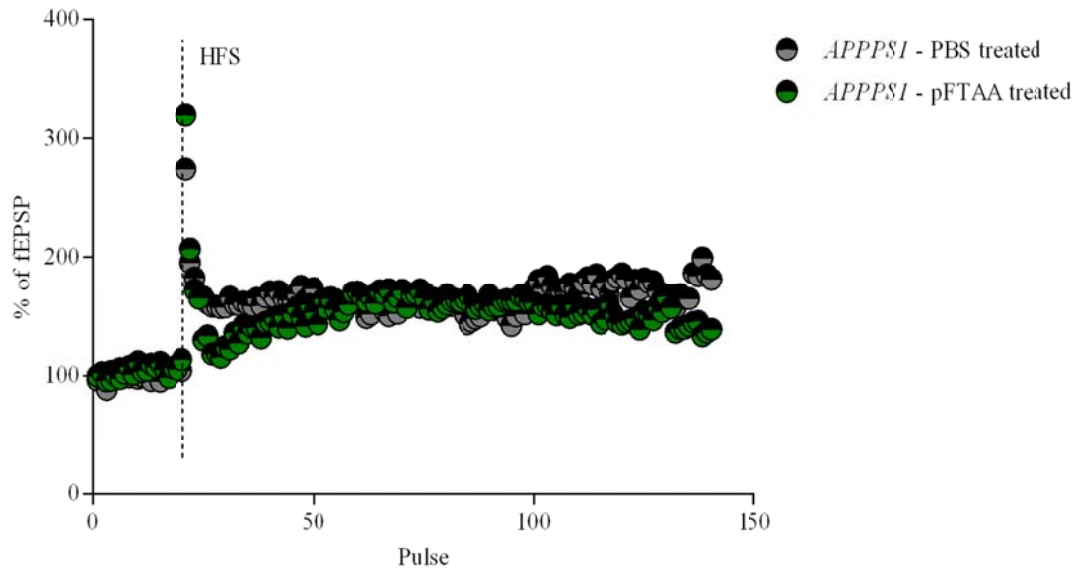


Figure 105: Hippocampal LTP measurement after pFTAA treatment of aged *APPPSI* mice. 7.5 month old *APPPSI* mice were treated for eight weeks with PBS (control, n = 7) or pFTAA (n = 8) to investigate the impact of pFTAA on synaptic plasticity *in vivo*. At 9.5 months of age treated animals were sacrificed and hippocampal slices of the left hemisphere were prepared to assess LTP in the hippocampal CA1 region. After recording a stable baseline potentiation for 20 pulses (10 min), slices were stimulated at high frequency and fEPSPs were measured for an additional hour. 30 min after HFS, fEPSP was compared between PBS and pFTAA treated *APPPSI* mice. Student's t-test was used for statistical analyses.

Additionally hippocampal PPF was measured using the same electrode placements as for LTP, to analyze synaptic short term plasticity, following eight week long PBS and pFTAA treatment of aged *APPPSI* mice. As already observed for synaptic long term plasticity by LTP, synaptic short term plasticity measured by PPF showed no major difference between the two experimental groups i) *APPPSI* – PBS treated and ii) *APPPSI* – pFTAA treated (Fig. 106). At the 25 ms interstimulus interval a statistical significant difference ($p < 0.05$) between both groups was observed (Student's t-test), but when comparing the entire set of PPF measurements with increasing interstimulus interval, there was no statistical significant difference detectable (ANOVA with Bonferroni's multiple comparison post-test).

Results

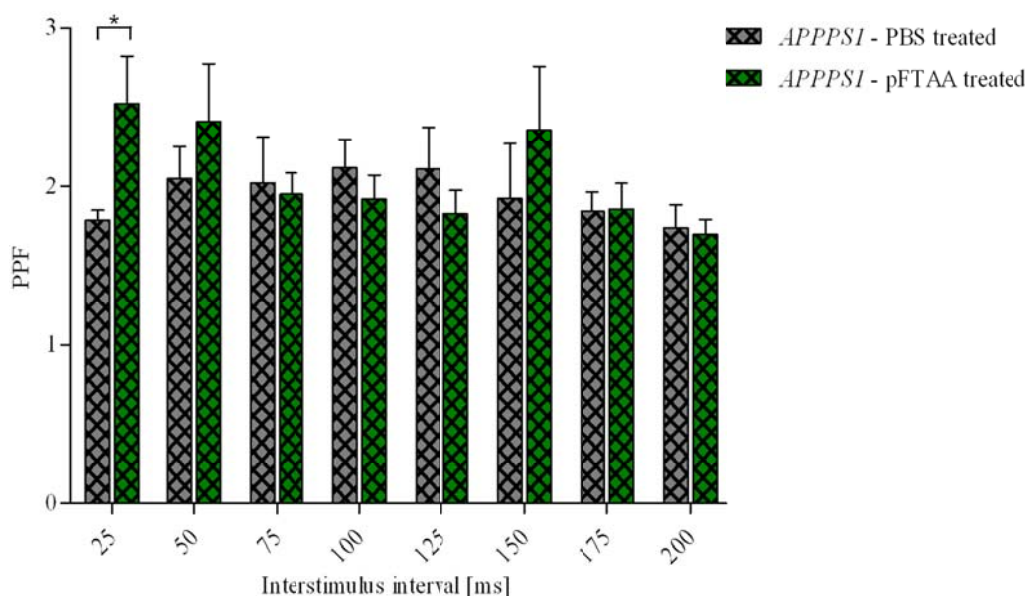


Figure 106: Hippocampal PPF measurement after pFTAA treatment of aged *APPPSI* mice. 7.5 month old *APPPSI* mice were treated biweekly with PBS (control, n = 5) or pFTAA (10 mg/kg, n = 5), up to a final age of 9.5 months. To analyze if peripheral short term treatment with pFTAA had an effect on synaptic short term plasticity in the hippocampus of aged *APPPSI* mice, PPF in the hippocampal CA1 region was measured for eight increasing interstimulus intervals (25-200 ms) after animals were sacrificed. Student's t-test was used to compare PBS and pFTAA treated mice at every single interstimulus interval measurements, ANOVA for overall comparison between experimental groups.

It was hypothesized, that due to the cerebral binding of pFTAA to soluble A β oligomers, their toxic potential on synaptic plasticity would be affected and a change in long or short term plasticity could be measured. But, short term pFTAA treated *APPPSI* mice revealed in comparison to PBS treated animals no difference in hippocampal synaptic transmission assessed by electrophysiological measurements for short (PPF) and long term plasticity (LTP).

As aged experimental animals of the short term treatment were sacrificed at 9.5 month of age, blood was sampled and peripheral A β amounts in the EDTA-plasma were quantified using biochemical analyses (MSD 4G8 assay). Since levels of soluble A β in the brain are in equilibrium with A β levels in the blood, EDTA-plasma A β was quantified in pFTAA treated animals to get a hint if short-term pFTAA treatment impacts levels of soluble A β . The biochemical quantification of A β_{40} (Fig. 107a) and A β_{42} levels (Fig. 107b) in the plasma, measure by the MSD 4G8 assay, revealed no statistical significant difference between PBS and pFTAA treated aged *APPPSI* mice.

Results

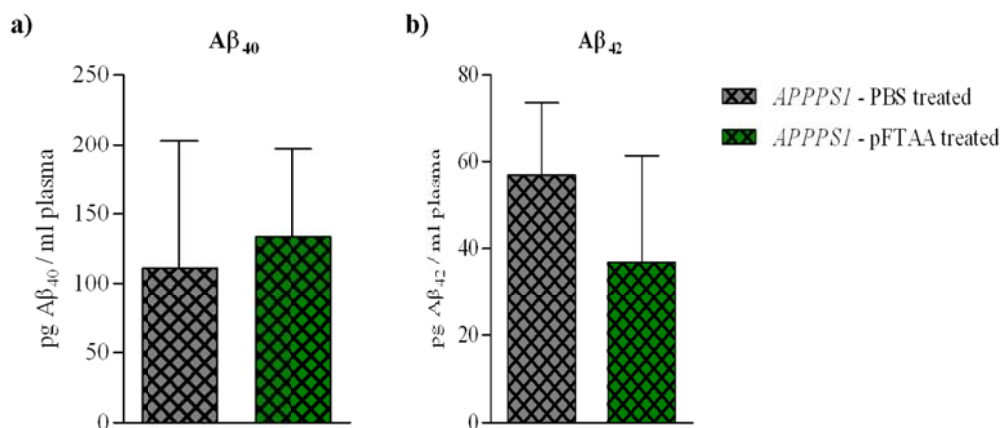


Figure 107: Biochemical quantification of Aβ₄₀ and Aβ₄₂ amounts in the plasma of aged *APPPS1* mice after short term PBS and pFTAA treatment. 7.5 month old *APPPS1* mice were treated twice per week over two month with PBS (n = 7) and 10 mg/kg pFTAA (n = 8). At a final age of 9.5 month mice were sacrificed and plasma was sampled for biochemical Aβ detection. The MSD 4G8 assay with 4G8 as an Aβ specific detection antibody was used to measure and differentiate between Aβ₄₀ (a) and Aβ₄₂ levels (b). Student's t-test was used for statistical analyses.

After short term PBS (control) and pFTAA (10 mg/kg twice per week) treatment of aged *APPPS1* mice no statistical significant differences in synaptic long (LTP) and short (PPF) term plasticity as well as no significant changes in peripheral (plasma) Aβ₄₀ and Aβ₄₂ levels were detected. In a further step, a histological quantification of cerebral Aβ burden by plaque size distribution analysis of brain sections was performed. Serial free floating sections of the frontal left hemisphere were stained with the Aβ specific antibody 4G8 and cortical Aβ plaques were classified into seven different plaque size classes: class 1 (10-500 μm), class 2 (500-1,000 μm), class 3 (1,000-1,500 μm), class 4 (1,500-2,000 μm), class 5 (2,000-2,500 μm), class 6 (2,500-3,000 μm) and class 7 (3,000-6,500 μm) using the cellSens Dimension software (Olympus). In none of the seven different Aβ plaque size classes a statistical significant difference of relative Aβ plaque size area between PBS and pFTAA treated *APPPS1* mice was detected (Fig. 108).

Results

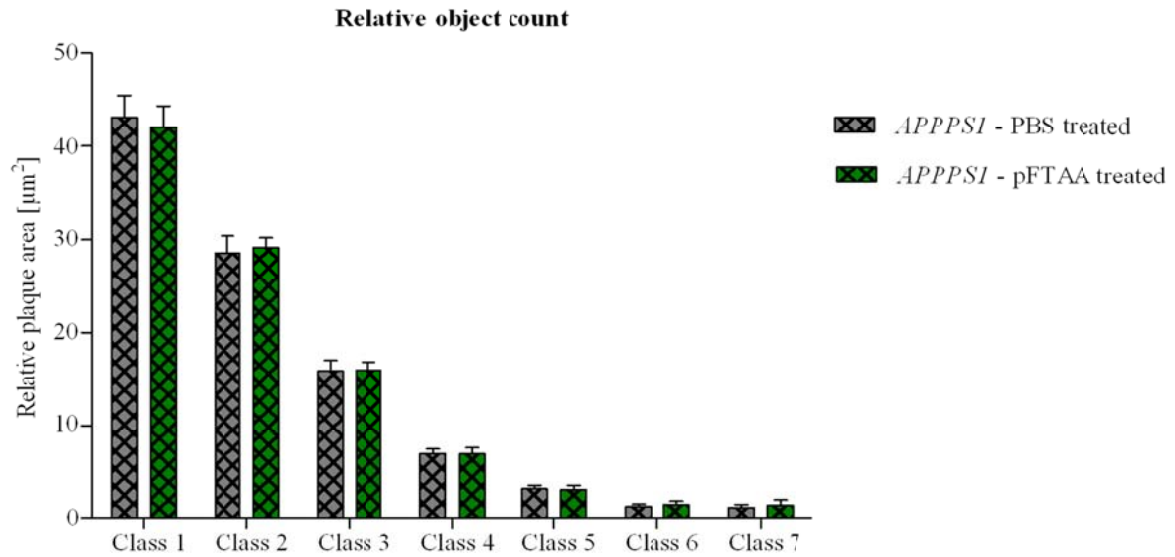


Figure 108: Cortical A β plaque size distribution analysis after short term PBS and pFTAA treatment of aged APPPSI mice. Following an eight week long peripheral PBS or pFTAA treatment of aged APPPSI mice, a cortical A β quantification was performed by immunohistochemical 4G8 staining. A β plaques of 10-12 frontal, coronal sections were classified into seven different plaque size classes: class 1: 10-500 μm , class 2: 500-1,000 μm , class 3: 1,000-1,500 μm , class 4: 1,500-2,000 μm , class 5: 2,000-2,500 μm , class 6: 2,500-3,000 μm and class 7: 3,000-6,500 μm by the use of the software cellSens. Student's t-test was used to compare plaque sizes after PBS and pFTAA treatment, ANOVA for overall comparison between experimental groups.

A peripheral short term treatment of aged APPPSI mice with the molecular marker pFTAA caused in comparison to PBS treated animals no changes in hippocampal, synaptic transmission but did also not affect the peripheral and cerebral A β load and the structure of A β deposits.

4. Discussion

Within this thesis LCOs, a class of multimodal fluorescent oligothiophenes, were evaluated with regard to their possible application as *in vivo* tracers for A β detection and as potential pharmacophores in the AD context.

For diagnostic applications LCOs coupled to MNPs were analyzed for the capability to cross the BBB after peripheral administration and for their applicability as *in vivo* MRI contrast agents. In a second line of research the potential of LCOs as pharmacophores was assessed in different treatment paradigms in young and old *APP/PS1* mice. While efficient crossing of intact LCO-MNP molecules across the BBB could not be demonstrated, which precluded further analysis of LCO-MNPs as MRI contrast agents, the long term treatment of young *APP/PS1* mice revealed an impact of LCOs on the structure of A β deposits in the brain.

4.1 LCOs as *in vivo* tracer for detecting A β in Alzheimer's disease

AD is the major neurodegenerative disease affecting about 4.6 million people worldwide¹⁴. In face of this disease epidemic an efficient treatment strategy is urgently needed. Since the damage of the brain is already far progressed when symptoms of dementia are apparent, better diagnostic techniques, ideally for a pre-symptomatic detection of cerebral amyloid pathophysiology in subjects at risk, are a prerequisite for effective therapeutic interventions. By assessing defined clinical symptoms in combination with the amyloid PET imaging technique, a clinical AD diagnosis can be assessed with high accuracy¹. But, although amyloid PET imaging represents a useful diagnostic tool in AD, it has distinct limitations for an urgently needed widespread application. Besides the usage of a radioactive tracer agent and the concomitant exposure of the patients to radiation, high costs and limited availability are the most deterrent ones⁵⁹.

In principle the amyloid binding agents LCOs might be useful alternative diagnostic marker for specific and selective *in vitro* and *in vivo* detection of amyloid, with the advantage to distinguish between structurally different amyloid lesions. Pre-fibrillar A β oligomers and aggregated A β fibers can be discriminated by the pentameric LCO pFTAA using spectral imaging during *in vitro* fibrillization⁹⁸. Distinct LCOs, for example pFTAA, hFTAA and qFTAA, are described to be usable also for *in vivo* imaging (for example 2-Photon imaging) of pathological protein aggregates in transgenic AD mice. Probes show quick and efficient crossing of the BBB after peripheral application and label cerebral A β plaques with high

selectivity and specificity^{39,75}. This is in contrast to the fact that, almost all of large-molecule pharmaceuticals (for example peptides, recombinant proteins, monoclonal antibodies, RNA interference-based drugs and gene therapies) and more than 98 % of all small molecule drugs are known not to pass the BBB^{76,99}.

Within the present thesis it was hypothesized, that LCO derivatives as precursors of coupled LCO-MNPs and LCO-MNPs bind cerebral A β plaques comparable to uncoupled LCOs and pass the BBB following an i.v. injection in *APPPSI* mice to function as novel *in vivo* imaging tracer for the detection of cerebral A β deposits in AD.

In a first step it was analyzed if LCO derivatives, after they revealed efficient and specific A β plaque labeling on *APPPSI* brain sections and showed amyloid binding properties *in vitro*, fulfill the requirements to cross the BBB after a peripheral administration in *APPPSI* mice. Since uncoupled LCOs pFTAA, qFTAA and hFTAA readily crossed the BBB after peripheral injection, it was hypothesized that slightly modified LCO derivatives would do so too. The results presented here did not confirm the hypothesis. Only LCO derivative 4011, where qFTAA was attached to a short spacer with a terminal phosphate group, achieved efficient cerebral A β plaque labeling, detected on cerebral sections after peripheral administration in *APPPSI* mice, and thus indicated BBB crossing. LCO derivatives where the quaternary LCO qFTAA was only attached to a reactive terminal propyne group (4004), a long spacer with a terminal phosphate group (4010) or to other short spacers (4020, 4021) revealed no specific A β plaque labeling after i.v. injection, assuming that distinct attached spacer components limited BBB crossing of those LCO derivatives.

As mentioned above, distinct uncoupled LCOs (pFTAA, qFTAA, hFTAA) readily crossed the BBB after systemic administration in AD transgenic mice^{39,75}. Other derivatives of Congo red penetrate the BBB after peripheral application as well. Congo red itself but also methoxy-XO4 as a small molecule A β -binding agent (SMA β BAs) or curcumin were described to pass the cerebral barrier after systemic application^{43,44,100}. The cationic dye methylene blue, belonging to a class of compounds known as phenothiazines, was also described to cross the BBB as potential drug for AD¹⁰¹. In contrast, LCO derivatives penetrated not readily into the brain. After peripheral administration only LCO derivative 4011 labeled cerebral A β plaques, indicating limiting properties for BBB penetration. This LCO derivative has three negatively charged groups. In contrast to cationic molecules, anionic substances have an improved bioavailability and are promising carriers for *in vivo* administration of therapeutics¹⁰². Additionally anionic surface charges of NPs were shown to enhance brain permeability¹⁰³. On

the other hand, LCO derivatives 4004 and 4010 reveal anionic charges as well but might have other limitations for BBB penetration.

Since administered LCO derivative 4011 (at a concentration of 1.36 mM), which was the only derivative penetrating the BBB, did not have the highest LCO concentration in comparison to other applied derivatives (0.52-8.5 mM), it is very likely that the BBB crossing and A β plaque labeling of LCO derivatives is not due to different concentrations of the provided LCO solutions. In contrast, for peripheral pFTAA applications (see chapter 3.1.1) a clear correlation between injected pFTAA concentration and fluorescent intensity of labeled cerebral A β plaques was detected.

As mentioned before, it is speculated, that spacer length and/or type limited BBB crossing and subsequent A β plaque labeling of several LCO derivatives after peripheral application in *APP/PS1* mice. LCO derivative 4011, which showed efficient BBB crossing after two i.v. injections in treated animals, consists of a qFTAA molecule attached to a short spacer with a terminal charged phosphate group. In contrast, LCO derivative 4010, where qFTAA is coupled to a long spacer with a terminal phosphate groups, was not able to pass the BBB, possibly due to the long spacer. Otherwise, LCO derivative 4004, where qFTAA was coupled only to a reactive propyne group, showed no BBB penetration after peripheral administration as well. These results indicate that the length of the attached spacer does not necessarily limit BBB crossing. The optimal conditions for efficient BBB passing based on the structure of derivative 4011 appear to be the presence of at least three charged groups^{102,103} in combination with the defined size and shape of the molecule, which are comparable to pFTAA (Fig. 108). Indeed pFTAA consist of five thiophene rings, but the size is similar to LCO derivative 4011, which has four thiophene rings and is additionally attached to a short linker. Also pFTAA is highly charged by four carboxyl side chains^{76,102,103}.

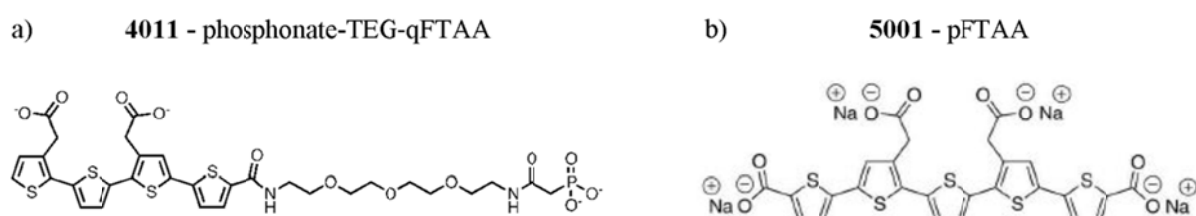


Figure 109: Chemical structures of LCO derivative 4011 and pFTAA.

In contrast to the hypothesis that all peripherally injected LCO derivatives would pass the BBB and show amyloid binding properties *in vivo*, the present thesis revealed different

results. Only one (LCO derivative 4011) out of five LCO derivatives tested passed the BBB after i.v. application and labeled cerebral A β plaques which argues for defined structural properties of the LCO derivative to allow BBB passage and cerebral A β plaque labeling.

In parallel, LCOs attached through distinct spacer components to MNPs were analyzed for their binding properties to cerebral A β plaques following peripheral i.v. injection. Efficient BBB passing after i.v. application of LCO-MNPs in *APP/PS1* mice was hypothesized, but in this project only optical signals of the LCO component were detected whereas significant MRI signals are missing.

All peripherally applied LCO-MNPs were assumed to have crossed the BBB on the basis of optical imaging results since all derivatives labeled cerebral A β plaques. Fluorescent labeling of cerebral A β plaques on sections of LCO, LCO derivative and LCO-MNP treated *APP/PS1* in mice was detected preferentially close to the ventricles. Due to this cerebral labeling pattern, it is assumed that LCOs and distinct derivatives penetrate into the brain through meningeal vessels. The passage of specific molecules between the bloodstream and the brain can be regulated by paracellular or transcellular pathways¹⁰⁴. Since applied LCOs, LCO derivatives and LCO-MNPs revealed an anionic surface charge, a transcellular passive diffusion through the BBB is less likely. Probes are further assumed not to penetrate into the diseased brain by receptor mediated endocytosis as shown for distinct FeO nanoparticles¹⁰⁵, because a specific receptor ligand was not attached to the surface of any tested particle. Also, these negatively charged molecules have probably not penetrated into the brain by adsorptive-mediated endocytosis and transcytosis as shown for positively charged molecules¹⁰⁴. Thus it is conceivable that tested probes crossed the BBB with the help of specific drug transporters. The adenosine triphosphate (ATP)-binding cassette (ABC) transporter superfamily (ABC transporter) and the solute-linked carrier (SLC transporter) are involved with influx and efflux transport function for cerebral drug uptake and export¹⁰⁶.

In comparison to pFTAA injections and applications of other LCO-MNPs, LCO-MNP 4026 and LCO-MNP derivative 5012 revealed most efficient fluorescent labeling of cerebral A β plaques after peripheral administration as assessed by fluorescence microscopy.

As discussed before for the brain penetration of LCO derivatives, structural characteristics like particle size and side chain charge of injected molecular markers play a major role for passing the BBB after peripheral administration. However LCO-MNP 4026 and LCO-MNP derivative 5012 are morphologically very different. LCO-MNP 4026 has a long spacer component, which was used to couple the quaternary LCO qFTAM with a FeO MNP. In contrast, LCO-MNP derivative 5012 represents a probe, where the pentameric LCO pFTAA is

coupled through a short spacer to a single gadolinium molecule, instead of a MNP. Thus, on the basis of optical imaging results, structure of distinct LCO-MNPs did not seem to be the limiting factor for BBB passing of LCO-MNPs and subsequent cerebral A β plaque labeling.

LCO-MNP 4026 (190 μ M) and LCO-MNP derivative 5012 (4 mM) showed the highest LCO concentrations among all MNP coupled probes tested (range 28.7 μ M – 4 mM), what could explain the efficient cerebral A β plaque labeling after peripheral administration in *APP/PS1* mice. This fact is in line with results, which were achieved after peripheral administration of pFTAA in *APP/PS1* mice. The intensity of pFTAA labeled cerebral A β plaques was previously shown to be LCO concentration related as well. In contrast, as discussed above, the differential ability of different LCO derivatives to cross the BBB is most likely not due to different concentrations of the provided LCO solutions.

It was hypothesized and initially assumed by optical imaging of cerebral sections after peripheral LCO-MNP treatment of *APP/PS1* mice, that all tested MNP coupled probes were able to cross the BBB. Simultaneously performed TEM analyses of ultrathin cerebral sections of LCO-MNP treated *APP/PS1* mice identified no MNPs around or within cerebral A β plaques. However, since just a small cerebral area and a distinct A β plaque number was investigated for MNPs by TEM, it cannot be excluded that MNPs were present in the brain tissue but were not detected. Since specific fluorescence but no significant TEM and MRI signals were detected on cerebral sections after peripheral administration of distinct LCO-MNPs, it needs to be further investigated if LCO-MNPs crossed the BBB. Fluorescently labeled cerebral A β plaques showed that at least the LCO component crossed the BBB. But it is not known if the attached MNP component penetrated into the brain as well.

In contrast to pFTAA and qFTAA alone, which cross the BBB readily (Aslund et al., 2009, personal communication with collaborators), LCO-MNPs are structurally much bigger in size, which could limit the BBB passing of coupled particles. To cross the BBB, MNPs need to be rather small – ideally smaller than 100 nm⁷⁸. The size distribution of GdF₃ and FeO MNPs conjugated to qFTAA and pFTAA was measured in PBS and particles revealed diameters of 40 nm in average (unpublished data, personal communication with collaborators of the Université Claude Bernard Lyon 1, France and Genovis AB, Sweden). Several NPs with sizes up to ~400 nm were previously shown to cross the BBB after systemic administration¹⁰⁷. Fe₄O₃ NPs with an average diameter of 16.5 \pm 1.6 nm passed the BBB by receptor-mediated transcytosis in rats and could be detected by MRI techniques¹⁰⁵. But also larger, fluorophore-embedded Fe₄O₃ NPs of ~ 100 nm were shown to pass the BBB in mice¹⁰⁸. Thus, the size of the injected LCO-MNPs (40 nm) used in the present thesis should not have limited BBB

crossing following a peripheral application in *APPPSI* mice and does not explain why the hypothesis, that LCO-MNPs would cross the BBB after peripheral administration could not be proven.

Nevertheless, low toxicity and sufficient stability in physiological environments are also crucial requirements for a successful *in vivo* application of MNPs. Polyethylene glycol (PEG) or triethylene glycol (TEG) as hydrophilic polymers and trimers, were coupled to the surfaces of all tested LCO-MNPs (see chapter 2.1). By attaching PEG or TEG to the surface of NPs, hydration of the particle is increased and attached proteins are known to be protected from enzymatic degradation during *in vivo* applications¹⁰⁹. The surface addition of PEG has the additional advantage to increase *in vivo* compatibility of NPs, since i.v. injected uncoated NPs are known to be rapidly cleared from the bloodstream by the reticuloendothelial system¹¹⁰. Prolonged half-lives, believed to result from decreased opsonization and subsequent clearance by macrophages, are described as well for hydrophilic polymer coated NPs¹¹¹. Consecutively it is assumed that LCO-MNPs *in vivo* were tolerated by the murine system and could in principle reach the brain, especially because they were targeted by surface attached LCOs.

As mentioned, qFTAA and pFTAA were attached at the MNP surface as LCO components of investigated LCO-MNPs. Both LCO probes reveal an anionic charge^{74,112}. It was shown previously, that the surface charge is involved in determining the ability of NPs to cross the BBB and low concentration anionic NPs do not affect BBB integrity¹⁰³. The surface of LCO-MNPs 5010 and 5011 was for example covered by 2 % (LCO-MNP 5010) or 10 % (LCO-MNP 5011) pFTAA, which might not have limited BBB penetration.

As mentioned, optical imaging revealed significant fluorescent signals after peripheral application of LCO-MNPs, but MRI measurements performed at the NTNU in Trondheim, Norway revealed no significant changes in T1 and T2 relaxation times. It is conceivable that technical limitations related to MRI measurements limited the detection of significant signals. For the paramagnetic gadolinium particles, which were mainly coupled to LCO-MNPs used in the present study, it is described, that they reveal small positive magnetic susceptibilities causing only modest decreases of relaxation times and therefore exhibit limited MRI sensitivity^{113,114}. In contrast, superparamagnetic FeO particles provide the largest change in signal per unit of metal⁸⁷. However, MRI measurements at the NTNU - Trondheim did not reveal significant signals in brains of *APPPSI* mice treated with Feo based LCO-MNP 4026. *Postmortem* iron staining on tissue sections was negative as well (data not shown). Thus, it is not clear, if the LCO-MNP 4026, qFTAM attached to FeO MNPs, or other MNP coupled

particles passed the BBB and entered the brain to bind cerebral A β deposits in *APP/PS1* mice after peripheral administration.

It is also imaginable that coupled particles termed LCO-MNPs dissociated *in vivo* following a peripheral i.v. injection. The LCO component crossed the BBB and labeled cerebral A β plaques and since MNPs alone were not targeted to the brain, they might have accumulated in the murine system or possibly been metabolized. Especially for FeO particles it was shown that they can be recycled by the organism⁸⁷. After peripheral administration of LCO-MNPs 5010 and 5011, where different amounts of pFTAA (2 % or 10 %) are attached to a GdF3 MNP, collaborators from the Linköping University in Sweden confirmed the finding of fluorescent A β plaque labeling on cerebral sections of treated *APP/PS1* mice by spectral imaging. However simultaneously fluorescent LCO signals were detected on liver and spleen sections (data not shown). These findings indicate that coupled LCO-MNPs might not have been able to cross the BBB and circulated in the periphery after i.v. application. But since fluorescent cerebral A β plaques were detected it is assumed that coupled particles partially dissociated, the LCO component reached the brain and achieved the observed fluorescent plaque labeling. With regard to the stability under physiological conditions, the properties of LCO-MNPs in solution were studied by collaborators at the Université Claude Bernard Lyon 1 in France and revealed sufficient stability in artificial physiological environments (data not shown). Finally it is not clear, if LCO-MNPs dissociated *in vivo* after peripheral administration.

Although it is described in the literature, that distinct MNPs are able to pass the BBB after peripheral administration^{103,105,108,115,116}, intact LCO-MNPs could not be detected in AD brains after peripheral administration. Further investigations like optimizing MRI protocols after peripheral administration of LCO-MNPs are necessary to finally proof the hypothesis that these particles can penetrate into the brain. Nevertheless, since LCOs alone were shown to readily cross the BBB after peripheral application, they represent a useful and promising tool for non-invasive diagnostic or therapeutic approaches targeting the brain.

4.2 Effect of LCOs on Alzheimer's disease pathology *in vivo*

4.2.1 Effect of pFTAA on A β plaque pathology *in vivo*

The neuropathological disease AD is characterized by cerebral aggregation and deposition of the pathological protein A β . Since cerebral A β plaque pathology is thought to drive disease progression¹⁹, many therapeutic approaches target A β aggregation and fibrillization.

Interference with A β aggregation as well as influence on A β fibrillization are known features of several amyloid binding dyes such as Congo red. LCPs as precursors of LCOs and LCOs are derivatives of Congo red^{117,118}. LCPs were previously shown to inhibit prion propagation by stabilizing PrP aggregates⁸⁰. Since prion diseases and AD share the common property of pathological cerebral protein aggregation, the potential of LCOs to act as pharmacophores for AD was further investigated.

If robust binding of LCOs, which are known to pass the BBB, influences cerebral A β pathology in a beneficial or detrimental manner, or causes side effects in the transgenic AD mouse model *APP^{PS1}*, was analyzed within the present thesis.

Long term pFTAA or PBS treated finally 120 d old *APP^{PS1}* mice revealed no significant difference in overall cerebral A β plaque burden. However, in contrast to control mice, pFTAA treated animals had more but smaller A β plaques. Spectral imaging confirmed this finding and in addition revealed structural differences of cortical A β plaques in *APP^{PS1}* mice after pFTAA treatment. Furthermore it was observed, that overall plaque associated pathology was not significantly affected by the pFTAA treatment. However, a trend towards less dystrophic neurites surrounding cortical A β plaques was demonstrated in pFTAA treated *APP^{PS1}* mice. This trend might be explained on the one hand by structural differences of cortical A β plaques after pFTAA treatment. A smaller area of cortical A β plaques could correlate with a decrease of associated toxic side effects as visualized by the appearance of plaque surrounding dystrophic neurites. On the other hand it is conceivable that this trend is only an artefact of the underlying analysis, since the decreased A β plaque covered area provides a reduced surface area exposed to neurites in general.

Different amyloid binding agents like Congo red or methylene blue were investigated as potential pharmacophores in AD previously and side effects of these treatments in AD animal models were monitored. Similar to methylene blue or SMA β BAs^{43,101}, the long term pFTAA treatment in young *APP^{PS1}* mice caused no obvious side effects. In contrast, an oral treatment of the AD animal model *Drosophila melanogaster* with the amyloid binding dye Congo red revealed side effects and resulted in an immobility even of Congo red treated control flies¹¹⁹. Since the pFTAA treatment revealed no toxic effects, its diagnostic and therapeutic potential is still promising.

Comparable to the presented long term pFTAA treatment in young *APP^{PS1}* mice, cerebral A β plaque pathology was analyzed after a systemic short term (three weeks) treatment with small molecule A β -binding agents (SMA β BA's, for example methoxy-XO4⁵⁸) of the AD mouse model *PS1/APP* previously⁴³. Although there are differences in the treatment setup (injected

concentration, treatment period, AD mouse strain), a shift in plaque size distribution towards smaller plaques was observed for both studies. Biochemical A β quantification after the pFTAA treatment could not be validated in this thesis, because of the observed A β precipitation during brain homogenization *in vitro*. This fact was not investigated by Cohen et al., possible because relative A β levels were decreased after biochemical and histological quantifications by equal amounts of about 60 %⁴³. Since both quantifications of cerebral A β amounts revealed the same result, it is speculated that SMA β BAs cause no A β precipitation *in vitro* as observed for pFTAA and that SMA β BAs may indeed be able to reduce cerebral A β burden.

As presented here, after pFTAA long term treatment of *APPPSI* mice with the Congo red derivative pFTAA, reduction of A β aggregation could be observed. For Congo red it has been shown, that it blocks A β oligomer toxicity *in vitro* and reduces A β plaque load due to a blockage of A β aggregation in brains of the AD animal model *Drosophila melanogaster in vivo*^{45,63,119,120}. *Postmortem* analyses of the cerebral A β plaque burden in pFTAA treated mice revealed more numerous but smaller cortical plaques. The increased number of cortical plaques might be explained by more amyloid seeds, which occur by pFTAA binding to A β fibrils triggering possibly a fibril breakage as shown for PrP aggregates¹²¹. Furthermore it is conceivable that the decreased mean area per A β plaque is caused by pFTAA masked plaques, what prevents further A β fibril aggregation. Due to these findings it is assumed that pFTAA acted in a similar manner as Congo red⁶³ and since pFTAA also binds pre-fibrillar A β oligomers, their further aggregation into insoluble A β fibrils, causing the growth of extracellular A β plaques, was prevented.

The plaque size distribution analysis and the spectral imaging of A β plaques after pFTAA treatment pointed to alterations in A β plaque morphology. In comparison to controls, pFTAA treated *APPPSI* mice revealed by spectral imaging a less developed amyloid core of cortical congophilic A β plaques. Recently, also differences of A β plaque morphology between young and aged *APPPSI* mice were observed⁷³. As *APPPSI* mice grow older than 10 months, the core of the plaques appears to rearrange and the LCO staining pattern of individual A β plaques changes⁷³. Mice of the pFTAA treatment were much younger than animals, which revealed age dependent morphological differences in cerebral A β plaque deposition. The pFTAA treatment was initiated before plaque deposition started at 6-8 weeks of age and plaque burden was analyzed already at an age of 120 d. But since it is shown in the present study that pFTAA bound to cerebral A β deposits decelerates cortical plaque growth, overall plaque pathology in *APPPSI* mice treated with pFTAA for up to an age of at least ten months

might be changed. It is further known, that from approximately 8 months of age on, almost no formation of new plaques is detected but present A β plaques appear to grow in *APPPSI* mice¹²². Due to these facts it would be of high interest to analyze the structure of cerebral A β plaques in pFTAA treated *APPPSI* mice at an age about 10 month and older.

The amyloid binding dye methylene blue apparently has beneficial effects in the treatment of cognitive disorders and was shown to slow down the cognitive decline in AD within clinical trials¹⁰¹. *In vitro* studies revealed the ability of methylene blue to inhibit the assembly of tau proteins into filaments¹⁰¹. The aggregation of hyperphosphorylated tau proteins is a hallmark of human AD and these proteins accumulate also in dystrophic neurites around cerebral A β plaques in *APPPSI* mice⁶⁴. After the peripheral long term pFTAA treatment of young *APPPSI* mice, a trend to less dystrophic neurites, surrounding cortical A β plaques and containing hyperphosphorylated tau aggregates, was observed. However this trend did not reach statistical significance. In contrast to methylene blue, a direct effect of pFTAA on tau pathology in treated *APPPSI* mice was not investigated but this finding indicates an influence of the peripheral pFTAA treatment on plaque associated pathology und fits to the fact, that pFTAA treated *APPPSI* mice also showed a decrease in mean area per cerebral A β plaque. A positive correlation of A β plaque size and the area covered by dystrophic neurites around cortical A β plaques can be hypothesized.

4.2.2 Effect of pFTAA on A β oligomer toxicity in vivo

An impairment of synaptic transmission in AD, determining finally deficits in cognition and memory, is assumed to be mainly caused by neurotoxic soluble A β oligomers. It was hypothesized within the present thesis, that a peripheral pFTAA treatment in aged *APPPSI* mice might have a functional effect on synaptic transmission. This hypothesis was based on the fact that pFTAA is described to bind beside deposited A β assemblies also the neurotoxic pre-fibrillar A β oligomers^{33-35,39,123}. Impairments in synaptic transmission are described to be observed in *APPPSI* mice older than 8 month⁹⁷, why the pFTAA treatment was initiated at 7.5 month of age in *APPPSI* mice. However, a peripheral pFTAA treatment of aged *APPPSI* mice revealed no differences in synaptic transmission to PBS treated *APPPSI* controls and the underlying hypothesis could not be proven.

pFTAA is described to bind pre-fibrillar A β oligomers during *in vitro* fibrillization and it is speculated that an pFTAA binding of these species might block their toxicity⁷⁴. Congo red was shown to reduce the concentration of oligomers *in vitro*⁶³. Furthermore it was shown recently,

that a systemic vaccination using anti-oligomeric A β antibodies improves cognitive functions by reducing A β deposition and tau pathology in AD mice¹²⁴. However an *in vivo* effect of pFTAA on synaptic transmission in hippocampal slices of treated *APPPSI* mice could not be detected. Additionally no significant effect of the peripheral pFTAA treatment in aged *APPPSI* mice on cerebral A β plaque pathology and A β plasma levels (see chapter 3.4.2) was observed. It is questionable if pFTAA affected cerebral A β pathology in aged mice with advanced disease pathology at all.

The pFTAA treatment was initiated in *APPPSI* mice at 7.5 month of age because it is known that impairments of hippocampal synaptic transmission does not occur before 8 months of age⁹⁷. But it is assumed, that pre-fibrillar oligomeric A β species occur in the diseased brain already before A β plaque deposition¹²⁵ and based on this knowledge the pFTAA treatment might have been initiated too late, to influence synaptic transmission and possibly rescue neurotoxic effects of A β oligomers. When combining the results of the two peripheral pFTAA treatment approaches in *APPPSI* mice (see chapter 3.3 and 3.4) it is assumed, that pFTAA influences cerebral A β plaque formation in young animals but not plaque maintenance in aged *APPPSI* mice. Furthermore the treatment period of two month in aged animals might have been too short, to affect cerebral A β plaque maintenance. These results are comparable to previous observations, where a combination treatment (inhibition of A β production and passive immunization using antibody Ab9) influenced especially the formation of newly formed A β deposits¹²⁶. Therefore, it would be of interest to measure synaptic transmission in aged animals, where the pFTAA treatment was initiated before or with cerebral A β plaque deposition and neurotoxic A β oligomers were pFTAA bound before first cognitive impairments in animals occur.

4.2.3 Conclusions of peripheral pFTAA treatment in *APPPSI* mice

Taken together, no substantial effect of pFTAA on overall cerebral A β pathology was observed, however detailed analyses revealed an influence on cortical plaque assembly. After a peripheral pFTAA treatment, young *APPPSI* mice revealed an increase of A β plaque number and a shift to smaller cerebral A β plaques when compared to controls. A conformational change of cortical A β plaque morphology was observed, which indicates a slower cerebral A β plaque growth and maturation after systemic pFTAA treatment in *APPPSI* mice. The observed effect might even decelerate or moderate AD progression, but therefore cerebral A β load of longer treated aged *APPPSI* mice needs to be analyzed and additional

Discussion

functional studies need to be assessed. A peripheral pFTAA treatment does not influence A β oligomer toxicity on a functional level, but as discussed it is speculated that the treatment was initiated too late and disease pathology was already too advanced. It is conceivable, that a treatment initiated earlier, for example before plaque deposition starts in *APP/PS1* mice (6-8 weeks of age) might alter not only fibrillar A β deposition (see long term pFTAA treatment) but also toxic effects of oligomeric species. Since a remarkable effect of pFTAA on *in vitro* precipitation of A β was observed it is of high interest why only a minor effect on A β plaque pathology *in vivo* and no effect on synaptic transmission in *APP/PS1* mice was observed. An earlier and longer peripheral pFTAA treatment but also a local i.c. treatment of pFTAA, allowing for higher local concentrations of pFTAA via an osmotic minipump might influence cerebral A β pathology in *APP/PS1* mice differently^{85,127,128}.

5. Zusammenfassung

LCOs (*luminescent conjugated oligothiophenes*) als neue β -Amyloid-bindende Substanzen zur Diagnose und Therapie der Alzheimer'schen Erkrankung

LCOs sind neuartige, konformations-sensitive optische Amyloid-Marker, die je nach Struktur der gebundenen, pathologischen Amyloid-Ablagerungen Fluoreszenzlicht unterschiedlicher Wellenlänge emittieren. Nach einer intravenösen Injektion in dem transgenen Alzheimer Mausmodell *APP/PS1* sind bestimmte LCOs, beispielsweise pFTAA, in der Lage die Blut-Hirn-Schranke (BHS) zu passieren und zerebrale β -Amyloid-Plaques sowohl langfristig als auch spezifisch zu markieren.

Im Rahmen dieses Promotionsprojektes wurden LCOs zum einen auf ihre Verwendbarkeit als neuartige diagnostische Marker zur Detektion von zerebralen β -Amyloid und zum anderen als potentielle therapeutische Substanzen im transgenen Alzheimer Mausmodell *APP/PS1* untersucht.

Innerhalb des diagnostischen Versuchsansatzes wurde analysiert, ob an magnetische Nanopartikel gekoppelte LCO-Derivate (LCO-MNPs) für den Einsatz als Kontrastmittel nach einer intravenösen Injektion ebenfalls in der Lage sind, die BHS zu passieren und an zerebrale β -Amyloid-Ablagerungen in *APP/PS1* Tieren zu binden. Nach intravenöser Applikation der LCO-MNPs wurden mittels Fluoreszenz-Mikroskopie in *APP/PS1* Tieren LCO-markierte β -Amyloid-Plaques detektiert. Magnetische Nanopartikel konnten bisher mittels der Magnetresonanztomographie und Elektronenmikroskopie allerdings nicht im Hirn der behandelten Tiere nachgewiesen werden.

Verschiedene Amyloid-spezifische Marker wie beispielsweise Kongo Rot oder Methoxy-XO4 wiesen zuvor anti-amyloidogene Eigenschaften *in vitro* und in transgenen Alzheimer Tier-Modellen *in vivo* auf. Auch LCPs (*luminescent conjugated polythiophenes*) als Vorläufer von LCOs reduzieren die Ausbreitung von Prion-Proteinen *in vitro* und wiesen somit einen Amyloid-hemmenden Effekt auf. Innerhalb des vorliegenden Promotionsprojektes wurde weiterhin untersucht, ob die langfristige *in vivo* Bindung von pFTAA an zerebrale β -Amyloid-Plaques in *APP/PS1* Tieren einen Einfluss auf die Plaque-Pathologie in kortikalen Hirnregionen hat und LCOs somit möglicherweise als neue therapeutische Substanzen eingesetzt werden können. Nach einer *in vivo* Behandlung von transgenen *APP/PS1* Tieren, wurden keine toxischen Nebenwirkungen beobachtet und Analysen der Gesamt-Plaque-Belastung im Hirn der behandelten Tiere zeigten im Vergleich zu Kontrolltieren keine signifikanten Unterschiede. Allerdings wiesen pFTAA-behandelte *APP/PS1* Tiere signifikant

Zusammenfassung

mehr kleinere β -Amyloid Plaques und geringere durchschnittliche Flächen pro Plaque auf. Zusätzlich wurden signifikante morphologische Unterschiede zwischen pFTAA gebundenen und unbehandelten zerebralen β -Amyloid Plaques aufgezeigt, die auf eine langsamere β -Amyloid Plaque-Reifung hinweisen. Die erhöhte Anzahl an kortikalen Plaques könnte auch auf eine mögliche, verstärkte Nukleation der Amyloidablagerungen auf Grund der pFTAA Bindung hinweisen. Zusammenfassend könnten diese beiden Ergebnisse die unveränderte Gesamt-Plaque-Belastung im Hirn pFTAA behandelte Tiere erklären. Da pFTAA auch pre-fibrilläre, toxisch wirkende $A\beta$ -Oligomere bindet, wurde ausserdem der Effekt einer pFTAA Behandlung auf die synaptische Transmission in *APPPSI* Tieren untersucht. Es wurde jedoch kein signifikanter Einfluss der pFTAA Behandlung in *APPPSI* Tieren auf die synaptische Transmission im Hippokampus nachgewiesen.

Zusammenfassend demonstrieren die Ergebnisse keinen substantiellen therapeutischen Effekt während einer Langzeit-Behandlung von transgenen Alzheimer Tieren mit pFTAA. Allerdings unterstützen die generierten Daten die Anwendung von pFTAA beziehungsweise LCOs in der humanen *in vitro* Diagnostik und potentiell auch in der *in vivo* Diagnostik.

6. Abstract

Luminescent conjugated oligothiophenes as diagnostic tools and potential pharmacophores in Alzheimer's disease

Luminescent conjugated oligothiophenes (LCOs) are novel molecular amyloid binding agents, which identify their targets with high sensitivity and specificity, and additionally provide structural information about bound amyloid lesions due to changing emission spectra. The pentameric LCO pFTAA readily crosses the blood brain barrier (BBB) after intravenous injection and efficiently labels cerebral A β plaques in Alzheimer's disease (AD) transgenic *APP/PS1* mice.

Within the present thesis, LCOs were investigated as *in vivo* tracers for detecting cerebral A β deposits and as potential pharmacophores in *APP/PS1* mice, a model of early and robust cerebral amyloidosis.

To test LCOs for neuroimaging of cerebral A β deposits using magnetic resonance imaging (MRI), they were attached by distinct spacer components to magnetic nanoparticles (MNPs), resulting in coupled probes termed LCO-MNPs. LCO-MNPs were peripherally applied to *APP/PS1* mice and BBB passing as well as labeling of cerebral A β plaques was investigated using optical imaging and MRI. Results revealed a specific optical signal of LCO labeled cerebral A β plaques after peripheral administration of LCO-MNPs, however no significant MRI and transmission electron microscopic signals were detected so far.

Since different amyloid dyes showed anti-amyloid effects by preventing A β fibrillogenesis or by inhibition of A β toxicity, pFTAA was further investigated as potential pharmacophores in AD. After crossing the BBB of *APP/PS1* mice following peripheral application, pFTAA binds deposited fibrillar A β plaques but possibly also pre-fibrillar toxic oligomers, which were described to primarily cause impairments in memory and cognition. To analyze the effect of cerebral bound pFTAA on AD pathology, *APP/PS1* mice were treated with pFTAA, and cerebral A β plaque load and hippocampal synaptic transmission were determined. Although no functional impact on synaptic transmission was observed after peripheral pFTAA treatment, an influence on A β plaque pathology in *APP/PS1* mice was detected. The overall cerebral A β plaque burden was not changed, however pFTAA treated *APP/PS1* mice revealed more numerous and smaller plaques when compared to PBS treated controls, which could in addition be structurally distinguished from A β plaques of control animals. Thus *in vivo* pFTAA binding to cerebral amyloid deposits in *APP/PS1* mice slows A β plaque growth and

Abstract

maturation. The significant increase of cortical A β plaque number might be explained by elevated amyloid seeding through pFTAA binding to cerebral A β .

The results of the present thesis show, that pFTAA or LCOs have the potential to be further investigated for human AD diagnostic, since they caused no obvious toxic side effects in long term treated *APP/PS1* mice and did not substantially alter cerebral plaque burden.

7. References

1. Tarawneh, R. & Holtzman, D. M. The clinical problem of symptomatic Alzheimer disease and mild cognitive impairment. *Cold Spring Harb. Perspect. Med.* **2**, a006148 (2012).
2. McKhann, G. M. *et al.* The diagnosis of dementia due to Alzheimer's disease: recommendations from the National Institute on Aging-Alzheimer's Association workgroups on diagnostic guidelines for Alzheimer's disease. *Alzheimers. Dement.* **7**, 263–9 (2011).
3. Yuan, Y., Chen, Y.-P. P., Boyd-Kirkup, J., Khaitovich, P. & Somel, M. Accelerated aging-related transcriptome changes in the female prefrontal cortex. *Aging Cell* **11**, 894–901 (2012).
4. Beal, M. F., Lang, A. E. & Ludolph, A. . *Neurodegenerative Diseases: Neurobiology, Pathogenesis and Therapeutics*. (Cambridge University Press: UK, 2005).
5. Grand, J. H., Caspar, S. & Macdonald, S. W. Clinical features and multidisciplinary approaches to dementia care. *J. Multidiscip. Healthc.* **4**, 125–47 (2011).
6. Koo, E. H., Lansbury, P. T. & Kelly, J. W. Amyloid diseases: abnormal protein aggregation in neurodegeneration. *Proc. Natl. Acad. Sci. U. S. A.* **96**, 9989–90 (1999).
7. Serrano-Pozo, A., Frosch, M. P., Masliah, E. & Hyman, B. T. Neuropathological alterations in Alzheimer disease. *Cold Spring Harb. Perspect. Med.* **1**, a006189 (2011).
8. Luk, K. C. *et al.* Intracerebral inoculation of pathological α -synuclein initiates a rapidly progressive neurodegenerative α -synucleinopathy in mice. *J. Exp. Med.* **209**, 975–86 (2012).
9. Aguzzi, A. & Rajendran, L. The transcellular spread of cytosolic amyloids, prions, and prionoids. *Neuron* **64**, 783–90 (2009).
10. Kukull, W. A. *et al.* Dementia and Alzheimer Disease Incidence. **59**, (2002).
11. Alzheimer Association. 2013 Alzheimer's disease facts and figures. *Alzheimer's Dement.* **9**, 208–245 (2013).
12. Schneider. *Facharztwissen Psychiatrie und Psychotherapie*. (Springer-Verlag, 2012).
13. Mayeux, R. & Stern, Y. Epidemiology of Alzheimer disease. *Cold Spring Harb. Perspect. Med.* **2**, (2012).
14. Ferri, C. P. *et al.* Global prevalence of dementia: a Delphi consensus study. *Lancet* **366**, 2112–7 (2005).
15. Holtzman, D. M., Mandelkow, E. & Selkoe, D. J. Alzheimer disease in 2020. *Cold Spring Harb. Perspect. Med.* **2**, (2012).
16. Jonsson, T. *et al.* Variant of TREM2 associated with the risk of Alzheimer's disease. *N. Engl. J. Med.* **368**, 107–16 (2013).
17. Guerreiro, R. *et al.* TREM2 variants in Alzheimer's disease. *N. Engl. J. Med.* **368**, 117–27 (2013).
18. Tanzi, R. E. The genetics of Alzheimer disease. *Cold Spring Harb. Perspect. Med.* **2**, (2012).
19. Hardy, J. & Selkoe, D. J. The amyloid hypothesis of Alzheimer's disease: progress and problems on the road to therapeutics. *Science* **297**, 353–6 (2002).

References

20. Love, S. Neuropathological investigation of dementia: a guide for neurologists. *J. Neurol. Neurosurg. Psychiatry* **76 Suppl 5**, v8–14 (2005).
21. Kimura, T. *et al.* Aggregation of detergent-insoluble tau is involved in neuronal loss but not in synaptic loss. *J. Biol. Chem.* **285**, 38692–9 (2010).
22. Gómez-Isla, T. *et al.* Neuronal loss correlates with but exceeds neurofibrillary tangles in Alzheimer's disease. *Ann Neurol* **41(1)**, 17–24 (1997).
23. Iqbal, K. & Grundke-Iqbal, I. Neurofibrillary pathology leads to synaptic loss and not the other way around in Alzheimer disease. *J. Alzheimers. Dis.* **4**, 235–8 (2002).
24. Mandelkow, E. Tau in Alzheimer's disease. *Trends Cell Biol.* **8**, 425–427 (1998).
25. Masliah, E. *et al.* Immunoreactivity of CD45, a protein phosphotyrosine phosphatase, in Alzheimer's disease. *Acta Neuropathol* **83(1)**, 12–20 (1991).
26. Beach, T. G., Walker, R. & Mcgeer, E. G. Patterns of Gliosis in Alzheimer's Disease and Aging Cerebrum. **36**, (1989).
27. Glenner, G. & Wong, C. ALZHEIMER'S DISEASE AND DOWN'S SYNDROME: SHARING OF A UNIQUE CEREBROVASCULAR AMYLOID FIBRIL PROTEIN. **122**, 1131–1135 (1984).
28. Serrano-Pozo, A., Frosch, M. P., Masliah, E. & Hyman, B. T. Neuropathological alterations in Alzheimer disease. *Cold Spring Harb. Perspect. Med.* **1**, a006189 (2011).
29. Wisniewski, T., Ghiso, J. & Frangione, B. PEPTIDES HOMOLOGOUS TO THE AMYLOID PROTEIN OF ALZHEIMER'S DISEASE CONTAINING A GLUTAMINE FOR GLUTAMIC ACID SUBSTITUTION HAVE ACCELERATED AMYLOID FIBRIL FORMATION. **179**, 1247–1254 (1991).
30. Seubert, P. *et al.* Isolation and quantification of soluble Alzheimer's β -peptide from biological fluids. *Lett. to Nat.* **259**, (1992).
31. Querfurth, H. W. & Laferla, F. M. Alzheimer's Disease. 329–344 (2013).
32. Hardy, J. A hundred years of Alzheimer's disease research. *Neuron* **52**, 3–13 (2006).
33. Walsh, D. M. *et al.* Naturally secreted oligomers of amyloid beta protein potently inhibit hippocampal long-term potentiation in vivo. *Nature* **416**, 535–9 (2002).
34. Selkoe, D. J. Soluble oligomers of the amyloid beta-protein impair synaptic plasticity and behavior. *Behav. Brain Res.* **192**, 106–13 (2008).
35. Shankar, G. M. *et al.* Natural oligomers of the Alzheimer amyloid-beta protein induce reversible synapse loss by modulating an NMDA-type glutamate receptor-dependent signaling pathway. *J. Neurosci.* **27**, 2866–75 (2007).
36. Lue, L.-F. *et al.* Soluble Amyloid β Peptide Concentration as a Predictor of Synaptic Change in Alzheimer's Disease. *Am. J. Pathol.* **155**, 853–862 (1999).
37. Mclean, C. A. *et al.* Soluble Pool of A β Amyloid as a Determinant of Severity of Neurodegeneration in Alzheimer's Disease. 860–866 (1999).
38. Van Dam, D. & De Deyn, P. P. Drug discovery in dementia: the role of rodent models. *Nat. Rev. Drug Discov.* **5**, 956–70 (2006).

References

39. Aslund, A. *et al.* Novel pentameric thiophene derivatives for in vitro and in vivo optical imaging of a plethora of protein aggregates in cerebral amyloidoses. *ACS Chem. Biol.* **4**, 673–84 (2009).
40. Hirth, F. *Drosophila melanogaster* in the study of human neurodegeneration. *CNS Neurol. Disord. Drug Targets* **9**, 504–23 (2010).
41. Schenk, D., Basi, G. S. & Pangalos, M. N. Treatment strategies targeting amyloid β -protein. *Cold Spring Harb. Perspect. Med.* **2**, a006387 (2012).
42. Estrada, L. D. & Soto, C. Disrupting beta-amyloid aggregation for Alzheimer disease treatment. *Curr. Top. Med. Chem.* **7**, 115–26 (2007).
43. Cohen, A. D. & M.D. Ikonomic, E.E. Abrahamson, W.R. Paljug, S.T. DeKosky, I.M. Lefterov, R.P. Koldamova, L. Shao, M.L. Debnath, N.S. Mason, C.A. Mathis, and W. E. K. Anti-Amyloid Effects of Small Molecule A β -Binding Agents in PS/APP Mice. **6**, (2010).
44. Frid, P., Anisimov, S. V & Popovic, N. Congo red and protein aggregation in neurodegenerative diseases. *Brain Res. Rev.* **53**, 135–60 (2007).
45. Lorenzo, A. & Yankner, B. A. by Congo red . 8-Amyloid neurotoxicity requires fibril formation and is inhibited. **91**, 12243–12247 (1994).
46. Wood, S. J., MacKenzie, L., Maleeff, B., Hurle, M. R. & Wetzel, R. Selective Inhibition of Abeta Fibril Formation. *J. Biol. Chem.* **271**, 4086–4092 (1996).
47. Ono, K., Hasegawa, K., Naiki, H. & Yamada, M. Curcumin Has Potent Anti-Amyloidogenic Effects for Alzheimer ' s □ -Amyloid Fibrils In Vitro. **750**, 742–750 (2004).
48. Estrada, L. D. & Soto, C. Disrupting beta-amyloid aggregation for Alzheimer disease treatment. *Curr. Top. Med. Chem.* **7**, 115–26 (2007).
49. Sperling, R. a *et al.* Amyloid-related imaging abnormalities in amyloid-modifying therapeutic trials: recommendations from the Alzheimer's Association Research Roundtable Workgroup. *Alzheimers. Dement.* **7**, 367–85 (2011).
50. Blennow, K., Zetterberg, H. & Fagan, A. M. Fluid biomarkers in Alzheimer disease. *Cold Spring Harb. Perspect. Med.* **2**, a006221 (2012).
51. Ray, S. *et al.* Classification and prediction of clinical Alzheimer's diagnosis based on plasma signaling proteins. *Nat. Med.* **13**, 1359–62 (2007).
52. Hébert, S. S. *et al.* Loss of microRNA cluster miR-29a / b-1 in sporadic Alzheimer ' s disease correlates with increased BACE1 / □ -secretase expression. **105**, (2008).
53. Hébert, S. S., Sergeant, N. & Buée, L. MicroRNAs and the Regulation of Tau Metabolism. *Int. J. Alzheimers. Dis.* **2012**, 406561 (2012).
54. Mapstone, M. *et al.* Plasma phospholipids identify antecedent memory impairment in older adults. *Nat. Med.* **20**, 415–418 (2014).
55. Attwell, D. & Laughlin, S. B. An energy budget for signaling in the grey matter of the brain. *J. Cereb. Blood Flow Metab.* **21**, 1133–45 (2001).
56. Francisco, S. References and Notes I. To be described as superstitious, behavior 26 (1975). 5. **26**, 723–725 (1979).

References

57. Mathis, C. a, Lopresti, B. J. & Klunk, W. E. Impact of amyloid imaging on drug development in Alzheimer's disease. *Nucl. Med. Biol.* **34**, 809–22 (2007).
58. Klunk, W. E. *et al.* Imaging Abeta plaques in living transgenic mice with multiphoton microscopy and methoxy-X04, a systemically administered Congo red derivative. *J. Neuropathol. Exp. Neurol.* **61**, 797–805 (2002).
59. Johnson, K. a, Fox, N. C., Sperling, R. a & Klunk, W. E. Brain imaging in Alzheimer disease. *Cold Spring Harb. Perspect. Med.* **2**, a006213 (2012).
60. Braak, H. & Braak, E. Acta H ' pathologica Neuropathological staging of Alzheimer-related changes. 239–259 (1991).
61. Jack, C. R. *et al.* Tracking pathophysiological processes in Alzheimer's disease: an updated hypothetical model of dynamic biomarkers. *Lancet Neurol.* **12**, 207–16 (2013).
62. Casey, D. A., Antimisiaris, D. & Brien, J. O. Drugs for Alzheimer ' s Disease□: Are They Effective□? **35**, 208–211 (2010).
63. Caughey, B. & Lansbury, P. T. Protofibrils, pores, fibrils, and neurodegeneration: separating the responsible protein aggregates from the innocent bystanders. *Annu. Rev. Neurosci.* **26**, 267–98 (2003).
64. Radde, R. *et al.* Abeta42-driven cerebral amyloidosis in transgenic mice reveals early and robust pathology. *EMBO Rep.* **7**, 940–6 (2006).
65. Findeis, M. a. The role of amyloid beta peptide 42 in Alzheimer's disease. *Pharmacol. Ther.* **116**, 266–86 (2007).
66. McGowan, E. *et al.* Abeta42 is essential for parenchymal and vascular amyloid deposition in mice. *Neuron* **47**, 191–9 (2005).
67. Yang, F., Uéda, K., Chen, P., Ashe, K. H. & Cole, G. M. Plaque-associated alpha-synuclein (NACP) pathology in aged transgenic mice expressing amyloid precursor protein. *Brain Res.* **853**, 381–3 (2000).
68. Götz, J. *et al.* A decade of tau transgenic animal models and beyond. *Brain Pathol.* **17**, 91–103 (2007).
69. LaFerla, F. M. & Green, K. N. Animal models of Alzheimer disease. *Cold Spring Harb. Perspect. Med.* **2**, (2012).
70. Klingstedt, T. & Nilsson, K. P. R. Conjugated polymers for enhanced bioimaging. *Biochim. Biophys. Acta* **1810**, 286–96 (2011).
71. Nilsson, K. P. R. *et al.* Imaging Distinct Conformational States of Amyloid-b Fibrils in Alzheimer's Disease Using Novel Luminescent Probes. *ACS Chem. Biol.* **2**, 553–560 (2007).
72. Nilsson, K. P. R. *et al.* Structural typing of systemic amyloidoses by luminescent-conjugated polymer spectroscopy. *Am. J. Pathol.* **176**, 563–74 (2010).
73. Nystrom, S. *et al.* Evidence for age dependent in vivo conformational rearrangement within Aβ amyloid deposits. *ACS Chem. Biol.* 130325011231004 (2013). doi:10.1021/cb4000376
74. Hammarström, P. *et al.* A fluorescent pentameric thiophene derivative detects in vitro-formed prefibrillar protein aggregates. *Biochemistry* **49**, 6838–45 (2010).
75. Wegenast-Braun, B. M. *et al.* Spectral discrimination of cerebral amyloid lesions after peripheral application of luminescent conjugated oligothiophenes. *Am. J. Pathol.* **181**, 1953–60 (2012).

References

76. Pardridge, W. M. Blood-brain barrier delivery. *Drug Discov. Today* **12**, 54–61 (2007).
77. Veiseth, O. *et al.* Specific targeting of brain tumors with an optical/magnetic resonance imaging nanoprobe across the blood-brain barrier. *Cancer Res.* **69**, 6200–7 (2009).
78. Lockman, P. R., Mumper, R. J., Khan, M. a & Allen, D. D. Nanoparticle technology for drug delivery across the blood-brain barrier. *Drug Dev. Ind. Pharm.* **28**, 1–13 (2002).
79. Pollack, S. J., Sadler, I. I. J., Hawtin, S. R., Taylor, V. J. & Shearman, M. S. *Neuroscience letters.* **197**, 211–214 (1995).
80. Margalith, I. *et al.* Polythiophenes inhibit prion propagation by stabilizing prion protein (PrP) aggregates. *J. Biol. Chem.* **287**, 18872–87 (2012).
81. Aguzzi, A. & Polymenidou, M. Mammalian prion biology: one century of evolving concepts. *Cell* **116**, 313–27 (2004).
82. Golde, W. T., Gollobin, P. & Rodriguez, L. L. A rapid , simple , and humane method for submandibular bleeding of mice using a lancet. *TECHNIQUE* **34**, 39–43 (2005).
83. Grathwohl, S. A. *et al.* Formation and maintenance of Alzheimer’s disease beta-amyloid plaques in the absence of microglia. *Nat. Neurosci.* **12**, 1361–3 (2009).
84. Kawarabayashi, T. *et al.* Age-Dependent Changes in Brain , CSF , and Plasma Amyloid \square Protein in the Tg2576 Transgenic Mouse Model of Alzheimer ’ s Disease. **21**, 372–381 (2001).
85. Vom Berg, J. *et al.* Inhibition of IL-12/IL-23 signaling reduces Alzheimer’s disease-like pathology and cognitive decline. *Nat. Med.* **18**, 1812–9 (2012).
86. Citri, A. & Malenka, R. C. Synaptic plasticity: multiple forms, functions, and mechanisms. *Neuropsychopharmacology* **33**, 18–41 (2008).
87. Bulte, J. W. M. & Kraitchman, D. L. Iron oxide MR contrast agents for molecular and cellular imaging. *NMR Biomed.* **17**, 484–99 (2004).
88. Perez Nievas, B. G. *et al.* Restraint stress increases neuroinflammation independently of amyloid β levels in amyloid precursor protein/PS1 transgenic mice. *J. Neurochem.* **116**, 43–52 (2011).
89. Cuadrado-Tejedor, M. *et al.* Chronic mild stress accelerates the onset and progression of the Alzheimer’s disease phenotype in Tg2576 mice. *J. Alzheimers. Dis.* **28**, 567–78 (2012).
90. Wilson, R. S. *et al.* Proneness to psychological distress is associated with risk of Alzheimer’s disease. *Neurology* **61**, 1479–1485 (2003).
91. Kang, J.-E., Cirrito, J. R., Dong, H., Csernansky, J. G. & Holtzman, D. M. Acute stress increases interstitial fluid amyloid-beta via corticotropin-releasing factor and neuronal activity. *Proc. Natl. Acad. Sci. U. S. A.* **104**, 10673–8 (2007).
92. Jucker, M. & Walker, L. C. Pathogenic Protein Seeding in Alzheimer’s Disease and Other Neurodegenerative Disorders. *Ann Neurol* **70**, 532–540 (2011).
93. Rupp, N. J., Wegenast-Braun, B. M., Radde, R., Calhoun, M. E. & Jucker, M. Early onset amyloid lesions lead to severe neuritic abnormalities and local, but not global neuron loss in APPPS1 transgenic mice. *Neurobiol. Aging* **32**, 2324.e1–6 (2011).
94. Barron, K. D. The microglial cell. A historical review. *J. Neurol. Sci.* **134 Suppl**, 57–68 (1995).

References

95. Prokop, S., Miller, K. R. & Heppner, F. L. Microglia actions in Alzheimer's disease. *Acta Neuropathol.* **2**, 461–477 (2013).
96. Walsh, D. M. *et al.* Naturally secreted oligomers of amyloid beta protein potently inhibit hippocampal long-term potentiation in vivo. *Nature* **416**, 535–9 (2002).
97. Gengler, S., Hamilton, A. & Hölscher, C. Synaptic plasticity in the hippocampus of a APP/PS1 mouse model of Alzheimer's disease is impaired in old but not young mice. *PLoS One* **5**, e9764 (2010).
98. Nilsson, K. P. R., Lindgren, M. & Hammarström, P. in *Methods Mol. Biol.* **849**, 425–34 (2012).
99. Pardridge, W. M. Alzheimer's disease drug development and the problem of the blood-brain barrier. *Alzheimers. Dement.* **5**, 427–32 (2009).
100. Orlando, R. a, Gonzales, A. M., Royer, R. E., Deck, L. M. & Vander Jagt, D. L. A chemical analog of curcumin as an improved inhibitor of amyloid Abeta oligomerization. *PLoS One* **7**, e31869 (2012).
101. Oz, M., Lorke, D. E. & Petroianu, G. a. Methylene blue and Alzheimer's disease. *Biochem. Pharmacol.* **78**, 927–32 (2009).
102. Tavitian, B. *et al.* Characterization of a synthetic anionic vector for oligonucleotide delivery using in vivo whole body dynamic imaging. *Pharm. Res.* **19**, 367–76 (2002).
103. Lockman, P. R., Koziara, J. M., Mumper, R. J. & Allen, D. D. Nanoparticle surface charges alter blood-brain barrier integrity and permeability. *J. Drug Target.* **12**, 635–41 (2004).
104. Barbu, E., Molnár, E., Tsibouklis, J. & Górecki, D. C. The potential for nanoparticle-based drug delivery to the brain: overcoming the blood-brain barrier. *Expert Opin. Drug Deliv.* **6**, 553–65 (2009).
105. Qiao, R., Jia, Q. & Hüwel, S. Receptor-Mediated Delivery of Magnetic Nanoparticles across the. 3304–3310 (2012).
106. Girardin, F. Membrane transporter proteins: a challenge for CNS drug development. *Pharmacol. Asp.* 311–321 (2006).
107. Wohlfart, S., Gelperina, S. & Kreuter, J. Transport of drugs across the blood-brain barrier by nanoparticles. *J. Control. Release* **161**, 264–73 (2012).
108. Kong, S. D. *et al.* Magnetic targeting of nanoparticles across the intact blood-brain barrier. *J. Control. Release* **164**, 49–57 (2012).
109. Harris, J. M. & Chess, R. B. Effect of pegylation on pharmaceuticals. *Nat. Rev. Drug Discov.* **2**, 214–21 (2003).
110. Brigger, I., Dubernet, C. & Couvreur, P. N anoparticles in cancer therapy and diagnosis. **54**, 631–651 (2002).
111. Moghimi, S. M. & Szebeni, J. Stealth liposomes and long circulating nanoparticles: critical issues in pharmacokinetics, opsonization and protein-binding properties. *Prog. Lipid Res.* **42**, 463–478 (2003).
112. Klingstedt, T. *et al.* Luminescent Conjugated Oligothiophenes for Sensitive Fluorescent Assignment of Protein Inclusion Bodies. *Chembiochem* 607–616 (2013). doi:10.1002/cbic.201200731
113. Caravan, P. Strategies for increasing the sensitivity of gadolinium based MRI contrast agents. *Chem. Soc. Rev.* **35**, 512–23 (2006).

References

114. De Backer, M. E., Nabuurs, R. J. a, van Buchem, M. a & van der Weerd, L. MR-based molecular imaging of the brain: the next frontier. *AJNR. Am. J. Neuroradiol.* **31**, 1577–83 (2010).
115. Lockman, P. R. *et al.* Brain uptake of thiamine-coated nanoparticles. *J. Control. Release* **93**, 271–282 (2003).
116. Sarin, H. *et al.* Effective transvascular delivery of nanoparticles across the blood-brain tumor barrier into malignant glioma cells. *J. Transl. Med.* **6**, 80 (2008).
117. Klingstedt, T. *et al.* Synthesis of a library of oligothiophenes and their utilization as fluorescent ligands for spectral assignment of protein aggregates. *Org. Biomol. Chem.* **9**, 8356–70 (2011).
118. Klingstedt, T. & Nilsson, K. P. R. Luminescent conjugated poly- and oligo-thiophenes: optical ligands for spectral assignment of a plethora of protein aggregates. *Biochem. Soc. Trans.* **40**, 704–10 (2012).
119. Crowther, D. C. *et al.* Intraneuronal A β , non-amyloid aggregates and neurodegeneration in a *Drosophila* model of Alzheimer's disease. *Neuroscience* **132**, 123–35 (2005).
120. Gellermann, G. P. *et al.* Alzheimer-like plaque formation by human macrophages is reduced by fibrillation inhibitors and lovastatin. *J. Mol. Biol.* **360**, 251–7 (2006).
121. Aguzzi, A. & Polymenidou, M. Mammalian prion biology: one century of evolving concepts. *Cell* **116**, 313–27 (2004).
122. Hefendehl, J. K. *et al.* Long-term in vivo imaging of β -amyloid plaque appearance and growth in a mouse model of cerebral β -amyloidosis. *J. Neurosci.* **31**, 624–9 (2011).
123. Cleary, J. P. *et al.* Natural oligomers of the amyloid-beta protein specifically disrupt cognitive function. *Nat. Neurosci.* **8**, 79–84 (2005).
124. Rasool, S., Martinez-Coria, H., Wu, J. W., LaFerla, F. & Glabe, C. G. Systemic vaccination with anti-oligomeric monoclonal antibodies improves cognitive function by reducing A β deposition and tau pathology in 3xTg-AD mice. *J. Neurochem.* **126**, 473–82 (2013).
125. Cleary, J. P. *et al.* Natural oligomers of the amyloid-beta protein specifically disrupt cognitive function. *Nat. Neurosci.* **8**, 79–84 (2005).
126. Wang, A., Das, P., Switzer, R. C., Golde, T. E. & Jankowsky, J. L. Robust amyloid clearance in a mouse model of Alzheimer's disease provides novel insights into the mechanism of amyloid-beta immunotherapy. *J. Neurosci.* **31**, 4124–36 (2011).
127. Herber, D. L. *et al.* Time-dependent reduction in A β levels after intracranial LPS administration in APP transgenic mice. *Exp. Neurol.* **190**, 245–53 (2004).
128. Wilcock, D. M. *et al.* Intracranially administered anti-A β antibodies reduce beta-amyloid deposition by mechanisms both independent of and associated with microglial activation. *J. Neurosci.* **23**, 3745–51 (2003).

8. List of publications

Luminescent conjugated oligothiophenes (LCOs) as pharmacophores in Alzheimer's Disease; S. Handrick, S. Nyström, J. Mason, N. Reitan, B. M. Wegenast-Braun, M. Lindgren, M. Jucker, K. P. R. Nilsson, P. Hammarström, F. L. Heppner, S. Prokop; *manuscript in preparation*

Evidence for age dependent *in vivo* conformational rearrangement within A β amyloid deposits; S. Nyström, K. M. Psonka-Antonczyk, P. G. Ellingsen, L. B. G. Johansson, N. Reitan, S. Handrick, S. Prokop, F. L. Heppner, B. M. Wegenast-Braun, M. Jucker, M. Lindgren, B. T. Stokke, P. Hammarström, K. P. R. Nilsson; *ACS Chem. Biol.*, 2013, 8 (6), pp 1128-1133

Gouléako Virus Isolated from West African Mosquitoes Constitutes a Proposed Novel Genus in the Family Bunyaviridae; S. Handrick, M. Marklewitz, W. Grasse, A. Kurth, A. Lukashev, C. Drosten, H. Ellerbrok, F. H. Leendertz, G. Pauli and S. Junglen; *J. Virol.* 2011, 85(17):9227

Declaration of Authenticity

I hereby declare that all work and writing contained within this thesis was conducted by myself, all used references are cited accordingly and any personal assistance has been acknowledged by name.

Berlin, April 23th, 2014

Susann Handrick